PARAMETER IDENTIFICATION AND HYBRID MATHEMATICAL MODELLING TECHNIQUES APPLIED TO NON-LINEAR CONTROL SYSTEMS

CRINELA PISLARU

A thesis submitted to the University of Huddersfield in partial fulfilment of the requirements for the degree of Doctor of Philosophy

November 2001

The University of Huddersfield in collaboration with
Micro Metalsmith ltd. and Renishaw plc.

To my parents, Irina and Emanuel

for their love and support

ABSTRACT

The study is concerned with the mathematical modelling and parameter identification of non-linear motion control systems. The control systems under review are the axis motion control systems for a 3-axis CNC machine tool.

The modelling process commences with lumped parameter methods applied to each element and then to each axis in turn. Comparing the dynamic performance of the simulated axis drive with the machine tool axis performance identifies the need for a modular load and the introduction of measured non-linear effects.

In order to achieve a realistic dynamic performance, a hybrid model incorporating a distributed load, explicit damping factors and measured non-linear effects was developed. The influence of factors like damping coefficients, the moving mass, velocity and positional gains, time constants of the servo control system on the servo characteristics of machine tool has been determined. Different friction models have been investigated and an effective simulation method has been developed for simulation purposes. This model represents to a large extent the dynamic behaviour of the drives from the actual machine, a fact proven by the comparison between the simulated and measured results.

For multi-axis control, measured geometric errors at the machine were needed to be included in the model in order to achieve realistic contouring performance. The models were validated by comparison with measurements at the machine.

A feature of this work is the developed measurement methods for parameter identification. This together with the definition of the stimuli provides a solid base for a universal identification process for application to non-linear machine tool axis drives. A novel wavelet algorithm for the determination of damping coefficients for CNC machine tools is introduced and this together with other developed parameter adjustment routines allows for the performance to be optimised.

ACKNOWLEDGEMENTS

I would like to thank to my Director of studies Professor Derek G. Ford for giving me the opportunity to join the Engineering Control and Machine Performance research group within Precision Engineering Centre at University of Huddersfield. It is a pleasure to express my profoundest gratitude for his tremendous enthusiasm in all phases, kind encouragement and willingness to devote time and energy to my work. This thesis owes much to his meticulous and enlightening supervision as well as encouragement.

I would like to thank Dr. J. M. Freeman for his advice with the software and helpful discussions, for his painstaking efforts in reading the entire manuscript and making constructive suggestions.

The support of my home university (Universitatea "Transilvania" din Brasov, Romania) which granted me leave and my fellow colleagues in the Department of Electrical Drives and Automation is gratefully acknowledged.

I am indebted to Mr. Geoff Holroyd for his help and constructive discussions during my research programme. Mr. Geoff Holroyd undertook a MSc project of two months duration carrying out measurement trials under my guidance and developing the initial model of the ball-screw. He later joined the research team to model ball-screws and we worked jointly to optimise the simulation of the model (see section 6.1.2) over another two months period.

I am grateful to my friends for their boundless hospitality, for their endless encouragement in all aspects towards my research work and future career.

Last and by no means least, my sublimest thanks and appreciation to my parents Irina and Emanuel for the love and support they have given me throughout my entire career. Their great moral support has been propelling me to overcome all possible barriers towards noble goals, with the help of almighty God.

Crinela Pislaru

Huddersfield

November 2001

CONTENTS

FIGURES

LIST OF TABLES

1. INTRODUCTION

1. 1. Machine tool performance

The ability to produce accurate components has many advantages; some of the most important ones are listed below:

- Tolerances can be reduced allowing the production of more accurate assemblies. Greater component accuracy often results in performance improvements.
- A reduction in hand fitting or selective assembly, resulting in shorter build times and greater interchangeability.
- A reduction in the costs incurred by re-manufacturing or scrapping out of tolerance components.
- An increased possibility of a part being roughed and finished on the same machine, resulting in reduced set-up time.

The three main areas of concern affecting component accuracy are environmental effects, user effects and machine accuracy. Temperature, humidity, pressure and external vibration are the variables contributing to environmental effects. Temperature change, the frequency of change, temperature gradients and radiation effects greatly influence the magnitude of the error. The user effects are those resulting from the work-piece, the tooling and the machining process. Work-piece considerations include its weight, stiffness, stress levels and distortion, datum surface quality, temperature coefficient and the way it is clamped. Tooling considerations include tool geometry, swarf build-up on the cutting edge, tool stiffness and wear, while machining considerations include the effects of speed and feed, chatter and coolant.

The environment in which a CNC machine tool operates and the user effects form part of the manufacturing process and they are the responsibility of the end user. The machine accuracy is the responsibility of the machine tool builder, and it is a particularly complex matter that depends on a large number of factors. The volume builder of machine tools cannot possibly provide specific operating criteria for the range of products likely to be manufactured using his machines, so a detailed understanding of the sources of error and how to counter them is imperative.

Research into the design process of any high precision CNC machine tool in order to achieve an ever increasing demand for greater accuracy and therefore a more stringent performance specification must embrace error avoidance, error measurement and error

correction. Careful measurement of the repeatable time and spatial errors can allow compensation methods to be applied for the correction of those errors provided sufficient resolution and good repeatability has been allowed for in the design. The ultimate accuracy limit for a particular machine is set by its measured repeatability figures. There is a need to review all design practices concerning the structural elements in order to meet high performance specifications.

Research is currently underway to investigate current methodology applied to the design, assembly, error measurement, and error correction practices of CNC machine tools [1]. Also to investigate "state of the art" practices and provide a generic guide to the machine tool builders and end users on techniques to improve high performance by applying volumetric accuracy correction. In order to achieve this there is the need to investigate the static and dynamic performance, and quantify the constituent errors for each structural element of the CNC machine tool.

Machine tool accuracy depends on its resolution, repeatability, quasi-static errors, dynamic errors and external vibration [2]. Quasi–static errors influence displacement/planar/volumetric accuracy and are caused by static deflections (static stiffness), thermal stability (thermal stiffness), spindle accuracy, and software limitations. Dynamic errors are influenced by control system velocity/acceleration lags, dynamic deflections, dynamic stiffness/damping, contour interpolation, and operating errors. External vibrations can be ground borne or acoustic vibrations.

There is a need with all CNC machine tools seeking high performance to quantify and understand systematic and random error content. Pre-calibrated correction practices are dependent on the machine tool error components being systematic. A correction practice is dependent on precise methodologies for the measurement and identification of the geometric, load and thermal errors.

The motion control system of the CNC machine tool is one of the major structural elements which, can be subdivided into its constituent elements such as controller, electrical drives, transmission, transducers and guide-ways. It is the key to the introduction of correction practices and is the major influence on the machine tool dynamic performance and clearly needs to be more fully understood, hence the need for this research activity.

Misalignments and imperfections within the structural elements cause geometric errors. Although they can be minimised by good design and careful assembly most new CNC machines will leave the manufacturer with some level of error remaining.

The movement of the machine tool axes result in changes in position of machine masses, which can further affect the error components of individual axes (such as yaw, pitch, roll and straightness). The level of each axis coupling is dependent on the machine tool configuration and the rigidity of the machine tool structure. If the structure of a machine tool is loaded then it will distort. If the loading is changed then the distortion of the structure will change and machining errors will result. Sources of loading are the moving weight of the slides, work-piece weight and cutting forces. At the University of Huddersfield (UoH), measurements have been taken over a wide range of machines and significant effects on accuracy were seen on circa half of the sample of machines under review [3]. For example it was shown that a moving slide and work-piece weight generally caused a change in angular error components.

Machine tools are inevitably subject to temperature changes. Thermal errors are produced by distortion occurring due to changes in the temperature of the machine tool structure. The two main causes of structural temperature change are internal heat generation (friction in spindle bearings and slide-ways, fluid losses in hydraulic systems etc.) and environmental temperature variation. The operating conditions of most machine tools means that the heat generated internally will vary significantly as the machine is used. This combined with the complexity of the structure and environmental temperature variations will give rise to complex, transient temperature distributions, making the resultant thermal errors difficult to quantify or predict.

Machine tool manufacturers and users will be well versed in the determination of geometric accuracy under no load, accuracy and repeatability of positioning axes, thermal distortion, and circular dynamic tests for their machines according to the major national and international performance standards [4-8]. These standards are used in the type testing of specific machines, acceptance testing of newly installed machines, comparison testing of a range of machines, periodic verification (i.e. annual re-calibration), and axis positioning compensation through the machine tool controller to ensure continuing accuracy.

AMTRI [9] and Ford [2,10] identified the following structural elements (Table 1.1) and those factors, which needed careful consideration in order to minimise the effect of the constituent errors that contribute to volumetric accuracy.

STRUCTURES	FACTORS TO CONSIDER FOR HIGH PERFORMANCE
Foundations:	High mass, stiff support, time dependent stability, good damping
Beds:	High stiffness, good thermal & time dependent stability, high damping, heat transfer capability, high humidity stability, levelling and alignment "of little significance" to "most important" dependent on machine type.
Columns:	High stiffness, high heat transfer, thermal stability, time dependent stability, alignment capability, low mass, low centre of gravity.
Heads:	High stiffness, high heat transfer, thermal stability, fatigue strength, time dependent stability, low mass, high damping, humidity stability, alignment capability "of little significance" to "most important" dependent on machine type.
Tables:	High stiffness, time dependent stability, alignment capability, static strength, fatigue strength, low mass, high damping.
Saddles:	High stiffness, thermal stability, humidity stability, time dependent stability, alignment capability, low mass, static strength, high damping.
Pallets:	High stiffness, time dependent stability.
Tooling:	Stiffness, balancing, damping.
Motion control	Resolution, stiffness, and noise rejection are general requirements.
Controller:	Sampling time, servo update, quantisation, avoid saturation limits, interpolation
Drives/transmission	Dead-band, backlash, friction , inertia matching, heat generation/cooling, velocity/ acceleration capability, mechanical stiffness.
Rotary/linear transducers	***Intrinsic***: laser wavelength, electronics, optical non-linearity, misalignment, spatial, mechanical set-up and interpolation. ***Environmental***: atmospheric, material thermal expansion, optical thermal drift. ***Installation***: dead-path, Abbe', misalignment, cosine, and acceleration/velocity capability.
Kinematics design	High load carrying capabilities without undue distortion surface fatigue and wear.
Guide-ways	Stiffness (static/dynamic), wear resistance, friction (coulomb/viscous), damping, heat (input/extraction), protection (covers/seals).
Rotary axes	Relative motion between work-piece and cutting: structural loop and thermal drift.

Table 1.1. Factors to consider in the design of high performance machine tools

1.2 CNC machine tool motion control systems

The increasing requirements of industrial applications for higher performance, better reliability and lower cost have imposed the necessity to produce realistic models of the motion control systems.

Many modern processes call for unattended operation, exceptional precision, high throughput, and flexibility for short runs for total manufacturing integration. Often in such

cases, humans cannot perform sufficiently well. Modern sensors and controls coupled with diverse and precise linear and rotary motion actuators, combine to fill the needs. They are elements of a dynamic system, which require continual development to be made in order to satisfy rapid changes in requirements.

A CNC machine tool is an example of such a dynamic system. The forces experienced by the motion control systems have different values depending on the duty cycles: acceleration, steady state, deceleration, cutting etc.

CNC machine tool control systems have errors due to geometric, non-rigid, thermal and dynamic effects. Previously work has largely concentrated on simulation methods based on "*lumped parameters*" methods and the assumption that it behaves as a linear system. The real system has non-linear control elements and the need is to move from the "*lumped parameters*" methods to a consideration of distributive elements if the structural dynamic effects are to be more deeply understood.

The behaviour of a lumped dynamic system is governed by a set of differential equations. Similarly, a set of partial differential equations can represent the dynamic behaviour of a distributed system. Physically all systems are distributed in nature. For practical modelling purposes they can be approximated by ordinary differential equations or by a combination of distributed and lumped elements as shown by Bartlett and Whalley [11]. For hybrid modelled systems represented by distributed –lumped parameter modelling, it is normal practice to treat the energy conversion and dissipating elements by a lumped approach, while energy – transporting elements are treated as distributed. Therefore in hybrid mechanical systems, such elements as long shafts (ball-screws) need to be analysed as distributed realisations, whereas the lumped parameter models are normally adequate for gears, bearings etc.

Modelling and simulation techniques have an established track record as system integration tools in engineering. Such approaches are typically used in the evaluation of new concepts and prototypes where direct experience and access to physical experimentation proves impractical, unsafe or simply too expensive. In promoting a "*systems perspective*" of complex engineering systems, it is therefore implicitly accepted that the whole may be more than just the sum of its parts. The potential problem in predicting and controlling the behaviour of such systems is due to the impossibility of being able to fix the inputs independently since these are dependent on the outputs from adjacent subsystems. This occurs even though localised relationship between inputs and outputs (through, for example the medium of a transfer function) is probably a relatively straightforward matter for each component in isolation. Hence it becomes necessary to view the system in its entirety, as

contrasted to the reductionist perspective which focuses, in detail, on the individually deconstructed parts.

An intuitive grasp of how such a system will behave, in total, is further obscured in the presence of delays, inertia and non-linearity. Hence in practice, simulation has often come to provide the most realistic means of understanding, controlling and improving such systems.

Simulation is arguably more than just science because judgement is required, particularly when the scope of the system and the requisite level of modelling detail are defined, matching the need to produce a representative, efficient and economic model of the real system. A range of human attributes is necessary to translate the physical world into a mathematical one, decide which experiments to perform, analyse results and map them back from graphical and tabulated simulation outputs into natural language.

The CNC machine tool has to be considered as a non-linear system because of friction, backlash and other non-linearities existent in it. The non-linear interactions are difficult to identify due to the immense number of possible combinations. The solution in this case is to structure the approach around a specific class of functions (such as a polynomial for example) that can be used to approximate arbitrarily the behaviour of a dynamical system.

Parameter estimation of linear continuous-time systems using stimuli techniques is well understood. Unfortunately these methods cannot be applied for the identification of non-linear continuous-time systems. The use of standard linear techniques has been mostly restricted to very special classes of non-linear systems only. Application to non-linear systems has been hindered by lack of computing power and suitable algorithms that can be implemented in real time. But the recent development of computers and real-time techniques provides the basis for an improved parameter estimation of non-linear systems.

The ideal situation for the improvement of CNC machine tools performance is to develop an intelligence-based system, which allows parameter identification adjustment on-line by utilising a fast and robust identifier for non-linear systems. To accomplish partially this requirement, the research carried out in this investigation is to develop an intelligence-based system for optimisation off-line by utilising a fast and efficient robust identifier for non-linear systems. The intelligence of the system will come from the ability to predict model parameters and check the system stability. The parameter identification of CNC machine tools or other non-linear continuous-time systems will later be possible to perform on-line on the basis of the intelligence-based system created for off-line application.

Modelling and system identification from measurements of input-output data on a dynamical system has been one of the most active fields of control engineering. However, all

the systems have been reduced using different methods to first or second order elements. This is not reflecting very accurately the behaviour of the real systems because a lot of them are non-linear systems with order number bigger than two (sometimes the order can go up to twenty). This thesis is focused on the development of a methodology for modelling and physical-based parameter identification for non-linear continuous-time systems of this kind.

Many researchers have studied the estimation of the modal parameters of a vibrating system using the *wavelet transform* of the system's free response. However reports, which include detailed technical know-how in determining the natural frequencies and damping factors of the machine tool by using *wavelet transform* are difficult to find in literature. This report represents an important contribution to the study of the wavelet transform used as parameter identification technique for machine tools.

The thesis extends the application of the *wavelet transform* by novel investigations aimed at producing a generic approach suitable for a large number of CNC machine tools and other Cartesian motion applications where non-linear control systems are in use.

The presented method increases the global performance of a modelled and simulated dynamic system. Because the shortcomings of traditional methods are overcome, this method is an important contribution to the motion control of CNC machine tool axis drives.

This new approach is useful for deriving a universal modular mathematical model of CNC machine tool axis drives from the diagnostic, condition monitoring and performance point of view. The errors in machine tools such as geometric, thermally induced and non-rigid errors are considered.

The method is applicable to robotics and other type of Cartesian motion control systems (where the equations of motion for every link are written, the algebraic equations representing the kinematics constraints are established, and the solution comes from solving the set of simultaneous algebraic and differential equations). A similar method could be applied to non-Cartesian machines in the future to extend the field of application.

1. 3. Aims and objectives

The present study is focused on the parameter identification and the mathematical modelling of a non-linear control system. The motion control of the Beaver 3-axis machining centre based at the University is the system under investigation.

In order to achieve this aim, distinct and definite objectives were set. The main objectives of this work can be summarized as follows:

- *Develop a universal 3D mathematical model for a Cartesian CNC machine tool* using three different methods: classical lumped parameter method, modular "*lumped parameter approach*" and hybrid modelling.
- *Simulate the functioning of the models* by implementing them into SIMULINK within the MATLAB environment.
- *Carry out modal analysis measurements* to determine significant structural resonance's.
- *Identify the control loop coefficients and non-linear parameters of the universal model.*
- *Perform physically-based parameter identification for CNC machine tool axis drives.*
- *Develop a robust identifier for modal parameter estimation of non-linear continuous-time systems using wavelet transform.*
- *Validate the robust identifier with respect to the parameter estimation of control model.*

The strength of the thesis lies in the building of an accurate model of the CNC machine tool by good analytical and proven measurement techniques. Then by simulation and practical application demonstrate that the identification technique developed can verify the model by the use of perturbation stimuli and optimisation routines. A feature of this project work is the development of an algorithm and a novel application of wavelet transform for the parameter identification of the CNC machine tools.

The successful outcome will help the machine tool industry to achieve or retain global competitiveness by cutting costs, increasing product and process quality and providing flexibility at the same time. As well as achieving time and spatial accuracy for the motion system the developed model and parameter identification technique is the first step towards producing a universal condition monitoring system

The scope of this research is to investigate an intelligence-based system for optimisation off-line by utilising a fast and efficient robust identifier for non-linear systems. Parameter identification of CNC machine tools or other non-linear continuous-time systems will later be possible to perform on-line on the basis of the intelligence-based system created for off-line application. Thermal effects although studied under this research program were also considered to be outside the scope of the project because of the long time constants involved.

1. 4. Thesis outline

The work presented in this thesis is structured into eight chapters, three of which provide the necessary background material whilst the main original work has been detailed in four relatively self-contained chapters.

Chapter 2 concentrates on a critical appraisal of the extensive literature and contains a brief historical perspective of modelling and simulation of CNC machine tool axis drives, errors in CNC machine tools and parameter identification methods for non-linear systems. The emphasis for the last aspect is on parameter identification and performance optimisation techniques applied to machine tool drives.

Chapter 3 describes briefly the motion control system of the CNC machine tool under review. A clear, simple yet relatively complete view about the elements of CNC machine tool axis drives and their characteristics is outlined.

Chapter 4 is the first of the four chapters that present original contributions. The lumped parameter model with load inertia reflected to the motor without backlash, friction and geometric errors is detailed using control system analysis techniques.

Then the lumped parameter model with modular load for one axis drive of a CNC machine tool is developed. The model includes non-linear effects such as backlash, friction and saturation. Two further models for the additional two axes are built by the same method. The three axis models were combined to demonstrate volumetric dynamic response.

The rigid body errors are included into the 2D model for the CNC machine tool axis drives. The combination of lumped and distributed parameters converts the system to a hybrid model. The final model develops one axis only and introduces a combination of lumped and distributed modelling for investigating the damping factors and stiffness of the different elements. These parameters are to be determined and validated using modal analysis techniques.

Chapter 5 describes the measurement techniques applied to a Beaver CNC machine tool for determining geometric and non-rigid errors using laser interferometer, precision electronic levels and ball-bar. Also it relates the measurement methods to determine:

- Transfer functions for the three- axis drives using HP3566A PC Spectrum / Network analyzer;
- System response to step, trapezoidal, swept sine inputs or white noise;
- Modal parameters for the structure and the drive.

The design of the experimental set-up and the formulation of tests to be performed are specified and the measurement data is analysed.

Chapter 6 presents the implementation of the modular systems for Beaver VC35 CNC machine tool axis drive in SIMULINK 2.0. The lumped parameter model with modular load, backlash and friction and the hybrid model with distributed load, explicit damping factors, backlash and friction are tested to step and trapezoidal inputs and the coefficients are altered

to match the machine parameters. The frequency responses to swept sine and white noise signals are also simulated.

The two-axis model built on the modular approach is used to simulate the ball-bar plot and the results are compared with those obtained from ball-bar tests. The comparison between the simulation results and the measured results is used to validate the models. The hybrid model with distributed load, explicit damping factors, backlash and friction proved to be the most accurate in reflecting the dynamic behaviour of the system.

Chapter 7 analyses the identification methods with regard to: control performance of CNC machine tools drives; bandwidths, gains and phases of different loops of the motion control system; resonance states of transmission (stiffness, damping factors).

The current state of the art of modal analysis is reviewed and some of the current limitations facing the application of modal parameter identification in practical situations are analysed.

Finally, the identification of the resonance states of transmission (stiffness, damping factors) using one of the advanced signal processing techniques – continuous linear wavelet transform - is treated in this thesis. A comprehensive study of evolutive time-frequency analysis using an advanced signal processing technique such as wavelet transform is given.

The critical appraisal of the different parameter identification methods highlights the novelty and advantages of the proposed method against the methods used previously.

Finally, **Chapter 8** summarises the salient points and draws conclusions. Also recommendations for future work are proposed.

2. LITERATURE SURVEY

2. 1. Modelling and simulation of CNC machine tool axis drives

Modelling and simulation are important aspects of engineering design for continuous dynamic systems. The design method usually applies several stages such as formulating the specification, building a mathematical model, preparing a good initial design, and simulating the systems to gather data then finalising the design.

Simulation is particularly important for complex systems where exact analytical approaches, especially with the existence of non-linearities, may not be possible.

In the design of a high performance motion system, the choice of the most adequate system structure is a key issue since normally each application presents specific requirements. Besides basic motor technology selection, a multitude of other factors, such as the interdependence of the functionality of the different elements, affects global performance.

This aspect has been illustrated very well by Ford [12], who developed a series of programs (in Enhanced Basic) and algorithms for the optimal design of the axis drives for use with the majority of machine tool configurations, types and sizes. The aim was to commence from the knowledge of the component shape prior to / after machining and the type of material, etc. and proceed through to the machine layout configuration.

The author noticed that " *mathematical models have apparently not been used extensively in machine tool design*" until that period (1987). Also, he demonstrated the effectiveness of using the lumped parameter models for analysis of the CNC (Computer Numerical Controlled) machine tool axis drives and for improvement of machine performance.

The axis drive simulation software developed by Ford was implemented in a high-level language (Turbo Pascal) by Green [13]. The central theme of this project was to produce two simulation programs that would operate on a PC of average specification:

- The first program generated the output of the mathematical model for a single axis drive system when a trapezoidal rate demand signal was introduced as an input signal.
- The second program simulated the dynamic action of a dual axis system (using two sets of mathematical models) in response to the circular interpolation. Applying a sine wave signal to the input of one axis and a cosine signal to the input of the other axis produced the circular interpolation. Both signals had to have a fixed and synchronised frequency.

Green used improved graphical routines allowing the user to enter values for the mathematical models and quickly assess the dynamic performance of the drives. The understanding of the system has therefore been increased because the user was able to simulate the effect of changing the values for system factors. However, the geometric, load and thermal errors from CNC machine tools were not introduced into the models and their effect was not examined in subsequent simulations.

Siemens AG sponsored special research studies centered on position control and feed drives at the University of Stuttgart. The scientific work for position control optimisation using frequency response methods has been summarized by Gross [14]. The author presents the theoretical treatment of the position control loop design and deals with different mechanical transmission elements and various proposed feed drive measurement methods for application with CNC machine tools. In this way the theoretical technical approach is successfully combined with the practical experience.

Leonhard [15] demonstrates that the most effective control scheme for drives is a cascade with a fast inner current loop, a superimposed speed control loop and an outer superimposed position loop. This control scheme has significant advantages: the stability problem can be broken down into several smaller sub-problems, design is done step-by-step beginning with the innermost loop, load disturbances (representing the mechanical parts of the machine) are suppressed by the integral part of the speed controller as fast as possible etc.

All the above-mentioned references analyse only the lumped-parameter models for CNC machine tool axis drives where the load inertia is referred to the motor. One of the significant shortcomings of this approach is the lost opportunity for examining the behaviour of individual mechanical transmission components and how they interact.

Classical CNC machine tool design utilises high efficiency switching power transistors, and high speed digital control technology to provide high performance servo systems. However, in the modern digital control environment, the analogue control interface does have some major drawbacks:

- The analogue signal is susceptible to electrical interference.
- The analogue interface at the CNC and drive ends is susceptible to drift.
- The analogue drive has a high level of noise because the PWM (Pulse Width Modulated) technique produces harmonics of high frequencies on top of the normal signal. The digital drives produce a clean signal because an encoder is used to measure the velocity and position signal.

All these factors limit the performance potential of the CNC servo system. Today, the capabilities of the modern 32-bit microprocessor based CNC have combined the improvements in mechanical and process technology to yield outstanding improvements in available productivity. The technology of the computer numerical control is advancing at an exceptional rate, such that it is the CNC that is pushing forward the capabilities of modern machine tools. A modern CNC is expected to provide an on-line multi-dimensional graphical interface to the operator, communicate part program and statistical process data via the cell controller. It needs to track tool locations and conditions, and concurrently maintain precise control over one or more multi-axis machining and/or part handling tasks. It operates with 5 times the resolution and 5 to 10 times the speed of previous machines.

Continued growth in CNC technology can be maintained only if it is accompanied by a parallel evolution in axis drive technology. The most significant development in this area over recent years has been the digital communications interface which led to the fully digital drive. SERCOS (**S**erial, **Re**al-Time **Co**mmunications **S**ystem) represents a standard for a serial communications interface in motion control systems with high performance and is based on a fibre optic ring.

With the decreasing cost of computation, the trend toward a broad application of digital control will certainly continue into the future. A permanently increasing number of modern CNC machine tools contain digital drives. This is the reason why controller producers (such as Siemens, Osai etc.) have supported research projects on digital controllers. Some major advantages of digital controllers are:

- Capability of making logical and conditional decisions on the basis of real-time data.
- Very easy reconfiguration through software.
- Implementation of filtering or non-linear conversion on data.
- Storage of operational data for later analysis etc.

Referring to digital drives Papiernik [16] shows that the quality of the machining process is mainly determined by:

- The tracking behaviour of the control / converter system - due to feasible path profiles generated from the programmed contour, time-optimised smooth motion control and a central feed forward control of acceleration and speed and the response to disturbances;
- The optimum response to disturbances - achieved by axial feed forward strategies for compensation of backlash and friction and by high sampling rates.

In another paper [17], the same author represents the CNC machine tool axis drive as a system of masses that vibrate. Because in practice it is very difficult to reduce the vibrations due to resonance frequencies of each element, the author considers only a two-mass-system and applies the frequency analysis as an identification method. Also Papiernik designs a state-space controller for the simplified model. The main shortcoming of this approach consists of the simplification of the real machine to only a two-mass-system.

By analysing the literature on the modelling of CNC machine tools, it is evident that the requirement for a detailed model of a CNC machine tool is very important with a need not previously recognised. All authors have derived lumped parameter models, even in the case of digital drives, which are components of the most recently produced CNC machine tools.

2. 2. Errors in CNC machine tools

In order to achieve high performance specification for CNC machine tools it is essential that all the axis drives have good dynamic performance. The motion control accuracy is a function of the dynamic performance of the control system and the effects of machine time and spatial errors.

The design process of CNC machine tools must embrace error avoidance, error measurement and error correction techniques in order to meet an increasing demand for performance. But first of all, it is necessary to identify the basic types of errors that influence the CNC machine tool performance.

Error avoidance attempts to eliminate the effect of the source of error on the machine tool or work-piece. Some methods for minimising the effects of the errors in machine tools are described by McKeown [18]. The author mentions that better mechanical design, machine tool construction techniques and the choice of better materials (from mechanical and thermal points of view) could improve the machine tool accuracy. Another way of improvement is by using more sophisticated controllers and transducers. However, these manufacturing solutions are extremely expensive to implement.

Error compensation consists of canceling or correcting the effect of the error. First of all, the errors are measured and after that, the correction is applied. There are two basic categories of error compensation techniques:

- *Active compensation* - when the measurement of the error is done at the same time as the compensation. Some methods are based on measuring the deviations from the desired form of the work-piece during the machining operation and correcting them by suitable adjustments of the process (*in process* error compensation). Other methods are based on

Calibration data can be captured dynamically due to recent advances in laser interferometry. Static calibration is time consuming because the machine axis is moved to targeted positions, stopped and a measurement is taken. To overcome these inherent problems, Postlethwaite et al [24] presents a dynamic calibration method. Data is captured on a time basis at a high sampling frequency while the machine axis moves at a constant feed rate. The measured data is processed using a conversion software package and the results can be analysed using the conventional calibration software. To prove the efficiency of the proposed method, experimental results are compared with those obtained from static compensation technique.

Chen et al [25] shows significant improvements by introducing compensation from the results of a static test method and applies correction whilst undertaking aluminium cutting trials. The proposed model comprises 32 error values (instead of 21 individual geometric error components presented by Postlethwaite) because space domain and time domain errors are taken into consideration. The additional 11 components represent thermal effects of the machine tool as drifts in the workpiece and spindle. The model contains load-induced errors introduced by the method of fitting curves to experimental data. To obtain this model it is necessary to perform extensive measurements and data fitting.

The study of thermal errors includes measuring temperature at various points on the machine structure. Hardwick [26] presents the variant of placing the thermal sensors intuitively around the machine structure. This method does not allow for the sensors to be in their optimum positions and the training period for coefficient identification is prohibitive.

A thermal error compensation system was implemented on a machine tool more quickly and practically by Allen [27]. He developed a thermal model which " *relates temperature measurements made at selected points on the machine structure to the overall temperature distribution*". The temperature distribution along a line is calculated from temperature measurements using a curve-fitting method applied between pairs of sensors. The position of thermal sensors is optimised by using a thermal imaging camera and associated cost function analysis software. The temperature model is then used to produce a distortion model that "*calculates the distortion of a structural element from the temperature distribution*". The system is able to determine the required amount of correction and apply it on-line.

The application of this technique to the head slide of a vertical machining centre is shown by Postlethwaite et al [28]. The software package performs two important functions:

- The optimum positions on the machine for thermal sensors are calculated from the thermal images of the machine while it runs through typical duty cycles. The parameter

estimation (off-line) for the temperature model is performed with special software written in MATLAB.

- The distortion corrections necessary to modify the rigid and non-rigid kinematics models are derived from the readings of thermal sensors. The software is written using Borland Turbo C V2.0 in the DOS environment. The main advantage of this novel technique for reducing work-piece errors caused by the machine's thermal distortion consists of cost and time effectiveness because the data is measured during short heating and cooling tests.

Chen et al [29] regards the identification of load induced effects as an integral part of a complete error compensation package. Collecting this data requires significant time for pre-calibration compensation when thermal effects can introduce errors to this measurement, so it is necessary to elaborate a clear and structured strategy for measurement. The effects of work-piece weight and the overall coupling of errors are not examined.

Blake [30] identifies a method for isolating load effects so that individual components can be predicted in the future. From tests done on a wide range of machines, he finds that the moving slide and work-piece weight generally cause a change in angular error components. Those changes, measured on-line, are introduced into the geometric model developed by Postlethwaite [21].

Ford et al [3] describes measurement strategies for the separation of the geometric and non-rigid errors, which will be used in a correction algorithm. The accent is on the angular error components which are the main geometric error components exhibiting a non-rigid effect. The effects of thermal errors on linear measurements are minimised by running the axes used during machining through a warm-up cycle.

The three categories of errors are discussed by Ford et al [2], who proposes various methods to compensate for these errors. The conclusion is that the best approach to reduce the errors in machine tools is a compromise between good design and compensation techniques.

A general algorithm for universal machine tool error compensation is developed by Ford et al [31] by combining the compensation systems mentioned above regarding geometric errors [21, 22, 23, 24], thermal errors [27, 28] and non-rigid errors [3, 30]. The motion of a machine is represented by a kinematics chain by using vectors to characterise the movement of the rigid bodies that make up the machine structure. Furthermore, the non-rigid effects are taken into account and the rigid-body model is modified. Also a temperature-based compensation system is used in validation tests. This dynamic compensation system constitutes a very powerful tool for improving machine tool accuracy due to its ability to compensate for all major sources of error. For example, the geometric error improvement

achieved is 10:1 and the thermal error improvement is 9.3:1 for a CNC vertical milling machine Beaver VC 35 and 7:1 for other types of machines on industrial sites.

The effectiveness of a volumetric error compensation scheme relies on a *calibration methodology* that can measure accurately the volumetric errors. Popular calibration techniques for acceptance testing and periodic checking of overall volumetric errors are the artefact inspection, telescoping ball bar and laser interferometer methods.

Kirkham [32] calculates the positioning errors using spheres of measurement (within the machine's working volume) provided by a machine-checking gauge. Many unknown set-up errors are likely to occur due to the large number of necessary measurements. The overall accuracy of the data is reduced in this way. To minimise the effect of the errors, the author uses statistical analysis techniques. The final model obtained is a compromise between static and dynamic performance.

Kakino et al [33] develops the double ball bar method for the measurement of 2-dimensional and 3-dimensional accuracy. The geometric deviations and those caused by numerical control can be recorded and analysed in a relatively simple way. The principle of error origin diagnosis by the circular interpolation test is explained. In order to optimise this method for motion error and accuracy evaluation it is necessary to obtain as much measuring data as possible.

Some experimental results obtained by using the telescopic ball bar, for a wide range of machining and turning centre configurations, are analysed by Smith et al [34]. The influence of different designs of machine tools and their axis configurations upon the profile-error plot of the ball bar must be appreciated. When error compensation is applied to the CNC controller from data provided by laser, precision levels etc. the ball bar system demonstrates that the contouring performance of the machine is improved.

Okafor et al [35] examines minutely the results of using this powerful tool for the fast, effective diagnosis/calibration of a vertical machining centre. The circular contouring errors are highly dependent on the feed rate used and the selected machine was shown to be overdue for maintenance because of the large backlash and servo mismatch errors. Today the ball bar has become one of the most popular checking-gauges for verifying machine performance, achieving manufacturing tolerances, comparing like machines, predicting maintenance, accepting new machines etc. The results of the dynamic test are analysed by-easy-to-use software that provides an overall picture of how the machine performs in accordance with ISO and ANSI standards. The accuracy and reliability of the estimated geometric errors are arguable when the machine produces significant noise during measurement.

The laser interferometer system is considered to be the most reliable and accurate calibration tool because the noise effects are minimised. The laser is largely a static method but it could be used in a dynamic way as was shown by Postlethwaite et al [24]. Blackshaw et al [36] describes the use of a laser interferometer to measure the linear positioning accuracy of one axis of a high precision lathe. On the basis of the measured data, the compensation was applied through the machine tool controller.

Okafor et al [37] determined the accuracy of a vertical machining centre motion control systems using a laser interferometer and other precision instrumentation. The X-axis (top table axis) was found to have the worst linear displacement accuracy and the X-axis pitch and the Y-axis yaw have the highest values among all the angular errors. The laser interferometer system has a lot of advantages such as its ruggedness portability, compatibility, high resolution and automatic data capture. The main shortcoming is that the optic set-up and laser-path alignment is time-consuming. To overcome this, Chen et al [38] has developed an auto-alignment laser interferometer capable of a diagonal measurement (when multiple machine axes are moved simultaneously) with automatic optic alignment. The complete calibration of a 3-axis machine can be achieved in one hour instead of several days using the conventional laser interferometer system. Again, the accuracy and reliability of the straightness errors are arguable when the machine produces significant noise during measurement. An averaging technique is proposed to overcome this problem. It is a method that is useful for comparative checking against similar machine types and configurations. Absolute volumetric error detail cannot readily be obtained by this method. Also the 21 sources of error that make up the volumetric error figure cannot be completely separated.

All of the above methods are to determine geometric, non-rigid or dynamic contouring effects, but the measurement practices try to keep the thermal effects to a minimum.

Thermal errors have been investigated by Allen [27] and White [39] and their effects demonstrated to be significant in terms of machine performance, but the changes are relatively slow and are outside of the scope of this research proposal. Ford et al [31] demonstrated that a geometric and thermal model can be combined to achieve compensation.

2. 3. Parameter identification methods for non-linear systems

2. 3. 1. General

No matter how well analytical modelling is performed, some parameter identification is necessary. Real systems contain difficult effects to model and have high sensitivity elements

within. There is therefore a need for good identification practices and stringent hardware testing procedures in order to determine the relevant parameters.

There is a strong link between identification, modelling and estimation. Modelling represents the process of setting up the mathematical model of the system, based on data relying on physical principles, empirical relations or other a priori information. Estimation refers to the process of obtaining the parameters of a given model, normally from stochastic linear differential or difference equations. Identification is the process of selecting a parameterised model and then obtaining its parameters. Hence identification refers to modelling followed by estimation. The modelling stage associated with process identification is often referred to as "*model structure determination*".

Ljung et al [40] formulated a sequence of questions that any user of identification methods must answer:

- Has system identification anything to offer to my problem?
- How should I design the identification experiment?
- Within which set of models should I look for a suitable description of the system?
- What criterion should I use for selecting that model set that best describes the data?
- Is the model obtained an adequate representation of my problem?

Bohlin [41] has shown that answering these questions is not an easy task; the answer depends on the knowledge existing beforehand about the system to be identified and on the powers and limitations of the available techniques.

The classical approach to process identification deals with the analysis of either the process time response to step or impulse inputs or the process frequency-domain response. The devices under consideration are assumed to be linear time-invariant (LTI) single-input, single-output (SISO) systems. Classical methods can be extended to multiple-input multiple-output (MIMO) systems. The input-output (I/O) observations are obtained by means of a band-limited measurement set-up. Guillame et al. [47] show that the frequency-domain approach has certain advantages in comparison with the time-domain approach:

- *Complex Normally Distributed Fourier Coefficients* – The *discrete Fourier transformation (DFT)* of the measured (periodic) I/O signals is the starting point of practical procedures for the estimation of dynamic system parameters in the frequency domain [42]. The discrete Fourier coefficient estimates thus obtained as primary observations are used by the subsequent parameter estimation stages. The Fourier coefficients are asymptotically complex, normally distributed and independent over the

frequencies, for a wide class of *probability density functions (PDF)* of the time-domain noise [43]. This detailed statistical knowledge could be used to determine and enhance the quality of the system parameter estimates.

- *Errors-in-Variables (EV)* stochastic models are needed [43] when the system identification methods presume that the applied excitation is an exactly known or quantifiable (zero-order-hold) signal [42]. In this case, only the output signal is subjected to disturbing noise and it is possible to obtain estimates for the system parameters as well as for a parametric noise model [44, 45]. These estimators are no longer consistent when the input is disturbed by noise so the errors in all variables must be taken into account to preserve the consistency of estimators. Examples of EV frequency-domain identification methods are the *generalised total least squares (GTLS), the bootstrapped total least squares (BTLS)* and the *maximum likelihood estimator (MLE)* which performs better than GTLS in the case of coloured noise. These frequency-domain estimators are only consistent when the "true" covariance matrix of the I/O disturbances is *a priori* known.
- *Validation* - A better insight into the dynamics of a system and an easy detection of modelling errors (by comparing the estimated transfer function with the frequency response data) are given by a frequency-domain representation. The frequency response method has proven to be an effective approach for the dynamic systems because rapidly varying forcing functions can often be expressed as periodic functions.
- *Large Dynamical Range* - Transfer functions with a large dynamical range can be estimated.
- *Wide Frequency Bands* can be covered due to the combination of the measurements gathered at different sampling frequencies.

The main drawbacks of a frequency-domain approach are:

- *Periodic Excitations* - required to be applied for the correct use of the DFT algorithms. Unless a sweep oscillator is used, a range of frequencies will have to be applied, the system allowed to settle to the steady state response at each frequency, and the magnitude and phase of the response measured. As an alternative, white noise can be used as the stimulus.
- *Off-line Identification* – due to the fact that the measurement results have to be processed off-line (or in batch mode). The output signal must be compared with the input signal in order to determine the gain and phase.
- *Covariance Matrix of the Fourier Coefficients* - has to be known a priori ([43]) to obtain consistent estimates within an EV stochastic framework. If this matrix is not available, the

consistency of the GTLS, the BTLS and the ML estimator are lost. To release this drawback, Feng and Zheng [46] constructed a modified least-squares (MLS) estimator by assuming white input and output noise. An estimate of the noise variances can be derived using a "known" first-order pre-filter. The asymptotic bias of the least squares method can be determined and subtracted from the system parameter estimates once the variances are known.

Guillame et al. [47] proposes an alternative solution which, does not require pre-filtering and can handle coloured I/O noise. The idea consists of constructing a parametric frequency-domain estimator whose consistency is robust to lack of prior noise information. An estimator that satisfies this objective is obtained by minimising a weighted sum of squared residuals involving complex logarithmic transforms of the transfer function model and the frequency response data. This *logarithmic (non-linear) least square estimator (LOG-LSE)* is shown to be more robust to lack of prior noise information than the GTLS, BTLS and ML estimators. However, when the noise information is available, it can be used to improve the efficiency of the estimator. The statistical properties of the parametric LOG-LSE are verified using Monte-Carlo simulations.

Pintelon et al. [48] perform a survey of frequency domain identification methods for rational transfer functions. When the goal is the design of a digital controller for a continuous-time process driven by a zero-order-hold (ZOH) reconstructor, the discrete time or z-transfer function models identified from noisy output observations are the most appropriate. Two identification approaches are possible in this case, according to the excitation signal:

- Classical time-domain (prediction error) identification methods - used for arbitrary excitations.
- Frequency - domain identification techniques - for periodic excitations. In the case when the classical discrete-time identification approach generates large model errors (for example, the plant is driven by a non-linear actuator or a signal-independent input-output model is required), ***the band limited (BL) signal*** assumption is used (the measured signals contain no energy above a certain specified maximum frequency).

Those methods can be divided into two classes:

- *Algorithms derived by "common sense" (deterministic) arguments.*

Levi [49] reduced the non-linear least squares (NLS) problem to a linear least squares one by multiplying the equation error with the denominator of the transfer function. Linearisation presents two major drawbacks: the high frequency errors are over emphasised

and there are generated poor low frequency fits and ill-conditioned normal equations for identification problems with a large dynamic frequency range.

The lack of sensitivity to low frequency errors is overcome by Sanathanan and Koerner [50] by an iterative procedure. Their idea is used for the iterative quadratic maximum likelihood (IQML) method, too. The non-linear optimisation problem of the maximum likelihood (ML) cost function is reduced to a linear weighted least squares problem by evaluating the denominator of the ML cost function at an initial guess of the model parameters. The *generalized total least squares (GTLS)* method [51] estimates are less efficient than the ML estimates due to the frequency-independent weighting of the equation errors. Its efficiency is enhanced by the *bootstrapped total least squares (BTLS)* method where the weighting is relaxed. The BTLS estimates can be seen as the GTLS method with an "optimally" weighted iteration. It combines the optimal ML efficiency with the global minimisation property of the GTLS estimates.

The previous estimators require a prior noise analysis (the variances and the correlation must be known at each frequency). This drawback is overcome by *"logarithmic" least squares (LOG)* estimator [47].

The *instrumental variable (IV) estimator* [52] can be obtained when two (or more) periods of the measured time signals are available. The measurements can be split up into two time records and the Fourier coefficients calculated for the second time record can be used as instrumental sequences for the linear least squares identification based on the Fourier coefficients of the first time record.

As a result of critical comparison of the above mentioned methods, the authors make some remarks:

- ML, GTLS, BTLS and LOG estimates are independent of the constraint used because their respective cost functions are scale invariant.
- There are ML and LOG extensions for models with an unknown (fractional) time delay (shift).
- NLS, ML, GTLS, BTLS LOG and IV estimators perform well on a second -order system.
- Estimates of the non-parametric noise model can be obtained by measuring the disturbing noise auto- and cross-power spectra (when no excitation signal is applied to the plant) and by calculating the sample (co-) variances of a set of noisy input and output spectra.

- *Algorithms derived using statistical arguments*

A fifth-order Butterworth filter with an extra transmission zero was simulated and one hundred disturbed data sets are generated. For each set are calculated the model parameters using LS, WTLS, NLS, GTLS, IQML, LOG, BTLS and ML estimators. Both WTLS and GTLS estimators perform well, however the WTLS error estimates are due to the bias, while GTLS are due to variance. The IQML estimator performs equally well as the ML estimator, due to the high signal-to-noise ratio and the absence of modelling errors. The conclusion of this survey is when prior noise knowledge is available, use ML and BTLS, otherwise use LOG or NLS estimators.

Balmer [63] investigates the problem of fitting a parametric model to frequency response data measured on-line by using the iterative method [50]. A general approach is developed because the application consists of on-line identification with time varying parameters. The best method of giving less weight to past data is the Kalman filter approach.

Zhang [54] develops an algorithm to identify interval models of multivariable systems from measurements in the frequency domain. The effectiveness of the identified interval model is guaranteed because the intervals are minimised with membership constraints. The resultant sizes of the intervals are related to the nominal model identification. The NLS algorithm is used for the identification of the nominal models. Both delay and non-delay multivariable systems can be identified with satisfactory accuracy, a fact proven by simulations.

One of the most challenging problems in system identification is that of model structure selection. Coca [55] underlined the importance of this aspect in the case of non-linear systems. Research into non-linear system identification is concerned with understanding the relationship between model structure and qualitative behaviour. Considerations are: effective initial structure specification, practical input sequences and the incorporation of behavioural constraints (e.g., stability, steady-state matching, etc.) into the model development process. Coca described the steps of a framework and methodology which allows the practitioner to derive a non-linear model of a system in a structured manner.

A detailed survey of methods for modelling and identification of non-linear dynamical systems has been performed by Sequare [56]. As a results of this thorough overview, the author presented the three main classes of models used for the identification of non-linear systems (Figure 2. 1.):

- *Non-parametric models* – based on functional series expansions or kernel regression estimation techniques;

- *Parametric models* – aimed at reaching the best possible or optimal estimate of the unknown system from normal noisy input-output data;
- *Semi-parametric models* – based on artificial neural networks and linguistic label fuzzy models.

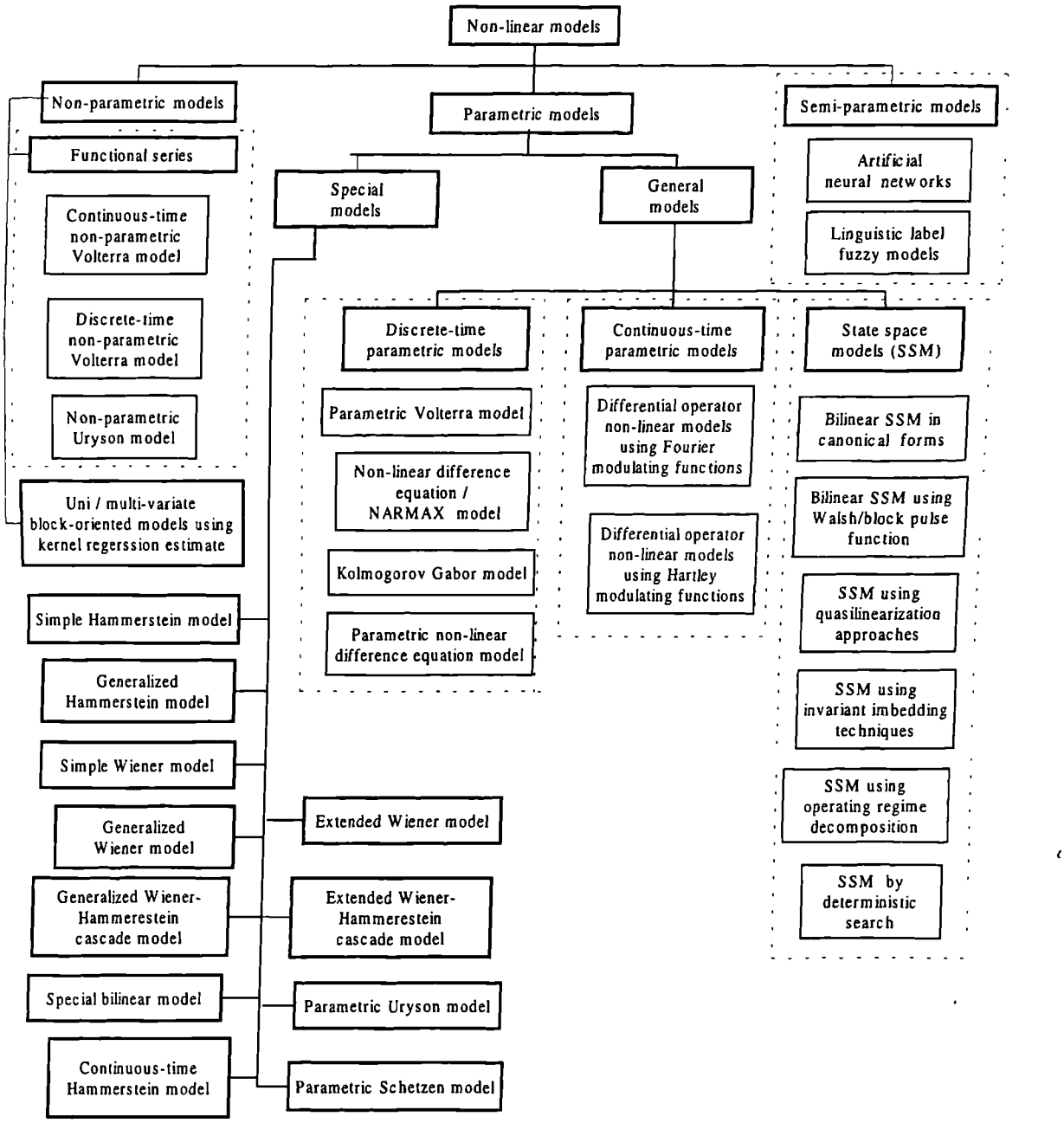

Figure 2. 1. Major structure of non-linear system identification models

These models are valid for continuous-time non-linear systems, but other methods have to be applied when analysing the dynamics of complex non-linear control systems (such as CNC machine tools for example) which require hybrid modelling. This is due to the fact that

some elements are represented as lumped masses (continuous-time elements with differential equations) while others are depicted as discrete masses (partial-differential equations).

2. 3. 2. Parameter identification methods suitable for use with machine tools

Different methods have been used for the identification of the parameters for machine tools. Pavelic and Cleek [57] present a technique for the analysis of a structural resonance in a prototype numerically controlled machining centre. Static stiffness of a machine structure is relatively easy to measure, but the dynamic stiffness is more difficult to determine. The paper describes the principles, instrumentation and test methods of an experimental approach analogous to that for static stiffness. In the theoretical approach it is assumed that the test structure is a linear system (restoring forces proportional to displacement and damping proportional to velocity). The compliance transfer function (force/displacement) is deduced for single degree-of-freedom and multiple degree-of-freedom systems.

A general test method to determine experimentally the resonant frequencies and the corresponding mode shapes is described. To excite the structure, a swept-sine waveform is used (produces the most accurate results when working with heavy, stiff structures). Analysing the experimental results, it is evident that the total displacement is divided into four identifiable components. One produced by compliance of bonded joints (between the steel foundation blocks and concrete floor), distortion of the bed structure, rotation and translation of the slide relative to the ways and rotation of the table base relative to the slideways. The resonance value could be shifted to a higher frequency by raising the system stiffness, by reducing the effective mass or by connecting in parallel a damped absorber. These solutions are not recommended due to the cost associated with them. The authors declare that "*the user will be advised of the importance of a secure foundation for the machine*".

Gustaveson [58] estimates modal parameters directly using the partial-fraction-expansion form of the frequency response function. This analytical technique (curve fitting) is based upon the minimisation of the least-squares-error of a set of non-linear equations using empirical frequency response data. In this way the natural frequencies, damping values and the mode shapes of a mechanical structure are estimated. The author displays the results considering the data with widely spaced modes, in the presence of noise and with highly damped modes. The technique demonstrates the ability to estimate modal parameters in the presence of noise and to uncouple modes that are closely spaced.

Banks and Wang [59] outline the theoretical foundations for general frequency domain parameter estimation techniques for second order systems described in terms of sesqulinear

forms and operators in a Hilbert space. It is calculated from the discrete Fourier transform (DFT) of the data and the cost function is defined by using this transformed data. The theoretical approach is used for estimating the damping parameters in Timoshenko beams.

Okabe et. al [60] proposes two methods for parameter identification of the non-linearity in machine tool elements, which use the impulsive response method. They are determined theoretically from the physical quantities, which describe the non-linear characteristics of spring and damping by using directly the displacement, the velocity and the acceleration of the element and the exciting force (measured with the impulsive excitation). The authors use the parametric least square method and non-parametric methods to perform the identification for a system with hardening spring, softening spring and clearances. The methods are evaluated by simulation in the noiseless case and when the noise components are included in the measurement. The conclusion is that the non-parametric method is more effective than the parametric one, when types and intensity of non-linearity from the actual machine components are known. The efficiency of the methods is verified experimentally by exciting a shaft element model with the impulsive response method.

Kim et. al [61] develop a new identification method for mechanical systems with friction. By making a critical appraisal to previous methods, they show that model-based friction compensation needs the precise knowledge of mass, and *Recursive Least Squares (RLS)* and *Least Mean Squares (LMS)* have good convergence properties only if the persistent excitation condition is satisfied. The highlights of this approach are: there is no need to know the acceleration; the conditions required for the feasibility of the method can be easily guaranteed in real applications; the mass can be identified accurately regardless of the modelling error of friction. The generality and practicality of this new method is demonstrated by simulation.

Meskell and Fitzpatrick [62] apply the frequency domain technique for the identification of a non-linear single degree of freedom model by reformulating the system as a multiple input single output (MISO) system. The linear and non-linear terms (mass, acceleration, velocity, displacement, damping, stiffness) are introduced as inputs and the excitation force is considered as output. First the system (a test rig excited by an electromagnetic shaker) was tested with no Coulomb damping and the transfer function between force and acceleration was calculated. This result is compared with that in the presence of Coulomb damping when the system is excited with band-limited white noise. It is important to realise that "*as the excitation level increases, the Coulomb damping becomes less significant*" because the friction force is not proportional to the velocity. A series of random forced tests were conducted to ensure linearity and to locate the modes of the structure.

Tsuei and Huang [63] discuss and compare two methods concerning the identification of a damping matrix:

- An iterative approach to viscous damping matrix identification when the matrix is constructed from the eigenvalues and eigenvectors. The method is valid only for small damping ratio and low noise. A two degree-of-freedom (DOF) lumped mass system is considered and simulations are performed for undamped, viscous, structural and viscous & structural friction cases. The estimation error is used for modelling the viscous damping to identify the system with combined viscous and structural damping
- The normal *frequency response functions (FRF)* extracted from the complex frequency response functions.

The authors stress the necessity to perform a critical review of structural damping and to carry out further research into the modelling of damping.

Blaszkowski et. al [64] developed a new technique for the identification of servo drives of machine tools and robots using the signal de-convolution method. This technique overcomes the drawback of the traditional non-parametric methods of identification - only the average value of the system properties is predicted. The authors consider a linear model to describe the servo drive dynamics and compare the measured servo drive response to white noise to an estimated response and a simulated response. The Taylor expansion is used to generalize the linear de-convolution to the non-linear case. In this way a powerful method is created for the identification of non-linear systems in the discrete time domain.

Best and Gordon [65] perform an extensive investigation of a new randomized integral error criterion (RIEC) method for the identification of reduced order models of complex mechanical vibration systems. The method overcomes the drawback of least-squares methods' resulting in the generation of an excessive parameter bias due to high variance and autocorrelation of the error process regarding to significant unmodelled modes. Simulation results are compared with those of direct least-squares identification method regarding tyre stiffness, masses and suspension force parameters of a quarter-car suspension system. The advantages of RIEC are evident:

- Successful in rejecting errors in the source data arising from unmodelled modes;
- Good degree of consistency for identification - the model is derived from four permutations of the dynamic equations of motion and in the presence of 3 different unmodelled modes;
- Successful identification of mass parameters where the reference method fails;

- Ability to extract a large number of samples from each single batch of data and to tune the integration step length depending on the system to be modelled.

The input signal is gaussian white noise chosen with sufficiently high bandwidth to excite all modes.

Verboven et. al [66] describe an improved modal parameter identification method based on non-parametric modelling of the measurement noise. The method uses a frequency domain MLE to perform a non-parametric FRF estimation for an EV model considering the process noise, the noise of the output and input signals. Experimental measurements using a random and periodic signal (multi-sine) excitation validate the method. Some interesting conclusions result from the analysis of these data:

- Lower resonance frequencies correspond to the most important structural modes, so it is important to estimate these values accurately in order to obtain correct modal parameters;
- The type of excitation signal affects the damping ratios and the mode shapes;
- The bias effect is less apparent in the measurements using a multi-sine excitation due to higher signal-to-noise ratio.

2. 3. 3. Previous work at the University of Huddersfield

The University of Huddersfield (UoH) was awarded a major research grant [67] to work with three collaborators covering applications to machine tools, aircraft simulators, power mills and metrology equipment.

The algorithms produced utilised a non-injective method for identifying non-linear dynamic systems, which adapts from machine vision the Hough Transform method of geometrical feature extraction [68]. The method uses statistical accumulators computed from condition monitoring data to fix the coefficients in an evolution equation. The coefficients are manifested as an accumulator peak, which must be found by a fast search of accumulator locations. If trending data suffers a change in trend due to a system change, a second peak appears to indicate that the monitored data supports two hypotheses about systems parameters.

The method is robust, performing well in the presence of additive noise, impulsive outliners in data, and partial loss of data. It can be refined to metrological levels of precision, but is computationally intensive. Also, different types of non-linear models require different accumulators to be used with the same monitored data.

One significant advantage of the technique is that the problem of parameter estimation of non-linear systems reduces to that of the estimation of linear expressions of model parameters. A critical comparison in performance found the Hough Transform technique to perform at least as adequately and often better than least-squares estimators [68].

The graceful degradation in performance of the Hough Transform as a parameter estimator in comparison with the more traditional least squares method has been shown by using a linear second order system and a Hammerstein model. The location of the peak was not affected by the heavy contamination of the output of the Hammerstein system with impulsive noise. In this way, the robustness of the Hough transform was illustrated as opposed to the least-squares based algorithm. The limitations of the method are that large amount of memory is required and the computational time is extensive.

2. 3. 4. Input signals for parameter identification

The accuracy of system identification depends on a number of factors, particularly in the choices for model structure and input excitations.

Morton and Brook [69] describe a simple method of injecting a perturbation signal on a D.C. machine and performing the transfer function analysis tests with a digital signal analyzer. Two types of signals are considered as perturbations:

- *Sine wave signals* for a range of frequencies - by comparing the shape of frequency response measured by the analyser with that expected for a postulated model, relevant parameters can be determined. Noise perturbations, independent of the sine wave input, corrupt the output and make accurate observation difficult. The measuring process can become time consuming because a separate test is necessary at each relevant frequency.
- *Gaussian wide band random signal* - which contains all relevant simultaneous frequencies. The analyser uses the Fast Fourier Transform (FFT) for the frequency-analysis of the signals. The cross correlation between the perturbing signal and the response signal is proportional to the system impulse response when the gaussian signal has an adequate bandwidth.

Araki et. al [70] compare the pneumatic system frequency characteristics obtained with M-sequence and the sinusoidal input methods. The M-sequence signal is a pseudo random pulse signal, periodical and with two levels of constant amplitude. The M-sequence is used because the digital simulation of the system frequency characteristics with a sinusoidal input signal is very time consuming. For the frequency characteristic analysis of a system, which includes non-linear components the *describing function method* is often used. This could work if the

non-linearity terms were reduced to friction and backlash only or other acceptable forms. The author's show that the bias error caused by the different waveforms of the two methods can be estimated and compensated for in the analysis.

Smith and Pratt [71] present a robust and practical method for obtaining open-loop frequency response data for a closed-loop system. The author's underline that the simplest technique to identify open-loop non-parametric constructions is to excite *sinusoidally* the plant and measure the frequency response. The technique is unacceptable in the presence of noise, disturbance and harmonic non-linearity. Accurate results are obtained by using correlation analysis - a very robust practical method, known to give very good noise immunity. *Step inputs* are introduced into the plant to investigate the response of the method to an unanticipated disturbance. The impact of the step disturbances was found to be negligible, apart from a small band of frequencies near 1 rad/sec. To check the performance of the method in a noisy environment, *white noise* scaled by 0.2 is introduced into the plant and its effect is obvious at high frequencies.

Jennewein and Fritzen [72] design optimal input signals for mechanical systems by maximising the trace of the Fisher information matrix. The Euler-Lagrange equations generate the input signal that maximises the integral with respect to the constraint (a limited amount of energy for the input signal). The authors recommend the following input signals for solving the identification problem:

- *Sinusoidal signal* - which generates large displacements in the response if its frequency is, near an Eigen frequency of the system resonance. The Eigen frequencies must be measured or system parameters must be first estimated (as the real values are not known yet).
- *Random noise* - stimulates a requested frequency range. The displacements of the system will be smaller compared with that resulting from a sine signal because of spreading the input energy over a wide frequency range.

To combine the advantages of both signal types, the authors multiply the sine signal peak with a flattop window in the frequency domain. So the frequency peak of the sine signal is opened up to a rectangle.

The calculated optimal input is used for parameter identification for two examples with simulated measurements:

- Horizontal ground movement using various signals excites a three-degree-of-freedom model of a multi-story building and the salient system parameters are the three masses and three stiffnesses.

- An elastic beam with a crack is modelled using the Finite Element (FE) method, according to the theory of Timoshenko. The parameter to be identified is the relative crack depth.

The identification results are compared with those obtained by using other types of inputs. The following observations can be made:

- The optimal input signals start with large magnitudes (the system gets excited comparable to a jump), decreasing over time and converging to zero. Large input magnitudes with frequencies near to system eigen frequencies are used.
- The time limitation of the input signal corresponds to the measurement requirements.
- The optimal input signal contains a range of frequencies around a dominating frequency because the signal is not periodic. Its "*effect is comparable to the flattop window effect: the eigen frequency of the real system is affected although it is not equal to the dominating frequency of the input signal*".

2. 3. 5. Parameter identification methods suitable for use with machine tools

When the input to a system changes as a function of time, the form of the resulting response is clearly dependent both on the nature of the input function and on the equations describing the dynamic characteristics of the system. The output response can be calculated for any input function of known mathematical form.

Three main types of input forcing excitations were considered when studying the dynamics of the CNC machine tools:

1. *Transient disturbances* such as step changes of magnitude, ramp changes, or impulsive changes which release the system from a non-equilibrium state (i. e. from an initial non-zero position and / or velocity) for the case of free vibrations;
2. *Sinusoidal input* (of position or force) for the case of forced vibrations;
3. *Statistical signals* with random characteristics.

1. Transient disturbances - Probably the most useful and frequently used forcing function is the *step change of input* where the input is changed suddenly from one value to a new constant value. It is mathematically simple and occurs commonly in practice. It is the most severe disturbance that can be applied, and knowledge of how the system output will be affected is of considerable interest.

Other simple forcing functions are:

- *Ramp function (derivative of step input)* - a less severe form of disturbance in some ways but a more difficult problem for the controller. This is relevant where step changes are not possible or not normal.
- *Impulse* - in practice is less valuable than the other two because to be large enough to produce an identifiable response (especially if there is some noise present), the amplitude of the impulse must be so high that the system may be damaged or driven into a region of non-linear operation.

Step, ramp and impulse functions are all transient disturbances because the system normally starts from a steady state and re-attains a steady state condition (except ramp functions) after the effect of the disturbance has died out. In analysis it is the nature of the transient response leading to the new steady state and the error between the steady state and the ideal value which are studied.

2. *Sinusoidal inputs* - have relevance since they commonly occur in practice (e. g. in mechanical systems undergoing vibratory movement). Pavelic and Cleek [57] have shown that a swept-sine waveform is the most suitable stimuli for heavy, stiff structures.
   By Fourier decomposition, any periodic signal of arbitrary waveform can be broken down into the summation of a series of sine and cosine waves with specific amplitudes at the fundamental frequency and integer multiples of this frequency. The response of the system to suitable swept sine input contains the response of all the modes of the system.

3. *Statistical signals* - have waveforms which are wholly or partially random. A random excitation causes all the modes to be activated and therefore, the response is the linear superposition of all the modes that are excited in the case of a linear system. The main disadvantage consists of the limited level of energy which is introduced into the system for various frequencies of excitation.
   Rivera [73] presented the principal sources of error in system identification:
   - Bias – systematic errors caused by input signal characteristics (i. e. excitation), choice of model structure, mode of operation (i.e. closed-loop instead of open-loop);
   - Variance – random errors introduced by the presence of noise in the data, which do not allow the model to reproduce exactly the system output. It is affected by the following factors: number of model parameters, duration of the identification test, signal-to-noise ratio.

From this point of view, understanding the various identification methods and associated decision variables in terms of bias-variance tradeoffs is an important key to successful system identification in practice.

The conclusion of the aspects presented above is that one who performs the system identification must have extensive background in a number of fields, including mathematics, control theory, signal processing, statistics, optimisation and many others.

2. 4. Conclusions

The literature survey brings out the strong link between identification, modelling and estimation. Ljung et al [44] expresses the needs for identification, good experimentation and validation of accurate models that fully represent the systems under review.

From a review of the literature survey when considering the development of robust algorithms for parameter identification applied to stiff heavy structures such as CNC machine tools, the following conclusions can be drawn:

- A robust system must be well served by good identification, modelling and estimation practices. Ljung et al [44] expresses the needs for identification, careful design of experimental methods and accurate modelling of the system under review.
- *Swept-sine excitation waveforms* produce the most accurate results when working with heavy, stiff structures such as machine tools [57].
- Four identifiable structural resonance components namely *compliance of bonded joints, distortion of the bed structure, rotation and translation of the slide relative to the ways and rotation of the table base relative to the slide* should be considered [57].
- The identification of servo drive parameters for machine tools using a signal de-convolution method derived by Blaszkowski et. al [64] merits consideration. Response to white noise used to predict average values of the system properties.
- Gaussian white noise of sufficiently high bandwidth could be tried to excite all modes. Its only doubt is how well it works with a heavy stiff structure [65].
- Frequency characteristic analysis of a system, which includes non-linearity's using a describing function method, could be investigated, provided only a few known non-linearity's are present [70].
- Stimuli inputs covering the time and frequency domains for consideration included *sine, step, impulse, ramp, trapezoidal, pseudo-random binary sequence, Gaussian white noise and composite signals* [41, 57, 65, 69, 70, 71].

- A robust and practical method for obtaining open-loop frequency response data for a closed loop system using sinusoidal and step inputs backed by correlation analysis was demonstrated [71]. Good noise immunity was achieved.
- *Errors in variables* (EV) techniques for consideration include least square methods (GTLS, BTLS, LOG-LSE) and *the maximum likelihood estimator* (MLE) [42, 43, 44, 45, 47, 50]. Frequency domains estimations are only consistent when the "*time*" covariance matrix of the I / O distribution is "*a priori*" known.
- A frequency domain representation gives a better insight into the dynamics of a system and allows for an easy detection of modelling errors by comparing the estimation transfer function with the frequency response data. Rapidly varying forcing functions can often be expressed as periodic functions, so the frequency response method is very attractive approach to this type of system.
- Estimates of the non-parametric noise model can be obtained by measuring the disturbing noise auto- and cross-power spectra (when no excitation signal is applied to the plant) and by calculating the sample (co-) variances of a set of noisy input and output spectra [72].
- Derivation of the basic servo drive model is best achieved for the specific machine tool under review by treating each element in turn [12, 13].
- Ford et al [3] describe measurement strategies for the separation of geometric and non-rigid errors for use with CNC machine tools.
- Geometric error 3-axis model for a machine tool has been derived and validated by Postlethwaite [21] which will need to be incorporated into a detailed model for the specific machine under review.
- Ford et al [31] and a more detailed thermal model approach by White [39] have described a combined geometric, non-rigid and thermal error model.
- Dynamic and static measurements of geometric errors by *laser interferometer, electronic precision level and a ball bar systems* have been defined [3, 33, 34, 35, 36]. The methods can be investigated for the measurement of machine tool system errors.

2. 5. Project plan

From this review a plan was formulated and the following investigation stages were outlined:

1. For the Beaver VC35 CNC machine tool under review, investigate each control axis in turn and produce a basic control model. This first stage was a theoretical appraisal of all elements.

2. Simulate each axis in turn using MATLAB and SIMULINK.
3. Carry out detailed measurements for each axis using laser interferometer, ball bar systems, electronic precision levels and other equipment to determine geometric and load errors. Thermal errors change slowly therefore they are not a consideration for parameter identification and outside the scope of this investigation.
4. Analyse the measurement data and revise the models.
5. Simulate the models for one, two and three axes drives.
6. Compare simulated single axis results for the model with actual system performance using sinusoidal, step and trapezoidal inputs. Adjust parameters in the model where appropriate.
7. Compare simulated two-axis model for sinusoidal input (X-axis) and co-sinusoidal input (Y-axis) with the ball bar results. Adjust parameters where appropriate.
8. Carry out modal analysis investigation of the machine tool structure dynamics and verify and identify the system resonances.
9. Carry out swept sine checks on the X-axis and Y-axis for the machine and compare with simulated performance. Modify the model to include for structural resonances and damping coefficients, previously not included.
10. Carry out parameter sensitivity check on the models.
11. Investigate stimuli methods in time and frequency domains for the identification of parameters.
12. Optimise on the stimuli methods and perform identification and estimation practices off-line. Validate against a similar machine type and configuration.
13. If the time allows, consider the validity of the practice for on-line use.

3. MODELLING THE COMPONENTS OF CNC MACHINE TOOL AXIS DRIVE

3. 1. Introduction to CNC machine tools axis drives

Electrical machines and actuators realise the basic function of converting electrical energy into mechanical energy. However, motion systems also perform additional high level functions such as the conversion of an input reference signal (both in digital or analogue form) into precise force, torque, speed or position. The implementation of such higher-level functions require additional elements such as sensors, encoders, power amplifiers, control electronics and communication links.

A machine tool axis drive consists of three major blocks:

- *CNC controller block* – calculates the motion of the various axes necessary to execute the required cutting path. It has a corresponding control algorithm for monitoring the motion and a communication interface for data exchange between the system and the exterior.
- *axis actuator* – realises the basic electromechanical energy conversion. It is usually an electrical motor (typically a DC drive as for the Beaver VC35 or an AC drive for the Takisawa MAC-V2). The electric drive will have a rotary encoder, drive (pre-amplifier, current control loop, power amplifier) and transducers.
- *mechanical system* – the mechanical linkage which transmits the motive force generated by the drive and converts it into relative motion between the tool and the work piece. Typically it contains the following: coupling between the drive and ball-screw, ball-screw and nut unit, slide and slideway and associated bearings.

All these blocks are presented in the block diagram of a CNC machine tool axis drive (Figure 3.1).

The CNC machine tool Beaver VC35 existing at the University of Huddersfield is a fixed column vertical spindle machine. It has two orthogonal axis in the horizontal plane (called X-axis and Y- axis) on which the worktable moves and upon which the work piece rests. The Z-axis is normal to this plane, and the cutting tool is moved in this axis. The data for this vertical machining centre is presented in Appendix A1.

In the control loop, the CNC controller is a software-based digital controller which generates the position demand signal from either a machine part program or from inputs

entered manually via the controller keyboard. The controller subtracts a positional feedback signal generated by the optical encoder from the position demand signal. A position error signal is thus produced and is converted to an analogue voltage which represents the output from the controller. This analogue voltage forms the velocity command signal that is used to drive the servo system. It is fed into the pre-amplifier where it is compared with the velocity feedback signal provided by the tachogenerator, to produce a velocity error signal. This signal is used by the amplifier to generate a suitable drive signal for the DC motor that drives the slide through a reduction pulley system and ball-screw. This is the basic *principle of operation* for the majority *of CNC machine tool position control systems.*

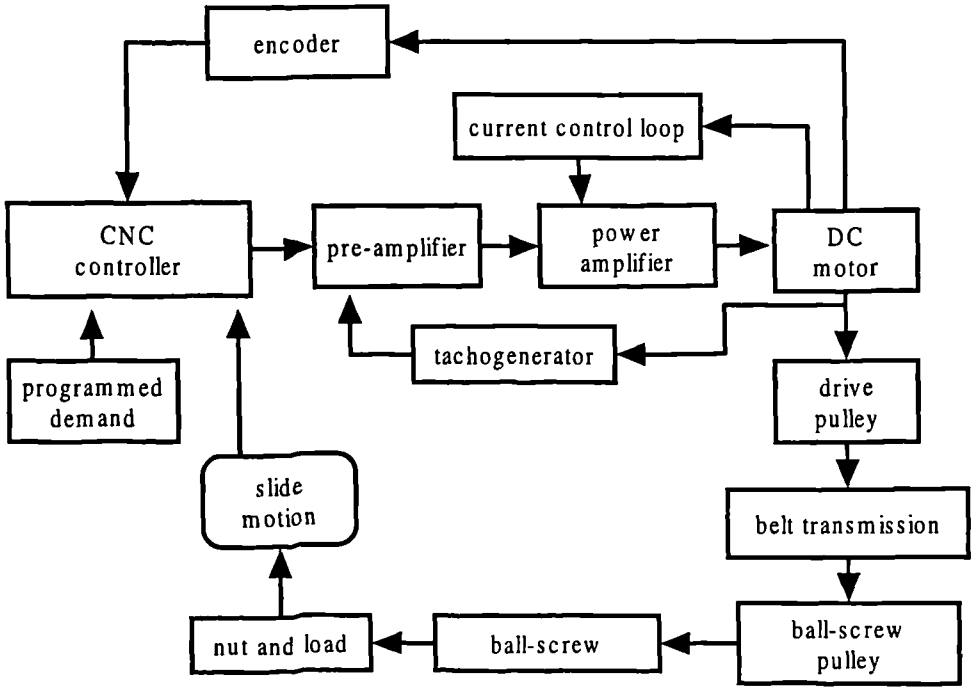

Figure 3. 1. Block diagram of CNC machine tool Beaver VC35

3. 2. Controller model

Computer numerical control (CNC) is a self-contained system for a single machine tool including a dedicated processor controlled by stored instructions to perform some or all of the basic numerical control functions.

The software of a CNC controller consists of at least three major programs:

- Part program data- consists of a description of the geometry of the part being produced and the cutting conditions (such as spindle speed and feedrate).
- Service program is used to check, edit and correct the part-data program.

- Control program that accepts the part-data program as an input and produces signals to drive the axes of motion.

Olivetti Corporation [74] has represented the block diagram (Figure 3. 2) of the circuits for an analogue controller that requires three input variables: acceleration (a), velocity (v) and position (s).

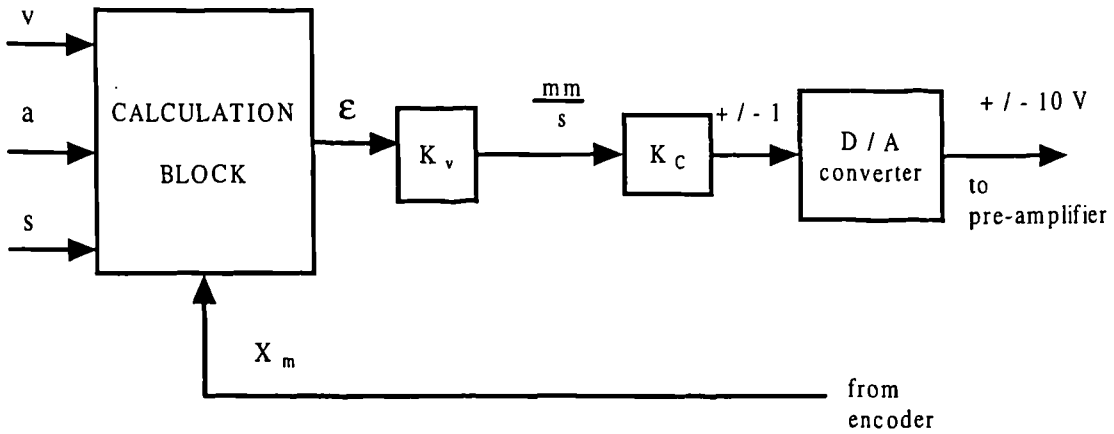

Figure 3. 2. Block diagram of an analogue controller

The demand feedrate and position are represented mathematically as a reference pulse frequency and a reference pulse stream duration respectively. The *Calculation* block, embedded within the controller, monitors the motion control of the machine tool using linear and circular interpolation routines. The position demand signal (X_C) for a single axis is generated as a function of the three motion control variables (a, v, s). Comparison is made between the calculated position demand (X_C) with the machine feedback position encoder signal (X_m). The encoder is modelled as a constant (K_{enc}) converting motor angular velocity to a pulse frequency. The difference between the two signals is called the *error* (ε) and is sent to control the machine tool motion system through a digital to analogue converter. Simultaneously, the controller is capable of generating a velocity feedforward (VFF) output to aid system response.

The error ε is multiplied by the gain of the position loop K_V and is converted into a velocity value. This is summed algebraically with VFF and the result is transformed into a digital value in the range ± 1 by the positive constant K_C. This value is converted by the D/A converter into analogue voltage because the pre-amplifier works with ± 10 V. By analysing the functioning of the controller, it could be expressed that:

- the velocity loop has a hardware-based (analogue) feedback;
- the position loop has a software-based (digital) feedback.

The interpolation techniques are used to generate the pulse count difference representing the positional error. The difference is kept into a register and the controller samples the contents of the register at fixed time intervals T (sampling time) and immediately clears it. An integrator and a zero-order-hold circuit could represent these operations. The integrator is introduced because the pulse number and phase difference are integrals of frequency. The zero-order hold (ZOH) is one of the most commonly used filters in which the value of the last sample is retained until the next sample is taken. More details about its functioning are presented in Appendix B1.

The digital to analogue (D/A) converter has the role to transform a digital dimensional signal into an analogue signal. It was represented by two constants (G_1 and G_2) and the quantisation effect exhibited by the D/ /A converter together with a function limiting the maximum and minimum voltages from the D / A converter have been considered.

In the case of multi-axis systems, each axis of motion is controlled by an identical control loop. Quadrature pulsed lines from the position rotary encoder are able to provide clockwise and counter-clockwise control data.

Due to considerations presented above, the transfer function of the controller Fanuc 6 M is:

$$H_{controller} = \frac{G_1\ G_2\ A}{s} \times \frac{1-e^{-sT}}{sT} = \frac{10}{s} \times \frac{1-e^{-0.01s}}{s} \qquad (3.1)$$

where A - a scaling term to simulate the potentiometer setting to control the preamplifier input demand

G_1 , G_2 – two-stage scaling of the D / A converter T - the controller sampling time [s]

The sample-and-hold has a sampling time of 10 ms, provides a unity gain and a small phase shift ($\omega T/2$). Over the bandwidth to be considered, this phase shift can be generally neglected (for example, when $\omega = 33$ rad / s and T=10 ms, the phase shift is 0. 165 rad = 9. 46 degrees).

A high gain velocity loop reduces the following error and enables the control system to respond to rapid movements. However, it also increases the bandwidth of the system making it susceptible to load disturbances. High gain increases the risk of an oscillatory behaviour and could result in an unacceptable overshoot to a step input. The risk is increased when an integrator is included in the controller, because it raises the order of the characteristic equation and reduces the limit of stability. Therefore selection of the gain is a compromise between performance and noise rejection.

The main advantages derived from the fact that the controller of a modern CNC machine tool being a digital computer are:

- Many loops can be controlled or compensated through time sharing;
- Changes in software (rather than hardware) allow parameter alterations to be made in order to achieve the desired control response;
- The controller is able to perform supervisory applications (such as scheduling required applications etc.).

3. 3. Pre-amplifier and amplifier models (see Figure 3. 3)

The output of the D / A converter (± 10 V) is compared with the output of the tachogenerator and the voltage difference is amplified by the servo amplifier. This has two components:

1. The pre-amplifier (PA) - consists of an operational amplifier sensitive to the difference between the reference signal generated by the D/A converter and the tachogenerator feedback and providing voltage amplification.
2. The power amplifier (Amplif) - supplies the DC motor with the required value of armature voltage. The armature voltage will be stabilised whenever the voltage difference at the input of PA reaches zero. This will ensure correspondence between the rotational speed of the DC motor and the reference signal generated by the D/A converter.

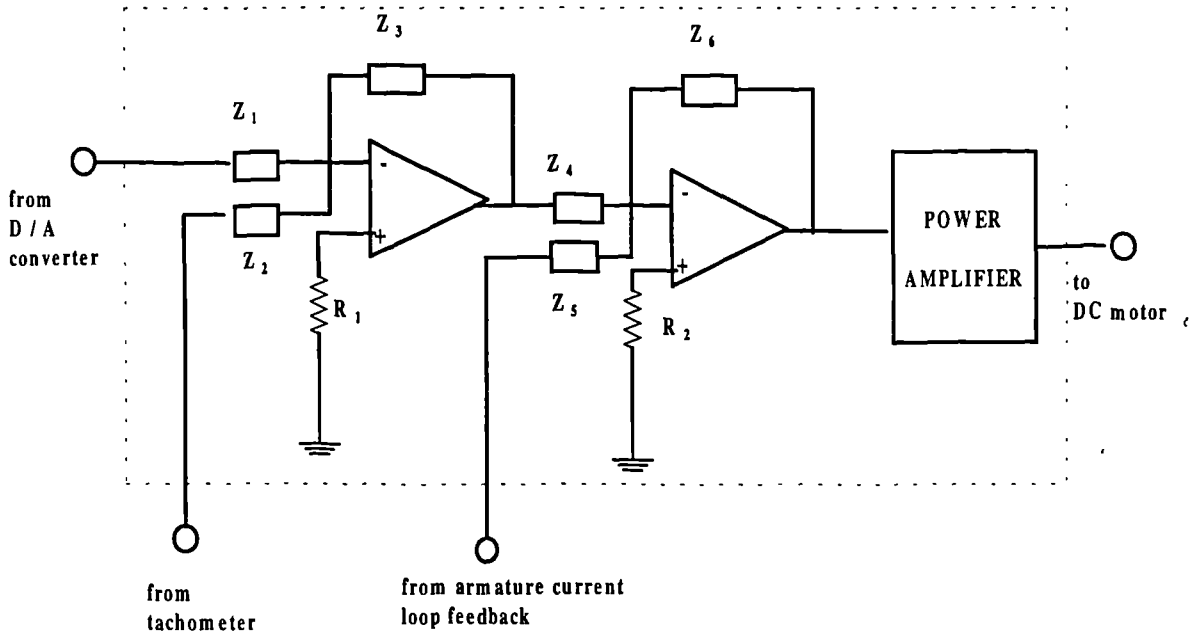

Figure 3. 3. Possible diagram of the servo amplifier considering the connections with other components of the DC drive

The two components yield good DC gain for steady-state functioning and a large bandwidth for good transient response. The pre-amplifier works with low voltage (± 15 V) and low

current (1 mA) while the power amplifier needs high voltage (110 V) and high current (60 A). Since the wiring diagrams for the Beaver VC35 Siemens drives were not available, it was considered that a good first estimate for the pre-amplifier would be to use a Gem drive Mk2 manufactured and described by GEC Ind. Controls [75]. The pre-amplifier and power amplifier are utilised in a velocity controlled closed loop system using a DC permanent magnet motor. The pre-amplifier is generating the PWM input voltage when armature current of the motor is kept under control all the time.

In Table 3. 1. are shown the relevant comparative data for the special lathe studied by Ford [12] and Beaver VC35 CNC machine tool which constitutes the subject of this investigation.

Characteristic	Lathe	Beaver VC 35
type of transmission for drive	belt and pulley	belt and pulley
reduction ratio	1. 5 : 1	2 : 1
System gain	33 mm / s / mm	33 mm / s / mm
Motor inertia	0. 0012 kg m^2	0. 0048 kg m^2
load inertia at the motor	0. 0047 kg m^2	0. 0069 kg m^2

Table 3. 1. Main characteristics of one of the drives studied by Ford [1] and Beaver VC 35 X-axis drive

It is evident that both drives are in a similar bracket of values, so the initial expression for the transfer function of the pre-amplifier was considered to be similar to that presented in [12] and [75]. Then it was optimised using the non-linear least square optimisation routine **lsqcurvefit** supplied with the *Optimisation Toolbox version 2. 0* on MATLAB 5. 3. A copy of the actual MATLAB code is included in Appendix A2.

After 8 iterations and 25 objective function evaluations, the equivalent transfer function for the pre-amplifier considering PI compensator yielded:

$$H_{preamplif} = 902 \times \frac{1 + 0.0048s}{s} \qquad (3.2)$$

The power amplifier is considered to be a four-quadrant transistor bridge. Its transfer function will be equal with a constant that is resulting from a product:

$$H_{amplif} = K_{br}\, K_{ia} = 32.5 \times 2 = 65 \qquad (3.3)$$

where K_{br} - the bridge voltage scaling [V /V] K_{ia} - the current loop scaling term [V / V]

3. 4. Permanent magnet motor model

The stator magnetic field of Permanent Magnet Motors (PMM) is generated by permanent magnets. The stator magnetic flux remains essentially constant at all levels of armature current and, therefore, the speed-torque curve of the PMM is linear over an extended range.

The significant advantages of PMM over wound-field types are the following:

- Linear available torque-speed characteristic
- High stall (accelerating) torque
- No need for electric power to generate the magnetic flux
- Reduced frame size and lighter motor for a given output power

Electro-Craft Corporation [76] developed the following electrical and dynamic equations and the transfer function for permanent magnet motors:

- *electrical equations* – by applying the Kirchhoff 's second law to the PMM equivalent circuit

$$U(s) = s L_a I_a(s) + R I_a(s) + E_g(s) \tag{3.4}$$

$$E_g(s) = K_e \omega_1(s) \tag{3.5}$$

Introducing E_g from second equation to the first one, results in the electrical equation of the motor:

$$U(s) = s L_a I_a(s) + R I_a(s) + K_e \omega_1(s) \tag{3.6}$$

where U – armature voltage [V] K_e – motor voltage constant [V / (rad/s)]

R - armature resistance [Ω] I_a - armature current [A]

L_a - motor inductance [H] E_g – induced voltage (counter e.m.f.) [V]

- *dynamic equations* – describing the relationship between the torque generated by the motor and the velocity of the motor

Since the magnetic field in the motor is constant, the current produces a proportional torque:

$$T_{1E} = K_T I_a(s) \tag{3.7}$$

The opposing torque in the motor is given by:

$$T_{1M}(s) = T_f + D \omega_1(s) \tag{3.8}$$

where ω_1 - angular velocity of the motor [rad /s] K_T – motor torque constant [Nm /A]

T_f - constant friction torque in the motor [Nm] T_{1E} – motor torque [Nm]

T_{1M} - the opposing torque in the motor [Nm] J_m – motor inertia [kg m^2]

Considering that the motor is coupled to a load, the relation between the torque and velocity represents the dynamic equation of the motor:

$$T_{1E}(s) = s(J_m + J_L)\,\omega_1(s) + D\omega_1(s) + T_f + T_L(s) \qquad (3.9)$$

where J_L – inertia of the load [kg m^2] T_L - load torque [Nm]

D – viscous damping factor for the motor [Nm s / rad]

The dynamic equation of the motor is based on a tacit assumption that motor velocity is the same as that of the load (motor and load may be approximated by a single body). While this assumption holds in most cases, for high-performance servo systems, one has to investigate the case where deflections of the motor shaft and other elastic parts lead to torsional resonance.

The transfer functions for permanent magnet motor are obtained when the Laplace transform is applied for the electrical and dynamic equations of the motor:

$$\begin{cases} U(s) = (sL_a + R)\,I_a(s) + K_e\,\omega_1(s) \\ T_{1E}(s) = K_T\,I_a(s) \\ T_{1E}(s) = s(J_m + J_L)\,\omega_1(s) + D\omega_1(s) \end{cases} \qquad (3.10)$$

From Equations (3. 10), the following block diagram (Figure 3. 4) may be established.

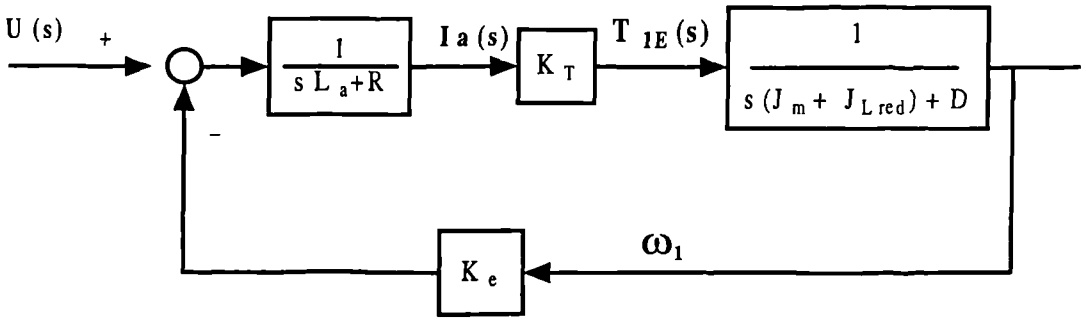

Figure 3. 4. D. C. motor block diagram

It should be noted that T_{1E} (electrical motor torque) is not identical to the torque available at the motor shaft. The difference between electrical torque and shaft torque is the torque required to accelerate the inertia of the motor itself and overcome the internal friction torque of the motor.

Notation $J = J_m + J_L$ - total moment of inertia

From the two expressions for the torque produced by current these results:

$$K_T I_a(s) = J\,s\,\omega_m(s) + D\,\omega_1(s) \qquad (3.11)$$

So the Laplace expression for armature current will be:

$$I_a(s) = \frac{1}{K_T}(sJ + D)\,\omega_1(s) \tag{3.12}$$

Introducing this expression in the relation for voltage:

$$U(s) = (sL_a + R)(sJ + D)\,\frac{1}{K_T}\,\omega_1(s) + K_e\,\omega_1(s) \tag{3.13}$$

Finally, the transfer function for the PMM (Permanent Magnet Motor) relating motor speed to armature voltage can be written:

$$G_m(s) = \frac{\omega_1(s)}{U(s)} = \frac{K_T}{(sL_a + R)(sJ + D) + K_e K_T} \tag{3.14}$$

Assuming that the motor damping factor is zero (D = 0), the transfer function is:

$$G_m(s) = \frac{K_T}{s^2 L_a J + sRJ + K_e K_T} \tag{3.15}$$

Considering the following notations:

- mechanical time constant for the motor $T_m = \frac{RJ}{K_e K_T}$
- electrical time constant for the motor $T_e = \frac{L_a}{R}$

the transfer function for PMM becomes:

$$G_m(s) = \frac{1/K_e}{(sT_m + 1)(sT_e + 1)} \tag{3.16}$$

The actual data for the Siemens DC motor can be seen in Appendix A3.

Electro-Craft Corporation [76] has shown that the assumption that velocity of all the parts in the motor-load system is identical is not accurate for high-performance servo systems since the mechanical parts of the system are elastic and they deflect under torque.

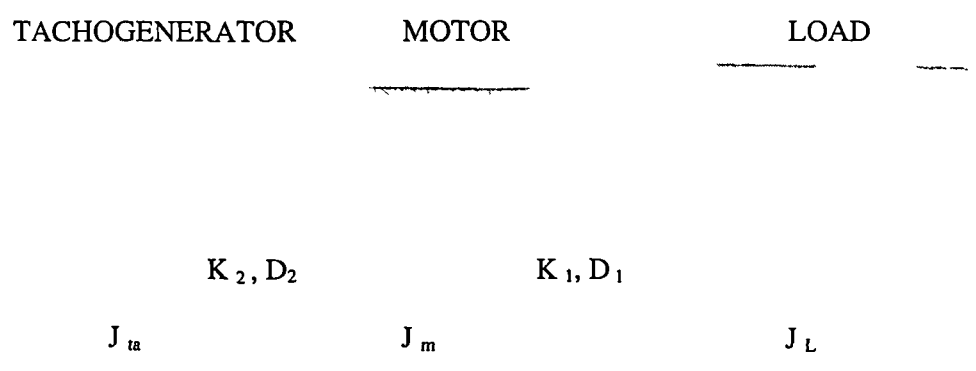

Figure 3. 5. Three-body model for load-motor-tachogenerator system

As a result, the instantaneous velocities of various parts are different, and at some frequencies will be in opposite directions. This condition allows the system to store a large amount of mechanical energy, which results in noticeable angular vibrations. This phenomenon is called *torsional resonance* and it arises when high precision and high-speed motion control is desired. Since many motors are coupled to both an inertial load and a tachogenerator, it is reasonable to approximate this mechanical system by three solid bodies, coupled by shafts (see Figure 3. 5). The dynamic equations of the three bodies are:

$$T_{1E}(s) = J_m \beta_1(s) + D\,\omega_1(s) + T_{1L}(s) + T_{2ta}(s) \quad (3.17)$$

$$T_{1L} = J_L \beta_L(s) \quad (3.18)$$

$$T_{2ta} = J_{ta} \beta_{ta}(s) \quad (3.19)$$

where J_L – load moment of inertia [kg m^2] β_L – load angular acceleration [rad /s^2]

J_{ta} - tachogenerator inertia [kg m^2] β_{ta} – tachogenerator angular acceleration [rad /s^2]

J_m - DC motor moment of inertia [kg m^2] β_m – motor angular acceleration [rad /s^2]

T_{1L} – torque delivered from the motor to J_L [Nm]

T_{2ta} – torque delivered from the motor to J_{ta} [Nm]

The deflections of the shafts are described by the following equations:

$$T_{1L}(s) = K_1(\Theta_1(s) - \Theta_L(s)) + D_1(\omega_1(s) - \omega_L(s)) \quad (3.20)$$

$$T_{2ta}(s) = K_2(\Theta_1(s) - \Theta_{ta}(s)) + D_2(\omega_1(s) - \omega_{ta}(s)) \quad (3.21)$$

where K_1 – stiffness of equivalent shaft between load and motor [Nm / rad]

K_2 – stiffness of equivalent shaft between motor and tachogenerator [Nm / rad]

D_1 – damping factor of equivalent shaft between load and motor [Nm s /rad]

D_2 – damping factor of equivalent shaft between motor and tachogenerator [Nm s /rad]

ω_1 – motor angular velocity [rad /s] ω_L – load angular velocity [rad /s]

θ_1 – motor angular position [rad] θ_L – load angular position [rad]

ω_{ta}, θ_{ta} – tachogenerator angular velocity, respectively angular position

Considering the deflections, the dynamic equations will be:

$$T_{1E}(s) = J_m \beta_1(s) + D\,\omega_1(s) + J_L \beta_L(s) + J_{ta} \beta_{ta}(s) \quad (3.22)$$

$$J_L \beta_L(s) + D_1 \omega_L(s) + K_1 \Theta_L(s) = D_1 \omega_1(s) + K_1 \Theta_1(s) \quad (3.23)$$

$$J_{ta} \beta_{ta}(s) + D_2 \omega_{ta}(s) + K_2 \Theta_{ta}(s) = D_2 \omega_1(s) + K_2 \Theta_1(s) \quad (3.24)$$

The quantity $J_L \beta_L$ could be extracted from Equation 3. 23:

$$J_L \beta_L(s) = D_1 \omega_1(s) + K_1 \Theta_1(s) - D_1 \omega_L(s) - K_1 \Theta_L(s) \qquad (3.25)$$

The quantity $J_{ta} \beta_{ta}$ could be extracted from Equation 3. 24:

$$J_{ta} \beta_{ta}(s) = D_2 \omega_1(s) + K_2 \Theta_1(s) - D_2 \omega_{ta}(s) - K_2 \Theta_{ta}(s) \qquad (3.26)$$

Introducing Equations (3. 25) and (3. 26) into Equation (3. 22) and neglecting D, it results:

$$J_m \beta_1(s) = T_{1E}(s) - J_L \beta_L(s) - J_{ta} \beta_{ta}(s) =$$

$$= T_{1E}(s) - [D_1 \omega_1(s) + K_1 \Theta_1(s) - D_1 \omega_L(s) - K_1 \Theta_L(s)] - \qquad (3.27)$$

$$- [D_2 \omega_1(s) + K_2 \Theta_1(s) - D_2 \omega_{ta}(s) - K_2 \Theta_{ta}(s)]$$

These equations could be introduced into a mathematical block diagram showing the dynamic properties of the DC motor (see Figure 3. 6).

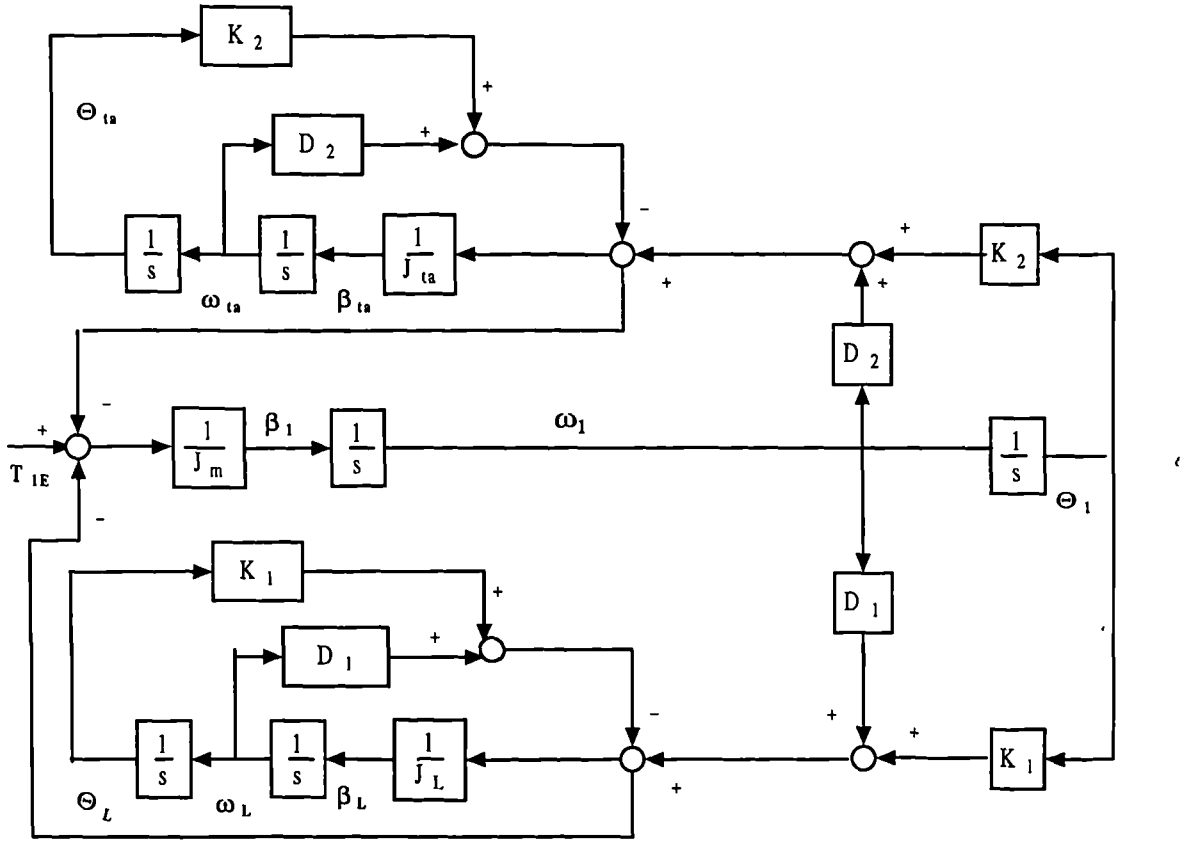

Figure 3. 6. Mathematical model block diagram of DC motor showing the dynamical characteristics

3. 5. Models for mechanical transmission components

The mechanical transmission of a CNC machine tool can be viewed as being constituted by a number of sub-systems. This allows a methodical derivation of the model and sufficient flexibility in the structure of the model.

This transmission can be considered as an input/output block; additional model details within the block have only little effect upon the input or output characteristics of the block. The modular approach allows for easy update of the model and examples of "block exchanges" could be:

- The belt-pulley transmission system instead of gear transmission
- The DC electric motor instead of AC motor etc.

The sub-systems that comprise the mechanical transmission of a CNC machine tool are represented in Figure 3. 7.

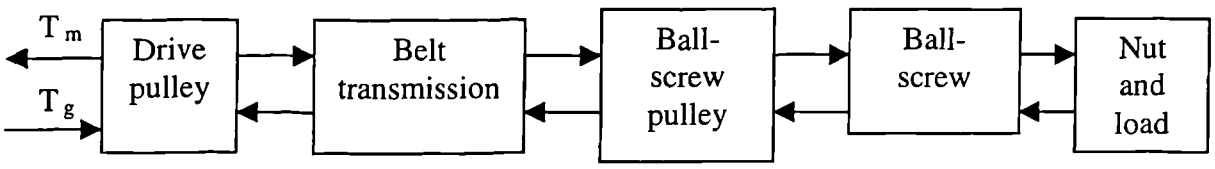

Figure 3. 7. Mechanical transmission components

Data for the Beaver VC35 CNC machine tool transmission components is presented in Appendix A4.

3. 5. 1. The drive- ball-screw coupling

To link a primary power source such as an electric motor to a rotating load requires the use of a belt drive, chain, spur gearing or a worm-gear drive. Often a first choice will be the belt drive because of its simplicity, performance, versatility and low cost. The choice of a belt still calls for a close assessment of efficiency, pulley and belt location, the provision of a means of access for maintenance and, not least, consideration of the environment in which the drive has to operate.

The drive-ball-screw coupling is achieved in the CNC machine tool Beaver VC35 by a timing belt as shown in Figure 5. 23.

Palmgren [77] underlines that synchronous (timing) belts need low belt tension because the power is transmitted by the mechanical interlocking of cogs or teeth on the belt in

corresponding recesses in pulleys. So the accurate transfer of speed in a drive is obtained with low loads on shafts and bearings.

The belt is usually surfaced with polyamide (nylon) fabric - usually as two crossed layers of polyamide cord fabric. The pulleys have integral hubs and bushings and flanges are used to prevent belts from running off the pulleys.

Normally, both lengths of the belt in a belt-pulley power transmission system are pre-tensioned. However, it is possible that "slackness" within one or other length of the belt could occur. The belt and pulley system is still capable of power transmission, but backlash will be present. This backlash can be modelled and its presence included in any machine tool model by using Heaviside step functions as gains on the appropriate belt tensions, with the "switch on / off" time set according to the value of an integral introduced later.

One side of the belt is tight and the second is loose during normal functioning. The original tight side of the belt becomes loose and the original loose side becomes tight before braking occurs. The effect of drive direction upon the location of belt slackness is illustrated in the Figure 3. 8.

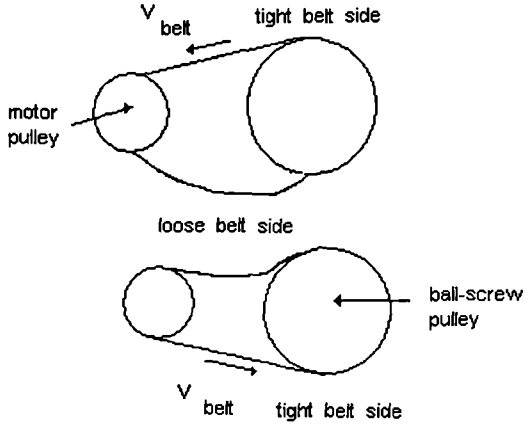

Figure 3. 8. Location of belt slackness when the pulleys rotate

When spring like behaviour is included in the model of the belt transmission system, then as tension in the newly tight section of belt increases, the belt will stretch. Thus two distinct phases of belt behaviour will be noted:

- slackness is taken up
- the belt stretches due to the increasing tension present in the belt.

Five distinct phases will be used to model the belt-pulley system, as the "tight side" transfers from one side of the belt pulley system to the other. A typical sequence is as follows:

1. One side of the belt is tight and one pulley drives the other pulley via the belt tension

2. As tension in the belt is reduced, it contracts due to its behaviour as a translational spring.
3. Slackness is transferred from one side of the pulley to the other. During this phase there is no effective torque on either pulley, due to the belt.
4. Once slackness is "transferred", the belt tightens and extends, as it again behaves as a translational spring.
5. Once taut, the belt again acts as a perfect transmission system.

For modelling purposes, the drive and ball-screw pulleys can be considered as moving due to the driving and resistive torques acting upon them. For convenience it will be assumed that resistive forces due to bearings (in the drive pulley and ball-screw pulley) are included in the drive shaft and ball-screw pulley models.

The belt transmission system includes the following:

1. Belt inertia
2. Belt-pulley interaction
3. Viscous drag due to the motion of the belt in air
4. The presence of pre-tension (slackness) in the belt
5. The elastic (translational) spring-like behaviour as tight side belt tension and loose side belt tension vary.

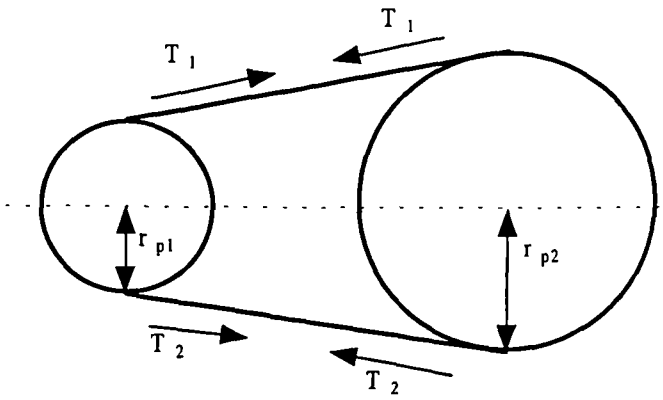

Figure 3. 9. The belt drive

In any correctly designed and installed belt drive, the belt will be under tension, will not be slack and will have negligible elastic behaviour. The motor load torque (τ_L) can be calculated on the basis of Figure 3. 9 with the following relation:

$$\tau_L(s) = \tau_{dp}(s) = \left(T_1(s) - T_2(s)\right) \times r_{p1} + J_{p1} \times s \times \omega_2 \qquad (3.28)$$

where ω_2 - drive pulley angular frequency [rad /s] T_2 - loose side belt tension [N]

J_{p1} - inertia of drive pulley [kg m^2] T_1 - tight side belt tension [N]

r_{p1} - drive pulley radius [m] τ_{dp} - torque delivered by motor to drive pulley [Nm]

The complete model of the ball-screw pulley would incorporate:

1. Friction due to the pulley bearing
2. Viscous drag due to pulley motion in air
3. Pulley inertia
4. Effect of belt tensions T_1 and T_2 upon the pulley
5. Effect of "load" τ_{bp} from the ball-screw upon the pulley

In the case of the ball-screw pulley, the driving force is delivered by the belt system and the resistive force is due to the load from the ball-screw:

$$(T_1(s) - T_2(s)) \times r_{p2} - \tau_{bp}(s) = J_{p2} \times s \times \omega_3 \tag{3.29}$$

where τ_{bp} - load torque from ball-screw [Nm] J_{p2} - inertia of ball-screw pulley [kg m^2]

r_{p2} - ball-screw pulley radius [m] ω_3 - ball-screw pulley angular frequency [rad /s]

It is assumed that the axis is modelled when functioning under normal conditions (the belt is not slack) so the following equalities apply:

$$T_1 - T_2 = 2T_x \tag{3.30}$$

$$\omega_m = \omega_2 \tag{3.31}$$

$$r_{p1} \times \omega_2 = r_{p2} \times \omega_3 \tag{3.32}$$

Substituting these values into Equations (3. 28) and (3. 29), the following expressions will result:

$$\tau_L(s) = 2 \times T_x(s) \times r_{p1} + s \times J_{p1} \times \omega_2(s) \tag{3.33}$$

$$2 \times T_x(s) \times r_{p2} - \tau_{bp}(s) = s \times J_{p2} \frac{r_{p1}}{r_{p2}} \times \omega_2(s) \tag{3.34}$$

The difference between tight and loose belt tensions (T_x) is obtained by eliminating $\omega_2(s)$ from equations (3. 33) and (3. 34):

$$T_x(s) = \frac{r_{p1} \times J_{p2} \times \tau_L(s) + J_{p1} \times r_{p2} \times \tau_{bp}(s)}{2\,(r_{p1}^2 \times J_{p2} + r_{p2}^2 \times J_{p1})} \tag{3.35}$$

The value of T_x is used to calculate the total magnitude of the forces acting upon the ends of the ball-screw-bearing model. These calculations have been presented by Pislaru et al. [78].

Toothed-belt transmissions produce considerable torques, operate with little pre-tensioning and absorb high specific loads. During operation, however, lateral oscillation of the belt fibres and torsional oscillations of the pulleys are observed. These are caused by contact between the belt teeth and periodic variation in tension of the belt fibres as a result of considerable differences in tooth pitch between the belt and pulleys.

Gross [14] has underlined two important aspects regarding to the mechanical transmission system of a CNC machine tool:

1. *the mechanical transmission elements possess mass and elasticity;*
2. *the transfer behaviour of the mechanical transmission elements is not linear.*

He derived these conclusions from two facts:

- reversal errors cannot be prevented between the different components of the mechanical transmission elements;
- the backlash, due to the finite stiffness of the mechanical transmission elements and the frictional forces, is always present.

The modelling aspects of the belt transmission dynamics are discussed in detail in Chapter 6.

3. 5. 2. Bearings

Each machine tool axis contains a number of shafts which require support. This is provided by bearings that are a source of frictional torque and hence must be included in the detailed model of the machine tool.

The bearings supporting the ball-screw are axially loaded when the ball-screw is loaded. In the case of the actual machine (Figure 3. 10), the X and Y-axis ball-screws are "fixed" at one end (using a set of four taper roller bearings), which takes the entire axial loading resulting from the linear motion of the nut and associated load. The axial loading F_a upon the fixed end bearings is a function (F_w) of slider mass, velocity and the more usual terms involving bearing construction, lubrication and geometry.

The "free" end (drive end) is connected to the pulley using a single row deep groove ball bearing. This bearing set only opposes the radial load imposed by the belt drive.

The low friction and the generally moderate lubrication requirements are two important advantages of rolling bearings. The friction conditions vary, however, in the individual rolling bearing types, since sliding friction of varying degree occurs in addition to rolling contact friction. Lubricant friction is also present.

The total resistance to running of a rolling bearing is very small in comparison with the transmitted forces so that, as a rule, no account need to be taken of the frictional losses in the

bearing when designing a machine. However, the friction determines the heat generated in a bearing thus influencing the operating temperature. The friction in a roller bearing is the determining factor where heat generation in the bearing is concerned and consequently the operating temperature. The friction depends on the load and on several other factors, the most important of which are the bearing type and size, the operating speed, the properties of the lubricant and the quantity of the lubricant.

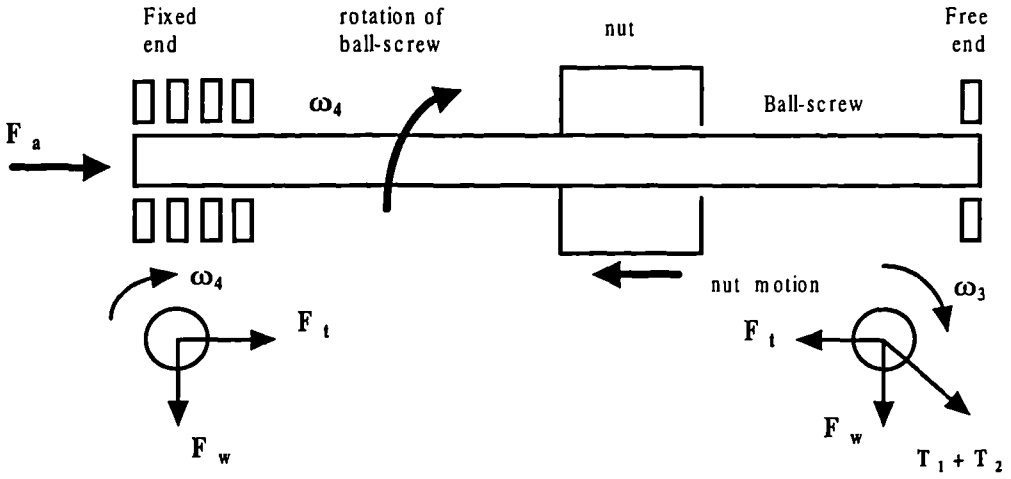

Figure 3. 10. Axial and radial loading upon the ball-screw bearings

The total resistance to rolling in a bearing is made up of the rolling and sliding friction in the rolling contacts, in the contact areas between rolling elements and cage as well as in the guiding surfaces for the rolling elements or the cage and the friction in the lubricant.

In tests, the total friction of a bearing (the sum of rolling, sliding, and lubricant friction) is measured as the resistance exerted against its movement. This resistance represents a torque and is generally referred to as the frictional torque $T_{friction}$. The value of the friction coefficient μ is different for various rolling bearings types.

Bearing type	Friction coefficient μ
Deep groove ball bearings	0. 0015 - 0. 003
Taper roller bearings	0. 002 - 0. 005
Thrust ball bearings	0. 0012

Table 3. 2. Friction coefficient μ for various rolling bearings types

The torque due to friction in bearings is calculated with the relation given by Eschmann [79]:

$$T_{friction} = T_{0f} + T_{1f} \qquad (3.36)$$

where T_{0f} - load - free component of the total frictional torque [N mm]

T_{1f} - load - dependent component of the total frictional torque [N mm]

The equation is valid provided that a lubricant film separates the surfaces that are rolling on each other in the bearing. If the lubricant film thickness is inadequate, the increased metallic contact means that the simple method of calculation shown here can no longer be used.

The load-free component of the frictional torque is not influenced by bearing load, but by the hydrodynamic losses in the lubricant and depends on the viscosity and quantity of the lubricant and also the rolling velocity:

$$T_{0f} = f_0 \times 10^{-7} \times (\upsilon n)^{2/3} \times D^3 \qquad (3.37)$$

where f_0 - coefficient taking into account the bearing design and lubrication method

ν - operational viscosity of oil or grease base oil at the operating temperature [mm^2 / s]

n - speed of bearings [rpm] D - pitch circle (mean) diameter of bearings [mm]

The load - dependent component of the total frictional torque arises from elastic deformations and partial sliding in the contacts and predominates in slowly rotating, heavily loaded bearings:

$$T_{1f} = \mu_1 \times f_1 \times F \times \frac{D}{2} \qquad (3.38)$$

where μ_1 - friction coefficient dependent on load and bearing design

f_1 - coefficient taking into account direction of load application

F - resulting bearings load [N]

Generally, angular contact ball bearings are subjected to combined loads (i.e. radial and axial loads acting simultaneously). In all such cases, it is necessary to calculate an equivalent bearing load that will have the same influence on bearing life, or produce the same permanent deformation in the bearing, as the actual load. The equivalent bearing loads can be obtained from

$$F = X \times F_r + Y \times F_a \qquad (3.39)$$

where F_r - radial component of bearing load [N] X - radial load factor

F_a - axial component of bearing load [N] Y - axial load factor

The assumptions that have been made to calculate the load upon bearing are:

- The axial component of bearing load (F_a) is the reaction of the motion of the slide caused by the motion of the ball screw nut

- There is no tangential component of bearing load (F_t)
- The ball screw weight and tangential component of bearing load (F_t) due to the ball screw rotation is evenly distributed over the bearing at both ends of the ball screw.

The value of the resultant bearing load is determined by the simple relationship:

$$F_{fixed} = \sqrt{F_a^2 + F_w^2} \tag{3.40}$$

The force due to ball screw weight will be:

$$F_w = \frac{m_{bs}\, g}{2} \tag{3.41}$$

where m_{bs} – ball-screw mass [kg] g - gravitational acceleration [m / s^2]

Because at the "fixed end" (non-drive end) there is a set of four tapered roller bearings and at the "free" end there is a single set of deep grove ball bearing, the force produced in the axial plane at "fixed end" will be 1/3 of the radial component of bearing load at the "free" end (drive end).

$$F_a = \frac{F_{free}}{3} \tag{3.42}$$

In the case of the "free"end for ball screw bearing model, it has been assumed that the axial component of bearing load (F_a) is determined by the belt tension:

$$F_a = 2\, T_x \tag{3.43}$$

where T_x - the difference between tight and loose belt tensions

$$F_{free} = \sqrt{F_w^2 + 4T_x^2} \tag{3.44}$$

3. 5. 3. Ball-screw model

A ball-screw is highly efficient due to the rolling motion of balls in the space between the screw shaft and nut, reducing the required driving torque to less than 1/3 of that which a conventional sliding screw requires. This makes it easy to convert not only a rotary into a linear motion, but also a linear into a rotary motion.

The most important features of a ball-screw are: positioning, movement, load carrying ability. The ball-screw was represented mathematically as a constant relating angular displacement to ideal linear displacement. By treating the ball-screw in this manner, it is assumed to be mechanically perfect. This is an incorrect assumption as all ball-screws exhibit an element of mechanical hysteresis or backlash. Backlash may be considered as a positional dead-band which manifests itself when the ball-screw changes its sense of direction. The

backlash has been represented in the model as a non-linear function relating ideal motor position to actual motor position.

The basic assembly of the ball-screw (Figure 3. 11) consists of a screw shaft, a nut assembly with a method of ball return, balls, and wipers (in applications where the screw is exposed to dust and dirt). An efficiency of up to 98 % can be achieved (as the balls are in rolling contact with precise ball races).

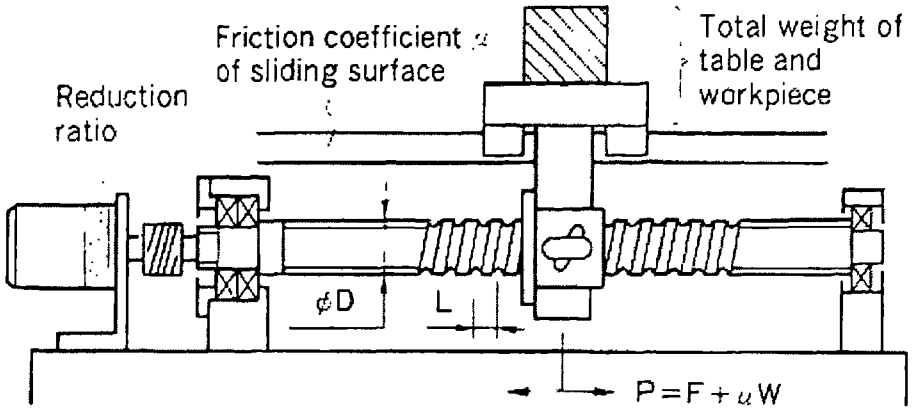

Figure 3. 11. Basic assembly of a ball-screw

Ball-screws have a very low friction loss that gives:

- high efficiency (up to 95 %)
- low wear
- long life
- precise positioning accuracy
- low drive power
- negligible heat generation
- high traversing speed
- absence of stick slip effects

An important feature of efficient ball-screws is the method of ball re-circulation within the nut. The internal transfer system is used because of its robust design and the advantage of smaller nut diameter, smooth movement, less balls per circuit therefore less friction and an absence of parts liable to early wear.

In order to produce a ball-screw completely free of axial play or to enhance the axial stiffness, the nut assembly has a preload built in between the nut and the shaft. Preload may be defined as the use of one group of ball grooves in opposition to another group to eliminate backlash (axial free play). Pre-loading enables the axial clearance to be below zero and provide a higher axial rigidity. When a ball-screw is preloaded through *the zero axial clearance point*, the rigidity of the ball-screw is increased, with the axial displacement becoming accordingly smaller. Normally the nuts are delivered with an adjusted preload

which is (1/ 2. 83) of the average operating load [12]. Higher values than this give increased resisting torque, lower efficiency and reduced service life.

The precision ball-screw is generally the type required for machine tool applications (for highly precise positioning requiring low reversal backlash with consequently high lead accuracy and stiffness values).

A detailed model for the ball-screw (Figure 3. 12) should include the following:

1. Ball-screw inertia
2. Axial load (due to slide inertia and cutting forces)
3. Ball-screw wiper and bearing friction
4. Slideway-guideway friction
5. Pre-load friction (at the nut)
6. Accumulated error in the ball-screw lead
7. Thermal expansion
8. Dynamic effects of loading upon the ball-screw (i. e. translational and rotational spring effects).

The effect of ball-screw angular pitch error can be considered to be a kinematic matter, so it can be omitted from the model of the ball-screw.

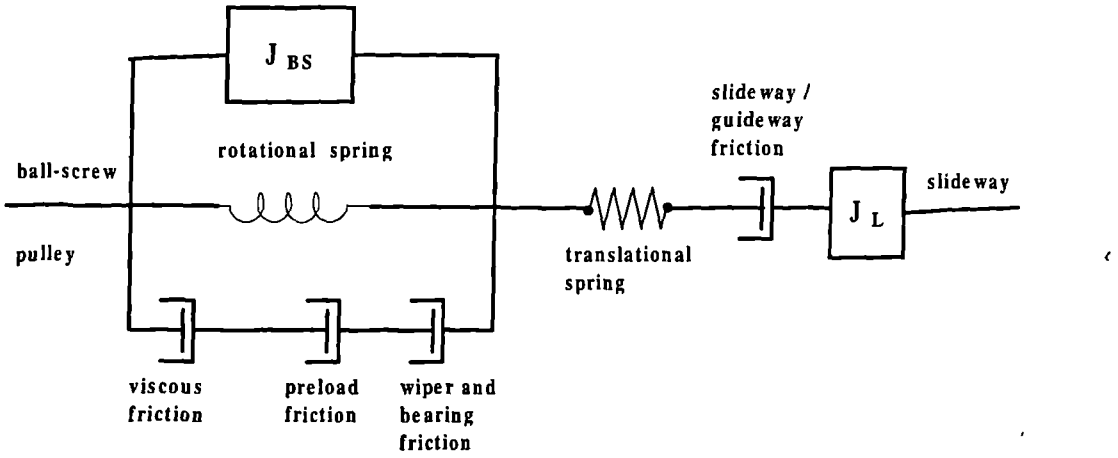

Figure 3. 12. The complete ball-screw model

It is evident that the ball-screw is not a rigid body from its complete model. The ball-screw will experience translational, rotational and axial motions (which are complex and not immediately open to analysis) but again are lumped into the geometric error model. It is noticeable that its propensity to compression when loaded axially and torsionally twisted. The compression is the result of translational spring behaviour of distance between the end of the

ball-screw and its nut. The torsional resonance can be viewed as arising due to the application of various torques at points along the length of the ball-screw.

In the catalogue elaborated by THK LM System [80] it is shown that the rotational torque required to give a ball-screw movement in the case of constant speed motion is:

$$T_t = \tau_n + \tau_{preload} + \tau_{other} \tag{3.45}$$

where T_t - rotational torque required [Nm] τ_n - torque due to external load [Nm]

$\tau_{preload}$ - torque due to preloading of ball-screw [Nm]

τ_{other} - torque of other origins (frictional torque due to the support bearings, oil seal and the like [Nm]

The torque required to the ball-screw to move a mass is :

$$\tau_n = \frac{F_a * p}{2 * \pi * \eta} \times R = \frac{(\mu * M_L * g) * p}{2 * \pi * \eta} \times R \tag{3.46}$$

where τ_n - torque at ball-screw nut [Nm] R - reduction ratio

F_a - frictional resistance of the guideway [N] M_L - load mass [kg]

p - ball-screw pitch [m] η - ball-screw efficiency

This torque has to counter the friction resultant from the rolling of the bearings inside the ball-screw nut, resistance of the guideways and external forces.

In the case that an accelerating motion is required, the rotational torque applied to the ball-screw has to be:

$$T_{acc} = T_t + J \times \theta = T_t + \left[M_L \times \left(\frac{p}{2\pi} \right)^2 \times R^2 + J_{BS} \times R^2 \right] \times \frac{2\pi \times n}{60\,t} \tag{3.47}$$

where T_{acc} - torque necessary for accelerating motion [Nm] t - acceleration time [s]

n - motor's rotational speed [rpm] J_{BS} - ball-screw moment of inertia [kg m^2]

Braasch et al. [80] showed that some of the errors appearing during position measurement using a rotary encoder and ball-screw are due to phenomena produced in the ball-screw:

1. *Pitch loss* - resulting from a shift of the balls during the positioning of ball-screw drives with two-point preloading;
2. *Positioning error resulting from thermal expansion of the ball-screw* which depends on the preloading of the ball nut and the fixed bearing. The thermal growth of the ball-screw is shown by the drift of position values measured with rotary encoder relative to starting values.

3. *Friction in the ball nut* - is the largest portion of the friction in a feed drive system and is due to the complex kinematics of a recirculating ball nut:

- *The balls are not completely held in the races and wobble.* The result is a continuous pressing and pushing with occasional slipping of the balls.
- *The friction among balls is aggravated by high surface pressure* due to the absence of a retaining device to separate them.
- As in every angular contact ball bearing, a spinning friction results from a contact diameter that is not orthogonal to the axis of ball rotation. Each ball rotates about its contact diameter.

In general, every ball-screw shows an efficiency of approx. 90%, due to rolling ball contact between screw and nut. The demands today however, are more complex than simply transforming a rotational movement into a linear movement and the manufacturers are performing intensive studies regarding the various phenomena produced by the ball-screw.

3. 5. 4. Guideways and slides

The Beaver VC35 slideway arrangement uses three guideways, two of which are to each side of their centrally placed ball-screw.

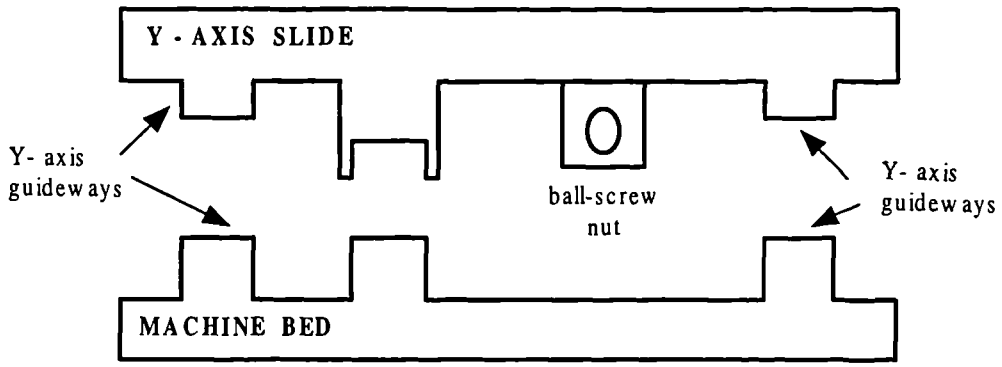

Figure 3. 13. Guideway arrangement for Y-axis of the Beaver VC35

This may be a design decision, arising from the probable asymmetric loading expected upon the Y-axis. The central guideway provides alignment in the Y-axis, while all three guideways provide vertical alignment. A second or third guideway is not used to provide Y-axis alignment, as conflict between the guideways would occur. The Y-axis guideways experience a number of forces (which are not necessarily simultaneous):

- Ball-screw axial thrust

- Y-axis slide weight and associated X-axis slide weight with workpiece load (if present)
- Guideway reactive forces
- Guideway friction forces (when Y-axis slide weight is moving on the guideways)
- Reactive and friction forces resultant from contact between the guideways resting upon machine bed.

The coefficient of friction for conventional slides varies with the slide velocity (see Figure 3. 14). The highest value of the coefficient corresponds to the lowest rates of slide velocity. This region where stiction is prominent is called the *"stick-slip range"* because when fine adjustment is needed, the oil-lubricated sliding surfaces are 'sticking' and a jerky action appears at low velocities movement.

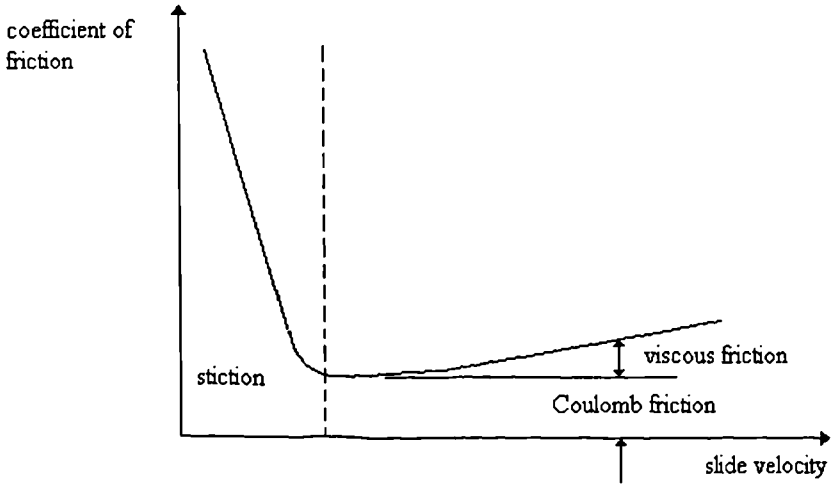

Figure 3. 14. Stribeck curve

Often the Y-axis is asymmetrically loaded, typically when the X-axis is at either end of its range of positions (see Figure 3. 15). The position of the X-axis affects the behaviour of the Y-axis, despite these axes being orthogonal.

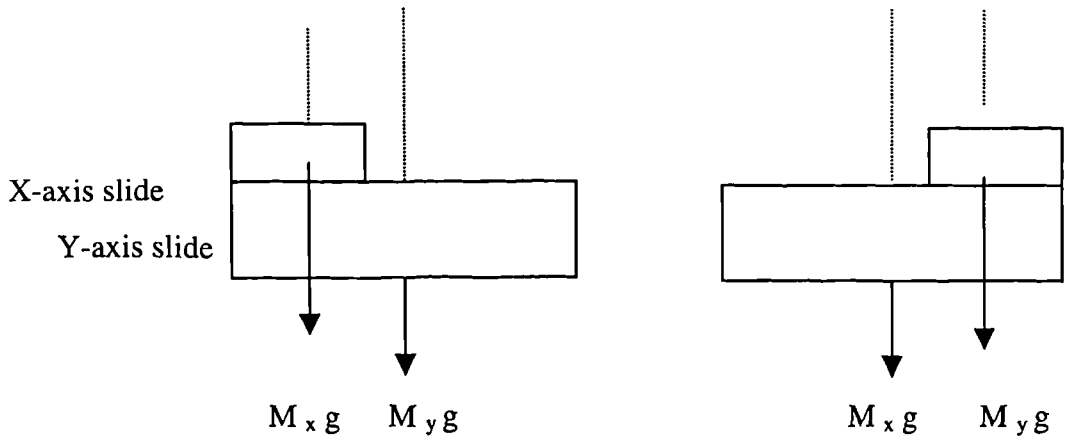

Figure. 3. 15. Extreme X-axis positions

The unbalance between load forces acting upon guideways creates unequal friction forces which generate a turning torque. Hence, the loads acting upon the Y-axis slide with asymmetric loading (function of the X-axis movement) are a torque and a linear force.

The ball-screw is positioned so that its thrust is along the centre of the Y-axis slide (to prevent the ball-screw alone generating axial thrust and torque). Hence, the Y-axis slide pivots around the ball-screw.

As the Y-axis moves, the effect of the torque is to rotate the slide to the limit of motion. This limit is determined by the geometry of the central guideway which provides the Y-axis alignment in a rigid body model of the machine tool. The effect of motion along the Y-axis and the yaw experienced is illustrated in Figure 3. 16.

Once the yaw has reached its fullest extent, an additional frictional force will come into play (see Figure 3. 17).

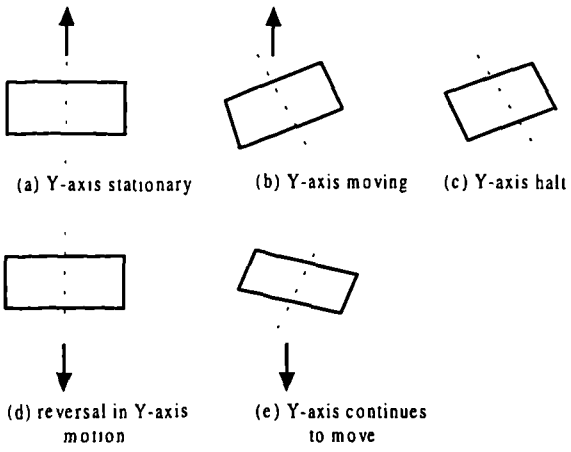

Figure 3. 16. Y-axis yaw during reversal

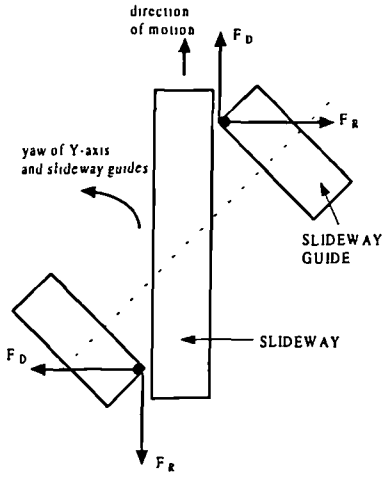

Figure 3. 17. Additional slideway friction

The CNC machine tool Beaver VC35 uses cast iron slideways with a turcite layer. The value of the coefficient of friction for such a junction is a constant $\mu = 0.1$ as shown in [12].

3. 6. Transducers

3. 6. 1. Tachogenerator

An ideal tachogenerator is a device whose output voltage (V_{ta}) is proportional to the shaft angular velocity ω_{ta}:

$$V_{ta} = K_{ta} \times \omega_{ta} \qquad (3.48)$$

In the real case, however, the voltage will have other components, which appear as ripple in the voltage given by the equation above. Expanding this equation to include ripple frequency and amplitude terms, we arrive at:

$$V_{ta} = K_{ta} \times \omega_{ta} \left[1 + k_1 \times \cos(u\,\omega t) + k_2 \times \cos(2u\,\omega t)\right] \qquad (3.49)$$

where k_1, k_2 – coefficients u - the number of commutator segments.

It is desirable to have k_1 and k_2 as small as possible to reduce the ripple factor, ξ, so that the tachogenerator output would be proportional to ω_{ta} only. The ripple factor is defined by:

$$\xi = \sqrt{k_1^2 + k_2^2} \qquad (3.50)$$

In most cases the tachogenerator is selected so that the ripple is not significant. Then the voltage output is simply proportional to ω_{ta} and the tachogenerator transfer function becomes:

$$\frac{V_{ta}(s)}{\omega_{ta}(s)} = K_{ta} \qquad (3.51)$$

3. 6. 2. Rotary incremental encoder (pulse generator)

The linear and rotary encoders operate on the photo-electrical measuring principle. The scanning unit consists of a light source, a condenser lens for collimating the light beam, the scanning reticule with the index gratings and silicon photo-voltaic cells. The Moiré patterns (similar to interference patterns) could be observed when the scale is moved relative to the scanning unit. The fluctuations of light are converted into electrical signals via photo-voltaic sensors. The output signals are sine waves that could be interpolated or digitized as necessary.

The rotary encoder is usually driven directly from the motor shaft, and contains a transparent disc marked with radial lines. A light source and photoelectric cell are arranged near the periphery of the disc such that rotation produces a train of pulses whose frequency is proportional to the speed. The direction of rotation can be determined if necessary by pulses from a second photocell, displaced 90° in phase from the first as shown below. Quadrature detection logic determines the sense of rotation from the phase relationship between the two channels.

The encoder has the advantage that its output is a pulse train whose frequency is not affected by temperature or attenuation of long cable runs as is the analogue signal of a tachogenerator; therefore it is potentially capable of contributing to extremely accurate digital speed control.

Rotary encoders are available with an additional once per revolution output, known as a marker pulse, which identifies a specific orientation of the disc. By counting pulses from the datum provided by the marker pulse, the absolute angle of rotation can be accurately measured. This feature is used in angular positioning systems, e.g. machine tool spindle orientation. Two channels (a and b) are necessary to know the direction of travel, as shown in Figure 3. 18.

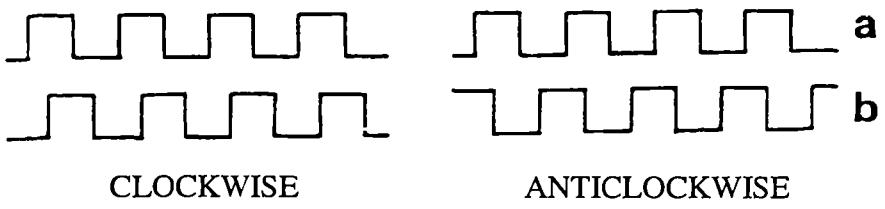

Figure 3. 18. Pulse trains corresponding to bi-directional rotation of an encoder

In most cases the encoder may be modelled as a gain term relating pulse counts to angular position.

3. 6. 3. Linear encoder

There are different categories of linear encoders, depending on the type of application: exposed - sealed, square wave – sine wave as output signal, incremental – absolute, etc.

In contrast to the earlier method of visually reading the graduations of measuring devices, today's encoders are usually scanned photo-electrically. When light falls onto the graduation of a measuring standard, it is diffracted. If the grating period is much larger than the wavelength of light, the diffracted beam components become insignificant. When collimated light is directed through such graduations, it projects an image of the grating pattern. If however the grating period approaches the wavelength of light, this generates a complex pattern of superposed light beam components (an interference pattern). Incremental encoders provide two sinusoidal or square-wave, 90° phase-shifted measuring signals and one reference mark signal. The sinusoidal signals are digitised and evaluated in the subsequent electronics, which results in a measuring step ¼ the signal period of the encoder.

The data for the transducers fitted on the actual machine under investigation is presented in Appendix A5.

This chapter has investigated the individual elements of the CNC machine tool axis drive. The next step is to put together a hybrid model by using lumped parameter and distributed modelling techniques.

4. MATHEMATICAL MODELS FOR CNC MACHINE TOOL AXIS DRIVES

Modelling and simulation are important aspects of engineering design and analysis for dynamic systems. Individual blocks are used in *block diagrams* to represent the separate functional parts of the system and the inter-relationships between the different parts of the system are shown. For the analysis of the system it is necessary to develop a *model*, which is a mathematical description of the system containing appropriate mathematical expressions for each of the elements.

The equations relating the outputs to the inputs of the blocks are in general differential equations, since dynamic conditions are considered. A single differential equation of high order results when these equations are combined to give an overall output-input relationship. One must be aware of the limitations of the mathematical model that are due to the mathematical and physical assumptions and simplifications contained within the model.

During the initial system modelling effort, some factors mentioned by Volland [82] should be taken into consideration:

- Identification of all significant system components
- Identification of all relevant system parameters and variables
- The range of variation in parameter values that should be investigated
- The structural organisation of the system, including the feasibility of alternative organisations
- The desired results (e. g. a description of the system response, maximum accuracy that can be achieved, the dependence of system performance on selected variables)
- The variables that can be controlled and the methods by which one will control these variables in the actual (physical) system
- Specification of the functional dependence on time of the system's inputs
- Identification of all assumptions contained within the system model, including a justification of the need for such assumptions and evidence of the validity of these assumptions for the system under analysis.

Generally, the main problems in obtaining adequate mathematical models for the real systems are due to the following factors: components cannot be easily represented as simple discrete ideal elements, non-linearities are dominant, measurement is difficult and noise is significant.

4. 1. Mathematical block diagram model of the CNC machine tool axis drives

The mathematical block diagram model for the single axis CNC machine is shown in Figure 4. 1. This model shows the mathematical relationships that describe the operation of the positional servo system. The operation of the system may be broken down into three sections:

1. the CNC controller
2. the servo current amplifier
3. the DC motor and mechanical transmission.

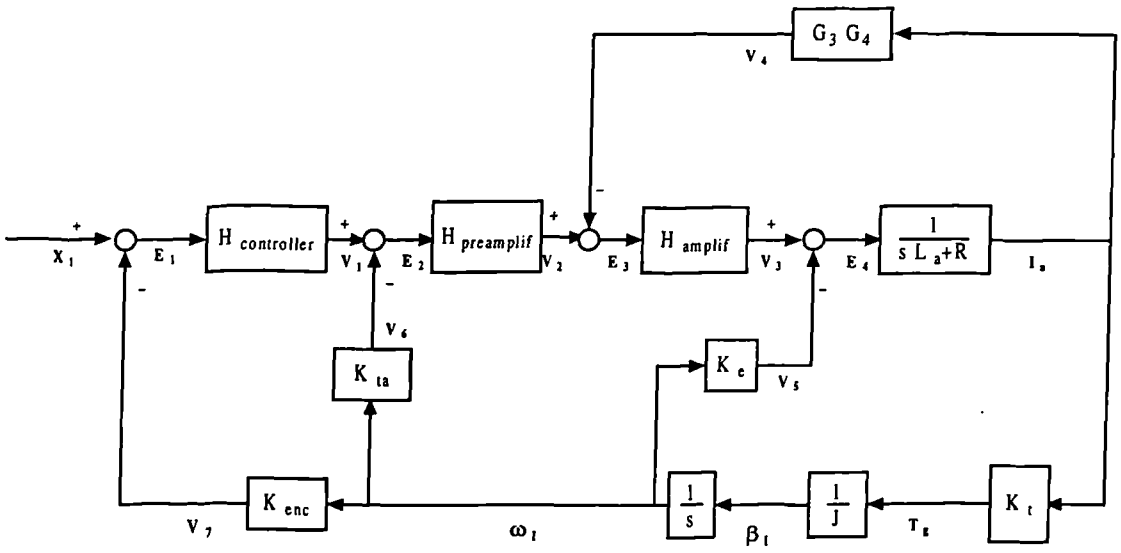

Figure 4. 1. General mathematical model block diagram of the CNC machine tool axis drive

The description of the behaviour of the elements of the drive (controller, pre-amplifier, power amplifier, DC motor, transducers) has been shown in Chapter 3.

The input (X_1) of the model can be arranged for various stimuli e.g. trapezoidal or sine wave or composite. The position error results by comparing this input with the encoder feedback pulse train:

$$E_1(s) = X_1(s) - V_7(s) \qquad (4.1)$$

where $E_1(s)$ - the position error [mm] $V_7(s)$ - the encoder feedback [m/s]

$$V_7(s) = K_{enc} \times \omega_1(s) \qquad (4.2)$$

where K_{enc} - the encoder constant $\omega_1(s)$ - the angular velocity of DC motor shaft [rad /s]

The sampled comparison is carried out in the controller (μs) and the position error is applied through a sample and hold (ms) and its associated D / A converter. The controller output depends on the transfer function of the controller described by the Equation (3. 1) and the controller input:

$$V_1(s) = H_{controller}(s) \times E_1(s) \quad (4.3)$$

where $V_1(s)$ - the controller output [V] $H_{controller}(s)$- the transfer function of the controller

The sample-order hold has a sampling time of 10 ms, provides a unity gain and a small phase shift ($\omega T/2$). Over the bandwidth to be considered, this phase shift can be considered to be negligible. For modern controllers, the update rate is 1 ms which further supports this assumption.

The output from the D/A converter is fed into the rate pre-amplifier, which compares the controller output and tachogenerator rate feedback generating rate error:

$$E_2(s) = V_1(s) - V_6(s) \quad (4.4)$$

where $E_2(s)$- the rate error [V] $V_6(s)$ - the tachogenerator output [V]

$$V_6(s) = K_{ta} \times \omega_1(s) \quad (4.5)$$

where K_{ta} - tachogenerator constant ω_1 - angular velocity of DC motor shaft [rad / s]

The output of the rate pre-amplifier depends on the transfer function of the pre-amplifier described by Equation (3. 6.) and the controller input:

$$V_2(s) = H_{preamplif}(s) \times E_2(s) \quad (4.6)$$

where V_2 - the rate pre-amplifier output [V] $H_{preamplif}$ - rate pre-amplifier transfer function

The voltage output from the rate pre-amplifier is compared with a feedback voltage, derived as a function of the DC motor armature current:

$$E_3(s) = V_2(s) - V_4(s) \quad (4.7)$$

where E_3 - the error voltage [V] V_4 - the feedback voltage [V]

$$V_4(s) = G_3 \times G_4 \times I_a(s) \quad (4.8)$$

where G_3 - scaling term G_4 - pre-amplifier forward path scaling [V /A]

I_a - the armature current of DC motor [A]

A second stage amplifier multiplies the error signal E_3 by a gain factor creating a voltage for feeding into the motor windings:

$$V_3(s) = H_{amplif}(s) \times E_3(s) \quad (4.9)$$

where $V_3(s)$ - the amplifier output [V]

$H_{amplif}(s)$ - the transfer function of the amplifier (Equation 3. 3)

The amplifier output is compared with the voltage depending on the motor voltage constant and the difference is an error voltage:

$$E_4(s) = V_3(s) - V_5(s) = V_3(s) - K_e \omega_1(s) \qquad (4.\ 10)$$

where $E_4(s)$ - the voltage input to the motor windings [V] $V_3(s)$ - the amplifier output

$V_5(s)$- the voltage depending on the motor voltage constant [V]

K_e - DC motor voltage constant [V s/ rad]

The armature current is derived from the following transfer function when considering the DC motor armature resistance and inductance of the windings:

$$I_a(s) = \frac{1}{sL_a + R} \times E_4(s) \qquad (4.\ 11)$$

where $I_a(s)$ - the armature current of the DC motor [A] L_a- DC motor inductance [H]

R - the armature resistance of the DC motor [Ω]

The torque generated by the DC permanent magnet motor is equal to:

$$T_g(s) = K_t \times I_a(s) \qquad (4.\ 12)$$

where $I_a(s)$ - the armature current of the DC motor [A]

K_t - motor torque time constant [s] $T_g(s)$ - torque generated by the motor [Nm]

This torque is required to overcome the inertial effects of the moving parts during motor acceleration and the load torque produced by friction between moving parts. The total moment of inertia of the system is a function of the dimensions and mass of all the moving parts, and has been analysed in terms of *motor moment of inertia* (a value for which has been obtained from manufacturers literature) and *load moment of inertia,* which has been calculated from the physical dimensions of the slideway.

The friction effects have been simplified to include only constant dynamic friction. Stiction had been considered insignificant due to high frequency oscillations on the machine being present while machine is active. The load friction has thus been modelled as a switching function sensitive to the sense of motor rotation. That is, positive load friction for a forward motor rotation and negative load friction for reverse motor rotation.

The angular acceleration of the motor shaft depends upon the torque generated by the motor and the effective motor inertia:

$$\beta_1(s) = \frac{T_g(s)}{J} \qquad (4.\ 13)$$

where $\beta_1(s)$- the angular acceleration of the motor shaft [rad / s^2]

$T_g(s)$ - the torque generated by the DC motor [Nm]

J – total inertia at the motor (Equation 4. 15) [kg m^2]

The angular velocity of the motor is obtained by integrating the angular acceleration:

$$\omega_1(s) = \frac{1}{s} \times \beta_1(s) \qquad (4.\ 14)$$

4. 2. Lumped parameter model for the Beaver VC35 CNC machine tool axis drive with load inertia reflected to the motor, without backlash, friction and geometric errors

Traditional methods for modelling and simulation of CNC machine tools have used lumped-parameter models. The behaviour of the machines could be determined by solving a set of differential equations. Ford [12] presented a detailed example of mathematical block diagrams for PWM brush and brushless DC drive systems. The analysis procedure consists of breaking down the cascaded loops of the system in smaller loops and then replace with first or second order system equivalents over the bandwidth to be considered.

The block diagram of the lumped parameter model of Beaver VC35 CNC machine tool axis drive is similar to the general one (Figure 4. 1) and is presented in Figure 4. 2.

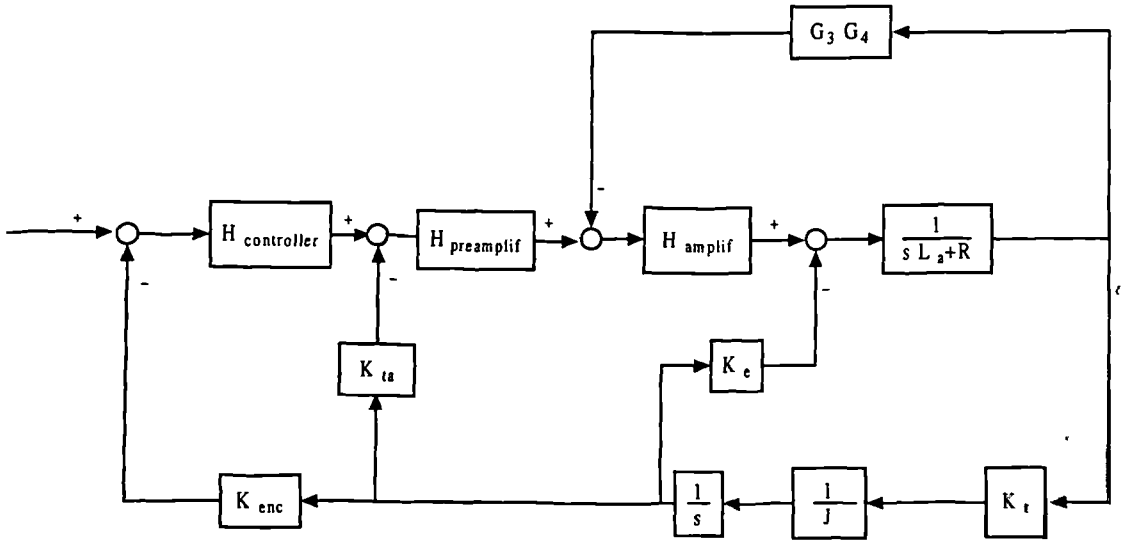

Figure 4. 2. Lumped parameter model of CNC machine tool axis drive

It is worth noting that the effective motor inertia is considered to be a combination of the DC servomotor inertia (J_m), associated drive shaft inertia (J_{shaft}), the driving pulley inertia (J_{pl}) and the load inertia referred to the motor (J_{Lred}):

$$J = J_m + J_{shaft} + J_{pl} + J_{Lred} \tag{4. 15}$$

$$J_{Lred} = \frac{J_{p2} + J_{bs} + J_L}{n^2} \tag{4. 16}$$

where J_{Lred} - load inertia referred to the motor [kg m^2] J_{bs} - ball-screw inertia [kg m^2]

J_{p2} - inertia of the second (driven) pulley [kg m^2] J_{shaft} - motor shaft inertia [kg m^2]

J_L - inertia of the load referred to the ball-screw [kg m^2] n - reduction ratio

The component loops are reduced to first or second order system equivalents using the Bode diagram frequency domain technique and considering only linear elements.

The calculations performed further are referring to Y-axis drive of the CNC machine tool Beaver VC35 and the results for X-axis and Z-axis are introduced in Appendix B2.

At the first stage, the total inertia at the motor is investigated:

$$J = J_m + J_{shaft} + J_{pl} + \frac{J_{p2} + J_{bs} + J_L}{R^2} =$$

$$= 48\times10^{-3} + 7.5\times10^{-6} + 0.46\times10^{-3} + \frac{23+27+17}{4}\times10^{-3} = 6.9\times10^{-3} \text{ kg m}^2$$

The calculations of the inertia for the different elements are presented in Appendix A4.

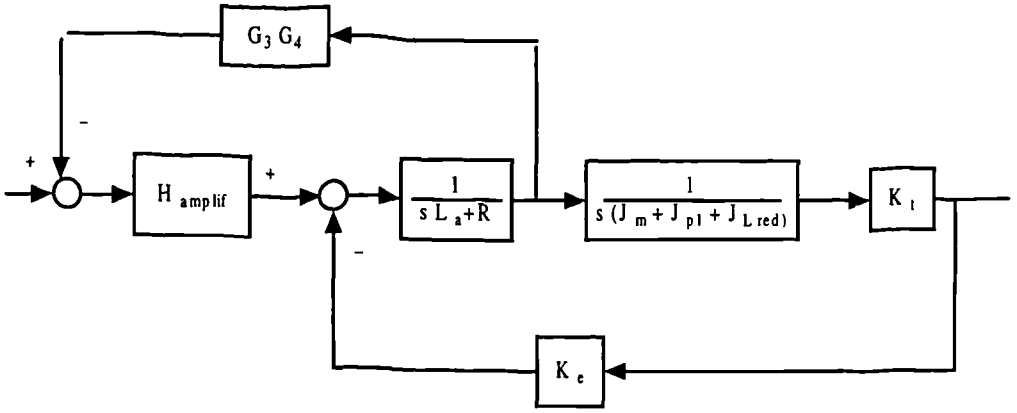

Figure 4. 3. The armature voltage - motor rate control loop

Consider now the armature voltage - motor rate control loop as shown in Figure 4. 3. It is possible to obtain an equivalent armature voltage - motor rate control loop (Figure 4. 4) by moving a summing point ahead of a block and considering both loops to have the same output point. The transfer function of the reduced loop is:

$$H_{motor+load} = \frac{\frac{H_{amplif}}{s L_a + R}\times\frac{K_t}{s J}}{1 + \frac{H_{amplif}}{s L_a + R}\times\frac{K_t}{s J}\times\left[G_3\times G_4\times\frac{s J}{K_t} + \frac{K_e}{H_{amplif}}\right]} \tag{4. 17}$$

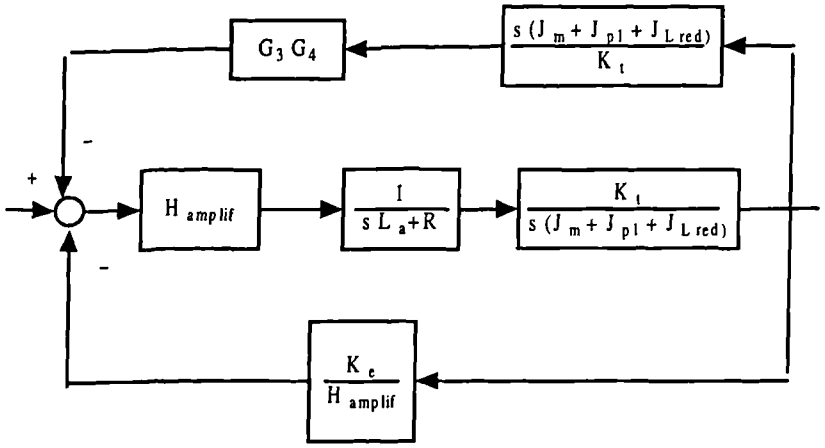

Figure 4. 4. The equivalent armature voltage - motor rate control loop

By introducing the effective values of terms, the transfer function of the reduced loop yields:

$$H_{motor+load} = \frac{H_{amplif} \times K_t}{s\,J\,(s\,L_a + R) + H_{amplif} \times K_t \left[\frac{K_e}{H_{amplif}} + G_3 \times G_4 \times \frac{s\,J}{K_t} \right]} \qquad (4.\ 18)$$

where $H_{amplif} = K_{br} \times K_2 = 32.5 \times 2 = 65\ V/V$

$K_{br} = 32.5\ V/V$ - bridge voltage

$K_2 = 2\ V/V$ - current loop scaling

$R = 0.804\ \Omega$ -armature resistance with brushes at 20° C

$L_a = 6.1\ mH$ - armature inductivity

$G_3 \times G_4 = 7.5 \times 0.095 = 0.7125\ V/A$ - armature current feedback scaling

$$H_{motor+load} = \frac{65 \times 0.735}{s\,0.0069\,(s\,0.0061 + 0.804) + 65 \times 0.735 \times \left[\frac{0.735}{65} + s\,0.0069 \times \frac{0.7125}{0.735} \right]} \qquad (4.\ 19)$$

$$H_{motor+load} = \frac{47.775}{0.000042\,s^2 + 0.4540\,s + 0.54} \qquad (4.\ 20)$$

The general form for second order element is

$$H(s) = \frac{\omega_n^2}{s^2 + 2\zeta\omega_n + \omega_n^2} \qquad (4.\ 21)$$

The transfer function of the equivalent armature voltage - motor rate control loop can be written as a general form:

$$H_{motor+\ load} = 88.47 \times \frac{12857}{s^2 + 10809.5\,s + 12857} \qquad (4.22)$$

The natural angular frequency for the second order element is:

$$\omega_n = \sqrt{12857} = 113.4 \ \frac{rad}{sec} \qquad (4.23)$$

The damping factor for this element is:

$$2\zeta\omega_n = 10809.5 \quad \rightarrow \quad \zeta = \frac{10809.5}{2 \times 113.4} = 47.66 \qquad (4.24)$$

DC gain = 88.47 DC gain [dB] = $20 \log_{10}(318.5) = 38.94$

Because ζ is much greater than 1, the result is an armature current loop that is very overdamped.

The gain curve will cut the zero dB axis at the frequency 59.76 rad / sec if the DC gain is removed. When the DC gain (38.94 dB) is included, the modified gain curve cuts the zero dB axis at 100 rad / sec (see Figure 4.5).

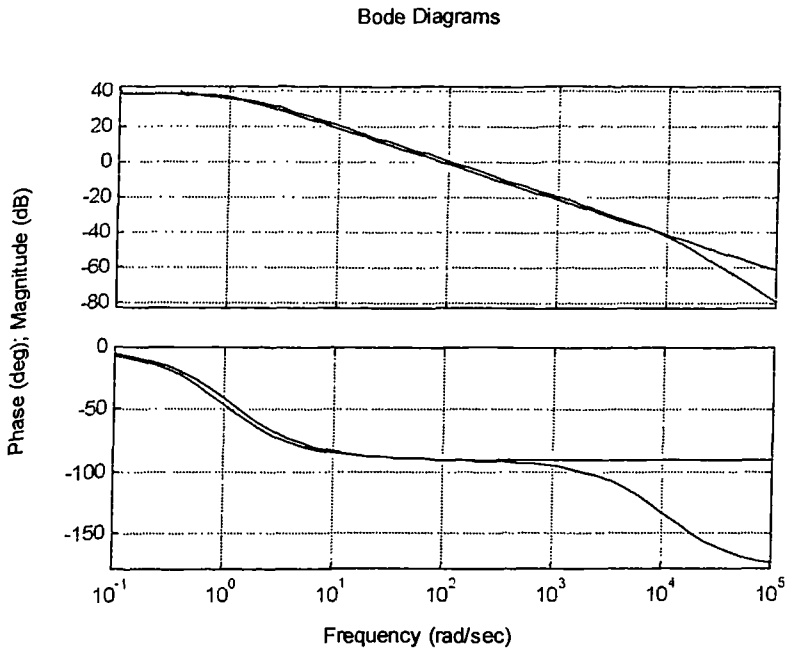

Figure 4.5. Bode diagrams for the calculated armature voltage - motor rate control loop (blue) and the equivalent first order element (red)

The transfer function from Equation (4.22) represents a second order element which is then reduced to a first order element using MATLAB. The method consisted in modifying the parameters of the first order element to achieve the best fit.

The equivalent first order element for the armature voltage - motor rate control loop is:

$$H_{motor+\ load\ equiv} = 88.47\frac{1}{s+1} \tag{4.25}$$

In Figure 4. 5 are shown the Bode diagrams for the second order element and the equivalent first order element on the same graphs using a MATLAB file presented in Appendix B2. It is evident that they are similar for the frequency in the interval (1 - 1000) rad / sec. This represents 17 times the natural frequency of the second order. So the first order element could be considered equivalent to the second order element over the bandwidth under consideration.

The expression for the reduced armature voltage - motor rate control loop (Equation 4. 25) is introduced into the next loop (velocity loop) as it is shown in Figure 4. 6.

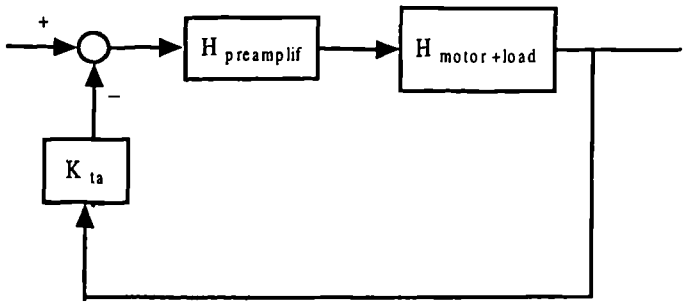

Figure 4. 6. Velocity loop

The transfer function of the velocity loop has the following form:

$$H_{velocity} = \frac{H_{preamplif} \times H_{motor\ +\ load}}{1 + K_{ta} \times H_{preamplif} \times H_{motor\ +\ load}} \tag{4.26}$$

where G_{PA}- pre-amplifier transfer function $\quad G_{PA} = 11000 \times \frac{0.00039\,s + 0.082}{s}$

$H_{motor\ +\ load}$- the equivalent transfer function for the loop containing the DC motor inertia and load inertia referred to the motor:

$$H_{motor+\ load\ equiv} = \frac{88.47}{s+1}$$

$K_{ta} = 20$ mV / min^{-1} = 0. 19 V / rad /s - tachogenerator constant

By introducing the effective values of the terms, the velocity loop transfer function becomes:

$$H_{velocity} = \frac{11000 \times \frac{0.00039\,s + 0.082}{s} \times \frac{88.47}{s+1}}{1 + 11000 \times \frac{0.00039\,s + 0.082}{s} \times 0.19 \times \frac{88.47}{s+1}} \tag{4.27}$$

$$H_{velocity} = \frac{902 \times (0.00476s + 1) \times 8.47}{s^2 + 73.12s + 15162} = \frac{379.54s + 79799.94}{s^2 + 73.12s + 15162} \quad (4.28)$$

The transfer function of the velocity loop contains a lead element and a second order element.

$$H_{velocity} = 5.26(0.00475\,s + 1) \times \frac{15162}{s^2 + 73.12s + 15162} \quad (4.29)$$

The Bode diagrams (Figure 4. 7) for the velocity loop are obtained by running a MATLAB file presented in Appendix B2.

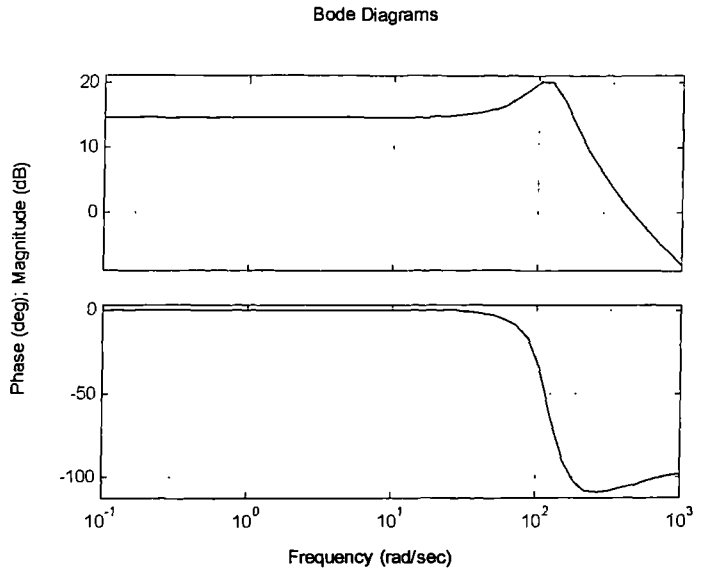

Figure 4. 7. Bode diagrams for the calculated velocity control loop

The natural angular frequency for the second order element is:

$\omega_n = 123$ rad / s and the damping factor is $\zeta = 0.3$

The DC gain of the lead element is :

DC gain = 5. 26 DC gain [dB] = 20 log $_{10}$(5. 26) = 14. 42

The expression for the velocity control loop (Equation 4. 29) is introduced into the position loop.

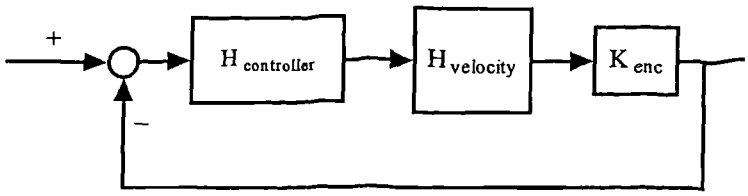

Figure 4. 8. The position loop

$$H_{position} = \frac{H_{controller} \times K_{enc} \times H_{velocity\_equiv}}{1 + H_{controller} \times K_{enc} \times H_{velocity\_equiv}} \tag{4.30}$$

$K_{enc} = p / 4\pi = 10 / 4 * 3.14 = 0.796$

$H_{controller} = 10 / s$

$$H_{position} = \frac{\frac{10}{s} \times 0.796 \times 7581 \times \frac{0.00476s + 1}{s^2 + 73.12s + 15162}}{1 + \frac{10}{s} \times 0.796 \times 7581 \times \frac{0.00476s + 1}{s^2 + 73.12s + 15162}} \tag{4.31}$$

$$H_{position} = \frac{287.24s + 60344.76}{s^3 + 73.12s^2 + 15449.24s + 60344.76} \tag{4.32}$$

A first estimate of the natural angular frequency for the equivalent transfer function for the position (final) loop is determined using the **damp** function from MATLAB (see Appendix B2). So the equivalent transfer function for the actual position loop (Figure 4. 9) is a second order element with natural angular frequency 35 rad/ s and damping factor ζ =1 (system critically damped).

$$H_{position\ equiv} = \frac{1225}{s^2 + 70s + 1225} \tag{4.33}$$

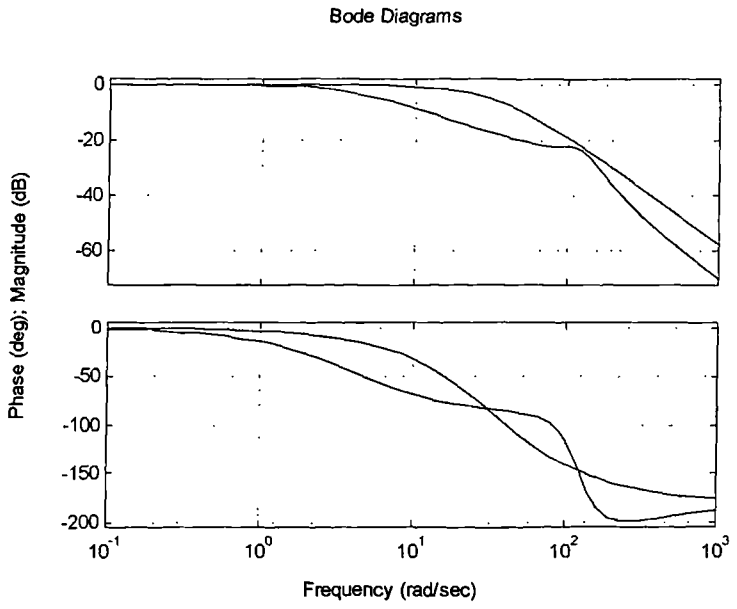

Figure 4. 9. Bode diagrams for the calculated transfer function of position control loop (blue) and the equivalent transfer function (red)

The value for natural frequency is expected because the bandwidth of the position loop for the Beaver VC35 CNC machine tool obtained from direct reading from the controller is:

$$\text{bandwidth} = \frac{\text{maximum following speed}}{\text{maximum following error}} = \frac{10000\,\frac{\text{mm}}{\text{min}}}{5\text{ mm}} = \frac{166.6\,\frac{\text{mm}}{\text{sec}}}{5\text{ mm}} \approx 33\,\frac{\text{rad}}{\text{sec}} \qquad (4.34)$$

The measurement is taken on the steady state part of a trapezoidal input signal.

The calculated natural angular frequency is bigger than the practical one because the behaviour of the load is more complicated than the load inertia reflected to the motor.

4. 3. Modular approach to modelling of CNC machine tool axis drives

The research on modular modelling and simulation of complex systems has made remarkable progress in recent years. This report presents the results of the research carried out in the field of *dynamic simulation of mechanical systems*. The main goal is to achieve an efficient modular approach to modelling, in order to make the modelling process easier, ensure its traceability and inspectability, and support model re-use.

In a modular approach, the model of any part of a complex system is defined as a module, whose behaviour should be independent of the context where it is used and of the procedure used for numerical solution. In fact, in the same way that the real mechanical system is built by assembling separate parts, it would be natural for the user to generate the dynamic model of the whole system by connecting graphically the modules representing the different parts. This modular approach permits the easy exchange of components without the need to alter the whole model. For example, the coupling between motor and load can be either direct, or with belts & pulleys or gears etc. and yet the rest of the modules remain the same.

In addition, the modular approach allows for the calculation of the forces that occur between model components. The lumped-parameter model does not offer this opportunity, which is very necessary for analysis as an aid to error avoidance design practices.

Of particular interest is the ability to generate models for friction developed by various components of the machine tool (such as the bearings and the axis slideway). An added advantage of the adopted technique is the ease with which geometric, load and thermal models of the machine tool can be incorporated into the dynamic model.

This new approach to the modelling of a machine tool axis drive will be useful in the development of diagnostic and condition monitoring systems when the errors in machine tools such as geometric, thermally induced and non-rigid effects are considered. Determining the

errors produced by different modules is beneficial for error avoidance because each component imposes errors on the CNC machine tool.

Finally, the modular approach will be very useful for the identification and performance analysis of dynamic errors from CNC machine tools.

4. 3. 1. Lumped parameter model of CNC machine tool axis drive using modular load with backlash and friction

The lumped parameter model with load inertia reflected to the motor has significant shortcomings:

- the lumping of any system removes the effect of model components with corresponding reduction in simulation accuracy
- changes in any system component requires the alteration of the entire lumped model
- it is not possible to examine the behaviour of individual components and how they interact.

To overcome these shortcomings, a modularised (distributed) model of the machine tool has been created. This is an alternative approach suggested by Leonhard [83], instead of that traditionally used [14].

The alternative approach for the modelling and simulation of a machine tool axis drive is similar to the Newton-Euler model [84] of a robot where kinematics motion is transmitted forward through the model and resistive force flows back through the model (Figure 4. 10).

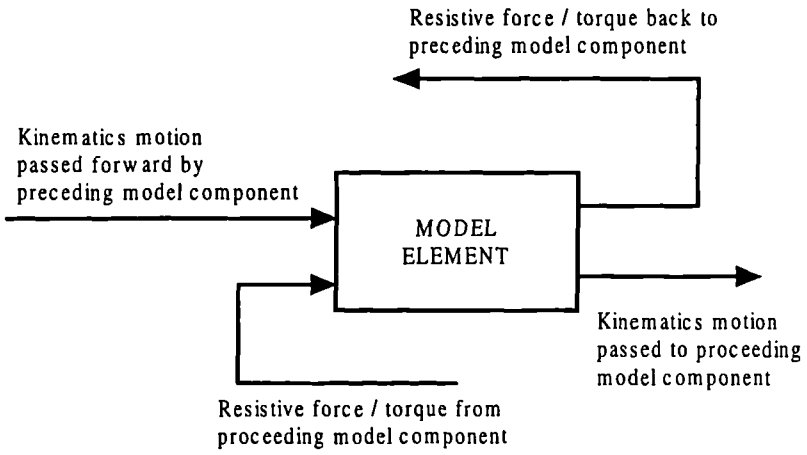

Figure 4. 10. Forces for one model element

Following this pattern, the reaction forces due to friction and components of inertia are transmitted as inputs to precedent modules. In this way the interaction between machine tool components can be studied.

The effective motor inertia is considered in this case to be a combination of the DC servomotor together with its associated drive shaft inertias (J_m) and the driving pulley inertia (J_{p1}):

$$J = J_m + J_{p1} \tag{4.35}$$

The remainder of the machine drive has been modelled as a series of mechanical components. This is still a lumped parameter model because the performance of the load elements in the time domain could be expressed by differential equations. Regarding the non-linearities which are introduced, *friction* can still be defined by a differential equation, but *backlash* is a function on two variables (time, space) and is described by a partial differential equation.

The influence of the load is characterised by its reaction torque due to inertia of the load elements, friction and backlash:

$$T_{reaction}(s) = R \times \left(T_{p2}(s) + T_{bsf}(s) + T_{bsi}(s) + T_{sr}(s) + T_{friction}\right) \tag{4.36}$$

where $T_{p2}(s)$ - torque due to driven pulley inertia [Nm]

$$T_{p2}(s) = J_{p2}\, s\, \omega_2 = 0.01778 s \omega_2 \tag{4.37}$$

J_{p2} - the driven pulley inertia [kg m^2] ω_2 - driven pulley angular frequency [rad / s]

T_{BSd} - torque due to ball-screw friction [Nm]

$$T_{bsf} = (\mu W_{bs} + F_{preload}) \times \frac{p}{2\pi} \times sign(\omega_2) = \\ = (0.16 \times 147 + 6896) \times \frac{0.01}{2\pi} \times sign(\omega_2) = 11 \times sign(\omega_2) \tag{4.38}$$

J_{BS} - ball-screw inertia [kg m^2] μ - the ball-screw friction coefficient

F - preload force [N] p - pitch of the ball-screw [m]

T_{BSi} - torque due to ball-screw inertia [Nm]

$$T_{bsi}(s) = J_{bs}\, s\, \omega_2 = 0.0027\, s\, \omega_2 \tag{4.39}$$

T_{sr} - torque due to slideway reaction [Nm]

$$T_{sr}(s) = \frac{p^2}{4\pi^2 \eta} (\mu W \omega_2 + m_L\, s\, \omega_2) = \\ = \frac{(0.01)^2}{4\pi^2\, 0.9} (0.1 \times 3518 \times \omega_2 + 359\, s\, \omega_2) = 0.00099\, \omega_2 + 0.001 s \omega_2 \tag{4.40}$$

where η - the ball-screw efficiency μ - the slideway friction coefficient

m_L - the load mass [kg] W - the slide weight [N]

$T_{friction}$ - torque due to friction in bearings (Equations (3. 36) - (3. 38))

$$T_{friction} = (T_{0\ fixed} + T_{1fixed}) + (T_{0\ support} + T_{1\ support}) \quad (4.41)$$

Introducing the actual data, the calculated value of this torque is obtained:

$$T_{friction} = 3.448 \times 10^{-5} \times (\omega_2)^{2/3} + 0.00407 \quad (4.42)$$

$$T_{0fixed} = T_{0\ support} = f_0\, 10^{-7} (\upsilon n_b)^{2/3} D^3 = 1.724 \times 10^{-5} \times (\omega_2)^{2/3} \quad (4.43)$$

$$T_{1fixed} = \mu_1 f_1 F_{fixed} (D/2) = 0.0105 \text{ Nm} \quad (4.44)$$

$$T_{1support} = \mu_1 f_1 F_{support} (D/2) = 0.031 \text{ Nm} \quad (4.45)$$

The torque generated by the DC motor has to overcome mainly the frictional forces in the slide guides, the bearing friction, the frictional losses in the ball-screw nut and the feed force necessary for machining. In this study, the cutting forces are not considered.

The approach described allows the easy construction of detailed machine tool drive models. It represents the basis for future incorporation of geometric, non-rigid and thermal models of machine tool behaviour.

The modular approach to the modelling and simulation of a CNC machine tool axis drive is an important contribution to machine tool theory. Simulation results considering trapezoidal and sinusoidal velocity demand signals were presented by Pislaru et al. [85].

The thesis presents further details on other aspects related to this first phase (the building of the model):

- Comparison with actual data from a CNC machine tool;
- Demonstration of the flexibility of the modular approach in the modelling of different axis drive systems;
- Development of the models for the other axes and finally, a three-dimensional model for the CNC machine tool axis drives. The modelling and simulation for 3 axes is discussed to show the performance of the whole simulation environment in terms of complexity management, efficiency, and accuracy.

It was intended to demonstrate that the technique allows the inclusion of the combined resonant states of the individual elements when it is difficult to obtain exact constituent damping factors. Also it demonstrates the modular approach to be more appropriate for parameter identification when compared to lumped-parameter models.

4. 3. 2. Two-axis and 3D model of CNC machine tool axis drives using modular load with backlash and friction

In order to produce a two-axis model for the horizontal plane (X and Y axes), the previous single axis model was duplicated, with a number of parameters changed to represent the two different axes.

In the case of the model for the vertical axis (Z-axis), the action of the counter-weight system must be included (see Figure 4. 11).

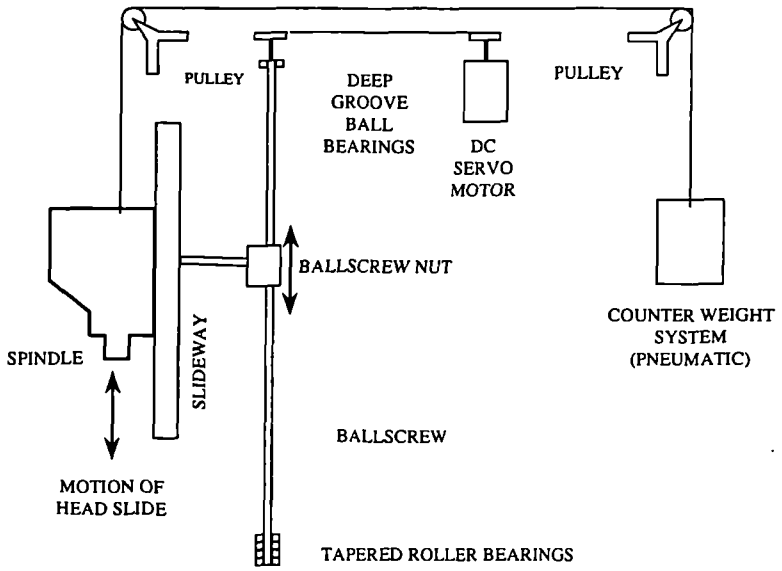

Figure 4. 11. The elements of the Z-axis drive

Using the assumption that the counter-weight system compensates for the mass of the Z-axis slide, the tension in the counter-weight belt is equal to the following weight:

$$T_{cw} = m_z \times g \qquad (4.46)$$

where T_{cw} - tension in the counter-weight belt [N] m_z - mass of the Z-axis slide [kg]

The axial force at the pulley bearing could be assumed to be zero and the radial force experienced by the pulley bearing is:

$$F_r = 2\,T_{cw} = 2 \times m_z \times g \qquad (4.47)$$

This force is introduced into the model of the axis drive, similar to that presented previously.

The simulation results using one axis (Y-axis), two-axis (X and Y axes), respectively 3D models are presented in Chapter 6 and Appendix D8.

4. 3. 3. The hybrid model of CNC machine tool axis drive with distributed load, explicit damping coefficients, backlash and friction

As an alternative to the model with distributed parameters outlined in section 4. 3. 1., an explicit damping coefficient method was investigated. This method became apparent when comparing lumped parameter and distributed model techniques discussed in sections 4. 2. and 4. 3. 1. with the measurements at the machine (see Figures 5. 26 and 6. 34).

Calculations on stiffness and the damping of systems have become more accurate due to the progress made in research into the dynamics of drives. The knowledge of the parameters of the elastic system: i.e., the mass of the various units, and the stiffness of the linkages between the masses and the damper mechanisms, is required when calculating the dynamics of machine tools.

The Beaver VC35 milling machine can be subjected to a wide range of frequency disturbances considering the complexity of the drive vibratory systems. These disturbances are due to spindle revolution variation, number of cutters teeth etc. and will sometimes operate under resonance conditions.

The modelling of these resonant states represents an important aspect in the study of the dynamics of machine tools. The different elements of the machine tools have to be modelled considering explicit damping coefficients in order to simulate the resonant states of the system. Effectively, the damping coefficients are introduced into the individual elements of the modelled system presented in section 4.3.1 by not relying on the damping effects existing in them and transmitted from preceding stages.

The hybrid model is developed on the considerations expressed by Bartlett and Whalley [11]. A mixture of ordinary differential equations and partial differential equations could describe this combination of distributed and lumped elements. According to normal practice, the ball-screw is modelled with distributed parameters, while the models for the other components (bearings, belt and pulleys etc.) have lumped parameters.

As shown in Figure 4. 12, the structure of the vertical machining centre contains five modules: the headstock, the column, the worktable, the saddle, and the bed unit. A spindle set is mounted on the flange of the headstock and the cutting tool is attached to the spindle. The workpiece has a horizontal movement relative to the cutting head by displacing the table parallel to the column (X direction) or perpendicular to the column (Y direction).

When predicting the dynamic behaviour of the drives, it is necessary to consider as many as possible of the factors involved in the energy dissipative processes which occur during the operation of the drive. These dissipative processes include:

- Resistance in the motor bearings and seals
- Damping in the motor shaft
- Friction and damping in the drive belt
- Resistance in the ball-screw bearings and seals
- Damping in the ball-screw (both torsional and axial)
- Friction and damping between the ball-screw and its nut
- Friction between the table and the saddle (X drive) or between the saddle and the bed (Y drive)

Though not directly "dissipative", the backlash between the ball-screw and its nut is also taken into account.

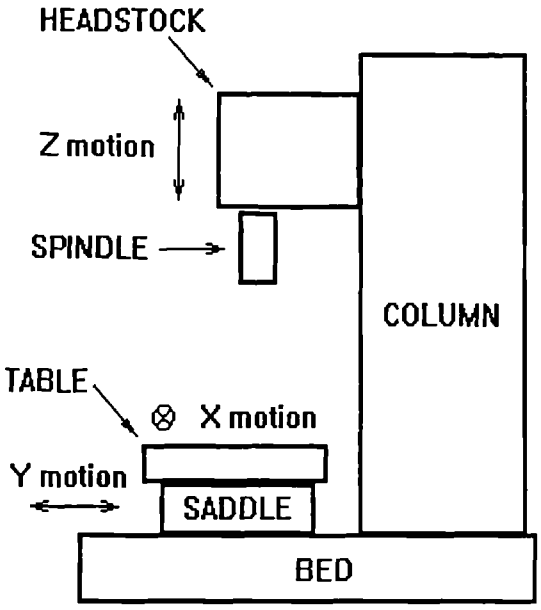

Figure 4. 12. The five major modules of the structure of the Beaver VC 35

There are five main inertia elements in the drive: motor, driving pulley, driven pulley, ball-screw and ball-screw load. Also there are three main stiffness elements: motor shaft, belt drive and ball-screw. Only the static stiffness of the system elements is examined in this investigation.

The motor, pulleys and load are represented as single lumped inertia elements and the ball-screw divided into 9 pieces with the ball-screw flexibility apportioned between each. The load is assumed to be in central position along the ball-screw length.

The mechanical elements are modelled considering the following categories

a) Mass and inertia elements

The acceleration could be calculated from Newton's second law for the linear case:

$$\frac{d^2x}{dt^2} = F/m \tag{4. 48}$$

The velocity results by integrating the acceleration:

$$\frac{dx}{dt} = \int \frac{d^2x}{dt^2}.dt \tag{4. 49}$$

and the displacement is obtained by integrating the velocity:

$$x = \int \frac{dx}{dt}.dt \tag{4. 50}$$

In the case of a torsional element, the angular acceleration is:

$$\frac{d^2\theta}{dt^2} = T/J \tag{4. 51}$$

b) Spring / damper elements

In this investigation, the elements representing shafts are considered as a spring in parallel with a viscous damper. Using the linear case as an example, if x_1, x_2 = displacements, k = stiffness and c = the damping coefficient, the force F generated by the spring / damper is

$$F = k \times (x_2 - x_1) + c \times (\frac{dx_2}{dt} - \frac{dx_1}{dt}) \tag{4. 52}$$

So the viscous damping part gives rise to a force which is proportional to the relative velocity of two parts of a system.

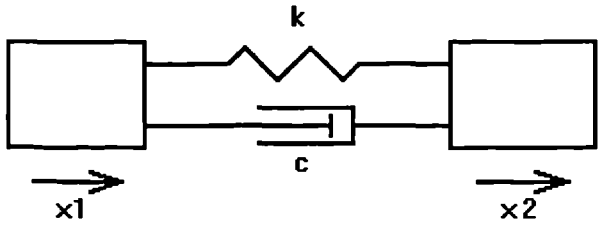

Figure 4. 13. The spring / damper element

The torsional case can be represented by a similar equation for the torque:

$$T = k_\theta \times (\theta_2 - \theta_1) + c_\theta \times (\frac{d\theta_2}{dt} - \frac{d\theta_1}{dt}) \tag{4. 53}$$

c) Rotational damper

A rotational damper element is used to model that part of bearing resistance that is proportional to the speed of the shaft. The element is basically a spring / damper without the spring. It is connected to the shaft at one end and, in principle, "earthed" at the other. The torque generated is thus

$$T = c_\theta \times \frac{d\theta}{dt} \tag{4. 54}$$

d) Linear (Coulomb) friction

Consider first that the surfaces are not moving relative to one another and are held in contact by a force F_n acting normal to the surfaces (see Figure 4. 14).

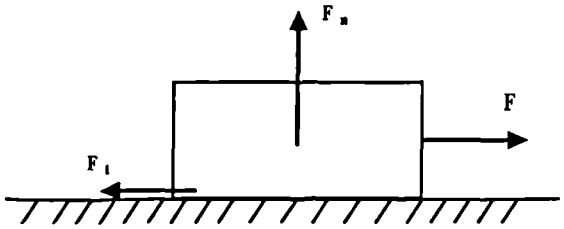

Figure 4. 14. Forces acting between two moving surfaces

If a force F is applied parallel to the surfaces, friction gives rise to a resistive force F_t on the body which has two values depending on F and F_n :

$$F_t = F \text{ ,when } F \le \mu \times F_n \tag{4. 55}$$

$$F_t = \mu F_n \text{ ,when } F > \mu \times F_n \tag{4. 56}$$

The force F_a available to accelerate the body to which F is applied is

$$F_a = 0, \text{ when } F \le \mu \times F_n \tag{4. 57}$$

$$F_a = F - \mu F_n \text{ ,when } F > \mu \times F_n \tag{4. 58}$$

The effect of friction is to act opposite to the direction of motion. Friction is a non-linear effect because the magnitude of the frictional force is dependent on a variety of conditions that are not always proportional to the forces applied.

e) Rotational frictional element

Rotational friction is used to model that part of bearing resistance which opposes motion with a constant torque provided the shaft is moving. The maximum torque T_{max} normally transmitted by the shaft is used instead of the normal contact force and a "friction ratio" is used instead of the coefficient of friction. The torque T_b absorbed when the bearing is subjected to torque T is:

$$T_b = T \quad \text{when } T \leq \mu \times T_{max} \tag{4.59}$$

$$T_b = \mu\ T_{max} \quad \text{when } T > \mu \times T_{max} \tag{4.60}$$

It is necessary to examine and consider not only the stiffness of single elements, but also the cumulative stiffness of the groups and systems formed by these elements. The cumulative stiffness of the machine parts, the elements which join them (bolted connections, oil films in bearings, slideways etc.), of the driving elements (oil columns, ball screws etc.), and of the resulting combinations of these must be such as to ensure that the resulting static and dynamic relative displacements between tool and workpiece are within permissible limits.

f) Stiffness and Rigidity

The term 'stiffness' has to be considered from the following points of view:

- *static stiffness* against deformation under static loads. The more important static deformations are those which are caused by bending and torsional loads because these produce misalignments and displacements of the guiding elements and thus working inaccuracies of the machine.

Longitudinal (axial) stiffness could be calculated in the case of bending:

$$K_L = \frac{F}{dL} = \frac{E_{ym} A}{L_1} \tag{4.61}$$

where F - longitudinal force (thrust) L_1 - length under compression or tension

dL - extension or contraction E_{ym} -Young' s modulus of elasticity

A - second moment of area

Torsional stiffness could be calculated in the case of torsion:

$$K_\tau = \frac{\tau}{\phi} = \frac{G J_\tau}{L} \tag{4.62}$$

where τ - applied torque ϕ - resulting angle of twist

J_τ - torsional second moment of inertia $J_\tau = \frac{\pi D^4}{32} \times L \times \rho$ (4.63)

G - modulus of rigidity

So the stiffness is influenced by the material, the size and the shape of the section under load.

- *dynamic rigidity* - showing the behaviour during vibrations under pulsating and inertia forces. The parameters which influence the vibration behaviour are: the vibrating mass, the static stiffness, the damping factor and the natural frequency.

g) Further modelling considerations (see acknowledgements)

By taking into consideration the aspects mentioned above, the various parts of the drive are modelled as follows:

- *the motor* - as inertia element and rotational frictional element to represent bearing resistance;
- *the belt drive* - the pulleys are represented as inertia elements and in the case of the driven pulley, it is introduced as a rotational frictional element. Also the Coulomb friction that arises from the teeth of the pulleys and the teeth of the belt is considered.

  There are two types of vibrations for the belt that could occur accordingly to Palmgren [77]:

  - *transverse vibrations* - the belt behaves like the string of a guitar or a violin;
  - *longitudinal vibrations* - due to the fact that the belt is an elastic link between two rotating masses (driving and driven pulleys) with given moments of inertia.

  Transverse vibrations are not considered because it is assumed that there is no imbalance of belt or pulleys that could be caused by dimensional variations, improper mounting, etc.

  The dynamic behaviour of the belt material is modelled as a spring/damper type element. However, it is possible for the belt to go slack on one side when the belt is tensioned and sufficient torque is applied. In this case only half of the belt will be in play and this is a non-linear situation. The details of the method used to model these effects are shown in Chapter 6.

  The synchronous belt was supplied by Uniroyal and no information is available for it. A preliminary estimate of the belt drive stiffness was therefore made based on Fenner's Poly Chain GT belts and the results were similar in many ways to those revealed by measurements (see Chapter 5). The details about the preliminary estimation are shown in Appendix B4.
- *the ball-screw* - the torsional flexibility of the ball-screw is represented by two torsional spring/damper elements. The axial stiffness of the ball-screw and its mounting bearings is represented by a linear spring/damper element.

  The *dynamic behaviour of the ball-screw middle* is represented by a special element that performs several functions:

  - Inertia element which calculates the torsional movement of the ball-screw middle (the portion nearest to the nut);
  - The torsional rotation of the ball-screw is converted into linear movement of the nut using the factor equal with the screw pitch divided by 2 π;

- Inertia element for the linear movement (axial behaviour) of the ball-screw middle caused by the reaction force from the nut acting on the ball-screw and its support bearings;
- The total axial movement of the part of the ball-screw acting on the nut is calculated.

The *dynamic behaviour of the ball-screw nut* is also represented by a special element which performs several functions:

- Spring / damper element connecting the ball-screw middle to the table (X drive) or the saddle (Y drive);
- The backlash is taken into consideration;
- The ball-screw could act in a 'positive' mode (the screw drives the nut) or in a 'negative' mode (the nut drives the screw). The force and torque created are calculated;

The *dynamic behaviour of the ball-screw end* is modelled by an inertia element and a rotational frictional element. At this stage, the ball-screw sag under its own weight is not considered.

- *the worktable / saddle* - as a Coulomb friction element and an inertia element.

A schematic representation of the model for the mechanical transmission of the CNC machine tool axis drive is presented in Figure 4. 15.

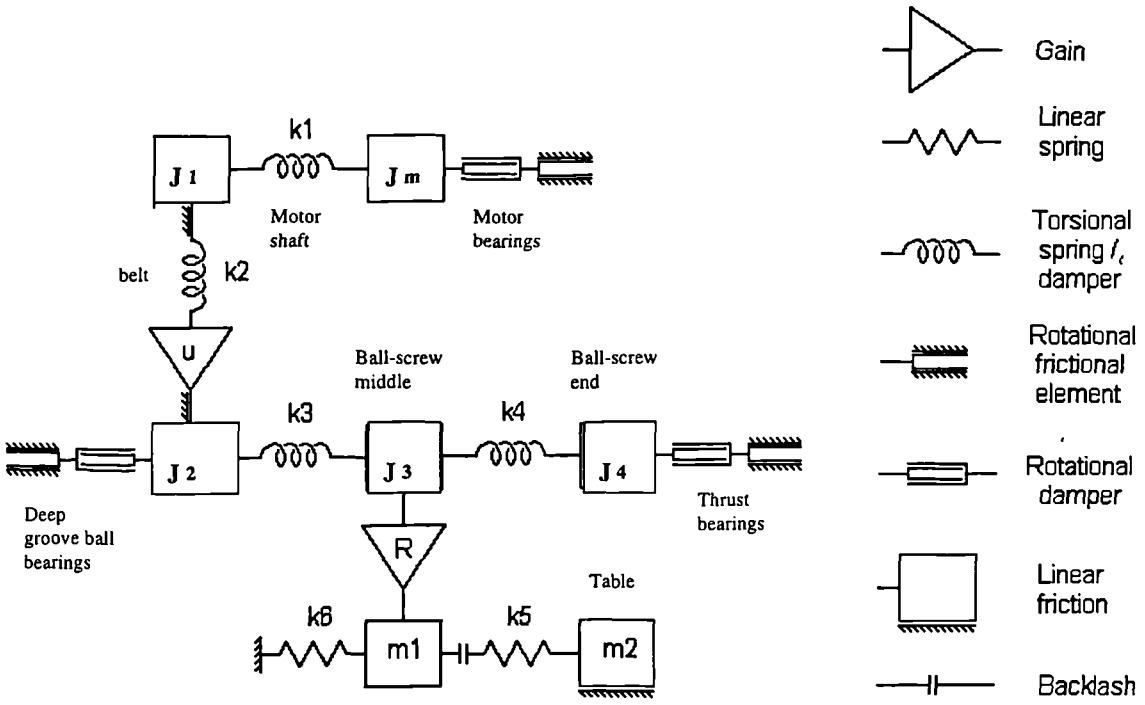

Figure 4. 15. Schematic representation of the mechanical elements of the model

Details for the models of special inertia elements (ball-screw middle, worktable / saddle) and special spring / damper elements (belt drive, ball-screw nut) are presented in Chapter 6.

The first estimates of the coefficients for this model are determined considering the experimental data for the closed-loop position control and the calculations are shown in Appendix B5.

This chapter has dealt with the construction of the hybrid model using a theoretical appraisal technique. The next step has to be the development of adequate measurement techniques for use at the machine tool under review. The techniques will include for measurement of geometric, load and thermal errors. Further measurement practices will comprise vibration and the response of the system to various stimuli.

5. MEASUREMENT TECHNIQUES APPLIED TO BEAVER VC35 CNC MACHINE TOOL AXIS DRIVES

The performance of each axis drive system is of critical importance in the accuracy of the component to be produced (see section 1. 1). The performance of this system can be specified in terms of its static and dynamic accuracy. *The static accuracy* is an assessment of the system's ability to accurately position the axis slide in the steady state. It is affected by static stiffness, thermal drifts and software limitations. *The dynamic accuracy* of the axis drive is an assessment of the system performance in response to changing demand signal. It is influenced by the control system velocity and acceleration lags, dynamic deflections, dynamic stiffness, damping, contour interpolation and operating errors.

There are three main sources of errors in machine tools that determine machine tool accuracy:

1. geometric errors;
2. thermally induced errors;
3. load induced (non-rigid) errors;
4. control system errors.

5. 1. Geometric error measurements

5. 1. 1. Machine tools geometric errors

The geometric errors generate small and unwanted motions of the machine's moving parts. The machine tool geometric errors are produced by:

- Mechanical imperfections in the machine tool structure;
- Misalignments of the machine's axes;
- Slight angular rotations of axes due to structural deformations;
- Wear of the elements of the machine structure.

They are inherent in machine tools and cannot be eliminated, but may be controlled. Their values change gradually due to wear of the machine. The geometric errors are sometimes referred to as *rigid body errors* since they are measured without specific consideration of load.

A single axis motion has six degrees of freedom resulting in six directions as illustrated in Figure 5. 1.

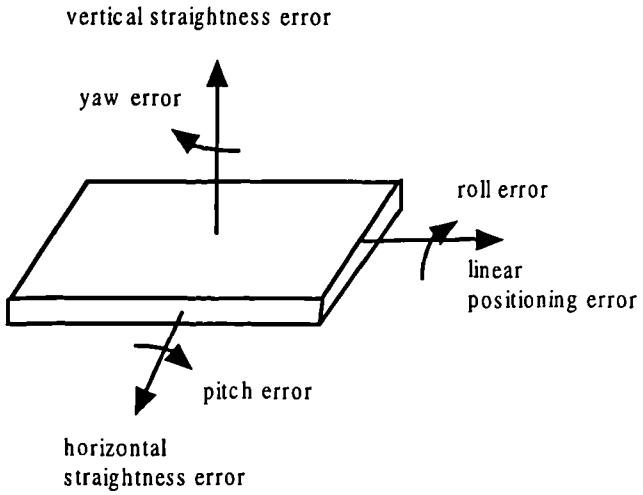

Figure 5. 1. Geometric sources of error for a single axis of a machine tool

The geometric errors can be classified into three categories:

1. *Translational errors* - vary as a function of axis position, produce positional offsets in axis direction due to two classes of error:
   - *linear positioning errors* - in the desired direction of axis travel. Kakino [33] illustrates that the origins of this type of errors are the ball-screw pitch error, backlash between nut and ball-screw etc.
   - *straightness errors* - perpendicular to the desired direction of axis travel. They are profile errors of guide way and could be produced during manufacturing and assembling, due to improper installation of base, shift of weight or due to the bearing interfaces in machine tools.
2. *Rotational errors* - are produced only when a second axis moves, are proportional to movement and are measured in μm/m or ArcSec. They have different denominations:
   - roll error - about the axis of travel
   - pitch and yaw errors - about axes perpendicular to the axis of travel.
3. *Squareness errors* - reflect the angular deviation from the perpendicular of associated axes, do not vary with axis position and are measured in μm/m or ArcSec.

For the three-axis Beaver VC35 machine tool, each axis produces six sources of error (see Figure 5. 1). This results in 18 sources of error when all three axes are considered. An

additional three sources of error consists of squareness errors for the Cartesian machine, bringing the total of geometric errors (rigid body) to 21 as shown in Table 5. 1.

Error	Number of components
Linear positioning errors	3
Straightness errors	6
Rotational errors	9
Squareness errors	3
TOTAL	21

Table 5. 1. Sources of geometric errors in a three-axis CNC machine tool

The constituents of a geometric error can be classified into the following:

- *systematic (repeatable) constituent* - is measured to quantify the accuracy of the machine.
- *random (non-repeatable) error* - is measured to quantify the repeatability and give an indication on the quality or condition of a machine. Measurement technique and temperature can influence the measured value.
- *progressive constituent* - relates to the general form of the error component and is measured during normal calibration.
- *cyclic constituent* - exhibits repetitive pattern of variation and is normally related to transmission (i. e. ball-screw) or position transducer.
- *backlash (reversal) constituent* - is an apparent dead-band during changes in sense of direction due to the mechanical hysteresis.

Rotational and straightness errors normally change slowly and progressively and do not exhibit a cyclic effect. Linear positioning errors are generally progressive in form and have a significant cyclic element. The backlash can be significant due to the ball-screw nut combination and in particularly dominant when a rotary encoder attached to the motor or ball-screw (as in Beaver VC35 machine tool) is used as the feedback element. A linear encoder compensates for positional error due to this type of backlash.

The size and configuration of a machine tool can often give a good indication as to the magnitude and effect of the machine's geometric errors. In general the magnitude and effect of errors are directly proportional to the machine size. For instance, for a machine that has a ball-screw drive and a rotary position transducer, the linear positioning error will normally increase in proportion to axis length. In the case of angular errors, their effect on machine

accuracy is directly related to the length of travel of the rotated axis. Measuring the geometric errors can provide important information about the accuracy of the machine. First, if there are any problems with the machine, the source can be more easily diagnosed by observing which errors are beyond acceptable limits. A secondary benefit of measuring these errors is that the tool positioning error can be calculated using a rigid body kinematics model.

5. 1. 2. Geometric errors measurement techniques

Three types of equipments are specified for the measurement of the geometric errors:

1. *the laser interferometer system* - used for linear and angular errors (pitch and yaw) measurement;
2. *electronic precision levels (talyvels)* - used for straightness errors to the horizontal such as roll.
3. *artefacts (precision squares)* - used for squareness errors.

The Renishaw laser interferometer system, used for measurements, comprises a laser head with detection unit, the signal processing and interpolation being carried out in a separate display unit. The laser head is a compact, robust and reliable Helium-Neon laser with the wavelength of 632.9 nm and resolution 1 nm in a vacuum. It is mounted on a suitably stable tripod, the interferometer and reflector optics being fixed to the table of the machine and the moving quill (or vice versa). The EC10 Compensation Unit is used to obtain corrected environmental results by continual and automatic compensation for variation in air temperature, relative humidity and material temperature.

The laser system uses the technique of interferometry which has the wavelength of light as the basic unit of measurement. An interferometer measures distance by counting the number of wavelengths of light that one element moves, relative to another. It is made possible by using the coherent properties of laser light, where all the light rays have exactly the same wavelength and are in phase with each other.

The Renishaw laser works by outputting one beam of coherent light of a given wavelength. The beam is then split, half of it is reflected at a fixed distance, the other is reflected from a changeable position. When the two beams are returned to the laser, wave interference occurs. The distance travelled can then be calculated.

The movement of the machine is programmed from the Renishaw software; a part program is generated to move the machine to a number of target positions. The error at each position is calculated from data obtained by using the laser interferometer. Data is captured automatically, by sensing that the machine has halted at each target position. The data

captured are repeated for a number of runs in accordance with the international standard ISO 230-2 [5] and the errors at each target are averaged.

The measurement investigation was carried out on the Beaver VC35 vertical machining centre. Details of the machining volume are presented in Table 5. 2. and the schematic diagram of the machine configuration is shown in Figure 5. 2.

Axis	Minimum	Maximum
X	0 mm	700 mm
Y	- 400 mm	0 mm
Z	- 450 mm	0 mm

Table 5. 2. Machining volume for the Beaver VC35 CNC machine tool

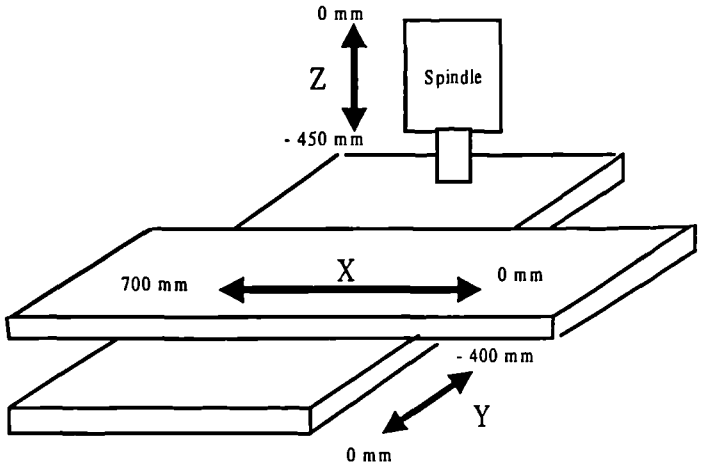

Figure 5. 2. Schematic diagram of the machine configuration

All geometric error components were measured: linear positioning, straightness (horizontal and vertical), yaw, pitch and roll for X and Y axes, squareness. The results of measurement are presented in Appendix C1. The conclusions derived by analysing the measurement results are :

- Linear position accuracy is at its optimum when the machine is in cold state and deteriorates with increasing machine operation (warm-up) time for all 3 axes.
- Generally all linear positional errors vary linearly with respect to axis nominal position and are highest at the end of axis travel range.
- Generally all angular errors are higher towards end of the travel of the respective axis.

In total, only 20 error components were determined because the Z axis roll could not be practically measured with the equipment available. Analysing the configuration and axis

construction of the machine, it is apparent that Z-axis roll error effect on the volumetric accuracy would be negligible (see Equations 5. 1 – 5. 3).

The measurements were done in conformity with the requirements of the standard ISO 230 - 2 [5]:

- Variation in temperature for 12 hours before test should not exceed 4 °C;
- Machine has to be completely assembled and fully operational in unloaded conditions;
- For axes up to 2 metres - approach each target position a minimum of 5 times in each direction and select a minimum of 5 targets positions per metre. Bi-directional runs identify the backlash constituent.

5. 2. Load induced (non-rigid) error measurements

Load induced errors (non-rigid body) errors are produced by varying mechanical loads applied to the machine tool. Loading could be due to:

- *The shift of weight owing to moving machine axes* - generates a new weight distribution on the machine structure;
- *Putting a heavy workpiece on the machine worktable* - which upon movement during machine operation will cause larger deformations than axis weight alone;
- *Forces present during the cutting process* - produce deformations within the machine structure that lead to inaccuracies. The effect of cutting loads can be reduced by careful selection of cutting speeds, tools, feedrate and depth of cut;
- *Variable tool weight* - multiple tool turrets introduce concentrated weight onto the headstock, causing extra loading close to the machining point.

Potentially, loading could change any geometric error component, but the major influence is over the angular error components. Therefore, to eliminate non-rigid effects it is advisable to concentrate on the angular errors.

Ford et al. [3] show that there was a definite correlation between the change in the angular errors produced by the non-rigid effects and the change in the linear positioning errors. The strategy depicted in the paper has been used to uniquely identify the presence of load induced errors on a Beaver VC35 vertical machining centre (its configuration is shown in Figure 5. 2). The measurements were made to identify the effects of moving slide mass, the principal cause of non-rigid errors.

Table 5. 2. shows the measured linear positioning, straightness, angular and squareness errors and how they are affected by non-rigid elements for the Beaver VC35 CNC machine

tool. Changes were seen for both X and Y linear positioning, and these were shown to be linked to angular error changes and could remain unaltered in the developed model. Non-rigid effects altered squareness and some angular errors. The effects of the non-rigid error changes for the machine represented as standard geometric components, can alter the various components of the rigid body model. There were no non-rigid effects apparent in any of the straightness measurements; therefore they remain in the model unmodified.

The denomination "Negligible" in Table 5. 2. means that the magnitude of the error is less than or equal to the machine repeatability value.

Axis	Component	Geometric effect	Non-rigid effect
X	Pitch	-8 arc sec	13 arc sec
	Yaw	5 arc sec	Negligible
	Roll	-20 arc sec	2.5 arc sec
	Linear positioning	55μm	-50μm
	Horiz. straightness	4μm	Negligible
	Vert. straightness	-10μm	Negligible
Y	Pitch	8 arc sec	3 arc sec
	Yaw	-3 arc sec	3 arc sec
	Roll	-2 arc sec	12 arc sec
	Linear positioning	-10μm	5μm
	Horiz. straightness	-2μm	Negligible
	Vert. straightness	-2μm	Negligible
Z	Pitch	4 arc sec	Negligible
	Yaw	4 arc sec	Negligible
	Roll	-	-
	Linear positioning	25μm	Negligible
	Straightness in X	1.5μm	Negligible
	Straightness in Y	2μm	Negligible
-	XY Squareness	13 arc sec	25 arc sec
-	YZ Squareness	7 arc sec	2 arc sec
-	XZ Squareness	-15 arc sec	5 arc sec
TOTAL	21		

Table 5. 2. Summary of measurements from the machine

Ford et al [3] derived a geometric error model for the Beaver VC35 type and configuration as follows:

$$Ex = ex(x) + ex(y) + ex(z) + \underline{\phi y(y,x)}.Z + \phi y(x).Z + \underline{\theta xz(y,z)}.Z + \underline{\theta xy(x,y)}.Y + \underline{\phi z(y,x)}.Y \quad (5.1)$$

$$Ey = ey(y) + ey(x) + ey(z) + \underline{\phi x\,(x,y)}.\,Z + \underline{\phi x\,(y,x)}.\,Z + \underline{\theta yz\,(y,z)}.\,Z - \underline{\phi z\,(x,y)}.X \qquad (5.2)$$

$$Ez = ez(z) + ez(x) + ez(y) - \underline{\phi x\,(x,y)}.Y - \underline{\phi y\,(y,x)}.X - \underline{\phi y\,(x,y)}.X \qquad (5.3)$$

Where X, Y, Z - position co-ordinates of the axes [mm]

ex (x) - X axis linear positioning error [μm]

ey (y) - Y axis linear positioning error [μm]

ez (z) - Z axis linear positioning error[μm]

ey (x), ex(y) - X, Y straightness errors in the XY plane [μm / mm]

ez (x), ex(z) - X, Z straightness errors in the XZ plane [μm / mm]

ez (y), ey(z) - Y, Z straightness errors in the YZ plane[μm / mm]

φx (x), φy (y) - X,Y axis roll errors [μm / mm]

φy (x), φx (y) - X,Y axis yaw errors[μm / mm]

φz (x), φz (y) - X,Y axis pitch errors [μm / mm]

θxy, θxz, θyz - squareness errors in the XY, XZ, YZ planes [μm / mm]

Ex, Ey, Ez - actual error movement of X, Y, Z axes [μm]

$\underline{\phi x\,(x,y)}$ - $\phi x\,(x)$ can be represented as one component relating to rotation around the X axis, as a function of X and Y position.

$\underline{\phi y\,(x,y)}$ - $\phi y\,(x)$ can be represented as one component relating to rotation around the X axis, as a function of X and Y position.

$\underline{\phi z\,(y,x)}$ - $\phi z\,(y)$ can be represented as one component relating to rotation around the Y axis, as a function of X and Y position.

$\underline{\phi x\,(y,x)}$ - $\phi x\,(y)$ can be represented as one component relating to rotation around the Y axis, as a function of X and Y position.

$\underline{\phi y\,(y,x)}$ - $\phi\, y\,(y)$ can be represented as one component relating to rotation around the Y axis, as a function of X and Y position.

$\underline{\theta xy\,(x,y)}$ - XY squareness magnitude changes as a function of the X and Y axis positions.

$\underline{\theta xz\,(y,z)}$ - XZ squareness magnitude changes as a function of the Y and Z axis positions.

$\underline{\theta yz\,(y,z)}$ - YZ squareness magnitude changes as a function of the Y and Z axis positions

Thus all of the significant non-rigid error components could be inserted into the error model for the Beaver VC35 machine as matrix elements (underlined elements). Underlining of the equation portion indicates the changing error components.

Because the non-rigid error contribution to geometric errors is outside the scope of this thesis, the Equation (5. 1 - 5. 3) were used in Chapter 6 without containing matrix elements. The underlined terms have only one single value when the equations are used for two axes simulation including geometric errors (see Equations 6. 33 and 6. 34).

5. 3. Modal analysis

5. 3. 1. Theoretical approach to modal analysis

The vibration which occurs in most machines, structures and dynamic systems is undesirable, not only because of the resulting unpleasant motions, the noise and the dynamic stresses (which may lead to fatigue and failure of the structure or machine), but also because of the energy losses and the reduction in performance which accompany the vibrations. The successful vibration reduction of machine tools during the machining process can improve productivity, increase quality and reduce tool wear.

Beards [103] showed that the dynamic analysis could carried out by following a three-stage approach:

1. *Develop a mathematical or physical model of the system* – whose derivation is not easy because the purpose of the model is to give useful and realistic information about the dynamics of the real system. Therefore, a number of simplifying assumptions can often be made during the modelling stage:
   - A distributed mass may be considered as a lumped mass;
   - The effect of damping in the system may be ignored in particular cases (i. e. when only resonance frequencies are needed or the dynamic response is required at frequencies very different from a resonance etc.);
   - A non-linear spring may be considered linear over a limited range of extension;
   - Certain elements and forces may be ignored completely when their effect is small.
2. *Write the equations of motion for the model* - by analysis of the free-body diagrams drawn for each element of the model or by using an energy method (such as Lagrange equation). The natural frequencies, modes of vibration, general response and stability are obtained from the characteristic or frequency equation derived from the equations of motion.

3. *Solve the equations of motion with the relevant excitation function* (force or motion, including harmonic, step and ramp) present - in order to determine the dynamic stress, noise, output position or steady state error. Usually, two forms of excitations are considered when studying vibrations in mechanical systems:
   - Release from a non-equilibrium state (i. e. from an initial non-zero position and / or velocity) for the case of free vibrations
   - Sinusoidal input - for the case of forced vibrations.

Analysis of vibration plays a role in product design, production test, architecture, and process control. Equally important is the role vibration analysis plays in improving machine performance and reliability. Analysing vibrations requires the following general procedure:

- Evaluate masses and elasticity of parts of the system
- Estimate the amount of friction
- Replace the actual mechanical system by an approximately equivalent system of masses, springs and dampers
- Write the differential equations of motion for the equivalent system
- Solve the equations and interpret the results.

Generally speaking, there are three types of vibration:

1. *Free vibration* - is a naturally characteristic vibration of a system with the amplitude decaying with time and produced by an initial impact;
2. *Forced vibration (steady deterministic vibration)* - is expressed as a Frequency Response Function (FRF) and happens at the frequency of the exciting force. The amplitude of motion depends on the amplitude of the force and on the frequency of the force. The natural frequency of the system ω_n is represented as:

$$\omega_n = \sqrt{\frac{k}{m}} \qquad (5.4)$$

   where ω_n - the natural frequency of the system m - the mass of the system
   k - the spring constant (force per unit deflection) or stiffness
3. *Self-excited vibration* - occurs when a steady input of energy is modulated into vibration. In metal cutting, an example of self-excited vibration is the chatter, which occurs between a tool and a workpiece and draws its excitation energy from the cutting process itself.

5. 3. 2. Modal analysis and frequency response measurements of a Beaver VC35 milling machine

Modal analysis was performed by a representative of AMTRI (Advanced Manufacturing

Technology Research Institute) under my guidance.

Brief cutting tests were carried out to establish the performance of the machine when operating under normal working conditions. The following conditions existed for the tests:

Tool type: 8 Teeth, Sandvik R262.2-100M (Diameter = 100 mm)

Material: S G Cast Iron Spindle speed = 350 rpm

X-axis feedrate = 150 mm / min Depth of cut = 3 mm Width of material = 70 mm

During the cutting trials, the vibration was measured using accelerometers fixed to the spindle nose and table, in all three orthogonal axes. The signals were processed using a Hewlett Packard 3567OA FFT analyser into plots of amplitude of vibration versus frequency.

The prominent vibration measured during cutting trials are at 300 Hz for spindle nose (Figure 5. 3) associated with electrical oscillation within spindle motor, and at 43. 5 Hz for working table (Figure 5. 5) due to the cutter tooth impact (8 times spindle speed). These vibrations are related to the cutting process and they do not appear to be amplified by any resonances (i.e. chatter vibration).

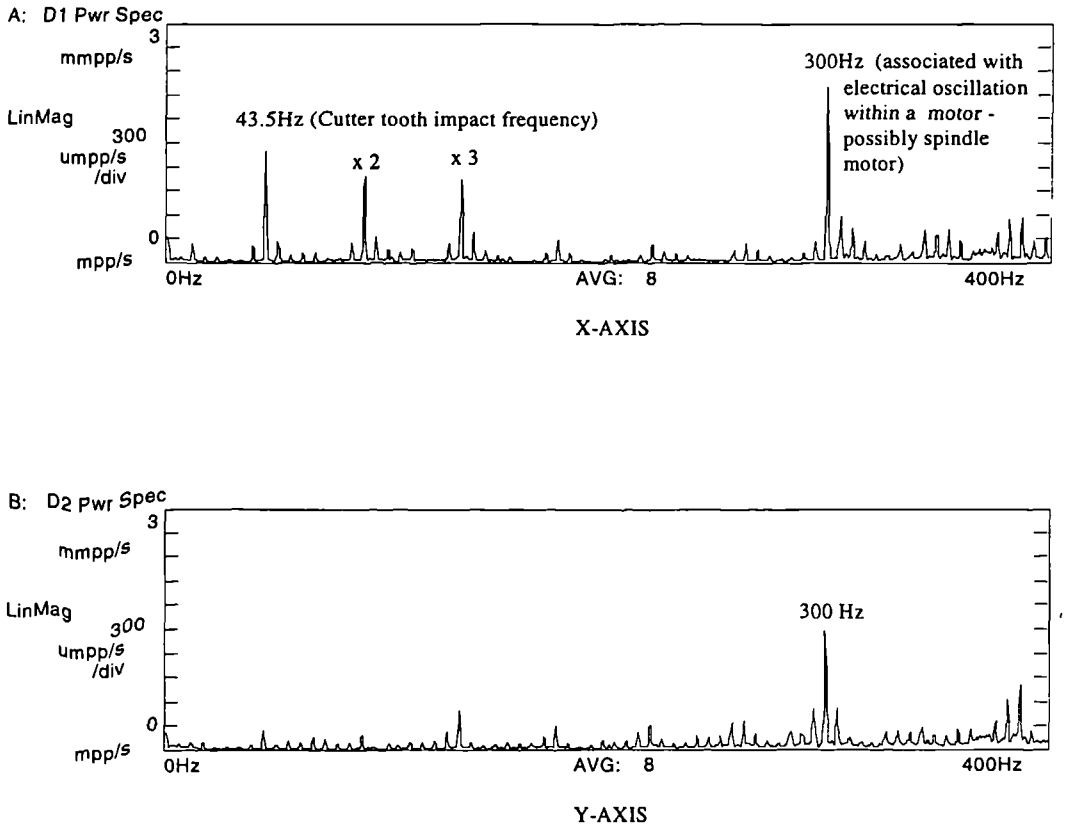

Figure 5. 3. Amplitude and frequency content of vibration measured on spindle nose during cutting trials (X-axis direction and Y-axis direction)

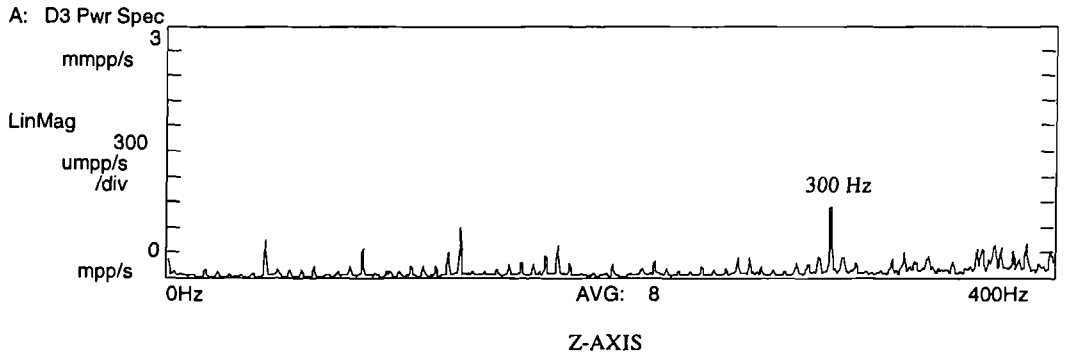

Figure 5. 4. Amplitude and frequency content of vibration measured on spindle nose during cutting trials (Z-axis direction)

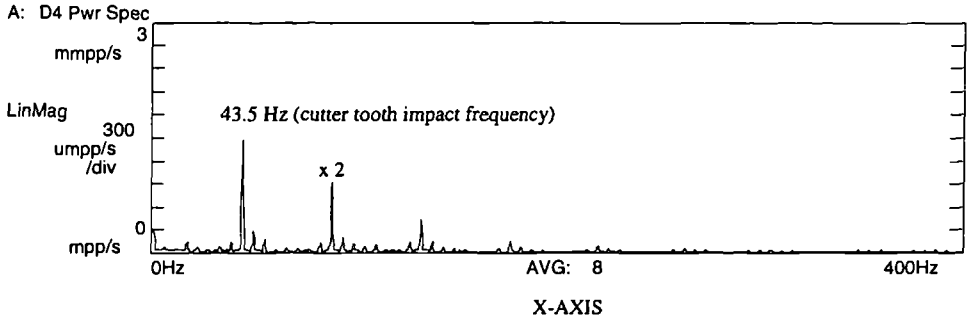

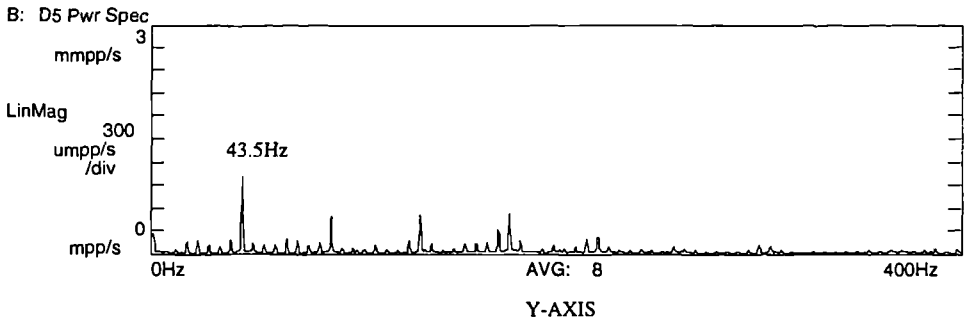

Figure 5. 5. Amplitude and frequency content of vibration measured on table during cutting trials (X-axis direction and Y-axis direction)

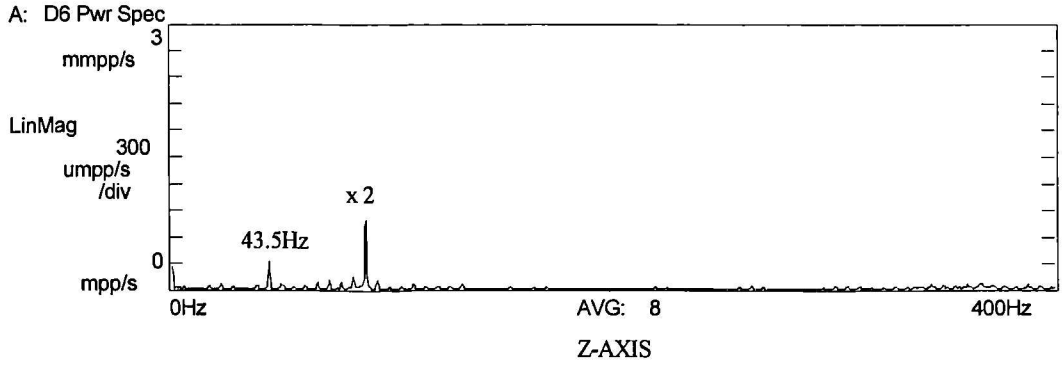

Figure 5. 6. Amplitude and frequency content of vibration measured on table during cutting trials (Z-axis)

Next, the frequency response of the structure was measured using the experimental set up presented in Figure 5. 7. An electrohydraulic shaker applied an oscillating force between the tool and an angle bracket attached to the machine table. The applied dynamic force was measured using a piezoelectric force transducer trapped between the shaker and the wheelhead. The response of the structure was measured using a relative displacement transducer fixed in parallel with the shaker. The displacement and force signals were input to the analyser for processing into the form of flexibility versus frequency plots. The peaks in the frequency response plots are indicative of the resonant behaviour of the structure.

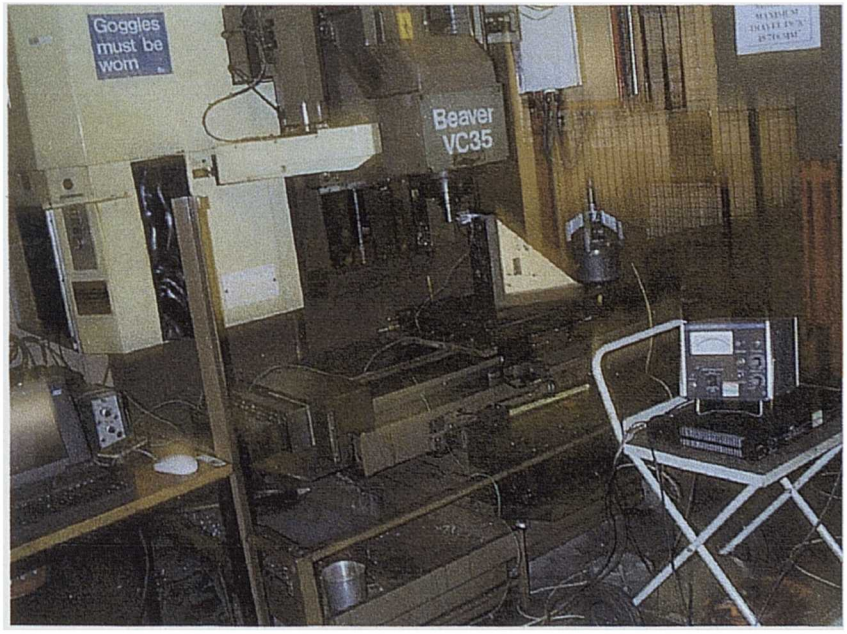

Figure 5. 7. Experimental arrangement for measuring vibrations of a milling machine

Figures 5. 8. and 5. 9. show X, Y and Z-axis frequencies of the machine with the spindle head in its lowest and mid height positions, respectively. It can be seen that the most prominent resonances occur at 51 Hz, 64 Hz, 113 Hz, 133 Hz and around 175 Hz. The amplitude of the first four resonances is the greatest in the X-axis of the machine with the last resonance more prominent in the Y and Z axes of the machine. The sources of these resonant frequencies were determined from the measurements described later.

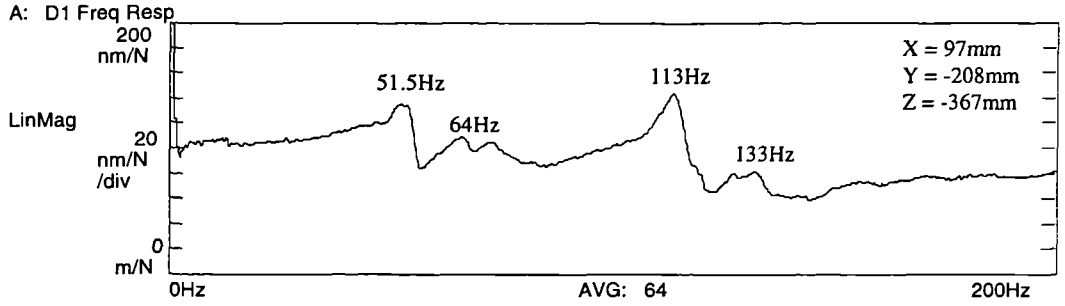

X -AXIS FREQUENCY RESPONSE

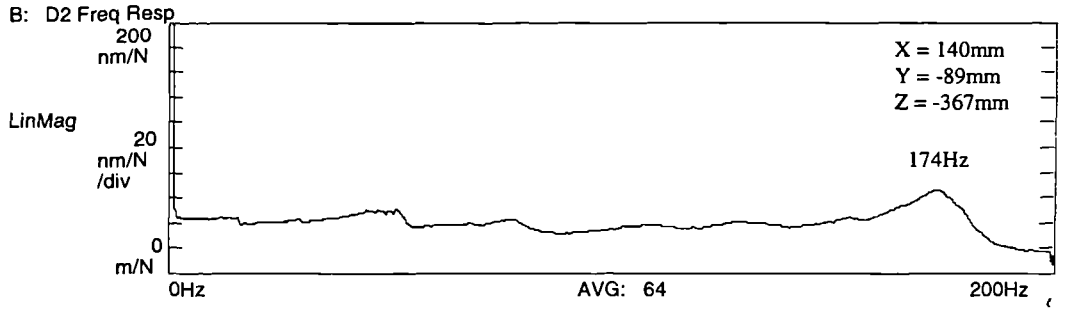

Y-AXIS FREQUENCY RESPONSE

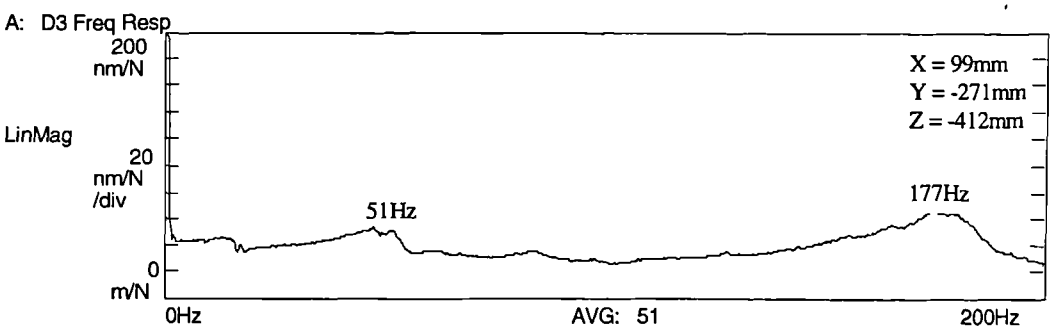

Z-AXIS FREQUENCY RESPONSE

Figure 5. 8. Frequency response in X, Y and Z axes with spindle head in lowest position

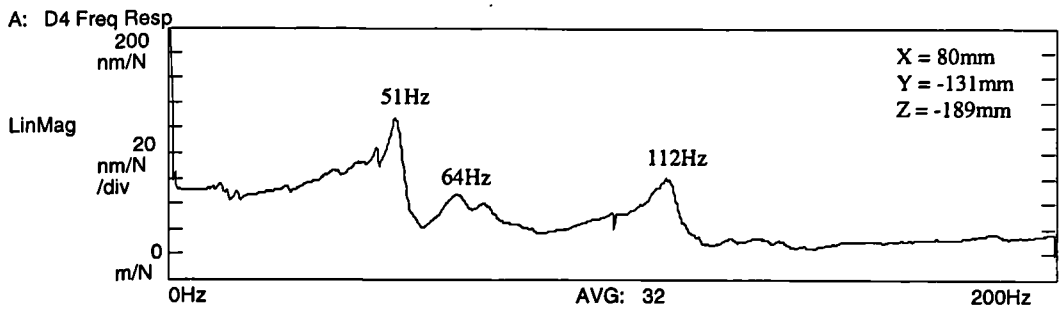

X-AXIS FREQUENCY RESPONSE

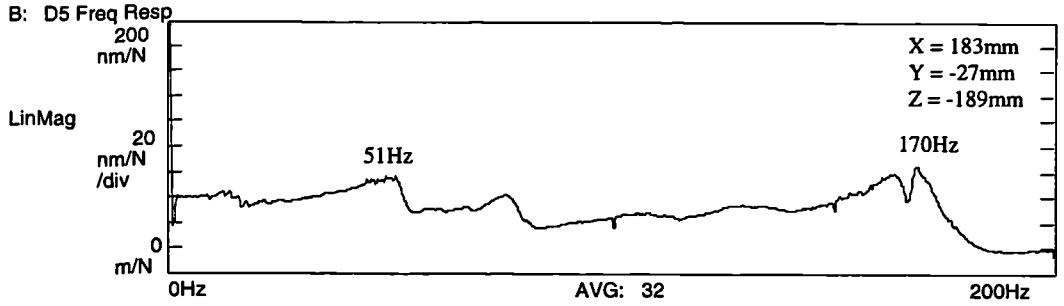

Y-AXIS FREQUENCY RESPONSE

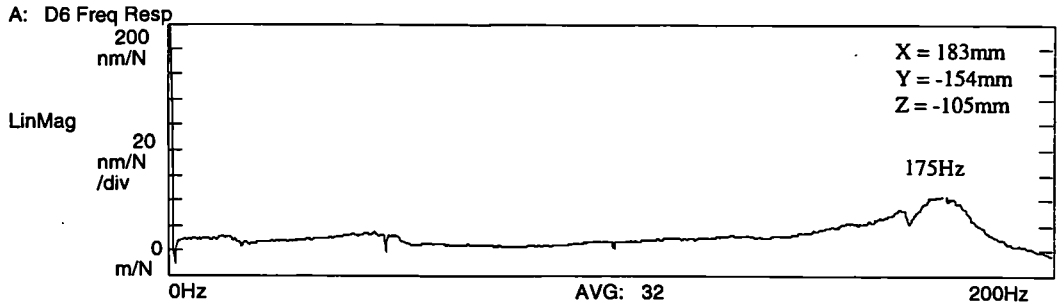

Z-AXIS FREQUENCY RESPONSE

Figure 5. 9. Frequency response in X, Y and Z axes with spindle head in mid-height position

The next part of the investigation was a modal analysis of the machine structure. First of all, a 3D representation of the machine structure (see Figure 5. 10) was developed considering the co-ordinates of the actual machine. The STAR system software displayed the deflection shapes associated with the measured resonant frequencies using this structural model produced by its 3D mesh generator. The software created deflection shapes by analysing the structure from frequency domain measurement data.

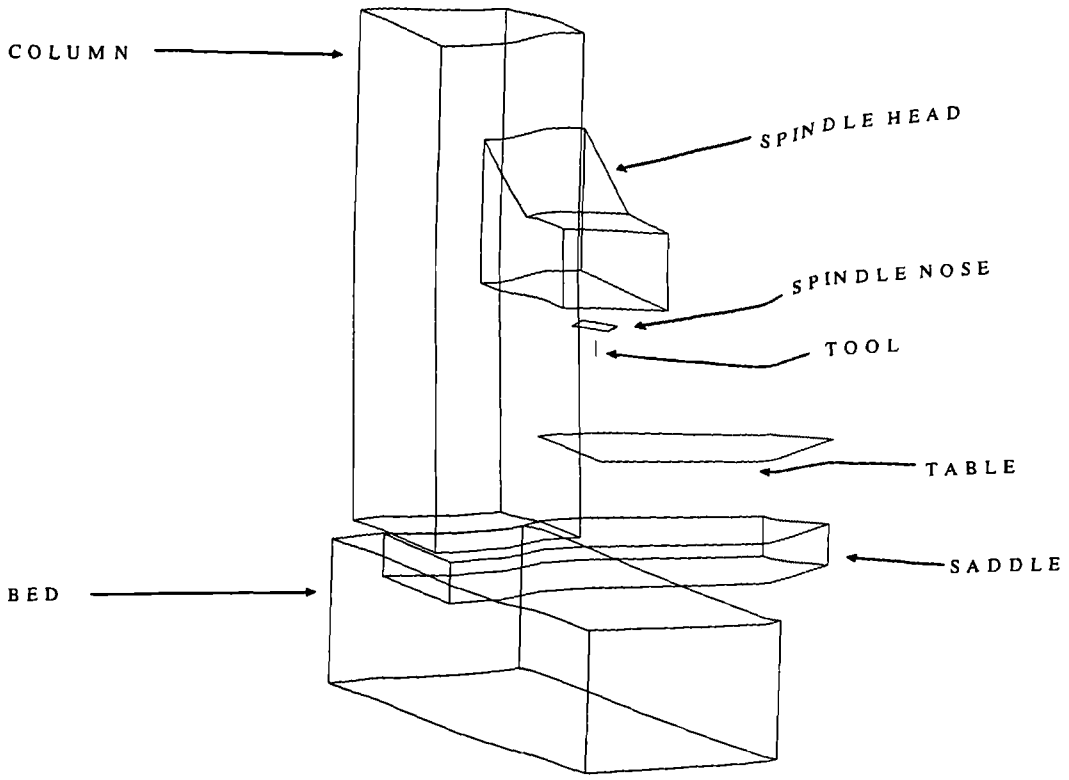

Figure 5. 10. 3-D representation of the structure used for modal analysis

The modal software was able to compute and display in animation the shape taken up by the structure at each of its resonant frequencies. The frequency-domain animation was performed because the operating deflection shapes and mode shapes show the motion of a structure at a single frequency and the overall vibration of a structure depends on the influence of multiple frequencies. The shapes were superimposed and the colour red was applied to show how the structure was moving at a certain frequency.

Figures 5. 11. to 5. 15 show the mode shapes of the structure at 51, 64, 112, 133 and 180 Hz respectively. The first three mode shapes show similar flexibilities. There appears to be a torsional flexibility of the machine bed and a bending of both ends of the saddle. There is also evidence of some torsion in the column allowing the spindle head to rock side to side as one body with the column. The fourth mode at 133 Hz shows the spindle head rocking side to side relative to the column whereas the fifth mode at 180 Hz show the spindle head rocking vertically relative to the column along with some bending of the saddle.

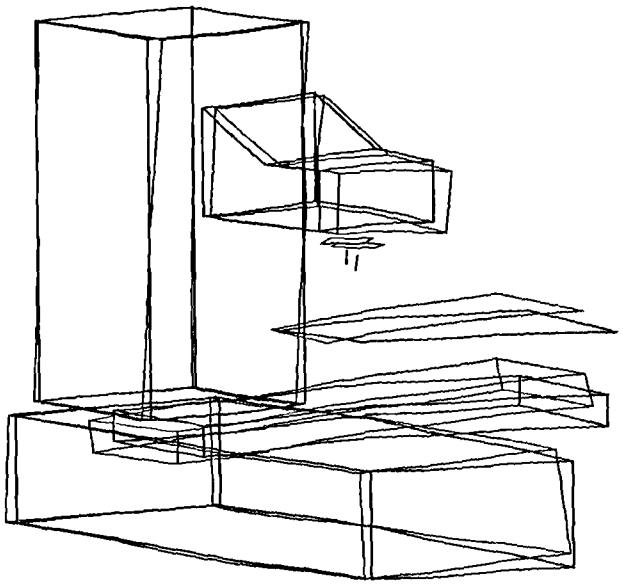

Figure 5. 11. Mode shape of structure at 51 Hz

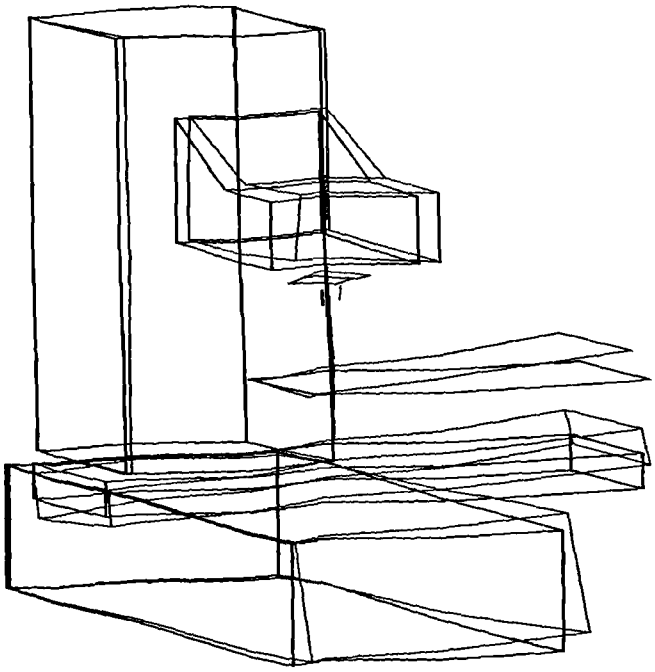

Figure 5. 12. Mode shape of structure at 64 Hz

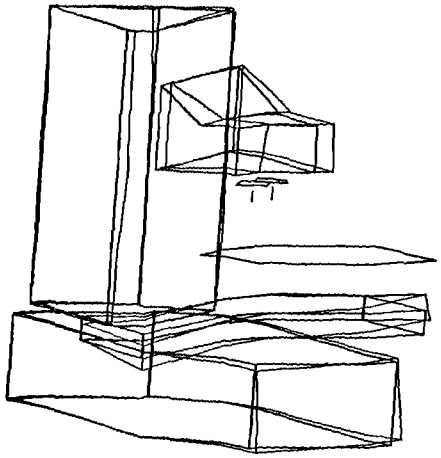

Figure 5. 13. Mode shape of structure at 112 Hz

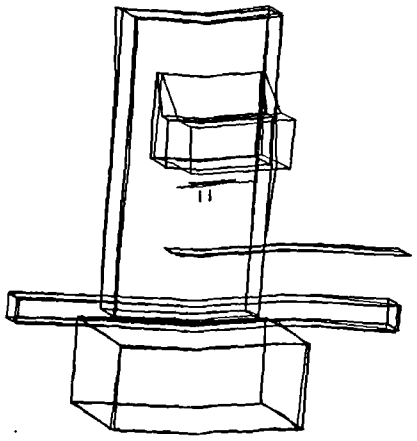

Figure 5. 14. Mode shape of structure at 133 Hz

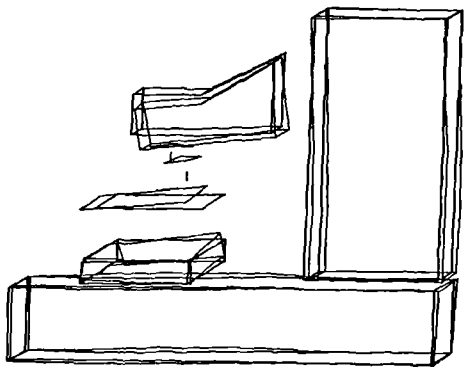

Figure 5. 15. Mode shape of structure at 180 Hz

Frequency response measurements were also taken of the drive motors, ball-screws and encoders for the three axes of movement. This was carried out by using an instrumented hammer to excite the component under test and measuring the resulting response of the component. The force applied was measured using a load cell trapped behind the head of the hammer and the response was measured using an accelerometer attached to the component under test. The analyser generated the frequency responses for the various components.

Figure 5. 16 shows the resonant characteristics of the X-axis drive motor. Two distinct resonances can be seen in the Y-axis and Z-axis with little evidence of resonances in the X-axis (along length of motor) over 200 Hz frequency range. The rotary encoder is attached to the motor so, the frequency response measurements taken on the encoder are the same as taken on the motor.

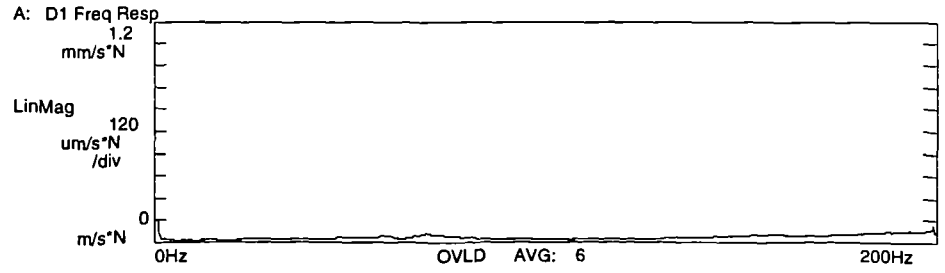

Measured in machine X-axis

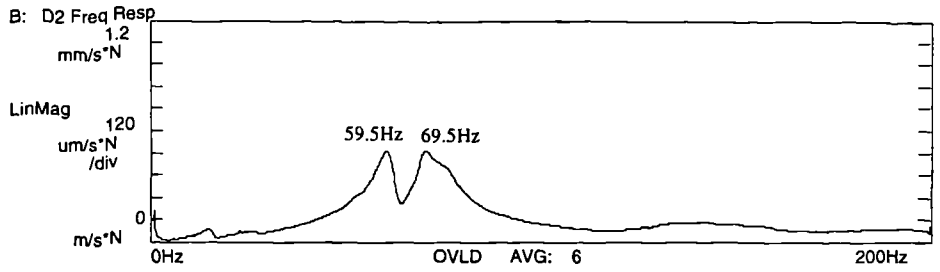

Measured in machine Y-axis

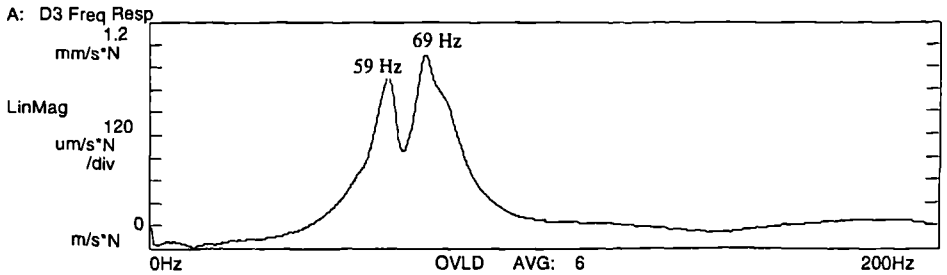

Measured in machine Z-axis

Figure 5. 16. Frequency response measurements of X-axis drive motor

Figure 5. 17 shows the frequency response measurements taken on the Y-axis drive motor. In the X-axis direction there is a resonance at 169 Hz and in the Z-axis direction there is a resonance at 142 Hz. No resonance was measured in the Y-axis direction within a 200 Hz bandwidth.

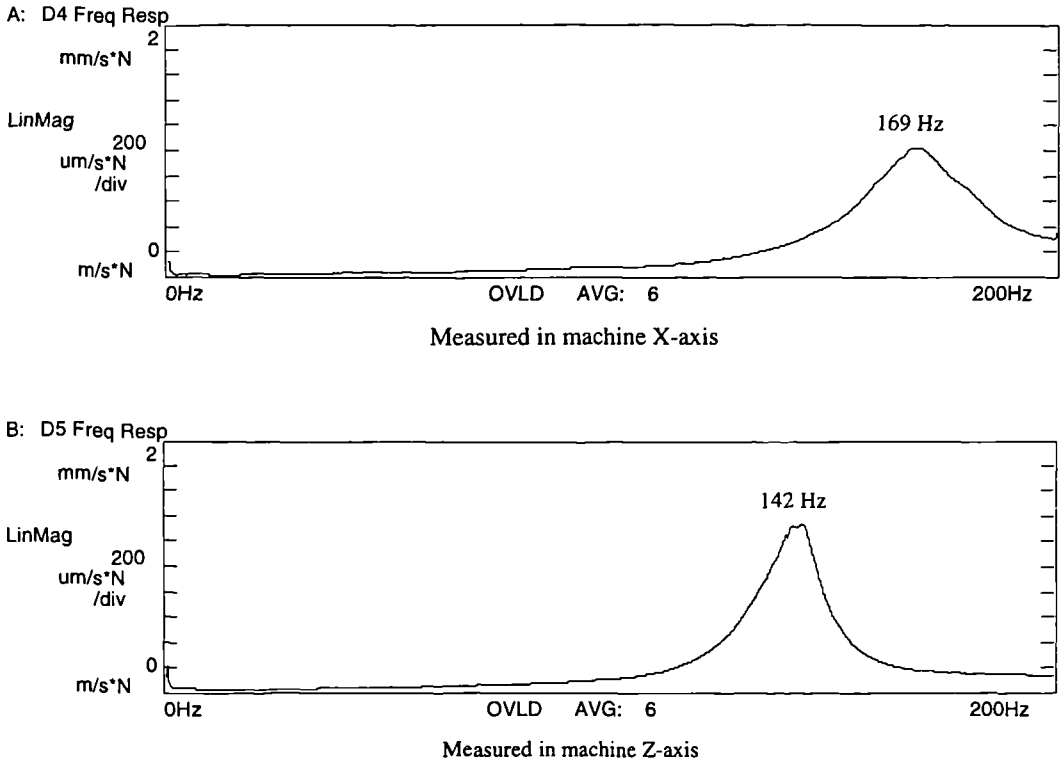

Figure 5. 17. Frequency response measurements of Y-axis drive motor

It was only physically possible to take a frequency response of the Z-axis drive motor in the X-axis direction and Figure 5. 18 shows there is a resonance at 132 Hz.

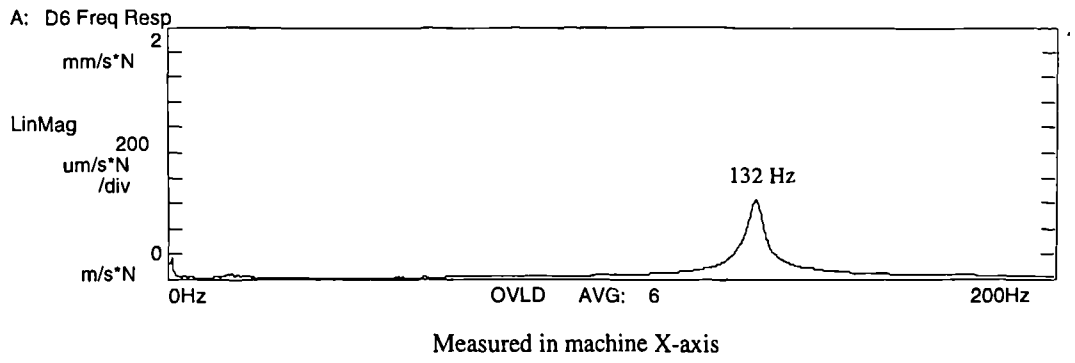

Figure 5. 18. Frequency response measurements of Z-axis drive motor

Figure 5. 19 shows the frequency response measurements of the X-axis ball-screw having two values for resonance: 119 Hz for X = 0 mm (full length of ball-screw)

240 Hz for X = 354 mm (approximately half length of ball-screw)

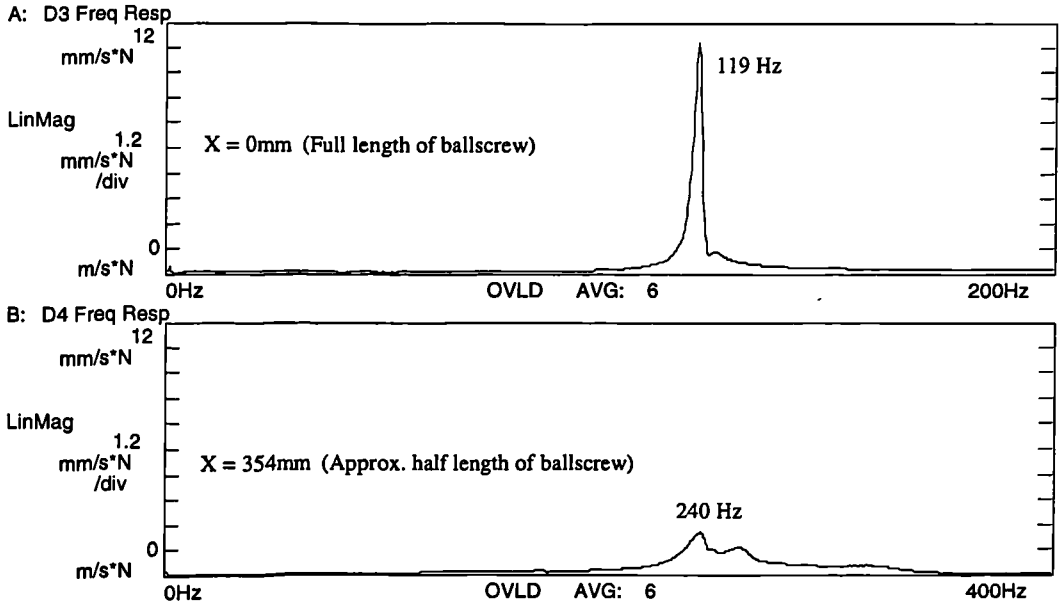

Figure 5. 19. Frequency response measurements of X-axis ball-screw

Figure 5. 20 shows the frequency response measurements of the Y-axis ball-screw having two values for resonance: 95 Hz for Y = 0 mm (full length of ball-screw)

122 Hz for Y = - 159 mm (approximately half length of ball-screw)

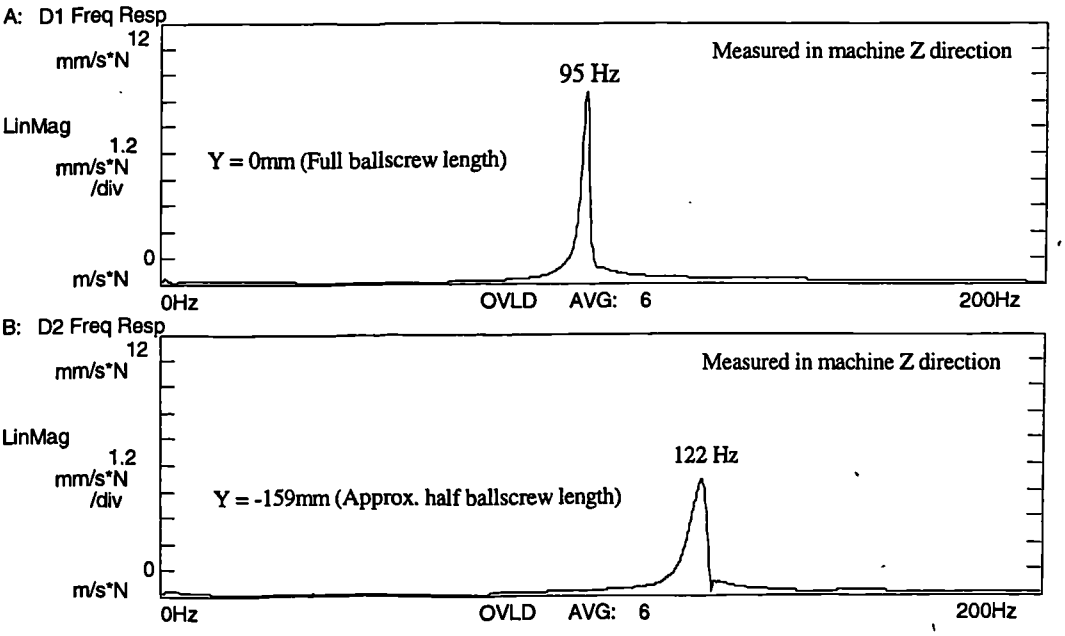

Figure 5. 20 Frequency response measurements of Y-axis ball-screw

It was not possible to remove the cover for the Z-axis ball-screw for practical reasons, Therefore, a frequency response measurement for this ball-screw was not obtained.

The theoretical calculations of the stiffness for the system composed of ball-screw - bearings - nut are presented in Appendix C4. It is obvious that is necessary to consider a more complicated system than one consisting of the axial stiffness of the both halves of the screw, bearings and nut connected in series. More details about the elements introduced into the model with explicit damping coefficients are discussed in Chapter 6.

The modes detected during modal analysis mainly involved "*whole body*" movement of parts of the machine. They could be due to bending or twisting of the saddle or table, but it was considered that these modes would only have an effect on transverse vibration. However, the levels of transverse vibration measured using accelerometers were all low. So no attempt was made to use the results of the modal analysis to calculate the stiffness and damping coefficients for the various parts of the system.

5. 3. 3. Measurement of the drive system vibrations using piezoelectric accelerometers

Mono-axial charge output accelerometers produced by D. J. Birchall (DJB) have been used for measuring the motion of the motor, belt drive, ball-screw and worktable / saddle. They include a truncated hollow piezoceramic cone, valve and concentric reaction mass whereas the sensing element is preloaded. This method offers good reliability, a rugged waterproof construction together with low sensitivity to environmental changes. More information about the accelerometer used is shown in Table 5. 3.

Type	Charge Sensitivity	Weight	Temperature range	Resonant frequency
A/20	25 / 38 pC /g	17 gm	-50 ° C / + 250 ° C	28 kHz

Table 5. 3. Technical characteristics of accelerometers used in measurements [86]

An accelerometer is a transducer which produces an electric charge proportional to the applied acceleration. A mass is supported on a piece of piezoelectric ceramic crystal which is fastened to the frame of the transducer body. Piezoelectric materials have the property that if they are compressed or sheared, they produce an electric potential between their extremities, and this electric potential is proportional to the amount of compression or shear. As the frame experiences an upward acceleration it also experiences a displacement. Because the mass is

attached to the frame through the spring-like piezoelectric element, the resulting displacement has different phase and amplitude than the displacement of the frame. This relative displacement between the frame and mass causes the piezoelectric crystal to be compressed, giving off a voltage proportional to the acceleration of the frame.

For frequencies much lower than the resonance frequency of the mass of the combined stiffness of the whole accelerometer system, the acceleration of the mass will be virtually the same as the acceleration of the whole transducer, and the charge produced will be proportional to the acceleration to which the transducer is subjected. This charge can be measured electronically at the output terminals of the accelerometer and is used for the accurate determination of vibration amplitude, frequency and waveform.

The accelerometers output signals need to be further amplified because their levels are inadequate for monitoring and control purposes. Another reason for amplifying these signals is the necessity of recovering the measurement data from additional data and noise of the accelerometer output. A charge amplifier is usually used for this purpose. The capacitive feedback of the amplifier compensates for the deviation in input signal due to varying capacitive loading of the accelerometer. In this way any length of cable can be used between the accelerometer and amplifier without changing the sensitivity of the measuring system.

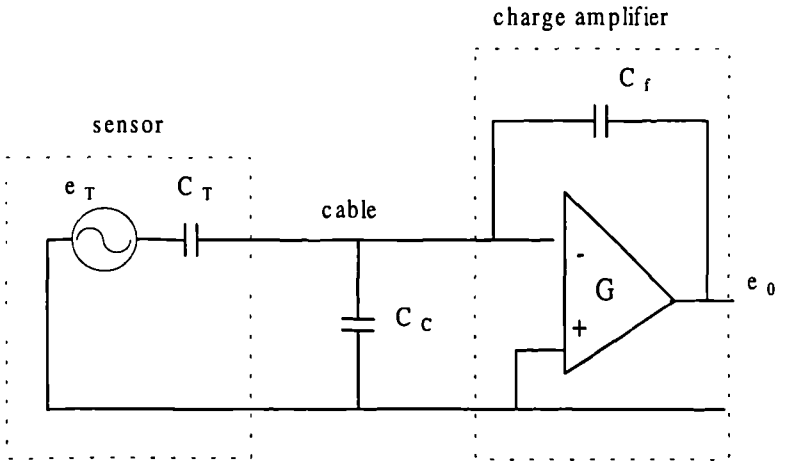

Figure 5. 21. Electrical diagram of the connection between accelerometer and charge amplifier [86]

From Figure 5. 21, the voltage e_0 at the output of the charge amplifier will be:

$$e_0 = \frac{e_T \times C_T}{C_f + \frac{C_c}{G}} \approx \frac{Q_T}{C_f} \qquad (5.5)$$

where e_T – accelerometer voltage [V] C_T – accelerometer capacitance [pC]

C_C – cable capacitance [pC] C_f – amplifier capacitance [pC]

G - loop gain of charge amplifier Q_T – accelerometer electrical charge

The main benefit of the charge amplifier is the virtual exclusion of the transducer connecting lead as the determinant of the system calibration. Still two drawbacks are noticeable:

1. A large amount of amplification is necessary to compensate for the great loss of signal voltage;
2. The noise increases with increasing cable length.

One important parameter for accelerometers is the *sensitivity* (mV/g) which allows the calculation of the measured acceleration from the voltage output generated by the charge amplifier connected to the accelerometer. Harris and Crede [87] state that there are three categories of methods for sensitivity calibration (derivation of sensitivity factor):

- *Absolute methods* - laser interferometry, earth's gravitational field, reciprocity techniques;
- *Comparison methods* - sinusoidal frequency-dwell method, sinusoidal swept-frequency method, random-excitation-transfer-function method;
- *Calibrators* which suppose the use of a vibration exciter with a known vibration level (physical pendulum, electrodynamic shaker etc.).

One of the comparison methods was used for the calibration of DJB accelerometers. The method consists of mounting in a back-to-back arrangement the accelerometer with the unknown sensitivity together with a reference accelerometer (see Figure 5. 22).

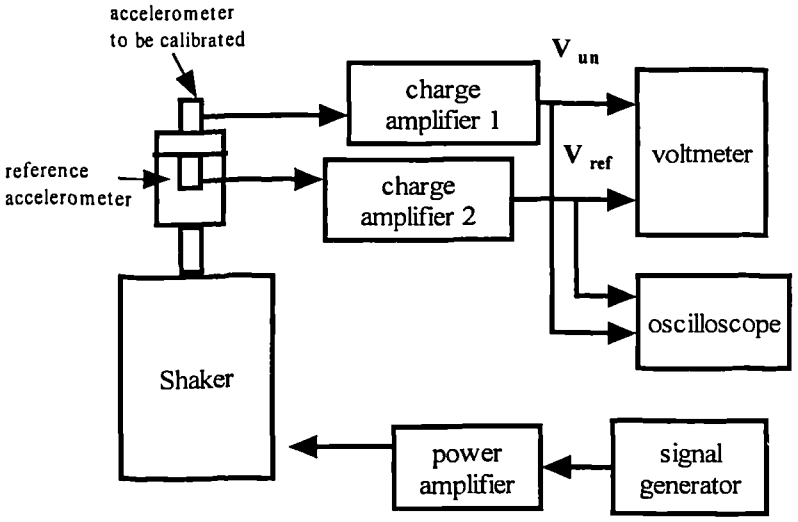

Figure 5. 22. Experimental set up for the comparison method

This arrangement is excited by a suitable vibration source producing a sinusoidal

acceleration with constant frequency and amplitude. The calibration frequency and acceleration level have to be within the normal working range of the accelerometer.

The output signals of the signal conditioning units (charge amplifiers) are measured individually by a high quality voltmeter with a known accuracy and an oscilloscope observes the shape of these signals (they have to be proportional).

The ratio of the accelerometers outputs is also the ratio of their sensitivities because the input acceleration is the same on both devices and the characteristics of the accelerometers are linear in frequency and dynamic range.

$$g_{ref} = g_{un} \tag{5. 6}$$

$$\frac{V_{ref}}{S_{ref}} = \frac{V_{un}}{S_{un}} \tag{5. 7}$$

$$S_{un} = S_{ref} \times \frac{V_{ref}}{V_{un}} \tag{5. 8}$$

where g_{ref}, S_{ref} - the measured acceleration and sensitivity of reference accelerometer

g_{un}, S_{un} - the measured acceleration and sensitivity of the unknown accelerometer

V_{ref}, V_{un} - the output voltage for the reference and unknown accelerometer

The instrumentation used for the calibration of the DJB A / 20 accelerometers is: Spectrum Analyzer HP3566A, voltmeter FLUKE 77, shaker LDS V201, power amplifier LDS PA 25E, reference accelerometer KISTLER 8630C50.

5. 3. 3. 1. Vibration measurements for closed-loop position control

A swept-sine signal generated by a PC Spectrum Analyzer HP3566A with the amplitude 250 mV is introduced as an external perturbation into the pre-amplifier of the Beaver VC35 CNC machine tool. The accelerometers were fitted on the machine on the following configurations:

a) *Two accelerometers on the first (driving) pulley and two accelerometers on the second (driven) pulley* to measure the torsional resonance frequencies of the system consisting of belt and pulleys (see Figure 5. 23). The two accelerometers were fitted diagonally opposite each other facing in the same sense of rotation close to the flange and were held in place by epoxy glue. Normal cables were used to transmit the output signal from the accelerometers to the charge amplifiers because the small amplitude (250 mV) of the excitation signal did not produce a movement of the driving pulley greater than 90°.

The arrangement of the accelerometers was chosen so that if there were to be a combination of torsional and transverse vibration these could be deduced by taking the sum and difference of the two readings. From the measured data it was determined that the vibration was almost entirely torsional.

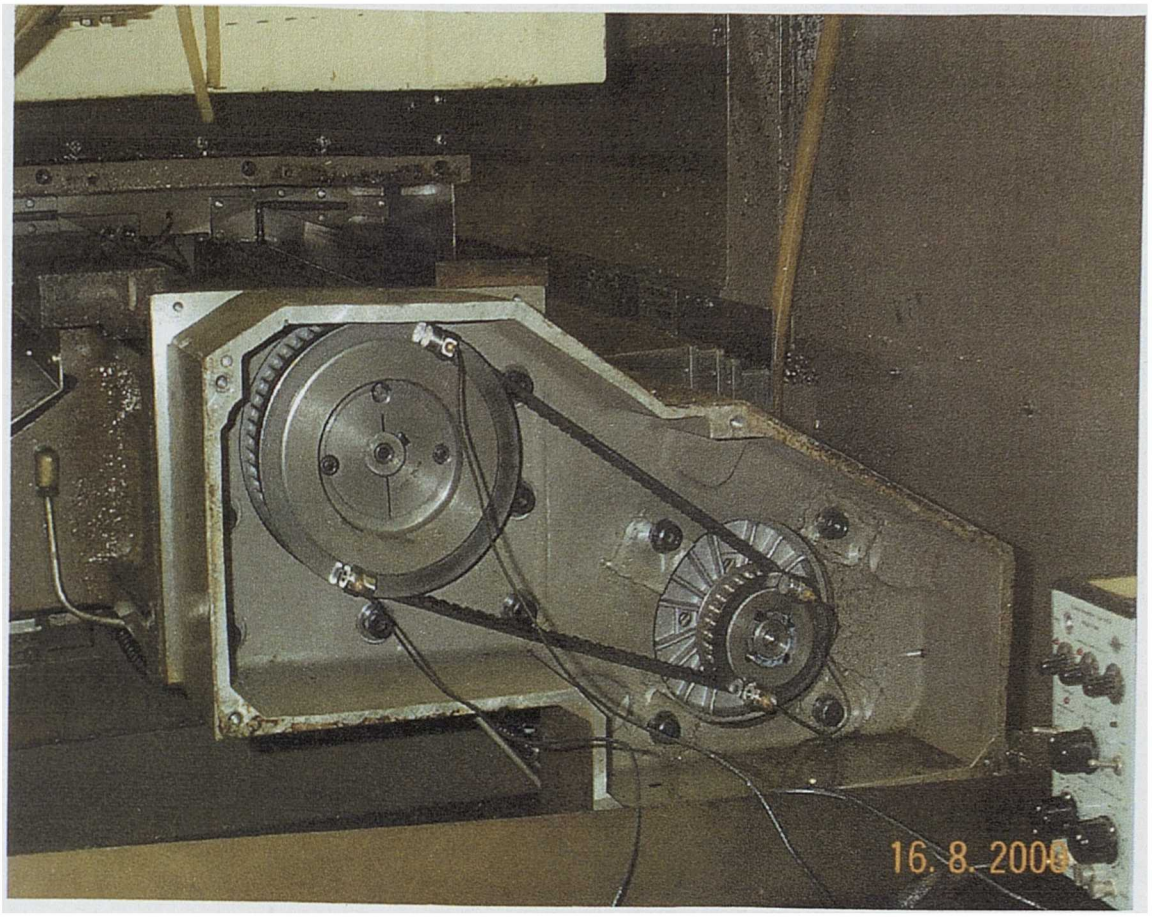

Figure 5. 23. Experimental arrangement of the four accelerometers for X-axis drive

The stiffness and the coefficient of viscous damping for the belt were calculated on the basis of the peaks of vibration activity (79 Hz for X-axis and 92 Hz for Y-axis – Appendix C2) when the CNC machine tool is functioning with closed-loop position control (see Appendix B5). A schematic diagram of the experimental setup is presented in Figure 5. 24 where the arrows indicate the directions in which the accelerometers measure displacements.

By comparing the results shown in Appendix C2 with the phenomena observed during the measurement session (a video was taken of the belt vibration), it was determined that the resonance frequencies are situated in the interval 85-179 Hz as follows:

85 Hz Belt resonance;

160 - 171 Hz	Upper part of the belt is vibrating
171 - 173 Hz	Lower part of the belt is vibrating;
173 - 179 Hz	" Beating " belt (both parts are vibrating simultaneously;
179 - 200 Hz	Flat belt (no resonance)

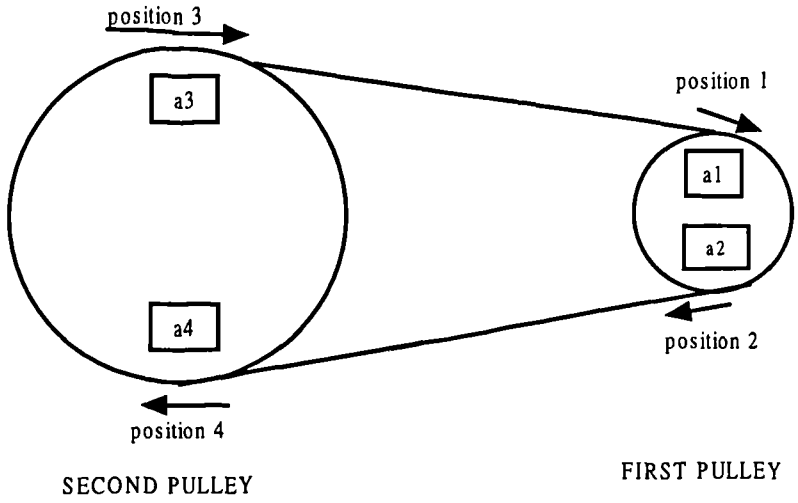

Figure 5. 24. Schematic representation of the experimental arrangement of the four accelerometers

b) One accelerometer on the driven pulley and one on the nut

An accelerometer screwed to a magnetic clamp was used to monitor the axial vibration of the table. After that, the accelerometer situated on the nut was moved on the worktable and some differences appeared in the results.

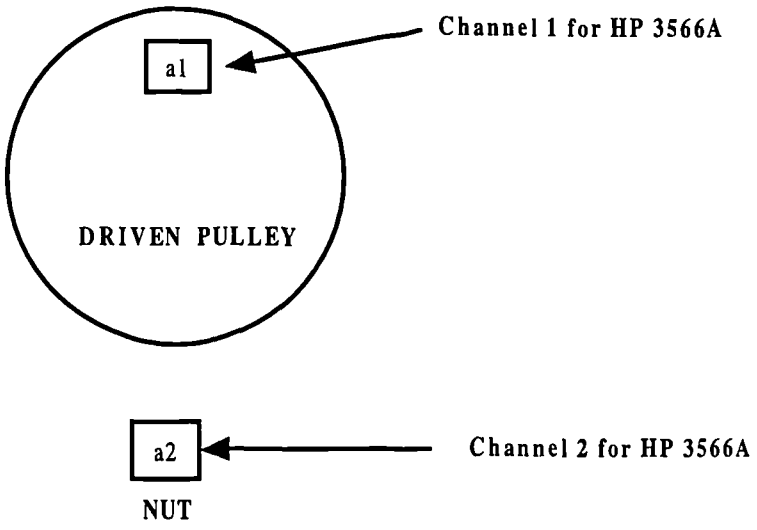

Figure 5. 25. Experimental arrangement of two accelerometers

This suggests that the nut is not attached solidly to the worktable (a spring/damper element has to be considered for this arrangement).

c) *One accelerometer on the deep groove ball bearing and one on the driven pulley*

In this way was determined the vibrations for axial movement and radial movement parallel to the belt and the transverse vibration of the deep groove ball bearing. It is noteworthy that all transverse vibrations observed were of low level.

d) *One accelerometer on the thrust bearing and one on the driven pulley*

The results show the vibrations for axial movement and radial movement of the thrust bearing versus driven (second) pulley. By analysing the results, it is obvious that the axial vibration of the main ball-screw thrust bearing is prominent.

The same experimental set-ups were used to determine the axial and torsional vibrations for the synchronous belt system and the ball-screw of the Y-axis of the machine.

The measured resonance frequencies of the various elements of the drives were used to calculate the damping coefficients as it was shown in Appendix B5.

The following conclusions could be derived by analyzing the experimental results from Appendix C2:

- A peak in the belt drive transfer function was observed at 79 Hz for X -axis and at 92 Hz for Y-axis;
- It was possible to use the model to refine the estimate of the belt stiffness;
- With the revised stiffness included in the explicit damping model, it was possible to estimate a value for the damping in the belt;
- The behaviour of the belt is more complex than that suggested by the theory used to derive its effective torsional stiffness;
- Transverse vibration of the belt may be responsible for some of the other vibration peaks;
- The possibility of the belt's going slack on one side then the other as it vibrates may bring in non-linear behaviour which will be studied in detail in Chapter 6.

5. 3. 3. 2. Vibration measurements for open- loop position control

To increase the amplitude of the input signal, it was decided to "open" the position loop for the Y-axis drive. The details of the procedure are presented in section 5. 6. 2. From the Bode diagrams measured for this arrangement, there was a resonance frequency at 35 Hz which was assumed to be due to the spring / damper existent between saddle and nut.

To confirm this theory, an input signal in the form of swept sine with amplitude 750 mV,

generated by the HP 3566A, was applied to the pre-amplifier of the Y-axis. The output was the signal generated by the charge amplifier connected to the accelerometer.

The Signal Analyser HP 3566A produced Bode diagrams by comparing the input with the output signal proportional to the acceleration measured by accelerometer.

By analysing the measured results (included in Appendix D3), it was necessary to introduce a spring between the worktable and the saddle to model the rocking of the worktable from side to side at 35 Hz. The results of the simulation when including this supplementary spring are presented in Chapter 6.

The experimental modal analysis method allows the user to determine the modal properties of mechanical elements through the measurement of frequency response functions. It requires knowledge of different scientific areas such as: modal analysis theory, digital signal processing, modal parameter estimation (curve fitting), excitation techniques and others.

5. 4. Transfer functions derivations for three axes

5. 4. 1. Theoretical approach

Spectral analysis consists of the examination of the frequency components from a signal and it has the following advantages:

- Small signals not visible in the time-domain displays (such as noise and distortion products) are revealed;
- Possibility to view many different signals at the same time because the frequency displays show frequency components distributed along the frequency axis;
- Opportunity to track subtle changes over time (for example the frequency drift of a signal source).

The PC/ Spectrum network analyzer HP 3566A has been utilised for measuring the frequency response of the system viewed via the Bode plot. It uses an FFT (Fast Fourier Transform) algorithm to convert an analog input (time-domain) signal to a digital signal displayed in the frequency domain. The Fourier decomposition is based on the fact that any periodic signal of arbitrary waveform can be broken down into the summation of a series of sine and cosine waves with specific amplitudes at the fundamental frequency and integer multiples of this frequency.

The swept sine mode has been chosen because it produces the most accurate results when working with heavy, stiff structures. Although measurement data available in swept sine mode is similar to measurement data available in FFT mode, there are important differences.

Swept sine is updated point-by-point as the analyzer measures the spectral energy at discrete frequencies - in contrast, measurements made in FFT mode are updated after each transform. Though much slower than frequency response measurements made with the analyzer's FFT mode, swept sine measurements nonetheless have several advantages:

- *Increased dynamic range* - the analyzer can adjust its input range (by auto-ranging both up and down) to provide an optimal signal-to-noise ratio at each point during the frequency sweep.
- *Better characterisation of non-linear devices* - if multiple swept sine measurements are made (each with a different sine level), the distortion changes could be observed.
- *More efficient excitation of mechanical structures* - because all the energy in a frequency response test is concentrated at only one frequency at any given time, unlike measurements made with random noise excitation.
- *Logarithmic sweeping to better characterise audio-frequency devices* - much faster and with better resolution than linear sweeping.
- *Faster measurements than traditional swept sine analyzers* - due to auto-resolution feature. When auto-resolution is on, the analyzer monitors the slope of the frequency response and changes the resolution accordingly (the analyzer sweeps faster in places where the frequency response is relatively flat, but slows down the sweep when more resolution is required).

5. 4. 2. Measurement technique

The measurements have been performed to validate the proposed theoretical models for the CNC machine tool axis drives. The theoretical model was changed accordingly with the data resulting from the practical measurements (the model has to reflect as close as possible to the real machine).

5. 4. 2. 1. Closed loop position control

The initial idea for determining the Bode plots of one axis at a time was to introduce sinusoidal inputs into the controller and to measure the controller output and the tachogenerator output. This was not practical to achieve therefore the alternative was to introduce a sinusoidal signal (generated by PC Spectrum Analyzer HP3566A) as a disturbance into the pre-amplifier as is shown in Figure 5. 26.

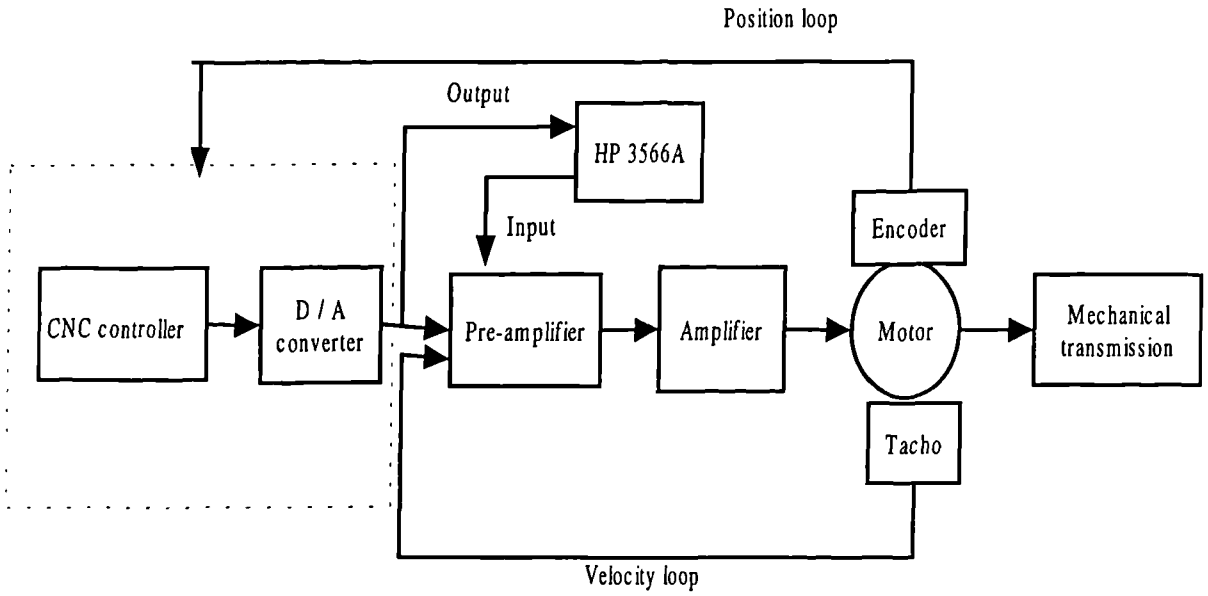

Figure 5. 26. Experimental setup for measurements on closed-loop position control

The amplitude of the signal was limited to 250 mV due to the fact that mechanical transmission must have a maximum acceleration limit of $0.5 * g = 0.5 * 9.81\ m / s^2$

The signal was introduced by using an electronic circuit which maintained unity gain with no phase shift between input and controller output. The diagram of this circuit is presented in Figure 5. 27.

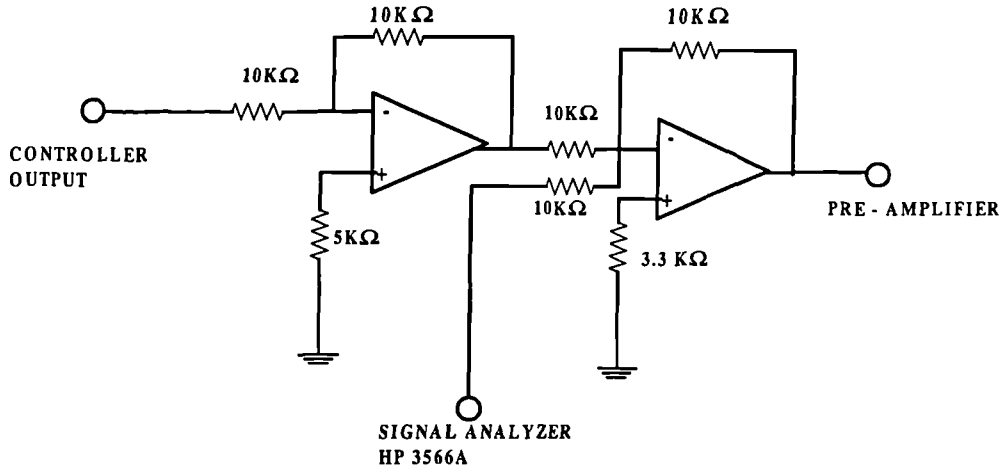

Figure 5. 27. Supplementary electronic circuit permitting the introduction of the signal generated by the signal analyzer

The results of measurements are presented in Appendix C5. The input signal (swept sine) was generated by the PC Spectrum / Network Analyzer HP 3566A and the output signal was the controller error. Digital signals were obtained from encoders fitted in three positions as follows:

- rotary incremental encoder Litton G60 attached to the DC motor;
- optical incremental rotary encoder Leine & Linde IS 632 fitted at the end of the ball-screw on Y-axis;
- sealed linear encoder HEIDENHAIN LS 106 attached to machine's bed for Y-axis.

The Bode diagrams obtained when the feedback signal was obtained from the rotary encoder attached to the DC motor ripples could be clearly seen. These ripples are due to vibrations which propagate from the assembly composed from ball-screw, nut, worktable through belt and pulleys back to the motor.

Also, while the Bode diagrams for the rotary encoder aplication do not present a resonance frequency below 200 Hz, the Bode diagrams for the linear encoder on the Y-axis show a first resonance frequency at 36 Hz. These values are due to the fact that velocity loop has high gain and high bandwidth and the position loop has low gain and low bandwidth.

The results of the measurements for the frequencies above 50 Hz are uncertain due to the sampling time of 10 ms for the FANUC 6M. If the sample rate is not fast enough, the presence of totally non-existent frequencies may be indicated due to aliasing.

The controller output was measured with increased precision using the *General Data Logging Software (GDLS)* [88]. This software package developed at the Precision Engineering Centre within the University of Huddersfield generates different stimuli (step, ramp, white noise, pseudo-random binary signals etc.), collects the data from transducers in real-time, provides on-line data analysis and reporting of results for further processing.

A sinusoidal signal with 250 mV amplitude and 50 Hz frequency (Figure 5. 28) was produced by the software and applied as an external perturbation to the pre-amplifier. The controller output was measured by the PC containing the GDLS software through an A / D card with 12 bit resolution. It is obvious that the amplitude of controller error decreases very much in time and the signal-to-noise ratio (SNR) becomes negligible. Considering this aspect, the limitation of the amplitude of the input signal to 250 mV and the influence of the sampling time of the controller, it was decided to "open" the position control loop.

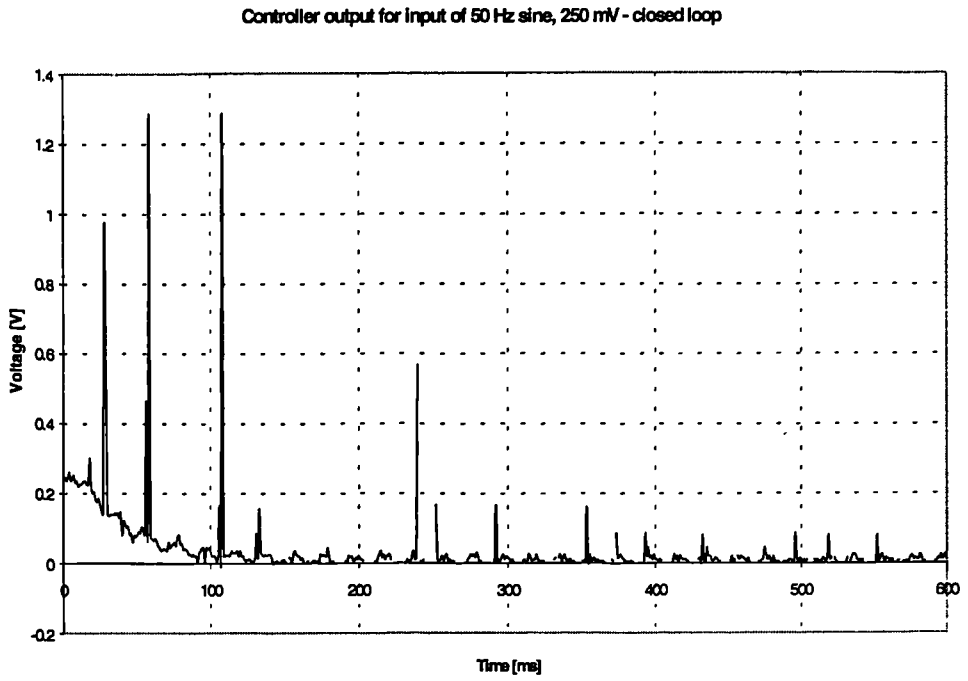

Figure 5. 28. Controller error when a sinusoidal signal of 250 mV and 50 Hz is introduced as a disturbance into the pre-amplifier

5. 4. 2. 2. "Open" Loop for Position Control

To measure frequencies above 50 Hz, it was necessary to "open" the position loop. In this way it was possible to introduce an input signal with a greater amplitude (750 mV) able to introduce sufficient energy thus making the output signal greater than the noise level and able to move the worktable measurable distances.

The pulses generated by the linear encoder are counted by the digital scalar card to determine the position of the slide. The input voltage is proportional to the velocity so the values measured by the linear encoder are differentiated in order to compare a like input and output signal. The differentiation is performed by the GDSL (1 ms sampling time) and the resulting digital signal is transformed into a voltage by a 16 bit D / A card. Then the analogue signal is introduced into the PC Spectrum / Network Analyzer HP 3566 A.

The GDSL contains subroutines to command the digital scalar card and the D / A card as it is shown in Figure 5. 30.

Comparing the general structure of measurement system presented by Bentley [89] with the experimental setup from Figure 5. 29, one could identify the following elements:

- The encoder is the sensing element;

- The signal conditioning operation is done by the digital scalar card;
- The computer and the D/A card installed in it perform the signal processing phase;

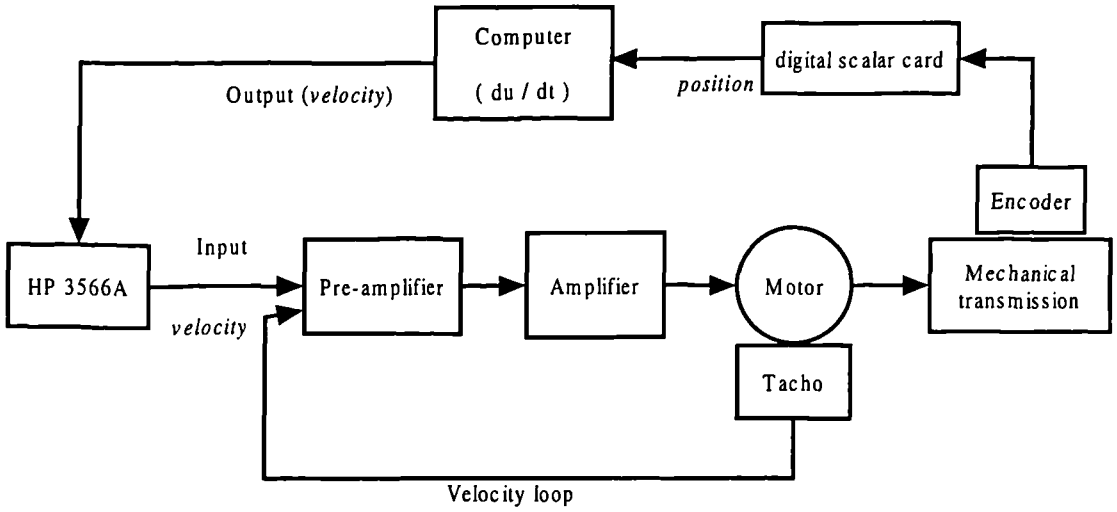

Figure 5. 29. Experimental setup for measurements in open-loop position control and closed-loop velocity control

The PC Spectrum / Network Analyzer HP 3566A is comparing the analogue input (swept-sine) to the system with the analogue output produced by D/A card. The results are shown in the form of Bode diagrams for the three encoders which could generate the feedback signal (see Figure 5. 31).

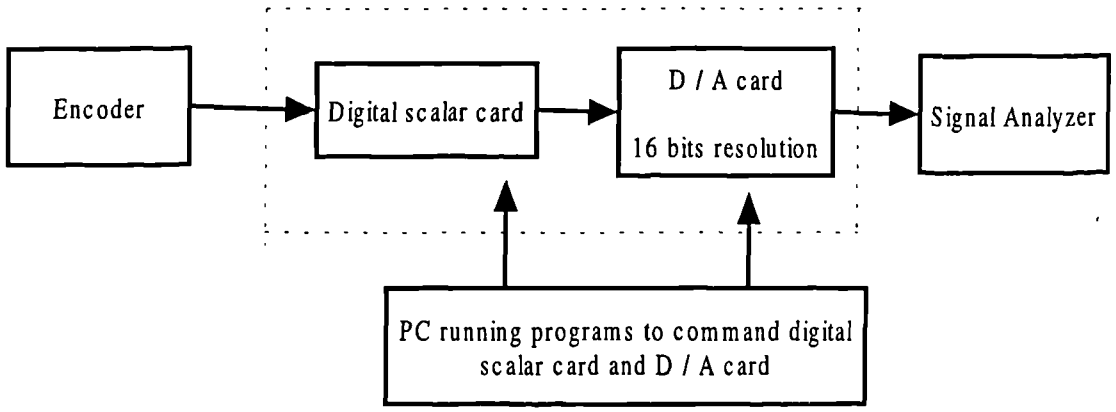

Figure 5. 30. Implementation of functional diagram for data acquisition in the case of open-loop position control

The input signal is a swept-sine generated by the PC Spectrum/Network Analyser HP 3566A. The output signal is the differential of the digital signal generated by:

- Rotary encoder attached to the DC motor (blue)
- Rotary encoder attached to the end of the ball-screw (green)
- Sealed linear encoder attached to the bed of the machine tool (red)

The experimental results measured with HP 3566A (plotted on a linear scale for frequency) show resonant peaks at 35 Hz, 119 Hz and 194 Hz (see Figure 5. 31). The phase diagrams contain large phase shifts due to these resonant states.

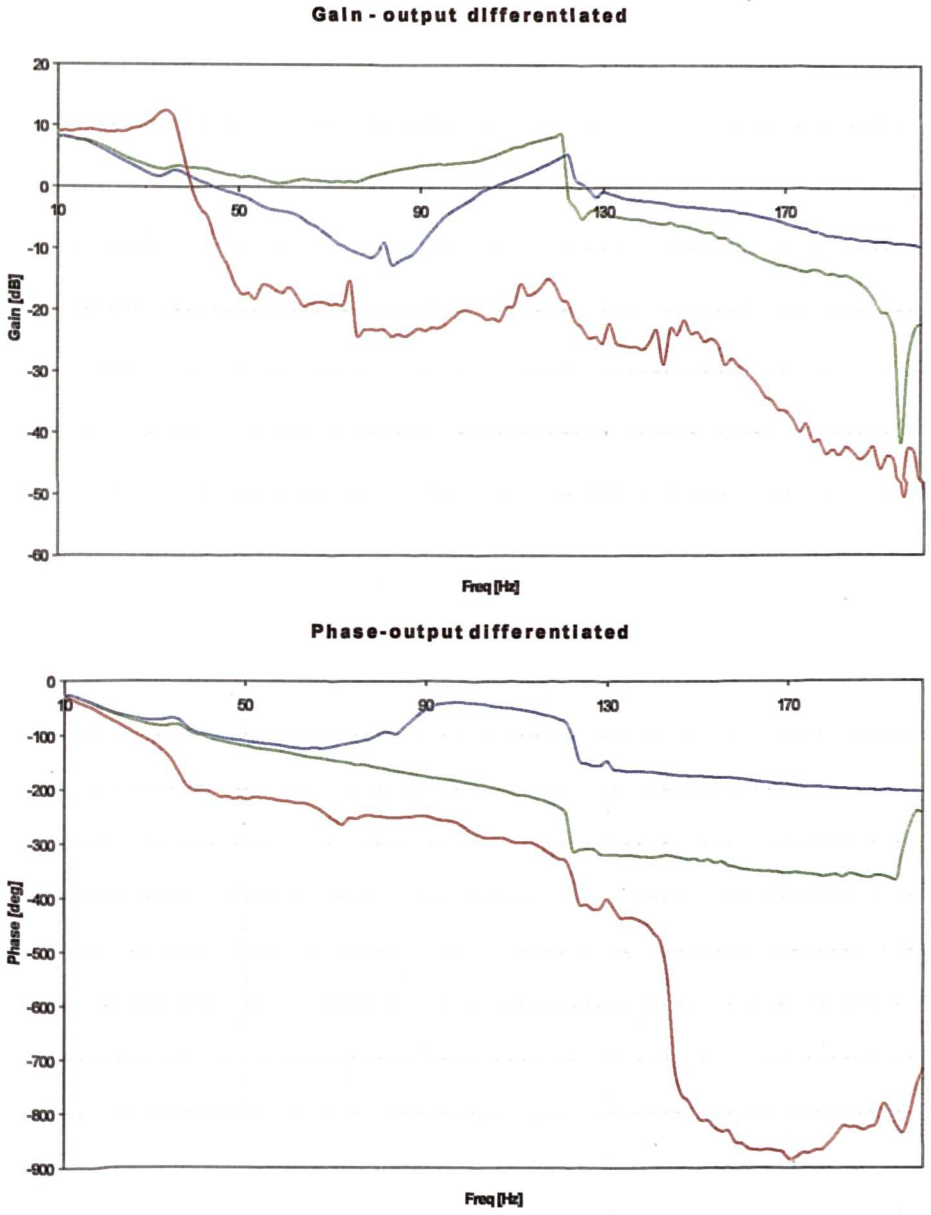

Figure 5. 31. Experimental results for measurements in open-loop position control using differentiation and a swept sine input

Possible causes of these resonance frequencies are:

- From the analysis of measurements performed by using accelerometers described in Chapter 5. 3., it was deduced that the main cause of resonance frequency at 35 Hz is the rocking of the worktable from side to side around X-axis.
- From the frequency response measurements of the Y-axis ball-screw (Figure 5. 20), it is obvious that the resonance frequency of 122 Hz is for half length of ball-screw. Thus 119 Hz could be due to this phenomenon.
- On the Bode diagrams for the linear encoder, there is a phase shift of approximately 180 degrees between 178 Hz (trough) and 194 Hz (peak). From the modal analysis of the Beaver VC35, it was detected that there are some saddle bendings occurred at 180 Hz.

From the measurement results it is obvious that it is better to measure the linear motion of the machine tool slide than to measure the rotation of the ball screw that drives the slide. This is because of losses (such as backlash and torsional wind-up) which contribute to positional inaccuracies.

There are some shortcomings introduced by differentiation such as:

- limiting the speed of calculation
- limiting the interval of frequency where precise data could be measured. For example, in the case of 2 ms sampling time, the maximum frequency of 250 Hz from Nyquist theorem. However, it is necessary to consider that an accurate differentiation using finite difference technique requires several times more points than a normal mathematical operation. Therefore the maximum frequency for which the measured data is reliable is approximately 100 Hz.

To overcome the above-mentioned shortcomings, it was decided to use the GDLS to read the digital scalar card and to send the information directly to the Signal Analyser without differentiation. The Bode diagrams then reflect the output position versus velocity demand. To obtain the velocity output versus velocity demand, it was necessary to take into consideration that if the signal is:

$$x = A \sin \omega t \tag{5. 9}$$

the differential will be:

$$\dot{x} = \omega A \cos \omega t = \omega A \sin (\omega t + 90^{0}) \tag{5. 10}$$

Thus the gain has to be multiplied by the angular frequency ω and a 90° phase shift must be added to the existing phase diagram.

A high pass digital filter was implemented by the GDLS to remove the position drift of the worktable in the case of open-loop position control. This filter is software re-configurable, won't drift with temperature or humidity, and does not require precision components. Its coefficients are calculated in Appendix C7 for the sampling time of 1 ms.

The measured results using this approach are shown in Figure 5. 32 and the curves are similar to those plotted for differentiated output, therefore the limitations of the differentiation are not prominent.

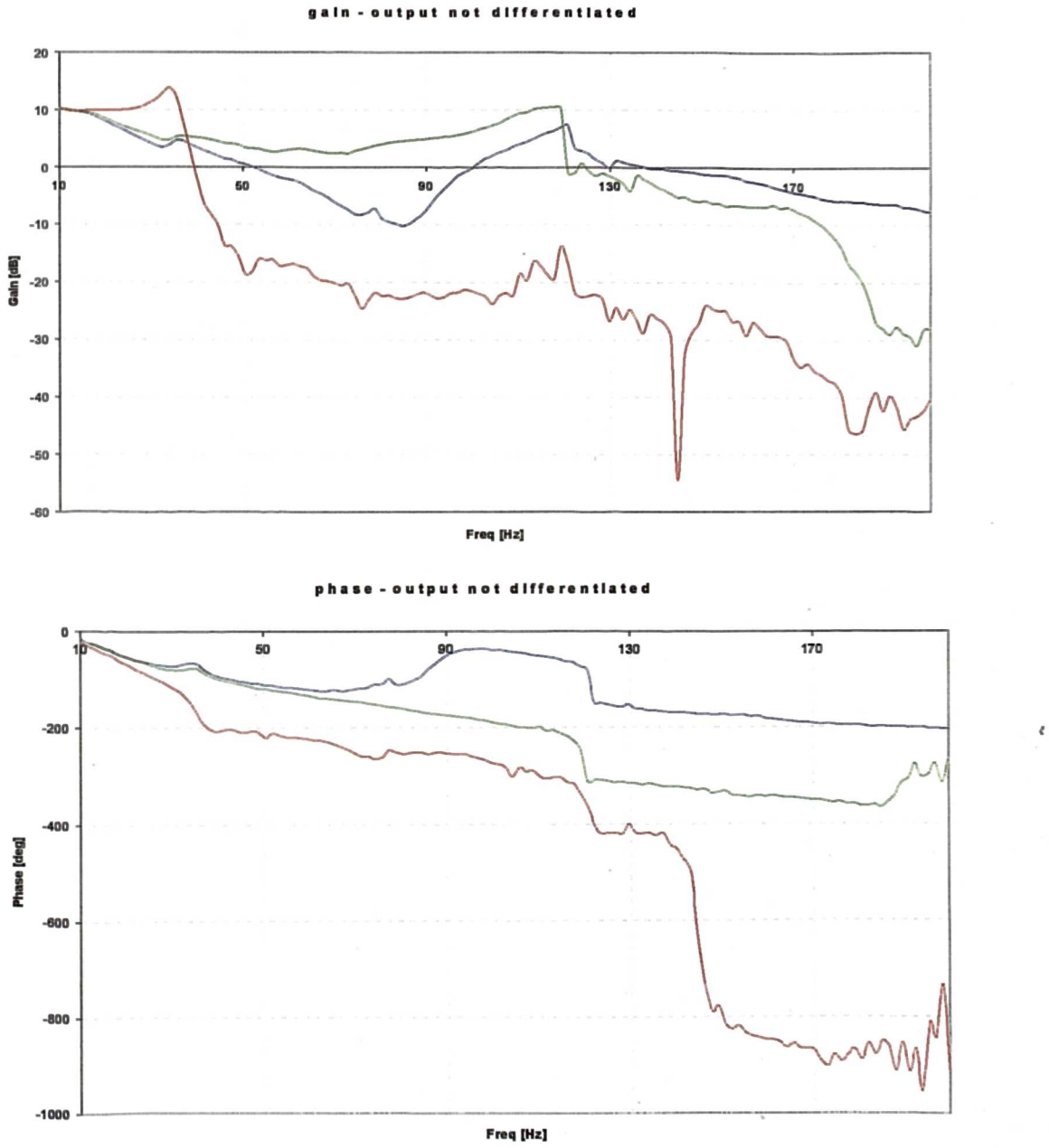

Figure 5. 32. Experimental results for measurements in open-loop position control without differentiation

5. 5. System response to step and trapezoidal inputs

The most useful and frequently used forcing function is the *step change of input* where the input is changed suddenly from one value to a new constant value. It is mathematically simple and occurs commonly in practice. It is the most severe disturbance that can be applied, and knowledge of how the system output will be affected is of considerable interest.

Although the results of sinusoidal testing give exactly the required result (the frequency response curve), the procedure is time consuming. The step response of the system on the other hand is very easily obtained. All that is required in this case is a step change in the input. The resulting output curve is a function of time and since a step function contains a Fourier series of odd frequencies, the step response contains all the information required to characterise the system. From the curve, which in the case of a simple second order system is usually in the form of a damped sinusoid, it is simple to evaluate the damping of the system from the envelope of the response and the natural frequency directly from the sinusoid.

If the slide of the machine tool has to move from position A to position B as quickly as possible, the signal to move will be given to the system in the form of a step function input. Clearly, the motor and mechanism driving the slide will need time to accelerate and move the slide at a constant velocity to the desired position. The time lag is due mainly to the inertia of the moving mass and the friction forces that have to be overcome.

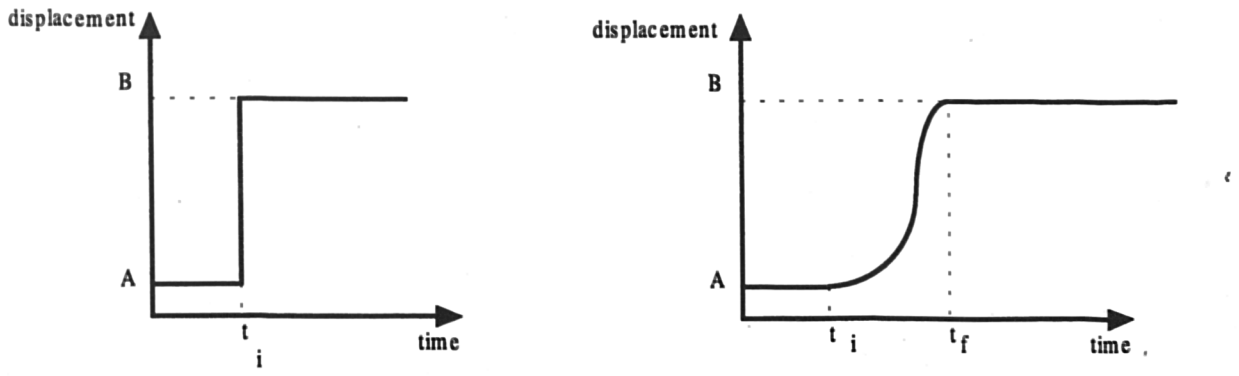

Figure. 5. 33. (a) Step function input for the control of a machine tool slide
(b) Time lag of the slide reaching the desired position
t_i - input time; t_f – response time

A step input of 1 V was introduced into the pre-amplifier when the measurement was performed for the open-loop position control. It was determined that 1 V at the pre-amplifier corresponded to 26 mm / s for the saddle (linear velocity obtained by differentiating the

position generated by the digital scalar card from the linear encoder output). The calculations were carried out by GDLS. The negative value is due to the fact that the worktable moved in the negative direction.

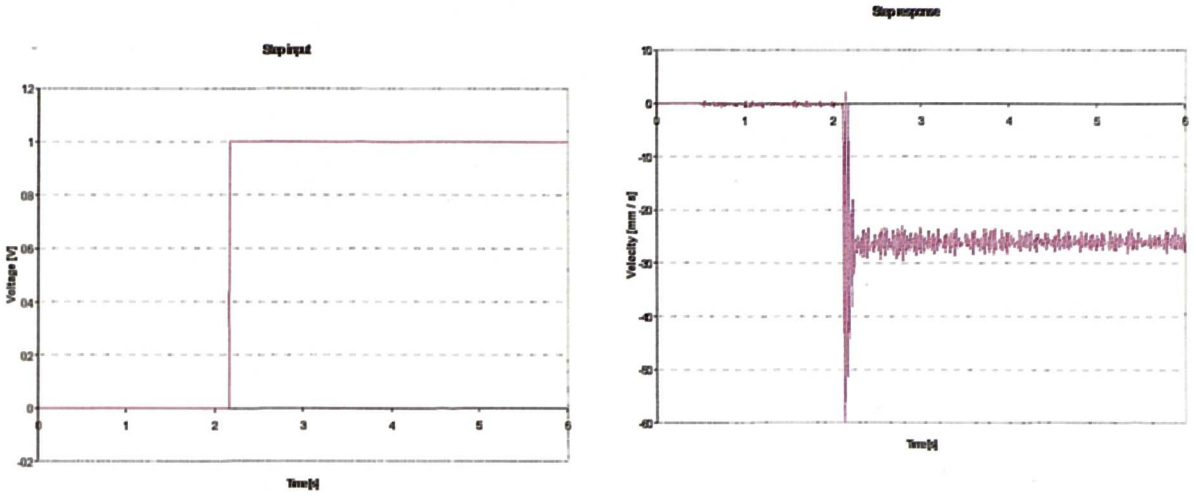

Figure 5. 34. Measured step input and step response for open-loop position control

The *trapezoidal velocity profile* (Figure 5. 35) is a typical shape for demand signals actually used in machine tool systems. It could be used to check out the performance of the CNC machine tool during different functioning regimes:

1. Acceleration phase - includes acceleration force and friction forces;
2. Running at constant rate - only friction forces are present;
3. Deceleration phase - includes deceleration force and friction forces.

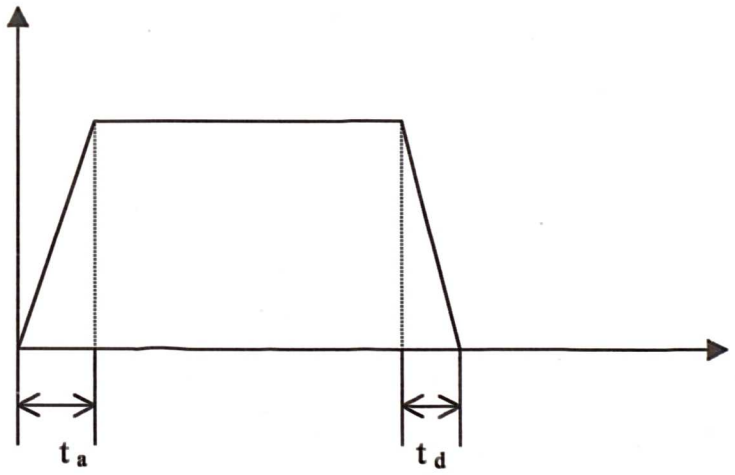

Figure 5. 35. Trapezoidal velocity profile

The acceleration time (t_a) and deceleration time (t_d) could be set up by modifying some parameters of the controller. The acceleration time is between 0 and 0. 16 seconds, depending

upon the fastest ramp-up time available with a typical controller due to finite electronics producing a transportation lag.

The CNC machine tool was programmed to move the worktable in Y–axis direction for 300 mm with a feedrate of 5000 mm / min and acceleration time t_a =140 ms, to have a dwell and to move the worktable back to the initial position (Figure 5. 36). In this way a trapezoidal rate demand was created with the machine functioning in closed-loop position control. The program for Beaver VC35 is shown in Appendix C8.

For this type of demand, the controller error was measured to determine how many volts corresponded to a certain constant feedrate.

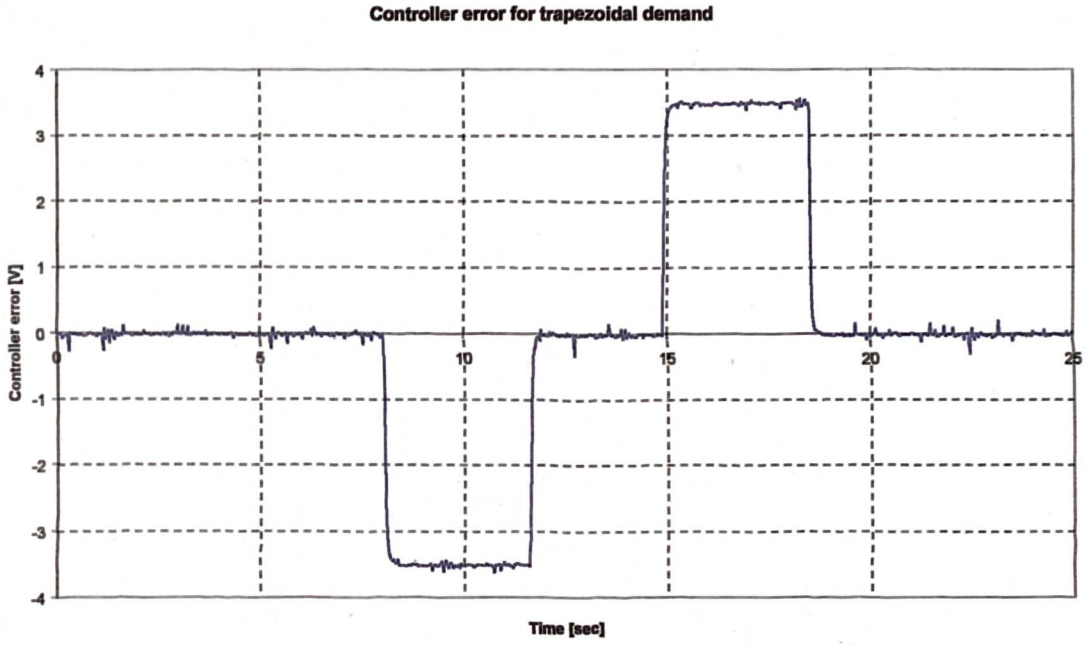

Figure 5. 36. Measured controller error for trapezoidal velocity demand with acceleration time 140 ms

It was determined that 3. 5 V for controller error correspond to 5 m / min feedrate. Therefore, for the maximum feedrate of 10 m / min will correspond 7 V. This value is confirmed from the following formula applied for the setting of servo loop gain multiple of each axis:

$$\text{Setting amount} = 2048 \times (E / L) \times \alpha \times 1000 \qquad (5.\ 11)$$

Where E - maximum voltage of controller output

L - machine movement amount per motor revolution 5 mm

α - detect unit = controller resolution / reduction ratio $\alpha = 0.\ 001 / 2 = 0.0005$ mm

Introducing these value into Equation (5. 11), yields:

$$1434 = 2048 \times (E / 5) \times 0.\ 0005 \times 1000 \qquad (5.\ 12)$$

The maximum voltage of controller output corresponding to maximum feedrate will be:

$$E = (5 \times 1434) / (2048 \times 0.0005 \times 1000) = 7 \text{ V} \qquad (5.13)$$

The first values of the measurement are negative because the worktable is going in the negative direction first.

The measurements were repeated for another value of the Y-axis constant linear acceleration (t_a =10 ms). From the rapid response (Figure 5. 37) in less than 0.1 s with no overshoot it is evident that the system (machine tool) is critically damped.

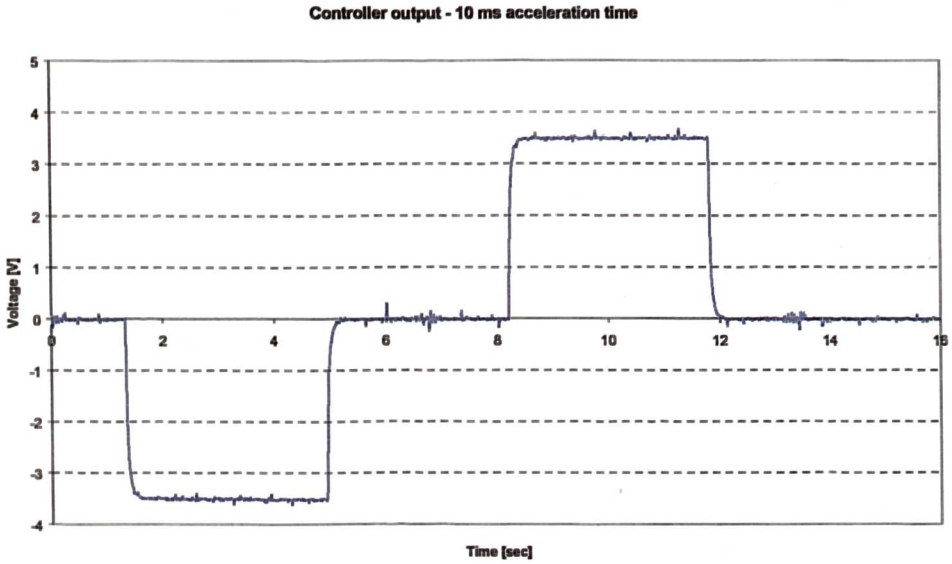

Figure 5. 37. Measured controller error for trapezoidal velocity demand with acceleration time 10 ms

Martin [90] showed that in the case when the slide of the machine tool has to start from rest and travel at a constant speed, the slide position will follow the input at the required velocity with a constant lag (Figure 5. 38).

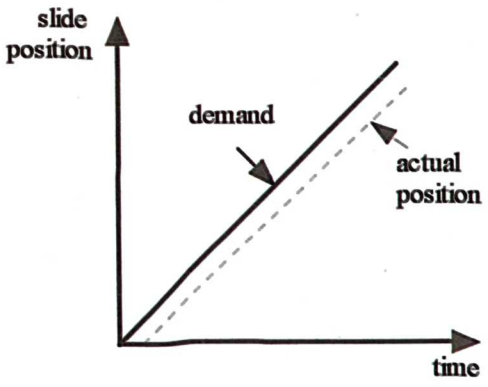

Figure 5. 38. Response to a ramp input

This lag is called *steady state error* and is due to the damping effect produced by introducing friction at the point of slide displacement. The motor has to generate a driving force to overcome the friction and to move the slide. This is the reason why the slide position follows the demand at the required velocity, but with a constant lag.

The steady state error has been determined by comparing the measurement results with the demand.

5. 6. System response to white noise signals

5. 6. 1. Theoretical approach

In the previous sections, the output response curves for deterministic input signals such as step, trapezoidal and sinusoidal signals were obtained. The amplitude of these signals was limited by the maximum acceleration of the mechanical transmission.

A statistical method of identification is applied to the determination of transfer functions to overcome the above-mentioned limitation. The method uses a non-deterministic forcing function (white noise) which has random characteristics. There are several main advantages of this technique:

- The normal operation of the system is not normally affected because the noise excitation energy is spread over a wide frequency range.
- The measurements are immune from the extraneous effects of unwanted noise provided they are stochastically independent of the input noise source.
- The amplitude of the input signal can be increased without risking damage to the system.

The impulse response of a linear system can be calculated from the cross-correlation of input and output signals [86]. The cross-correlation measurements indicate time domain similarity between input and output signals. The input signal is multiplied by a progressively time-shifted version of the output signal, highlighting similarities between the two while de-emphasising differences.

To avoid wrap-around error, the cross-correlation measurement for the HP system discards the last half of the output time record (amount of time domain data required to perform one FFT). The measurement display is therefore half the length of the time record.

In the case of a random signal, the behaviour of the signal is not known exactly once the observation period is over. However, the behaviour of random signals could be estimated from two points of view by using five statistical quantities:

- Amplitude behaviour could be specified by either the probability density function or mean and standard deviation;
- Frequency / time behaviour could be specified by either power spectral density or auto-correlation function.

The white noise does not characterise non-linearities because the system under test is excited differently each time record, so averaging over a number of time records tends to reduce the effects of non-linear distortion in the measurement. Averaging multiple samples to arrive at single measurement (and error) is a good way to improve the accuracy of measurements. The premise of averaging is that noise and measurement errors are random, and therefore, by the Central Limit Theorem, the error will have a normal (Gaussian) distribution. By averaging multiple points, one arrives at a Gaussian distribution and can then calculate a mean that is statistically close to the actual value. Furthermore, the standard deviation derived from the measurements gives the width of the normal distribution around the mean, which describes the probability density for the location of the actual value.

The main advantage of white noise resides in the fact that it contains equal-amplitude components at *all* frequencies, not just at integer multiples of a fundamental frequency. It can be used to probe the response properties of a system very rapidly. The white noise is a useful tool for research and in practice band-limited white noise must be used.

5. 6. 2. Measurement technique

The experimental setup for measurements in open-loop position control and closed-loop velocity control is as shown in Figure 5. 29. The only difference is that the GDLS program also performs a supplementary operation (see Figure 5. 39).

The Bode diagrams representing the frequency response of the system are calculated using the Fast Fourier transform (FFT). The FFT improves the computational efficiency of the Fourier transform of a signal represented by n discrete data points, from an order of n x n to n x log (n) arithmetic operations.

Despite the functionality of the Fourier transform, especially in regard to obtaining the spectral analysis of a signal, there are several shortcomings of this technique:

1. The inability of the Fourier transform to accurately represent functions that have non-periodic components that are localised in time or space, such as transient impulses. This is due to the Fourier transform being based on the assumption that the signal to be transformed is periodic in nature and of infinite length.

2. The inability to provide any information about the time dependence of a signal, as results are averaged over the entire duration of the signal. This is a problem when analysing signals of a non-stationary nature such as monitoring machine vibrations, where it is often beneficial to be able to acquire a correlation between the time and frequency domains of a signal. This shortcoming was overcome by the use of wavelet transform (see Chapter 7).

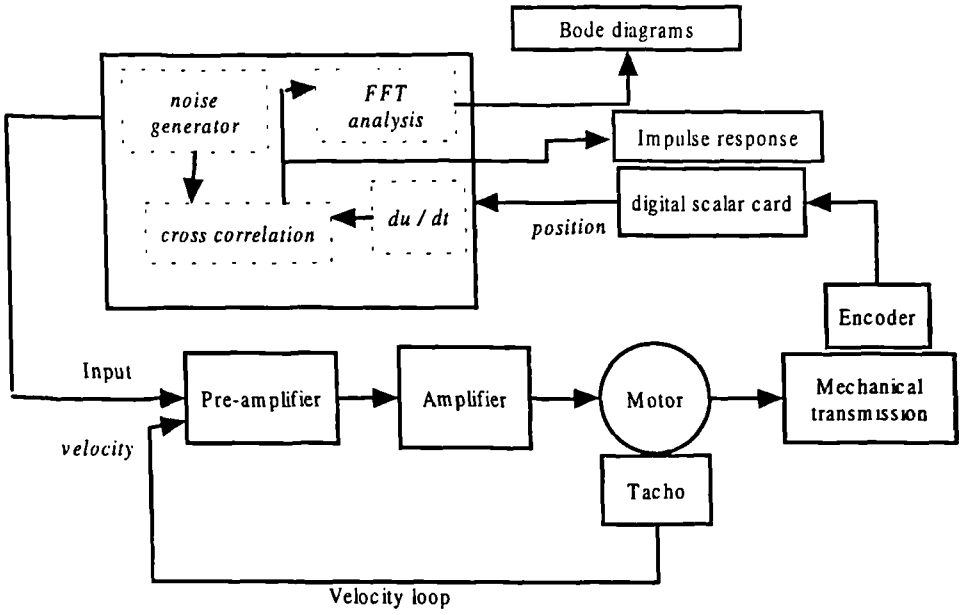

Figure 5. 39. Experimental setup for measurements in open-loop position control and closed-loop velocity control considering white noise as input

The impulse response of the system is estimated with the following formula [92]:

$$\hat{g}(\tau) = \frac{1}{\lambda N} \sum_{t=1}^{N} y(t+\tau)\, u(t) \qquad (5.14)$$

where u (t) - the input signal (white noise) y (t + τ) - the output signal delayed with time τ

g (τ) - the impulse response of the system λ - the variance of the input

N - the number of samples in the average

The measured results (with differential of the digital scalar card output) using GDLS are presented in Figure 5. 40.

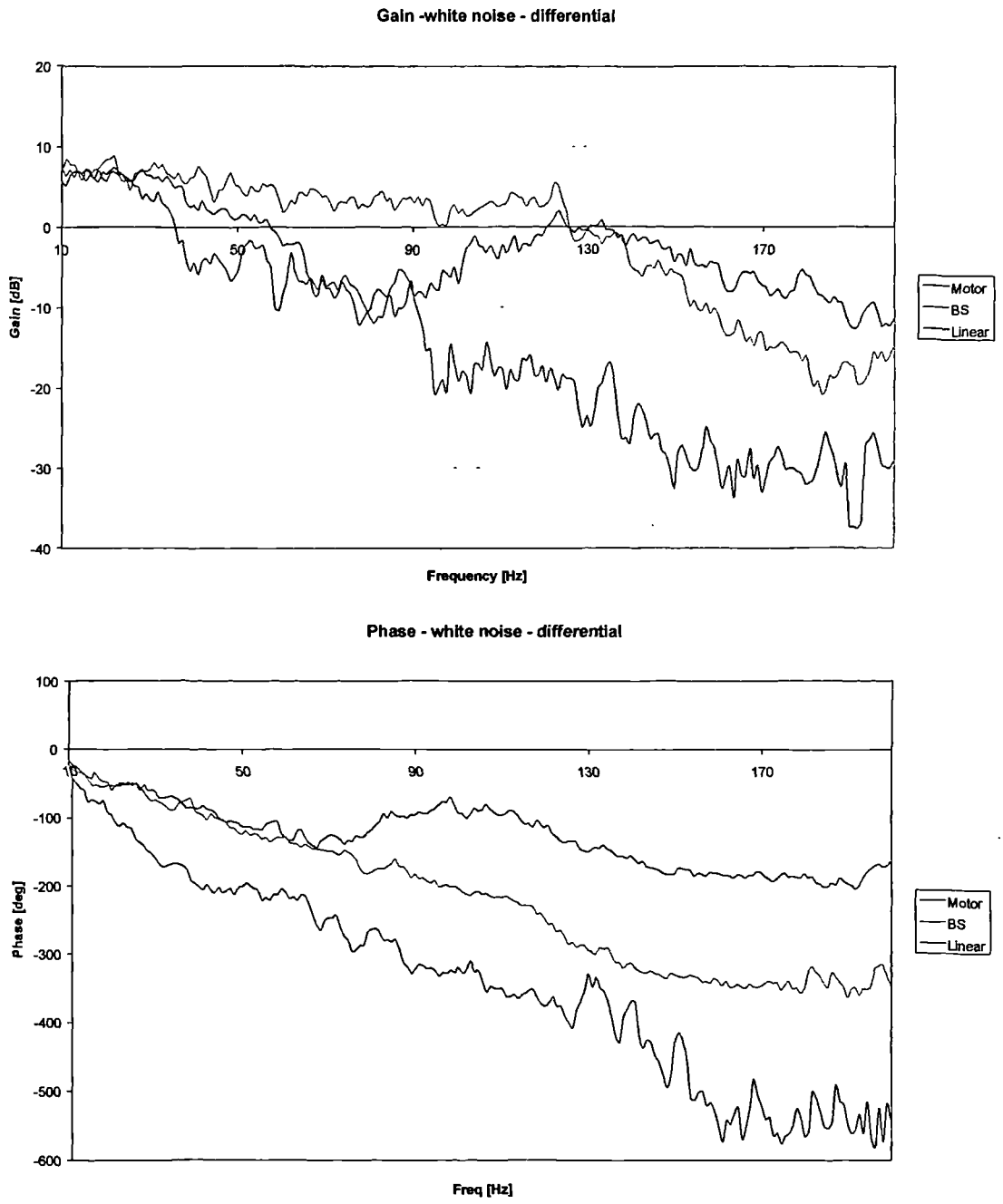

Figure 5. 40. Experimental results for measurements in open-loop position control considering differentiation and white noise input generated by GDLS

There are three sources of error in the output signal:

- *Number of points for sampling* - limited to 10000 points. The correlation between input and output is performed using direct computation (Equation 5. 14) rather than by FFT. Thus the accuracy of the estimate of the impulse response is of 1024 points limited by the sample size. To improve the accuracy, it would be necessary to increase the sample size,

which would extend the calculation time or to perform several separate estimations and find the average.

- *Quantization* - limited to 1 μm (rotary encoders) or 0. 1 μm (linear encoder);
- *Noise* - generated by the CNC machine tool. The amplitude of the output decreases with the increase of the frequency input. so the signal to noise ratio becomes very small and the Bode diagrams do not reflect the behaviour of the system at high frequencies.

Another set of measurements is performed with the output of the digital scalar card not differentiated by GDLS. The values for the Bode plots are calculated considering the Equations (5. 9) – (5. 10) and are displayed in Figure 5. 41.

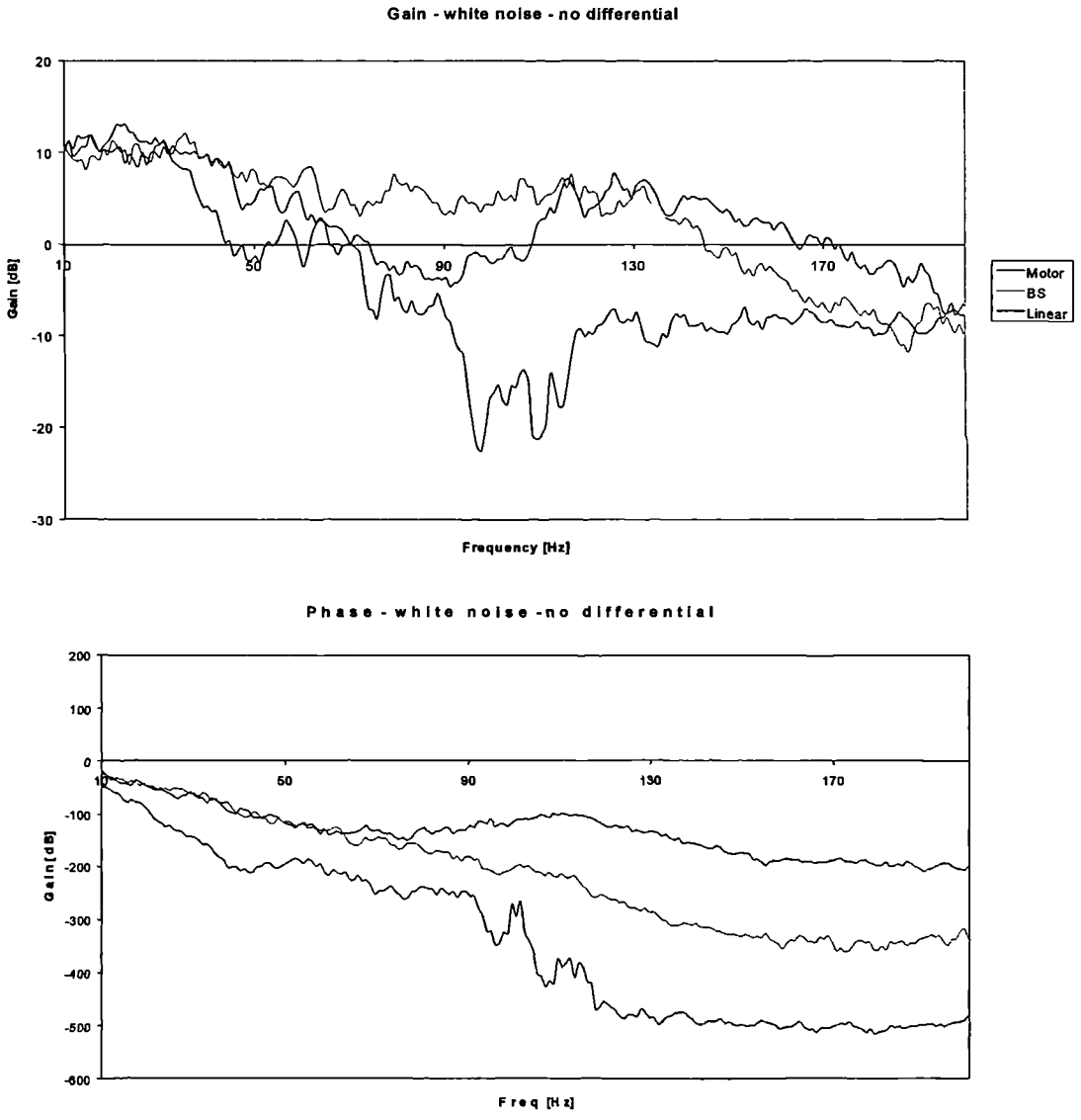

Figure 5. 41. Experimental results for measurements in open-loop position control for white noise input generated by GDLS and without differentiation

The measurements using white noise with 1.5 V amplitude generated by GDLS were repeated for 2 ms sampling time when the output signals from the encoders were differentiated and the resulting Bode diagrams are shown in Figure 5. 42.

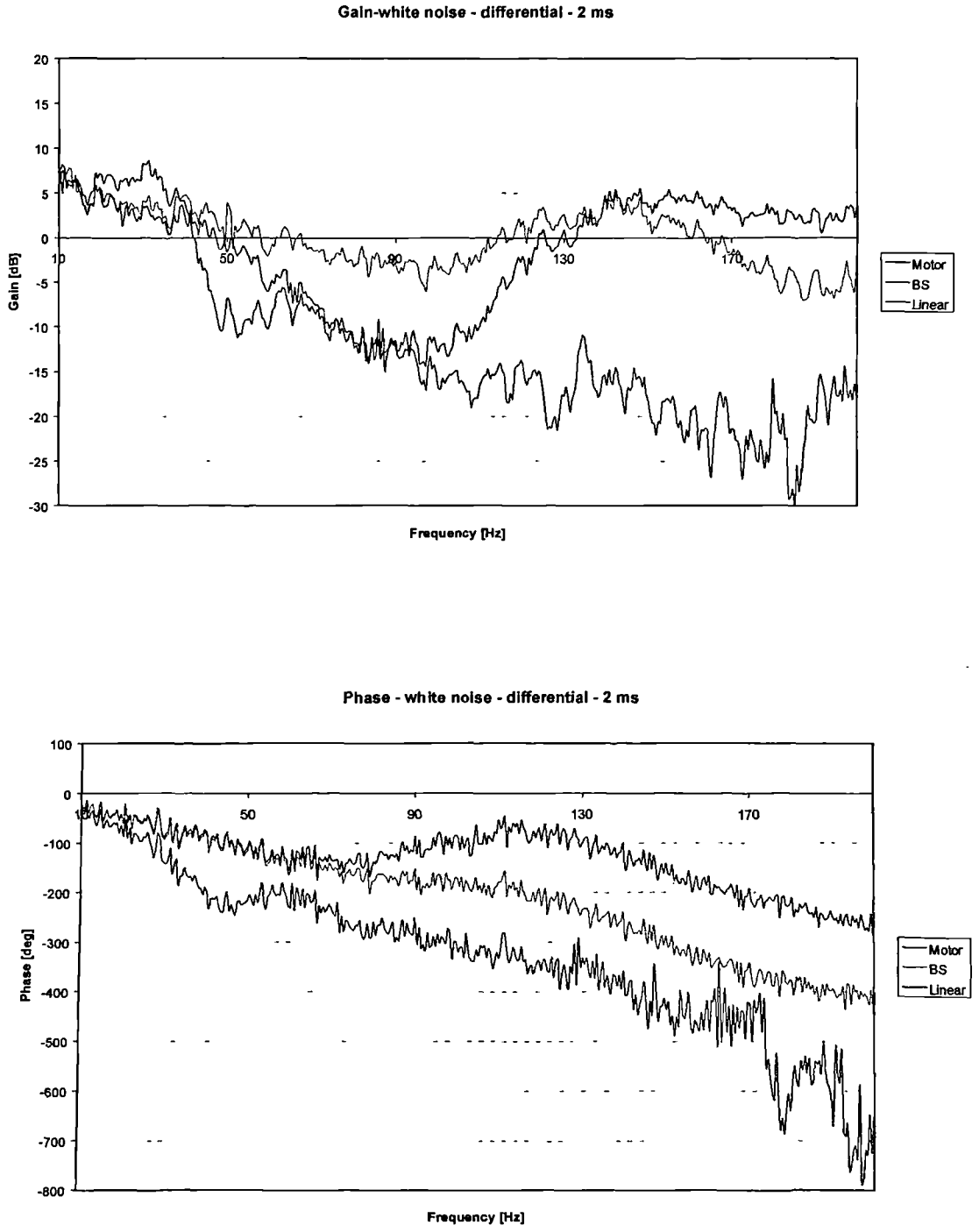

Figure 5. 42. Experimental results for measurements considering differentiation, white noise input generated by GDLS and 2 ms sampling time

Another set of measurements is performed for the case when the Signal Analyser HP3566A generates continuous random signal and plots the Bode diagrams when the digital scalar card output is differentiated in real time (0. 3 ms sampling time) by the GDLS. The measured results are shown in Figure 5. 43.

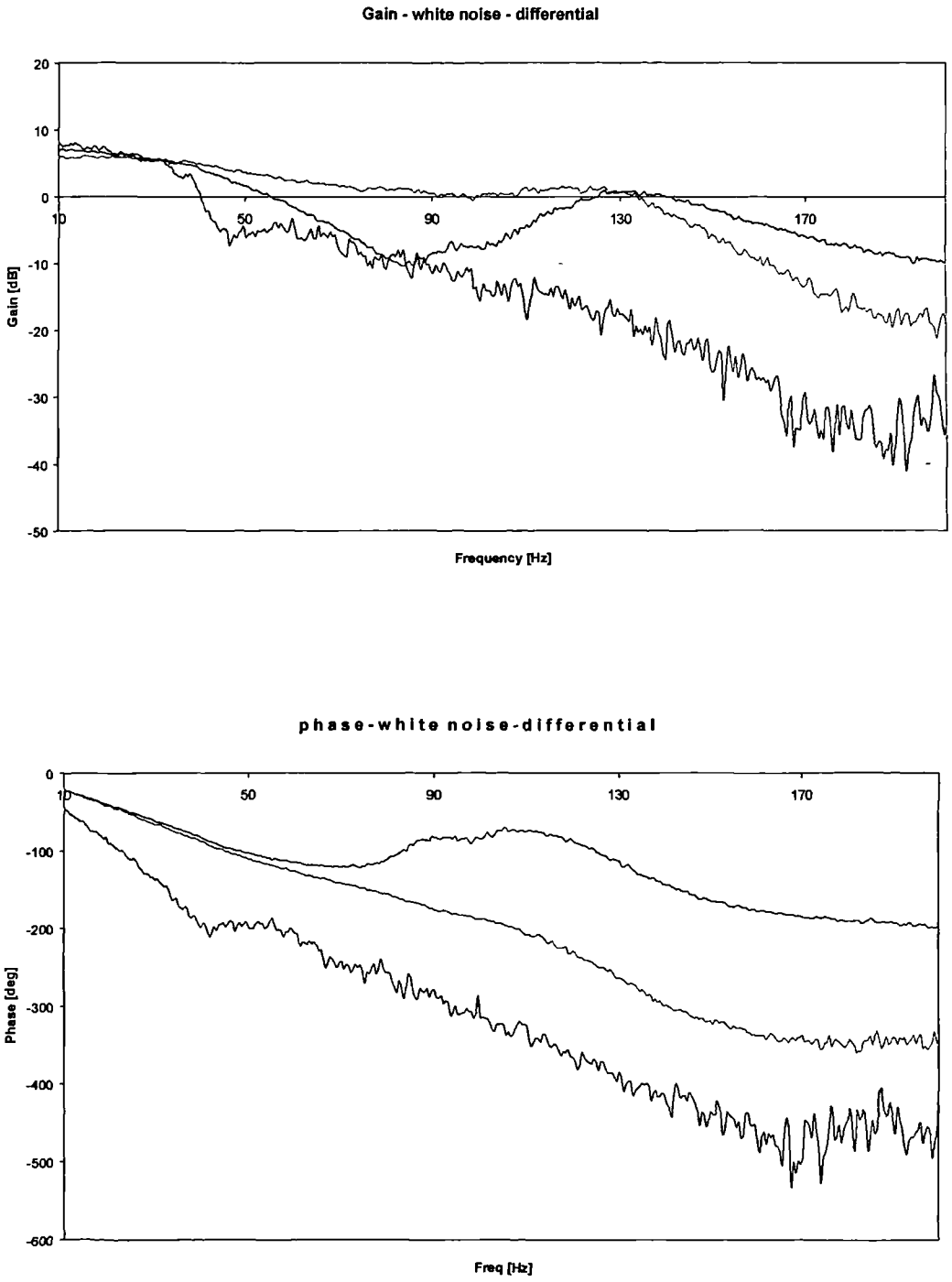

Figure 5. 43. Experimental results for measurements in open-loop position control considering differentiation and white noise input from HP3566A

Another case considered is when the Signal Analyzer HP3566A generates the continuous random signal and plots the Bode diagrams while the digital scalar card output is not differentiated. A high pass digital filter was implemented into GDLS to remove the position drift of the worktable in the case of open-loop position control. In conformity with Equations (5. 9) – (5. 10), the gain has to be multiplied by the angular frequency ω and a 90° phase shift must be added to the existing phase diagram. The results are shown in Figure 5. 44.

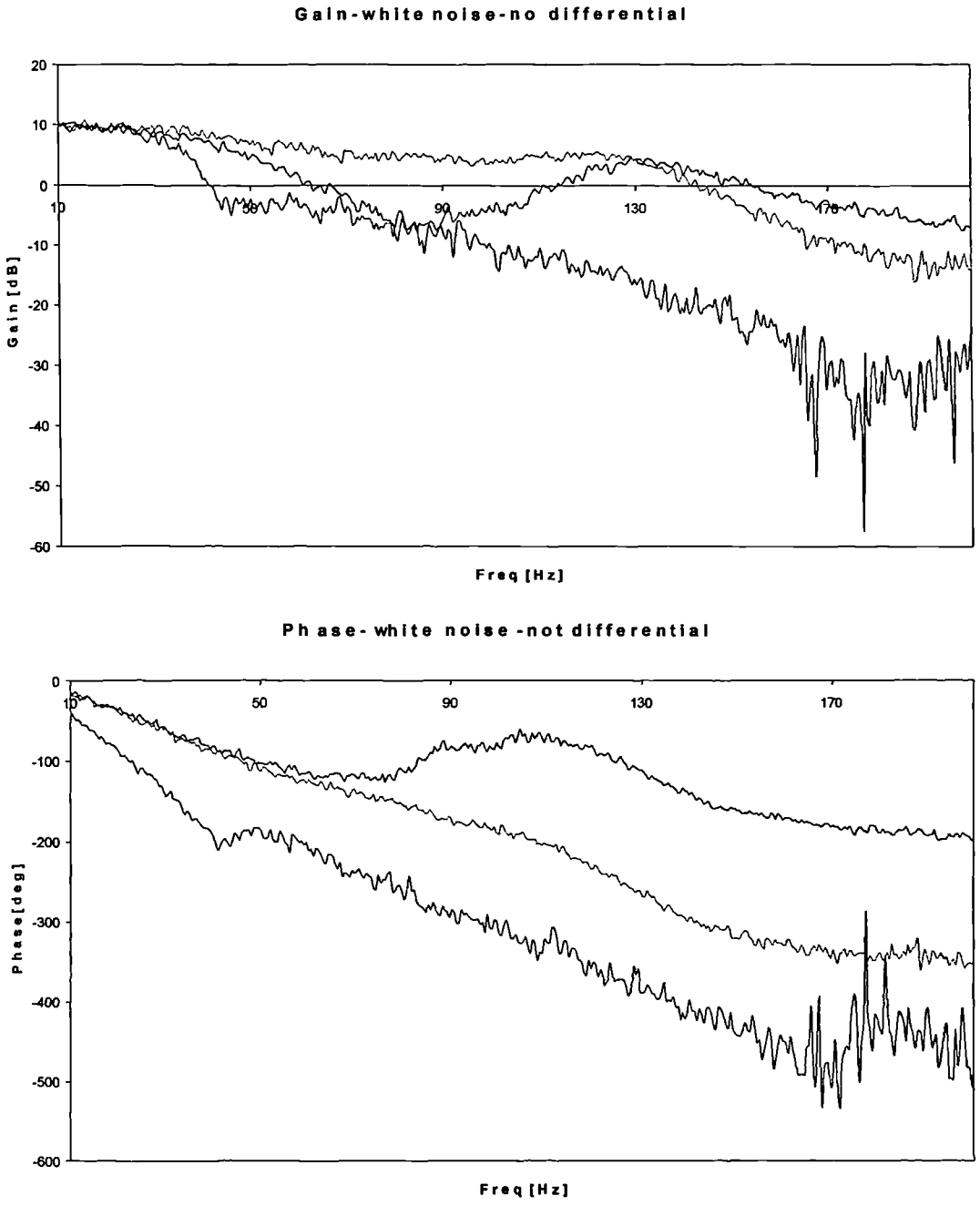

Figure 5. 44. Experimental results for measurements in open-loop position control with white noise input from HP 3566A and without differentiation

Also displayed on the same graph (Figure 5. 45) are the experimental data obtained using the three methods presented above:

- swept sine input generated by the signal analyser and output differentiated by GDLS (black);
- white noise input generated by the signal analyser and output differentiated by GDLS (violet);
- white noise input generated by GDLS and output differentiated by GDLS (orange);

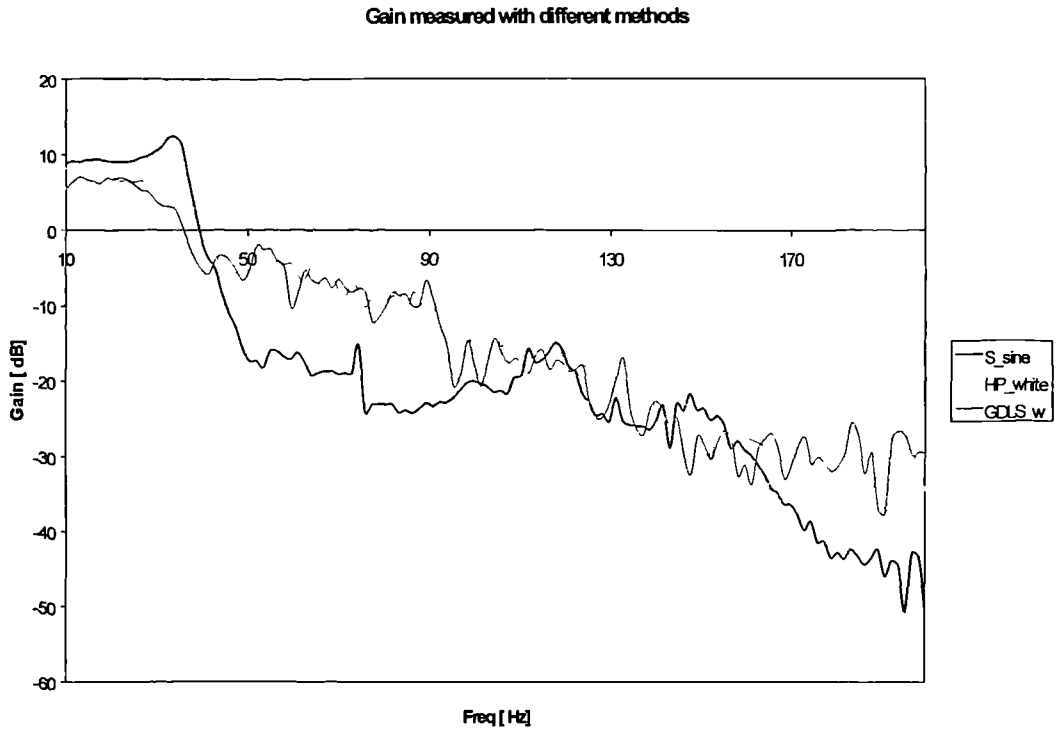

Figure 5. 45. Experimental results for measurements in open-loop position control with swept sine and white noise input from HP 3566A or GDLS considering differentiation

The resonant peaks are not so visible on the measured data using white noise because the effect of non-linearities depends on the amplitude of the input. The white noise signal has the energy spread on the whole range of frequency while the swept sine has the energy concentrated on every frequency. This is the reason why the resonant peaks are prominent on the experimental data in the case of swept sine input. This is a proof that swept-sine waveform produces the most useful results when working with heavy, stiff structures like as shown by Pavelic and Cleek [57].

5. 7. Ball bar plot for two axes

The dynamic and static accuracy of machine tool movement determine the results of machine tool measurement from the point of view of compliance to tolerances, surface

definition etc. For precision machining it is therefore important to measure and compensate for motion deviations.

The ball bar is a practical and efficient instrument for analysing and diagnosing the machine tool errors during circular contouring operations. Ball bar analysis provides the user with an overall picture of how the machine performs in accordance with ISO and ANSI standards. In addition, advanced mathematical techniques are used to identify the specific error sources on the machine.

The ball bar incorporates a precision measuring standard mounted between two telescopic precision balls. The ball bar is placed between a magnetic socket mounted into the spindle of the machine and a second magnetic socket placed into a small tower that is bolted to the machine's table. The balls are held in the sockets magnetically. Errors are measured by instructing the machine tool to scribe a circular arc or circle. Small deviations in the radius of this movement are measured by a transducer and captured by computer software. If the machine has no errors, the captured data will show a perfect circle. The presence of any errors will distort the circle by adding peaks along its circumference and possibly making it more elliptical. These deviations from a perfect circle reveal problems and inaccuracies in the CNC control, drives and position feedback systems.

For dynamic data capturing, the CNC machine tool Beaver VC35 was programmed to move in the XY plane using a 150 mm circular contouring radius in both clockwise (CW) and counter clockwise (CCW) directions. The program for the CNC machine tool is presented in Appendix D6.

The dynamic test provided information on the contouring ability of the machine tool. The feedrate was 3000 mm / min for the machine under test. Angular overshoot was 180 ° before and after data capture and a 360 ° data capture arc was utilised. The ball bar has a resolution of 0.1 μm and accuracy of ± 1 μm (at 20° C). Once the table started to move, the ball bar could begin taking measurements, which were outputted to a personal computer running evaluation software that captured and processed the test data. The measured ball bar plot is shown in Figure 5. 45.

The Renishaw calibration software system was used to generate circular plots and calculate error diagnostics as well as statistical repeatability. The values for following errors were determined by the software:

- *Circularity error* - is the difference between maximum outward deviation and maximum inward deviation from the best circle through captured data (in conformity with ISO 230-

1). This error is not very sensitive to spindle speed changes in both CW and CCW directions.

- *Servo mismatch error* - is the time in milliseconds by which one of the machine's axis servos leads the other. When the amplifier gains of the servo drives for the axis motion are not properly matched, steady state following error mismatch occurs between the axes. The errors can be corrected by balancing the loop gains of the servos which is achieved by adjusting the appropriate machine controller gain parameter. Negative sign indicates that X-axis leads Y in the XY axis plane and that the X-axis gain should be reduced. Therefore the test result plots have the shape of two ellipses in different contouring directions.
- *Bi-directional repeatability* - is calculated according to ISO 230-2.
- *Squareness error* - is the out of squareness between the two nominally orthogonal axes, and it is mainly due to the misalignment in the orthogonal axes. A negative value indicates that the angle between the two axes is less than 90°. This error may be caused by worn machine guide ways causing a certain amount of play in the axes or may be the axes are bent locally or perhaps there is an overall axis misalignment in the machine.
- *Scales mismatch error* - indicates that one of the machine's axes is either over travelling or under travelling. The higher the feed rate, the lower the scales mismatch error.
- *Backlash error* - the measured play between nut and screw observed when the moving direction of the machine is changed. It is mainly caused by the clearance in the ball-screw drive and elastic deformation in the drive. The precision of a ball-screw assembly depends strongly on the amount of backlash in it. Ball size and ball-and-ball-groove conformity dictate the amount of backlash. To avoid backlash, one ball circuit can be preloaded against another within the nut.
- *Dynamic backlash error (inertial spikes)* - occurs at the velocity changeover points similar to backlash error and is due to inertia of the elements of one axis.

There are several advantages of using the ball bar system such as:

- Quickly diagnoses the performance of machine tool
- Enables compliance to ISO, ANSI, QS9000 standards
- Forms the basis of predictive maintenance programs
- Reduces machine down-time and maintenance costs
- Tests a wide range of machines

The real advantage of the circular contour check is that it offers a quick snapshot of the machine's condition (15 minutes test) without having to take the machine out of production for long periods of time.

However, there are some disadvantages of using the ball bar for machine tool accuracy assessment:

1. It could be used in a limited space (a circle with 300 mm diameter for a ball bar with a nominal length of 150 mm or a circle with 600 mm when an extension bar is fitted) which does not cover the full travel of axes.
2. The squareness errors have to be measured for the whole length of axes

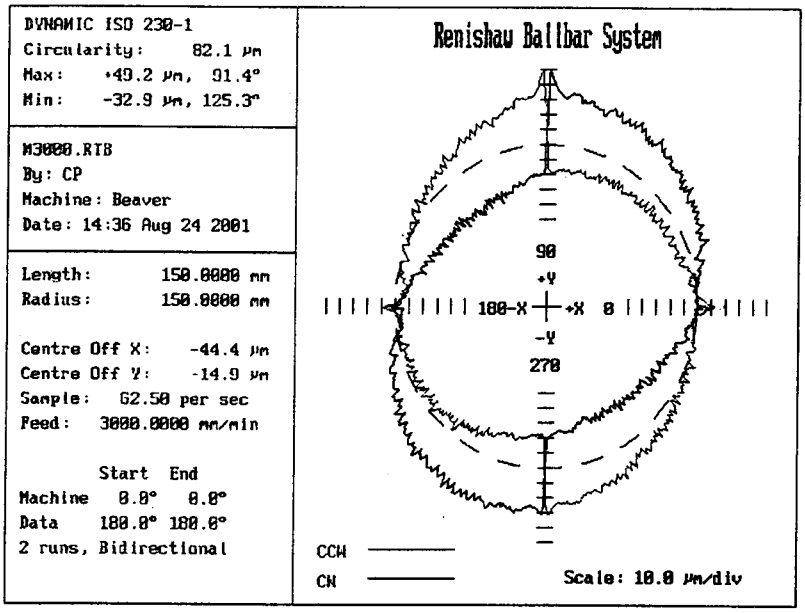

Figure 5. 46. Experimental ball bar plot for CNC machine tool Beaver VC35

From the experimental ball bar plot (Figure 5. 46), it could be observed that the error spikes at the pole position of the plot are due to axis inertia and the spikes are larger in Y direction because Y-axis is carrying X- axis.

The laser and ball bar systems were used as complimentary tools for CNC machine tool calibration. Firstly, a full laser calibration of linear, angular, straightness and squareness was performed. The ball bar test followed this and linking the laser calibration with ball bar test results formed a baseline.

The next step is to compile the models for one axis and for two axes and simulate their performance. This is undertaken in Chapter 6 using SIMULINK 2. 0. [93].

6. SIMULATION OF PROPOSED MODELS FOR ONE AXIS SYSTEM AND TWO AXES SYSTEM

From a *"systems perspective"*, complex systems are considered to be more than just the sum of their parts. So it is necessary to view the system in its entirety and not only focus on the individual parts. The prediction of a system's behaviour becomes very difficult in the presence of delays, inertia and non-linearity. Hence, simulation has come to provide in practice the means of understanding, controlling and improving such systems.

Simulation is more than just a science because translating the physical world into an efficient mathematical model, deciding the requisite level on modelling detail, analysing results and mapping these back from graphical and tabulated simulation outputs into natural language, requires a large range of human attributes.

The relationships between different stages of this process could be represented in a diagram (see Figure 6. 1).

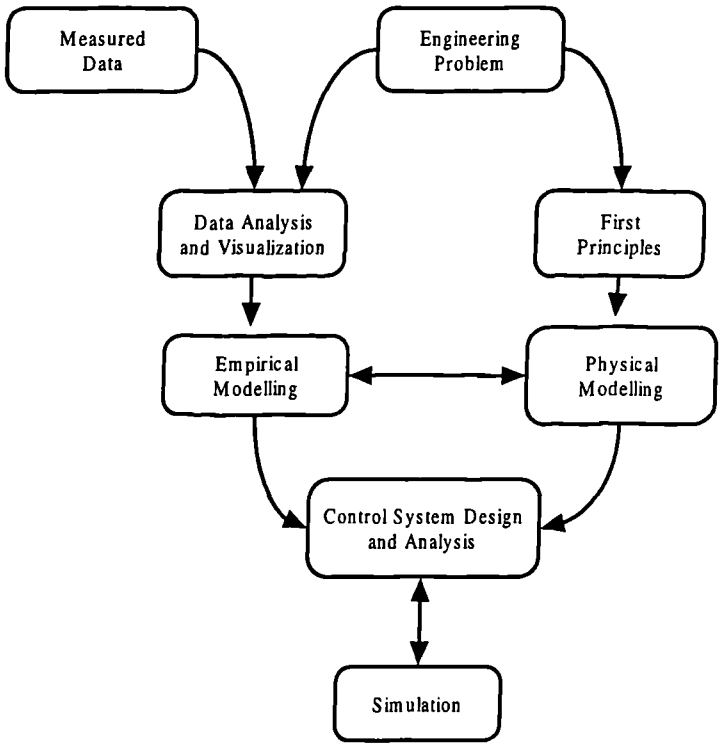

Figure 6. 1. The relationship between simulation and the real world

MATLAB [92] is an integrated computing environment that combines numeric computation, advanced graphics and visualisation, and a high-level programming language. The interactive nature of MATLAB makes it an excellent tool for rapidly developing insight into critical aspects of the problem including excitation simulation, linear dynamics simulation, control structure determination, stability analysis and controller design.

SIMULINK is an interactive environment for modelling and simulating a wide variety of dynamic systems including linear, non-linear, discrete-time, continuous-time and hybrid systems. With SIMULINK' s large library of building blocks, it is possible to easily model a system without writing a single line of code. The results of simulation can be viewed using scope blocks or saved to a file / MATLAB workspace for further analysis. Together, SIMULINK and MATLAB provide the ideal integrated environment for developing models, performing dynamic system simulations and designing and testing new ideas.

In the present study SIMULINK is employed for model analysis. The computer versions for the models of the modular systems depicted in Chapter 4 are used to simulate the dynamic behaviour of the non-linear control system, the CNC machine tool. Comparing the simulation results with the measured results performs the validation of the models.

6. 1. Implementation of the modular systems in SIMULINK

The models resulting from the modular approach described in detail in Chapter 4 were implemented in SIMULINK 2. 0. [93]. The version 2. 0. of SIMULINK has been chosen because of its advantages such as: reduced simulation time, high fidelity simulation (intrinsic zero crossing detection), ODE (Ordinary Differential Equations) solvers, improved algebraic loop solver, signal labels - attach labels to signals and propagate signal labels;

The mathematical model of the drive, resulting from the modular approach, produces data that can be analysed to predict the performance, accuracy, stability and safety of the drive system. By using SIMULINK, it was possible to analyse the signals present in the system.

6. 1. 1. Lumped parameter model with modular load with backlash and friction

SIMULINK has a large library of pre-defined blocks for use within system models. The only obvious disadvantage arises when the users model contains elements that are not defined in the libraries. Certain non-linear functions defined in the SIMULINK library [93] (such as Coulomb friction) do not generate the expected responses. This is the reason why they have been re-designed as it is shown in Figure 6. 2.

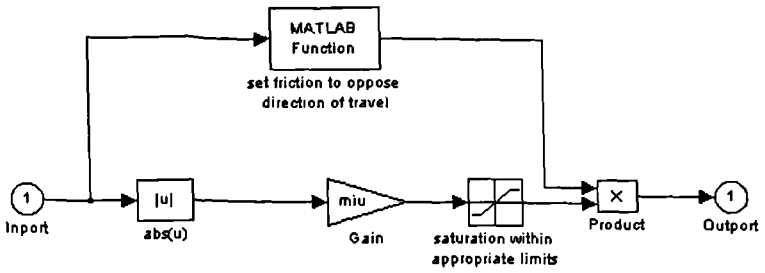

Figure 6. 2. SIMULINK implementation of Coulomb friction model

The Equations (4. 30 – 4. 40) of the model for CNC machine tool axis drive were implemented in SIMULINK 2. 0 (see Figure 6. 3), considering the velocity signal as an input.

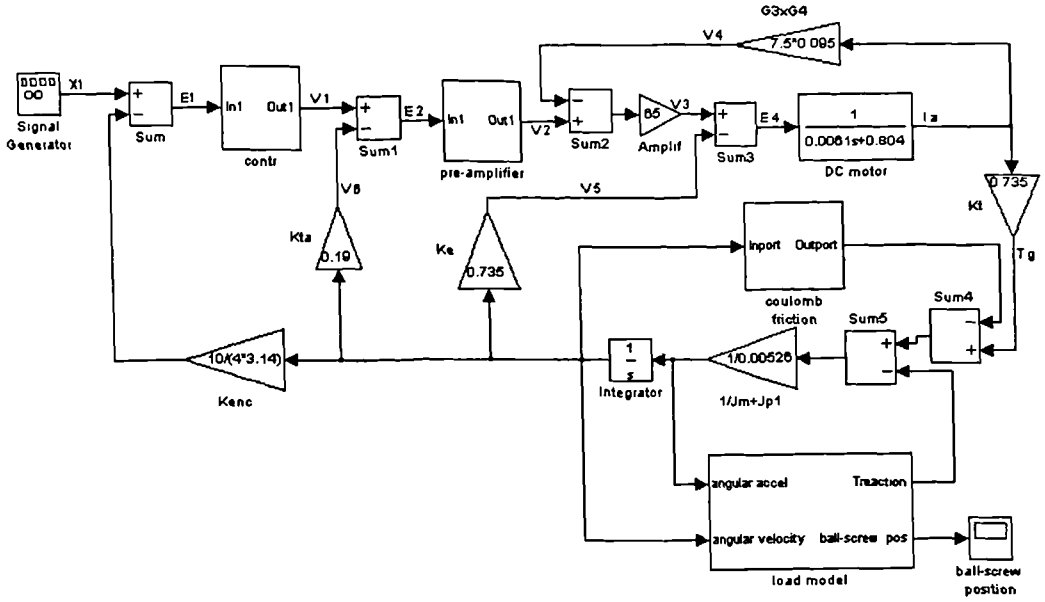

Figure 6. 3. Implementation in SIMULINK 2. 0. of the model with distributed parameters for Y-axis drive (rotary encoder attached to DC motor)

The controller was modelled on the basis of considerations discussed in Chapter 3 and was implemented in SIMULINK 2.0.

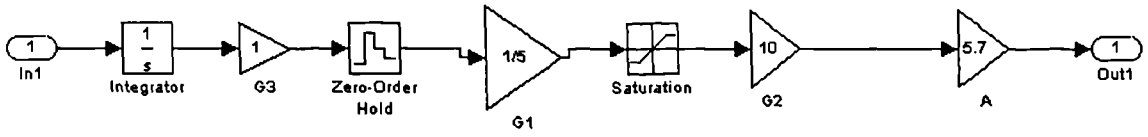

Figure 6. 4. Block diagram of FANUC 6M controller in SIMULINK 2. 0

The values for the elements included in the controller block diagram (Figure 6. 4.) are:

- Zero-order hold element has 10 ms sampling time
- The D / A converter scaling is 5 mm of error corresponds to 1 mA and the final stage of the D / A converter generates 10 V
- Saturation limits are ± 1 mA
- A = 5. 7 is a gain given by an operational amplifier connected with the D/A converter.

The subsystem " *Load model* " has been built on the basis of Equations (4. 31 - 4. 40) and its constituent elements are shown in the Figure 6. 5.

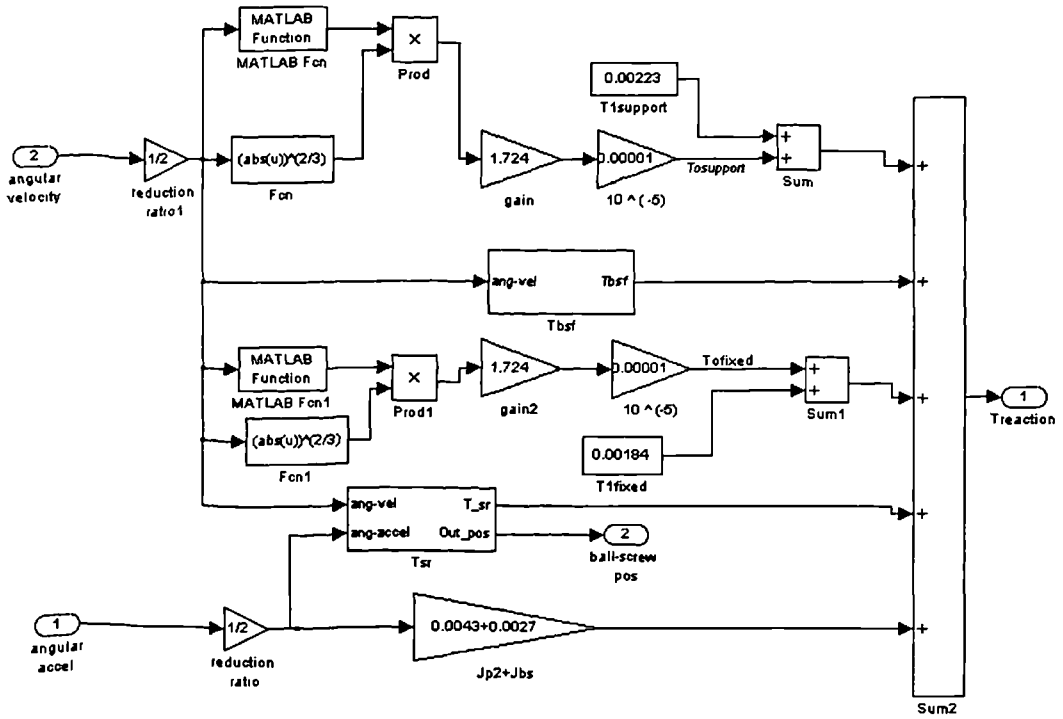

Figure 6. 5. Block diagram of " *Load* " model in SIMULINK 2. 0.

All other reaction forces that occur during machine functioning are considered. For the simulation their value is provisionally set to zero, but the place where they apply is determined. In future simulations, their calculated values will be introduced into the load model.

The torque due to slide reaction is calculated in conformity with Equation (4. 31) and the block diagram of the subsystem T_{sr} is shown in Figure 6. 6. The scaling factor 1000 converts the ball-screw position into millimetres since inside the load model the units are in metres.

The values of the parameters were calculated in Chapter 3 and Appendix A4. The requirements of the elements of the mechanical transmission are represented by reaction torques due to driven pulley inertia, ball-screw friction, ball-screw inertia, slideway friction and friction in the bearings.

The simulated results are compared later with the measured results and a two-axis model is built on the basis of the one axis model and used for simulating the ball bar plot. The simulated results are similar to the measured ball bar plot.

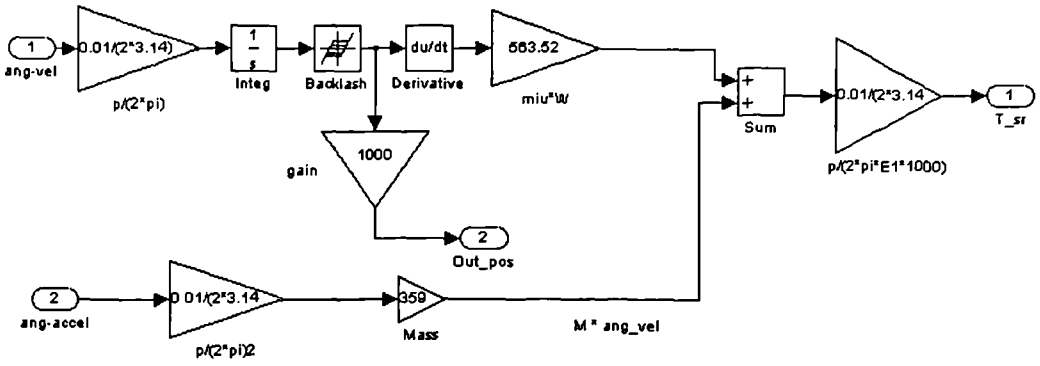

Figure 6. 6. Block diagram of subsystem calculating the torque due to slide reaction

However, the simulated results do not show the resonance frequencies that appear in the measured results and this is due to the fact that the damping coefficients are not introduced explicitly in the model. For this reason, another simulation is performed using a model with explicit damping coefficients.

6. 1. 2. Hybrid model with distributed load, explicit damping factors, backlash and friction

(This section was developed jointly with Mr. G. Holroyd – see acknowledgements).

Nowadays, it is not too difficult to construct an adequate dynamic model of mechanical systems of interest and even more so to assume numerical values for parameters of the dynamic model. If this is achieved, then it is straightforward to obtain a reasonably correct solution for the real-world problem.

The model with distributed parameters does not contain explicit variables to characterise the dynamics of the machine tool such as vibrations, equivalent multi-mass system, stiffness of different elements of the machine tools, toothed-belt transmissions etc. This is the reason why a *model with explicit damping coefficients* was developed. Calculations on the contact deformation of machine parts are performed taking into account their relative twist and displacement as solid bodies. In these calculations for a machine component, the natural stiffness of which is commensurate with its contact stiffness, beams on an elastic foundation

should be considered and their natural and contact deformation are examined in conjunction with one another.

During the effort of representing the dynamics of the CNC machine tools, there were taken into consideration some of the aspects such as:

- The relationships between the stiffness and damping of the machine elements;
- Four principal types of loading - tension, compression, bending and torsion - for the calculations of the stiffness of structural components;
- The basic factors defining the effective stiffness and damping for the elements of CNC machine tool axis drives were analysed. The dynamics of these drives depends on structural and contact deformations of the components, properties of the working (e.g. hydraulic or pneumatic) media, deformations of electromagnetic field in the drive motors, kinematic alterations of the stiffness properties, and so on.
- The interaction between the two aspects of stiffness - *structural stiffness and contact (joint) stiffness* – was treated in a systematic way. This interaction is due to the dependence of the contact area on structural deformations of the parts in precision-oriented structures. On the other hand, the form of contact area influences the calculations of the structural deformations. Contact stiffness and damping may be critical for accuracy of precision machine tools and other devices.

The non-linear phenomena in structural stiffness (pre-loading etc.) have not been studied in this thesis, though they are considered as important features and as very effective means for enhancing dynamic performance.

The general block diagram of the model with explicit damping factors in SIMULINK 2 is displayed in Figure 6. 7. where:

In2 - electrical torque generated by the motor *Out2* - DC motor angular velocity

Out3 - linear velocity of the worktable

This is similar with the implementation of the distributed parameters model (Figure 6. 3). The difference consists in eliminating the subsystem "*Load model*" and replacing with the subsystem " *Explicit* " (Figure 6. 8) to represent more accurately the dynamic behaviour of the elements from the mechanical transmission of a CNC machine tool.

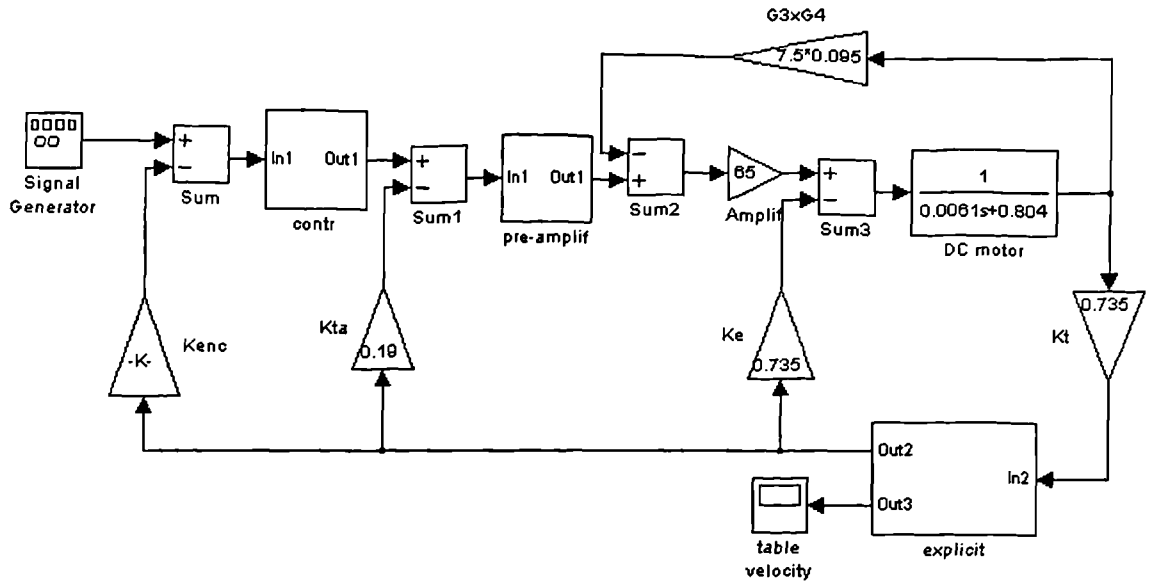

Figure 6. 7. Implementation of the model with explicit damping coefficients in SIMULINK 2 (rotary encoder attached to DC motor)

Some details about the modelling procedure were mentioned in Chapter 4. 4. and the way in which the elements were implemented in SIMULINK 2. 0. is described in this section.

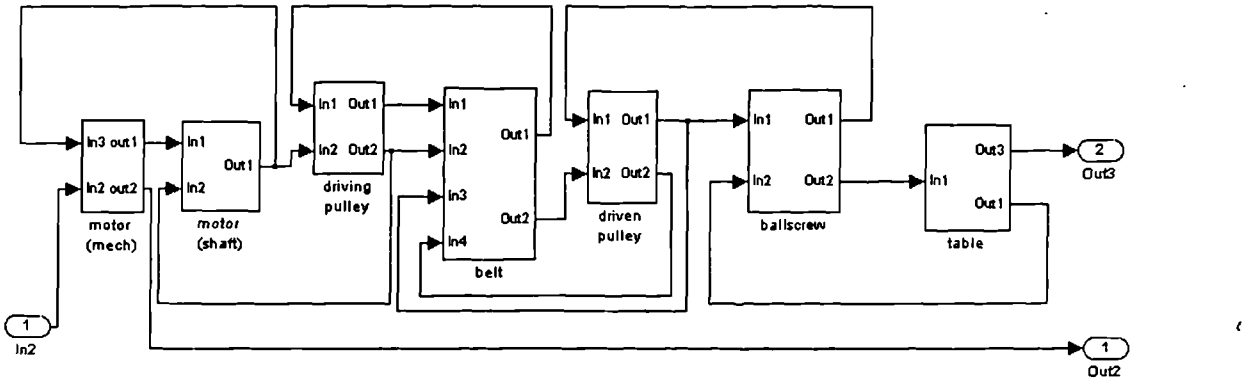

Figure 6. 8. Elements of the subsystem " *Explicit* "

The significance of the input / output ports is explained in the Table 6.1.

The ball-screw is modelled by six subsystems (see Figure 6. 9) taking into considerations the aspects of modelling discussed in Chapter 4. 3. 3. The significance of these subsystems is:

1. *Ballscrew1* - torsional spring/damper depicting the contact between ball-screw and driven pulley;
2. *Ballscrew middle* - represents the dynamic behaviour of the ball-screw middle;
3. *Ballscrew2* - torsional spring/damper depicting the contact between ball-screw and the structure;
4. *Ballscrew end* - describes the dynamic behaviour of the ball-screw end;

5. *Ballscrew nut* - portrays the dynamic behaviour of the ball-screw nut;
6. *Ballscrew axial stiffness* - contains the axial stiffness of the ball-screw and its mounting bearings.

Subsystem	Port name	Variable	Notation for variable
Motor (mechanical)	In3	Motor torque (mechanical)	T_{1M}
	In2	Electrical torque generated by the motor	T_{1E}
	Out1	Angular motor movement	$\{\omega_1, \theta_1\}$
	Out2	Angular motor speed	θ_1
Motor (shaft)	In1	Angular motor movement	$\{\omega_1, \theta_1\}$
	In2	Driving pulley movement	$\{\omega_2, \theta_2\}$
	Out1	Motor shaft torque	$T_2 = T_{1M}$
Driving pulley	In1	Torque from the drive belt	T_3
	In2	Motor shaft torque	$T_2 = T_{1M}$
	Out1	Driving pulley acceleration	β_2
	Out2	Driving pulley movement	$\{\omega_2, \theta_2\}$
Belt	In1	Driving pulley acceleration	β_2
	In2	Driving pulley movement	$\{\omega_2, \theta_2\}$
	In3	Driven pulley movement	$\{\omega_3, \theta_3\}$
	In4	Driven pulley acceleration	β_3
	Out1	Feedback torque to driving pulley	T_3
	Out2	Torque to driven pulley	T_4
Driven pulley	In1	Torque from *Ballscrew1*	T_5
	In2	Torque from belt drive	T_4
	Out1	Driven pulley movement	$\{\omega_3, \theta_3\}$
	Out2	Driven pulley acceleration	β_3
Ballscrew	In1	Driven pulley movement	$\{\omega_3, \theta_3\}$
	In2	Table linear movement	$\{v_6, x_6\}$
	Out1	Torque from *Ballscrew 1*	T_5
	Out2	Force generated by nut movement	F_3
Table	In1	Force applied to table from the nut	F_3
	Out1	Table linear movement	$\{v_6, x_6\}$
	Out3	Table linear velocity	v_6

Table 6. 1. Variables from the subsystem " *Explicit* "

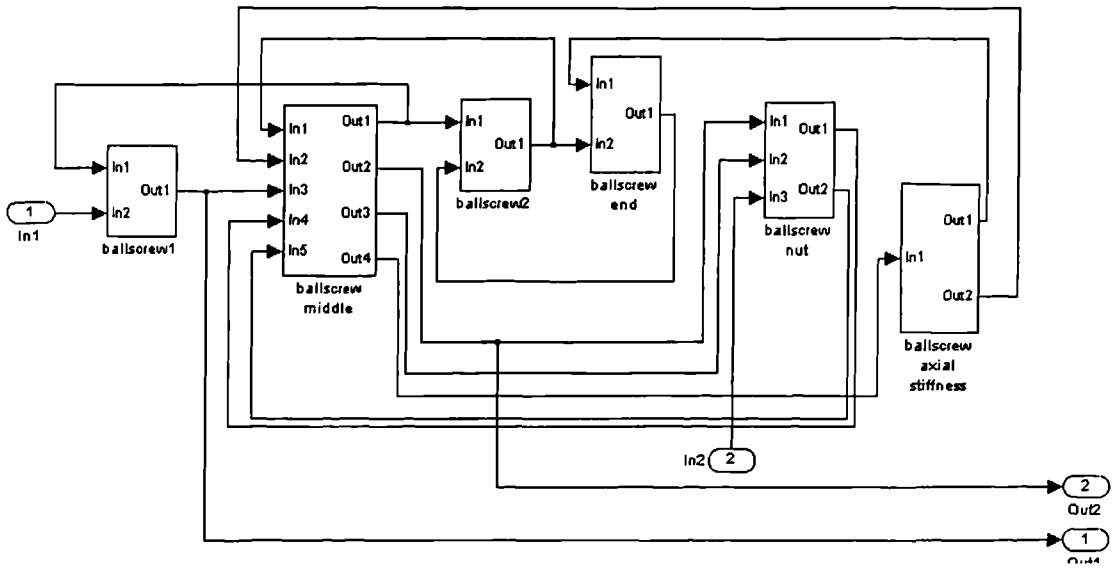

Figure 6. 9. Elements of the subsystem " *Ballscrew* "

The significance of the input / output ports is explained in the Table 6. 2.

The *ball-screw middle linear movement 1* has two components:

$$\{v'_4, x'_4\} = \{v_4, x_4\} + \{v, x\} = \{v_4, x_4\} + \{\omega_4, \theta_4\} x\, r_{BS} \qquad (6.1)$$

where $\{v_4, x_4\}$ - linear movement due to force acting on ball-screw middle inertia

$\{v, x\}$ - linear movement due to torque acting on ball-screw middle mass

r_{BS} – radius of the ball-screw

The configuration of the subsystem " *Ballscrew* " is described for the case of the rotary encoder attached to the end of the DC motor. For the situation when the position feedback is performed by the rotary encoder at the end of the ball-screw and linear encoder, the configurations of the subsystem " *Ballscrew* " are discussed in Appendix D1.

The coefficients of the model are calculated from the experimental data obtained during the closed-loop position control measurements (see Appendix B5). The model is validated by comparing the simulated results with measured data and by checking that the law of energy conservation (the sum of kinetic energy and potential energy is constant) is obeyed.

The particulars of the elements composing the model with explicit damping coefficients are explained furthermore.

Subsystem	Port name	Variable	Notation for variable
Ballscrew 1	In1	Ball-screw middle movement	$\{\omega_4, \theta_4\}$
	In2	Driven pulley movement	$\{\omega_3, \theta_3\}$
	Out1	Torque from *'Ballscrew 1'*	T_5
Ballscrew middle	In1	Torque from *'Ballscrew end'*	T_8
	In2	Force from *'Ballscrew axial stiffness'*	F_1
	In3	Torque from *'Ballscrew 1'*	T_5
	In4	Force from *'Ballscrew nut'*	F_2
	In5	Torque from *'Ballscrew nut'*	T_6
	Out1	Ball-screw middle movement	$\{\omega_4, \theta_4\}$
	Out2	Ball-screw middle velocity	ω_4
	Out3	Ball-screw middle linear movement 1	$\{v'_4, x'_4\}$
	Out4	Ball-screw middle linear movement	$\{v_4, x_4\}$
Ballscrew 2	In1	Ball-screw middle movement	$\{\omega_4, \theta_4\}$
	In2	Ball-screw end movement	$\{\omega_5, \theta_5\}$
	Out1	Torque from *'Ball-screw 2'*	T_7
Ballscrew end	In1	Axial force from thrust bearings	F_3
	In2	Torque from *'Ball-screw 2'*	T_7
	Out1	Ball-screw end movement	$\{\omega_5, \theta_5\}$
Ballscrew nut	In1	Ball-screw middle velocity	ω_4
	In2	Ball-screw middle linear movement 1	$\{v'_4, x'_4\}$
	In3	Table linear movement	$\{v_6, x_6\}$
	Out1	Force generated by nut movement	F_2
	Out2	Torque from *'Ballscrew nut'*	T_6
Ballscrew axial stiffness	In1	Ball-screw middle linear movement	$\{v_4, x_4\}$
	Out1	Axial force from thrust bearings	F_3
	Out2	Force from *'Ballscrew axial stiffness'*	F_1

Table 6. 2. Variables from the subsystem " *Ballscrew"*

Motor (mechanical)

The *" Torque acting on motor inertia"* subsystem calculates the motion of the motor. The torque acting on the motor can be calculated with the following relation:

$$T_{ef} = T_{IE} - T_{IM} - T_{mech} \tag{6. 2}$$

where T_{ef} – the effective torque acting on the motor inertia [Nm]

T_{IE} – the electrical torque generated by the DC motor (Equation (4. 12)) [Nm]

T_{IM} – the reaction torque generated by motor shaft [Nm]

T_{mech} – the reaction torque from the motor bearings [Nm]

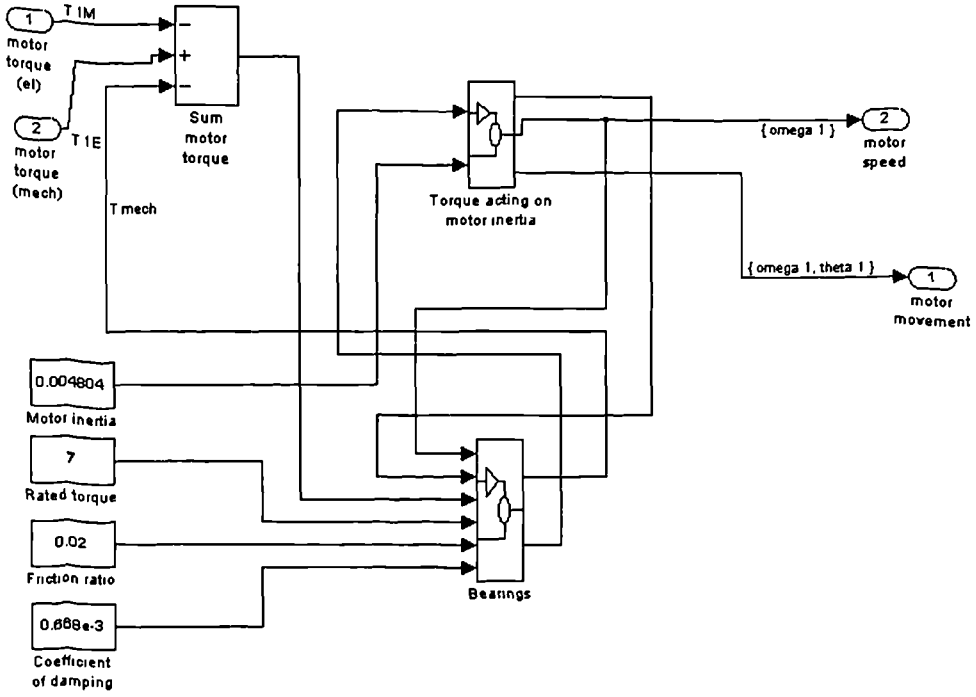

Figure 6. 10. Elements of the block *'"Motor (mechanical)"*

The angular speed of the DC motor yields:

$$\omega_1 = \int \beta_1 \, dt = \int \frac{T_{ef}}{J_m} dt \qquad (6.3)$$

where β_1 – the angular acceleration of the DC motor [rad / s^2]

J_m – the DC motor inertia [kg m^2]

The angular velocity and displacement are multiplexed to give the *"movement"* for simplicity of reading the model. The motor speed is given as a special output because it is used in the velocity loop to control the motor.

The dissipative effects of the bearing friction and viscosity are modelled by the *"Bearings"* subsystem that has two components:

1. *"Friction"* – estimates the torque transmitted to the inertia after subtracting torque generated by friction in the bearings from the rated torque. The friction in the bearings is considered to act like Coulomb friction, up to 2 % of the rated torque in this case:

$$T_{mech} = m_{0M} - 0.02 \times m_{0M} = 0.08\, m_{0M} = 0.08 \times 7 = 0.56 \text{ Nm} \qquad (6.4)$$

T_{mech} is transmitted as output signal through the out port 2 (force to sliding part).

The block " *Torque feedback* " represents the implementation of the Coulomb friction model. In this particular case, the variable is torque, but because this type of block is used as a Coulomb friction model considering forces, the discussion is held on forces.

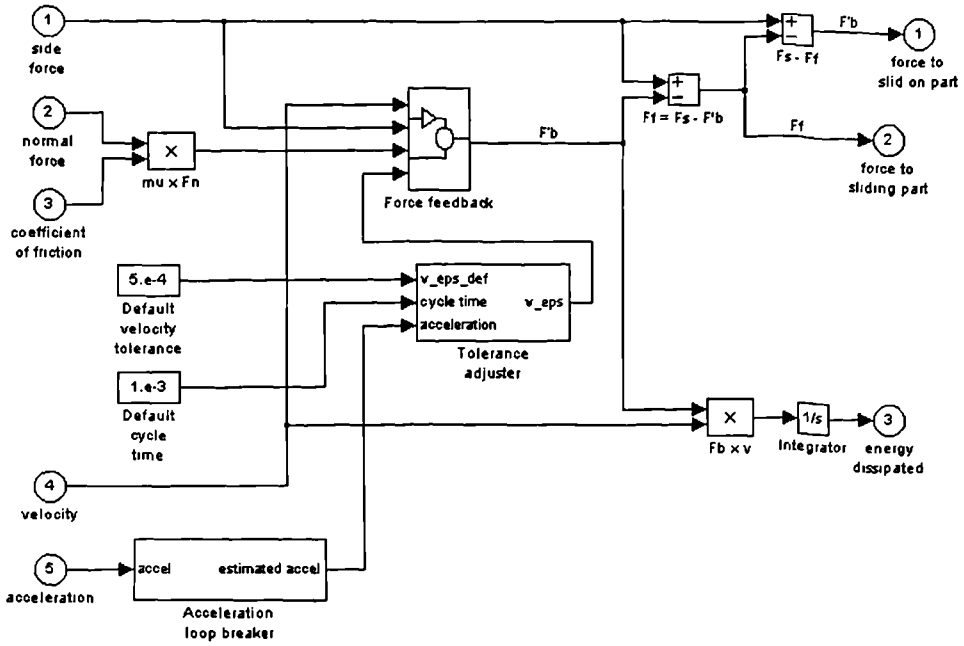

Figure 6. 11. Elements of the block " *Friction* "

During the development of the friction element, problems were experienced with bringing a mass to rest. SIMULINK solves the equations in a sequence of steps separated in time. When a mass is moving only slowly in the positive direction, the reaction force due to Coulomb friction μ x F_n is acting. If this force is sufficient to cause the mass to stop and start moving backwards in the cycle time of the solution process, the force μ x F_n reverses and starts to push the mass forwards again. This can cause the force to change signs again, and so on, generating a series of force "spikes" in the process. Although the nett effect is to keep the velocity of the mass close to zero, it was considered that the force "spikes" are not desirable. The following steps were followed to avoid this problem:

a) an interim feedback force F'_b was defined in two particular cases:

$$\text{if } \left|\frac{v}{v_\varepsilon}\right| < 1 \text{ then } F'_b = -F_s\left(\frac{v}{v_\varepsilon}\right)^2 + \mu \times F_n \frac{v}{v_\varepsilon} + F_s \qquad (6.5)$$

$$\text{if } \left|\frac{v}{v_\varepsilon}\right| \geq 1 \text{ then } F'_b = \mu \times F_n \frac{v}{|v|} \qquad (6.6)$$

where v – velocity

μ - coefficient of friction

v_ε - velocity tolerance

F_n – normal force [N]

F'_b - interim feedback force [N]

$|v|$ – velocity norm

F_s – applied force [N]

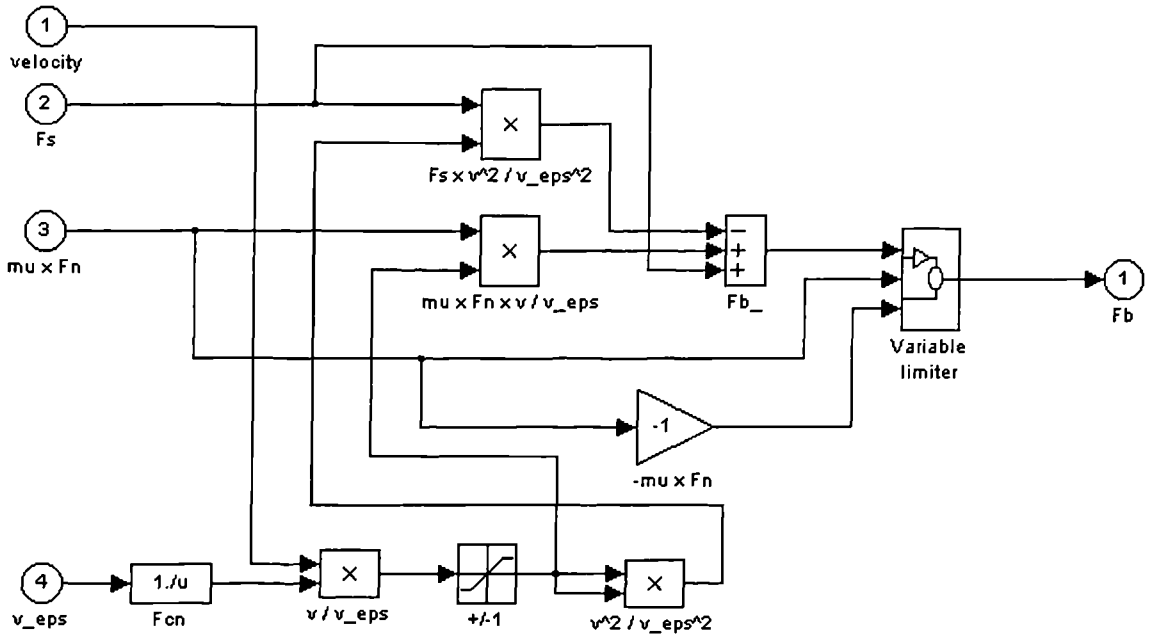

Figure 6. 12. Elements of the block " *Force feedback* "

The block " *Variable limiter* " is similar to " *Saturation* " block from SIMULINK library, but the upper and lower limits are estimated by the model rather being predefined (see Figure 6. 13).

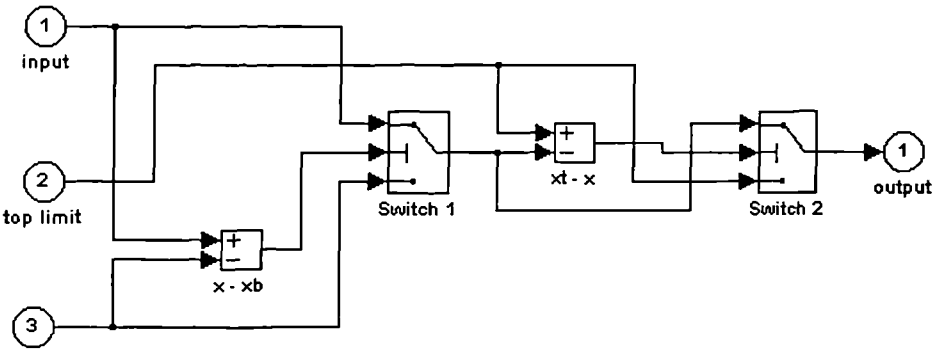

Figure 6. 13. Elements of the block " *Variable limiter*"

b) the block " *Tolerance adjuster* " (Figure 6. 14) is included to prevent instability when friction is bringing a part of the model to rest (relative to another part of the model or to zero).

The following logic was implemented into this block:

$$\text{If } v_\varepsilon < v_{\varepsilon\,def} \quad \text{then} \quad v_\varepsilon = v_{\varepsilon\,def} \tag{6. 7}$$

$$\text{If } v_\varepsilon \leq v_{\varepsilon\,def} \quad \text{then} \quad v_\varepsilon = 3.13 \times |a \times \delta t| \tag{6. 8}$$

Where $v_{\varepsilon\,def} = 5 \times 10^{-4}$ - default velocity tolerance v_ε - velocity tolerance

$\delta t = 1 \times 10^{-3}$ - solver cycle time a – acceleration [m / s^2]

The value 3.13 for zero trap width is chosen after different trials for the model.

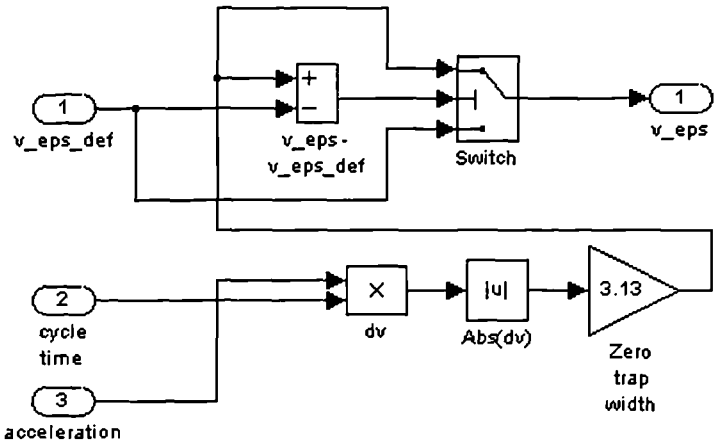

Figure 6. 14. Elements of the block " *Tolerance adjuster"*

c) the block " *Acceleration loop breaker* " has the role of avoiding problems with arithmetic loops from the *"Friction"* subsystem. The current calculated value of the acceleration is replaced by one estimated from the previous two values:

$$a_{estimat}(i) = 2 \times a(i-1) - a(i-2) \qquad (6.9)$$

where $a_{estimat}(i)$ – the current calculated value of the acceleration

$a(i-1)$, $a(i-2)$ – the previous two values of the acceleration

The estimated value is used in the setting of the velocity tolerance band which defines the smooth curves applied to calculate the forces used to bring a part of the model to rest.

2. " *Damper* " – calculates the resistive torque of the bearings which is proportional to motor speed. The force developed by damper is:

$$F = c \times \frac{dx}{dt} = c \times v \qquad (6.10)$$

where c – damping coefficient v – linear velocity x - displacement

Motor (shaft) is modelled as a torsional spring / damper element described by Equation (4. 46).

Driving pulley is represented as an inertia element by a block similar to " *Torque acting on motor inertia"* subsystem with the corresponding Equation (6. 3).

Belt (Figure 6. 15) - the block " *Spring / damper* " computes the spring torque and takes into account the damping effect of the material giving rise to the damping torque.

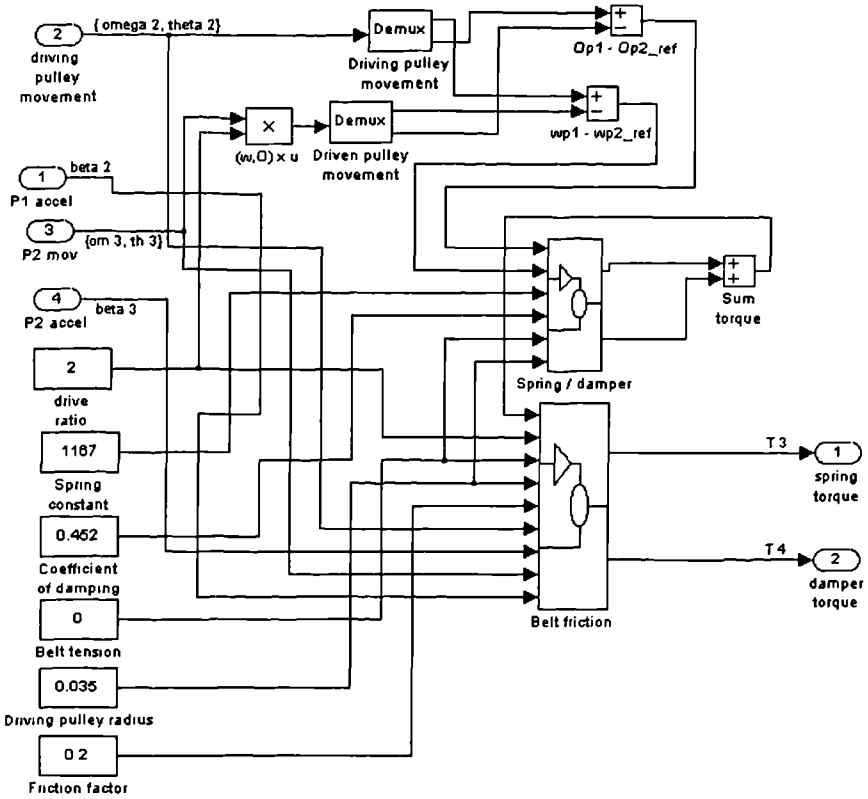

Figure 6. 15. Elements of the block " *Belt*"

The belt could run slack, depending on the belt tension and the transmitted torque. The effect consists of changing the stiffness and damping factor. The two parts of the belt, between pulleys, are treated separately in order to account for this phenomenon. The belt tension stretches the belt and the total stretch for the two parts could be expressed in terms of equivalent angle at the driving pulley:

$$\theta_1 = \frac{T_{belt} \times r_1}{K_\theta} + \theta \qquad (6.11)$$

$$\theta_2 = \frac{T_{belt} \times r_1}{K_\theta} - \theta \qquad (6.12)$$

where T_{belt} – tension in belt r_1 – driving pulley radius

K_θ – torsional stiffness of the belt $\theta_1, \theta_2, \theta$ - angular displacements

The torque referred to the driving pulley, transmitted by each portion of the belt is given by:

If $K_\theta \times \theta_1 < 0$ then $T_1 = 0$ else $T_1 = K_\theta \times \theta_1$ (6.13)

If $K_\theta \times \theta_2 < 0$ then $T_2 = 0$ else $T_2 = K_\theta \times \theta_2$ (6.14)

where T_1 – torque acting upon driving pulley T_2 – torque acting upon driven pulley

θ_1 - angular displacement of driving pulley θ_2 –angular displacement of driven pulley

The total spring torque is:

$$T_s = T_1 - T_2 \qquad (6.15)$$

The damping torque is considered to be dependent on whether one or two portions of the belt are transmitting the load:

If $T_1 \times T_2 < 0$ then $T_d = c_\theta \times \omega_1$ else $T_d = 2 c_\theta \times \omega_1$ (6. 16)

where c_θ - torsional damping coefficient ω_1 - angular velocity of driving pulley

The element " *Belt friction* " (Figure 6. 16) contains the models for the following:

- The frictional effect caused by the sliding of the belt teeth in and out of mesh with the pulley teeth;
- Any sliding of the belt within the pulley flanges;
- The hysteresis involved in flexing and unflexing the belt as it passes over the pulleys.

The belt friction is considered to act on each pulley separately as the belt teeth go in and out of mesh. The torque that determines the level of the "normal force" is given by:

$$T_{a1} = T_{belt} \times r_{p1} + |T_s| \qquad \text{for the driving pulley} \qquad (6.17)$$

$$T_{a2} = 2 \times (T_{belt} \times r_{p1} + |T_s|) \qquad \text{for the driven pulley} \qquad (6.18)$$

The torque which acts as the "sideways force" is the torque transmitted by the belt in the case of the driving pulley. This is multiplied by the drive ratio to give the torque on the driven pulley.

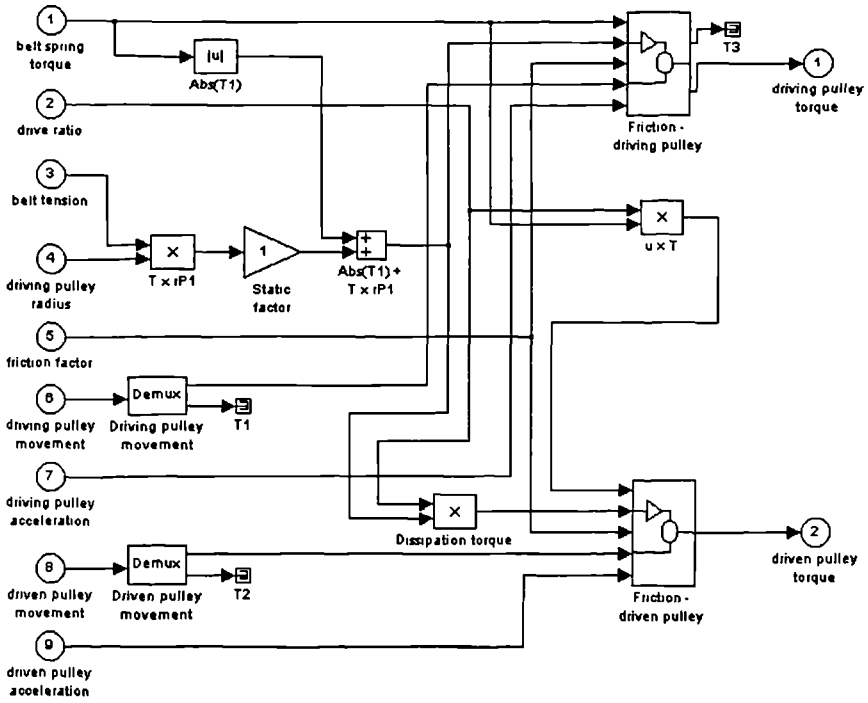

Figure 6. 16. Elements of the block " *Belt friction*"

The blocks " *Friction – driving pulley* " and " *Friction – driven pulley* " have the same structure as block " *Motor (mechanical)* " and calculate the feedback torque for the driving pulley and the driven pulley.

Driven pulley – is modelled as motor (mechanical) using " *Torque acting on inertia*" subsystem and " *Bearings* " subsystem. The friction in the bearings is considered to act like Coulomb friction up to 1% from the rated torque in this case:

$$T_{mech1} = 2\, m_{0M} - 0.01 \times 2 \times m_{0M} = 0.09 \times 2 \times m_{0M} = 0.09 \times 14 = 1.26 \text{ Nm} \quad (6.19)$$

Ball-screw - is modelled by six subsystems (see Figure 6. 9) and their content is as it follows:

1. ***Ballscrew 1*** – torsional spring / damper element described by Equation (4. 46).
2. ***Ballscrew middle*** (Figure 6. 17) – is a special element which portrays the dynamic behaviour of the ball-screw middle (the portion of the ball-screw on which the nut is sliding). It is called ball-screw middle because the nut is on the middle of the ball-screw during the performed experiments.

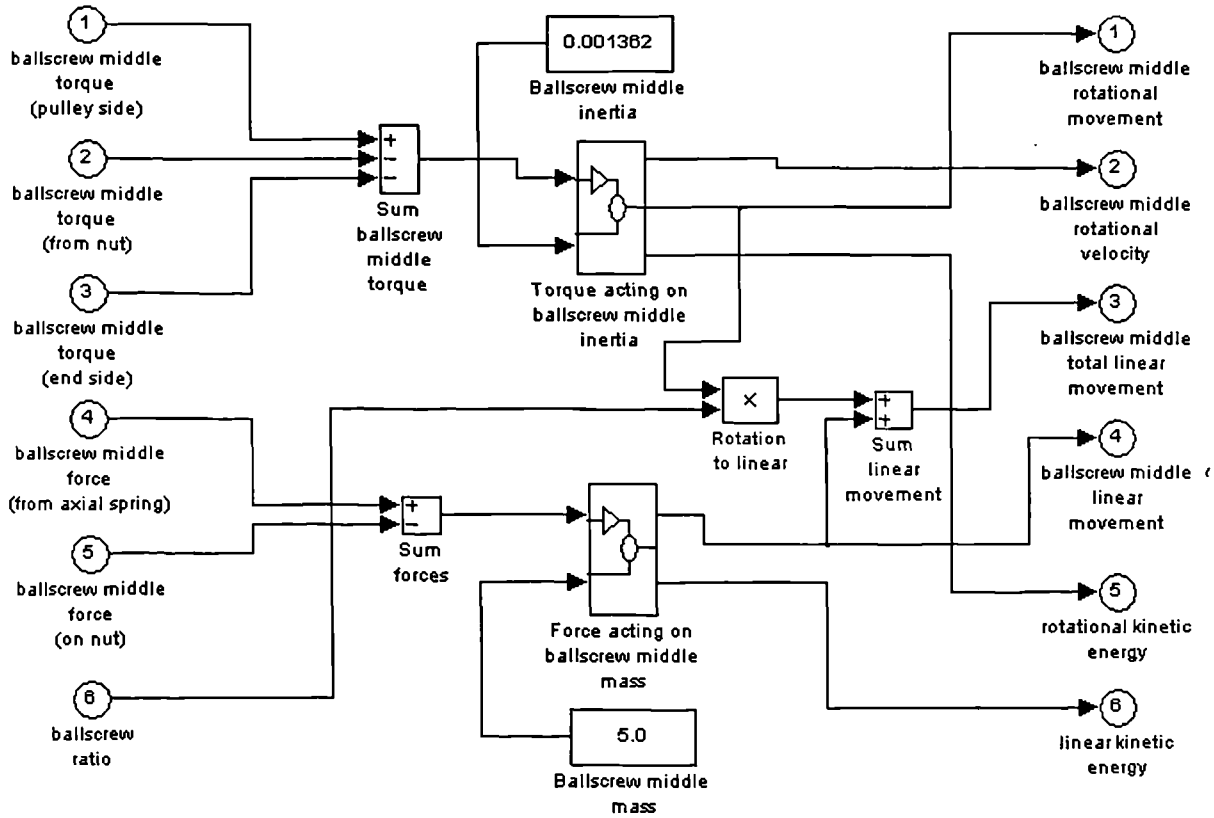

Figure 6. 17. Elements of the block "*Ballscrew middle*"

The functions executed by this element are:

- the torsional movement of the ball-screw middle is computed by an inertia element (*"Torque acting on ball-screw middle inertia "*);

- the torsional movement of the ball-screw centre is converted to the linear movement of the nut using the ratio (screw pitch / 2π);
- the linear movement of the ball-screw middle caused by the reaction force from the nut acting on the ball-screw and its support bearings is estimated by a mass element (*"Force acting on ballscrew middle mass"*). The force is computed with the following relation:

$$F_a = F_1 - F_2 \tag{6. 20}$$

where F_a – force acting on ball-screw middle mass

F_1 – force from axial spring F_2 – force from nut

The axial behaviour of the ball-screw middle is depicted by the linear speed of the ball-screw middle mass:

$$v_4 = \int a_4 \, dt = \int \frac{F_a}{m_1} dt \tag{6. 21}$$

and the linear displacement of the ball-screw middle mass:

$$x_4 = \int v_4 \, dt \tag{6. 22}$$

where v_4, a_4 – linear speed respectively linear acceleration of the ball-screw middle

F_a – force acting on ball-screw middle mass

$m_1 = m_{BS} / 3 = 5$ kg – equivalent with the effect of the ball-screw mass on the springs corresponding to each half of the total length (see Appendix 4)

x_4 – linear speed of the ball-screw middle mass

- the total axial movement of the part of the ball-screw that acts on the nut is calculated using Equation (6. 1).

3. ***Ballscrew 2*** – torsional spring / damper element described by Equation (4. 46).
4. ***Ballscrew end*** (Figure 6. 18) – is a special element which portrays the dynamic behaviour of the ball-screw end (the part attached to the structure through the thrust bearings). The torque acting on ball-screw end inertia is:

$$T_a = T_7 - T_{radial} - T_{thrust} = T_7 - T_{radial} - 0.5 \times F_3 \times D_{tb} \tag{6. 23}$$

Where T_a - torque acting on ball-screw end inertia T_7 – torque from *"Ball-screw 2"*

T_{radial} – torque arising from the radial action of the thrust bearings

The " *Tail end bearing radial* " block has the structure of " *Bearings* " block in which the *"Friction"* block works out the torque generated by the thrust bearings due to their radial action. This torque is obtained by subtracting from the rated torque, the torque generated by friction in the radial component of the bearings (assumed to be 1 % from 14 N). The

"Damping " subsystem calculates the resistive torque of the bearings which is proportional to the ball-screw speed.

The " *Tail end bearing thrust* " block has the structure of " *Bearings* " block in which the *"Friction"* block works out the torque created by the thrust bearings due to their thrust action. This torque is calculated by subtracting from the thrust torque T_{thrust}, the torque generated by friction in the thrust component of the bearings (assumed to be 1 % from T_{thrust}).

The thrust torque has the following relation:

$$T_{thrust} = F_3 \times (D_{tb} / 2) \qquad (6.24)$$

where T_{thrust} - torque generated due to axial thrust of the bearings

F_3 - axial force from thrust bearings D_{tb} – diameter of bearing race

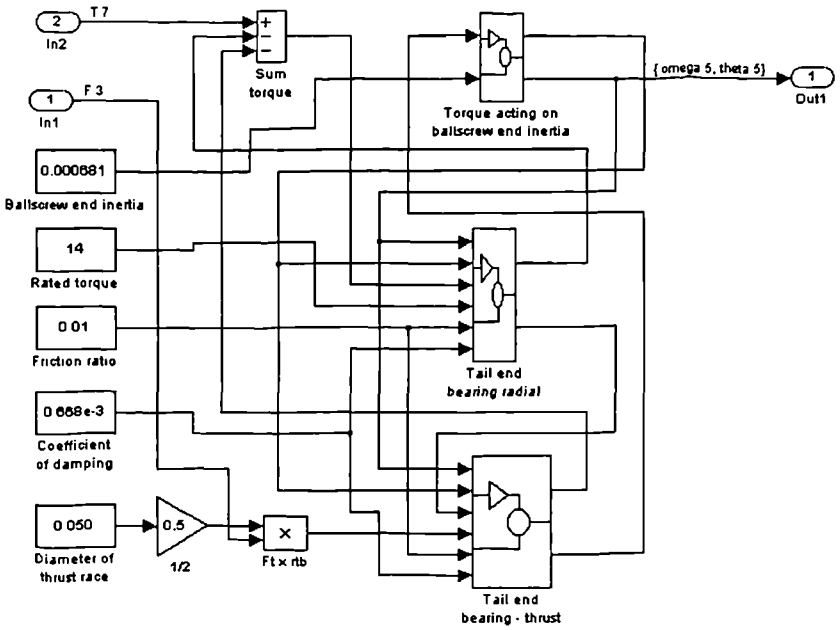

Figure 6. 18. Elements of the block *"Ballscrew end"*

5. ***Ballscrew nut*** – is a special spring / damper element which takes account of the backlash between the ball-screw and the nut by using a "dead zone" feature in series with the spring which represents the stiffness of the nut and its mounting feature.

   The *"Spring / damper "* element calculates the force transmitted by the ball-screw nut considering the effect of the relative displacement and velocity of the ball-screw centre and table on a notional "stiff "spring (spring constant K = 5 x 10^8 N / m, damping coefficient c = 58060 N s / m). This is done as a means of sharing the load between the ball-screw and the table because

$$F_2 = F_{spring} + F_{damper} \qquad (6.25)$$

(the force transmitted by the nut = spring force + damping force).

The backlash is taken into account at this stage.

In the case of the block " *Nut forces* "(see Figure 6. 20), for the computational convenience, the ball-screw is treated as an acme screw with the same lead angle as the ball-screw and an equivalent coefficient of friction (0. 01) to represent the resistive forces in the nut. The block " *Set sign* " defines a variable S which can take two values:

+ 1 - when the ball-screw is transmitting force to the nut (" forward " mode)

- 1 - when the nut is transmitting the force to the screw (" negative " mode)

When the applied force or the rotational velocity is zero, the variable S is zero.

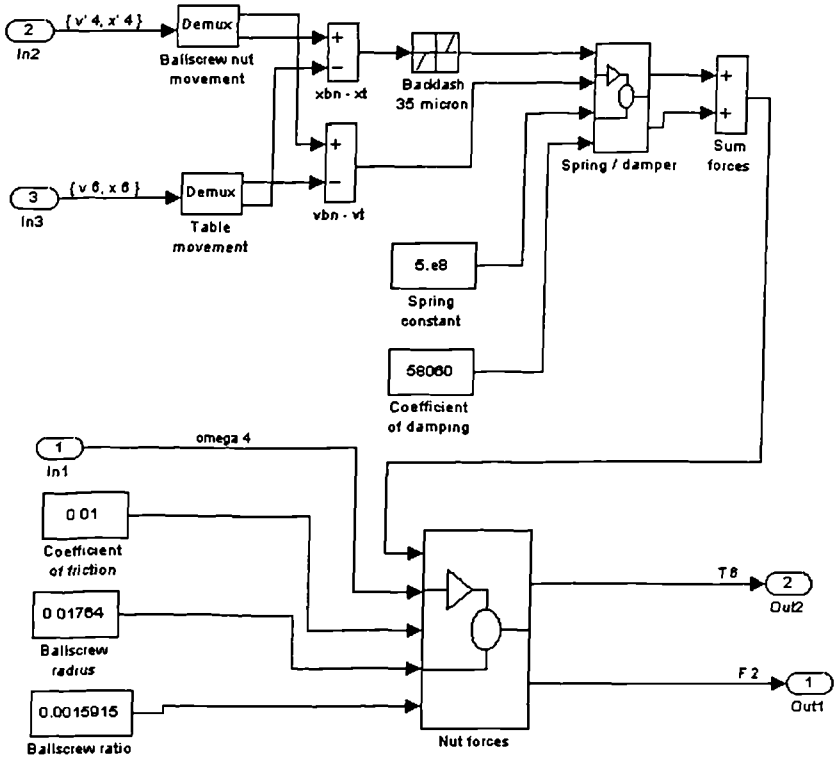

Figure 6. 19. Elements of the block "*Ballscrew nut*"

The block computes the forces transmitted by the ball-screw both in "driving" and "over-riding" mode. The sum of the normal forces acting along the screw is given by:

$$F_n = \frac{\sqrt{b^2 + r_{bs}^2}}{r_{bs} - S \times \mu_b \times b} \times F_2 \qquad (6.26)$$

where F_n – the normal force F_2 – force transmitted by nut

r_{bs} - ball-screw radius S – sign generated by "Set sign" block

μ_b - coefficient of friction b – ball-screw ratio

The sum of the tangential forces acting along the screw is:

$$F_t = \frac{b + S \times \mu_b \times r_{bs}}{\sqrt{b^2 + r_{bs}^2}} \times F_n \qquad (6.27)$$

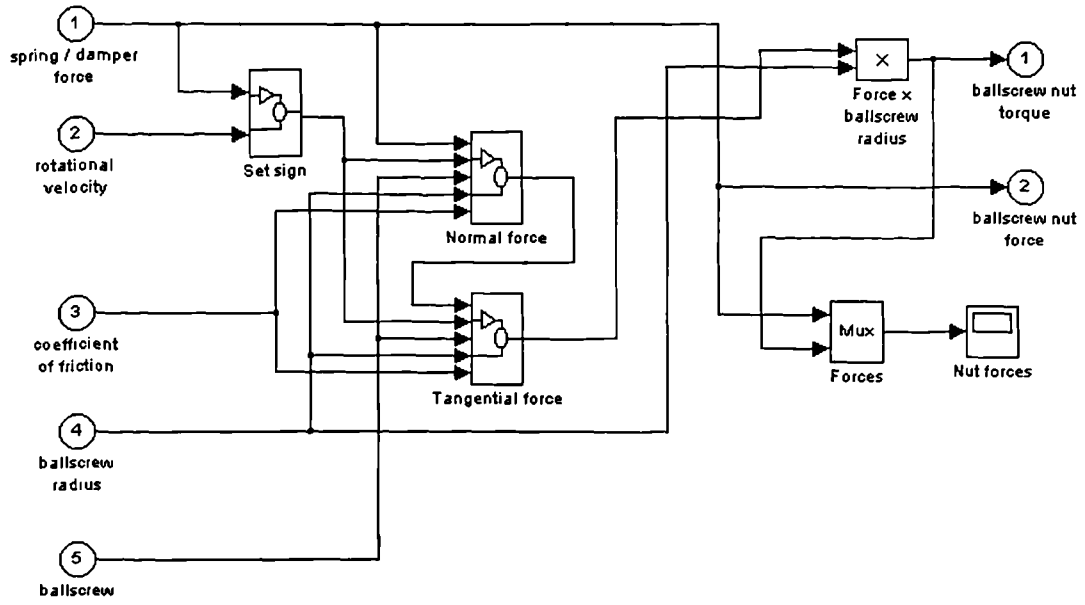

Figure 6. 20. Elements of the block " *Nut forces*"

6. *Ballscrew axial stiffness* – is a spring / damper element with spring constant $K_6 = 482.7 \times 10^6$ N / m and damping coefficient $c_6 = 8326$ N s / m. The axial force from thrust bearings applied to the ball-screw end is:

$$F_1 = F_s + F_d \qquad (6.28)$$

and the force applied to ball-screw middle is :

$$F_3 = -F_s - F_d \qquad (6.29)$$

where F_s – spring force [N] F_d – damping force [N]

Table – is a special element incorporating a friction element which takes into account the frictional behaviour of the table (X-axis drive) or saddle and table (Y-axis drive). The other subsystem entitled "*Force from ballscrew nut acting on mass*" is a basic inertia element (see " *Torque acting on motor inertia*" subsystem).

From the measurements performed with accelerometers to determine the source of the 35 Hz resonance (see Appendix C3), it resulted that the saddle and worktable are rocking around the X-axis. When the worktable and saddle move in the Y-axis direction, the reaction forces from the slides produce the tilting of the worktable and saddle around the X-axis. Also a torque is produced around the Y-axis because the movement of saddle and worktable is in the Y-axis direction. A graphical description of this phenomenon is portrayed in Figure 6. 21.

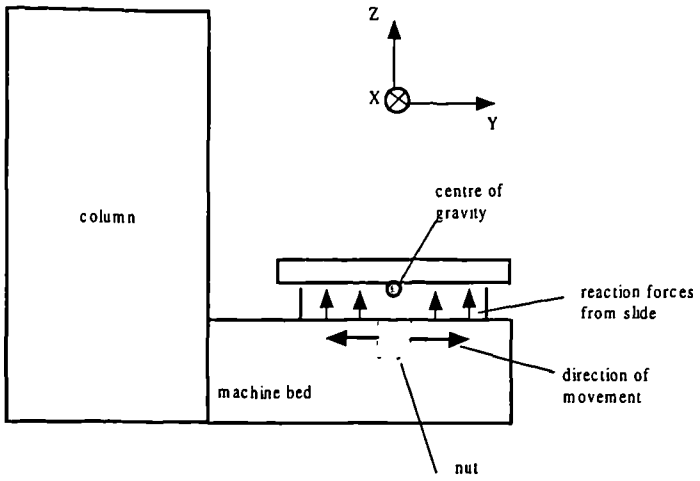

Figure 6. 21. The causes of worktable and saddle tilting around X-axis when the movement is in the Y-axis direction

The rocking around the X-axis can be represented as a torsional spring/damper element described by Equation (4. 46) and introduced into the block called *"Bed stiffness"* and added into the subsystem *"Explicit"*.

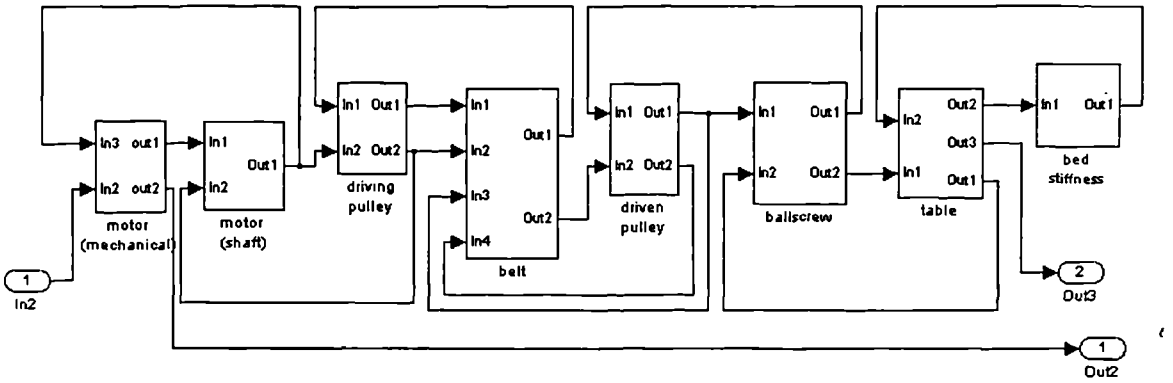

Figure 6. 22. Elements of the block " *Explicit"* when the rocking of the worktable and saddle is considered

The changes of the connections between *"Ballscrew"*, *"Table"* and *"Bed stiffness"* are shown in Figure 6. 22 and the significance of the input and output ports is described in Table 6. 3. The other blocks from the subsystem *"Explicit"* remain the same as in Figure 6. 8.

The block *"Table"* is different from that presented earlier (Figure 6. 11) because it has to incorporate the rotational movement of the saddle and worktable. The new structure of the block is presented in Figure 6. 23.

The blocks " *Force from ballscrew nut acting on mass* " *and "Torque from ballscrew nut acting on inertia* " have the same structure as the subsystem *"Torque acting on motor inertia"* (Equations 6. 2 – 6. 3).

Subsystem	Port name	Variable	Notation for variable
Ballscrew	In1	Driven pulley movement	$\{\omega_3, \theta_3\}$
	In2	Table linear movement	$\{v_6, x_6\}$
	Out1	Torque from *Ballscrew 1*	T_5
	Out2	Force generated by nut movement	F_3
Table	In1	Force applied to table from the nut	F_3
	In2	Torque applied to saddle / worktable	T_6
	Out1	Table linear movement	$\{v_6, x_6\}$
	Out2	Rotational movement of the saddle and worktable	$\{\omega_6, \theta_6\}$
Bed stiffness	In1	Rotational movement of the saddle and worktable	$\{\omega_6, \theta_6\}$
	Out1	Torque applied to saddle / worktable	T_6

Table 6. 3. Variables from the blocks *"Ballscrew"*, *"Table"* and *"Bed stiffness"* when the rocking of the worktable and saddle is considered

The angular velocity of the saddle/worktable is calculated using the following relation:

$$\omega_6 = \int \beta_6 \, dt = \int \frac{T_7}{J_7} \, dt = \int \frac{(F_3 \times z_1) - (F_f \times z_2) + T_6}{J_7} \, dt \qquad (6.30)$$

where ω_6 - angular velocity of the saddle / worktable J_7 - saddle / worktable inertia

β_6 - angular acceleration of the saddle / worktable

T_7 - torque from ball-screw nut acting on saddle / worktable inertia

F_f – friction force due to nut movement (see Appendix A4)

F_3 - force generated by nut movement

z_1, z_2 - the distances between the point of application for F_3 and F_f respectively and the centre of gravity for saddle/worktable (practically measured)

In order to validate the model, the various conditions of the experiments are simulated and the simulated results are compared with the measured ones.

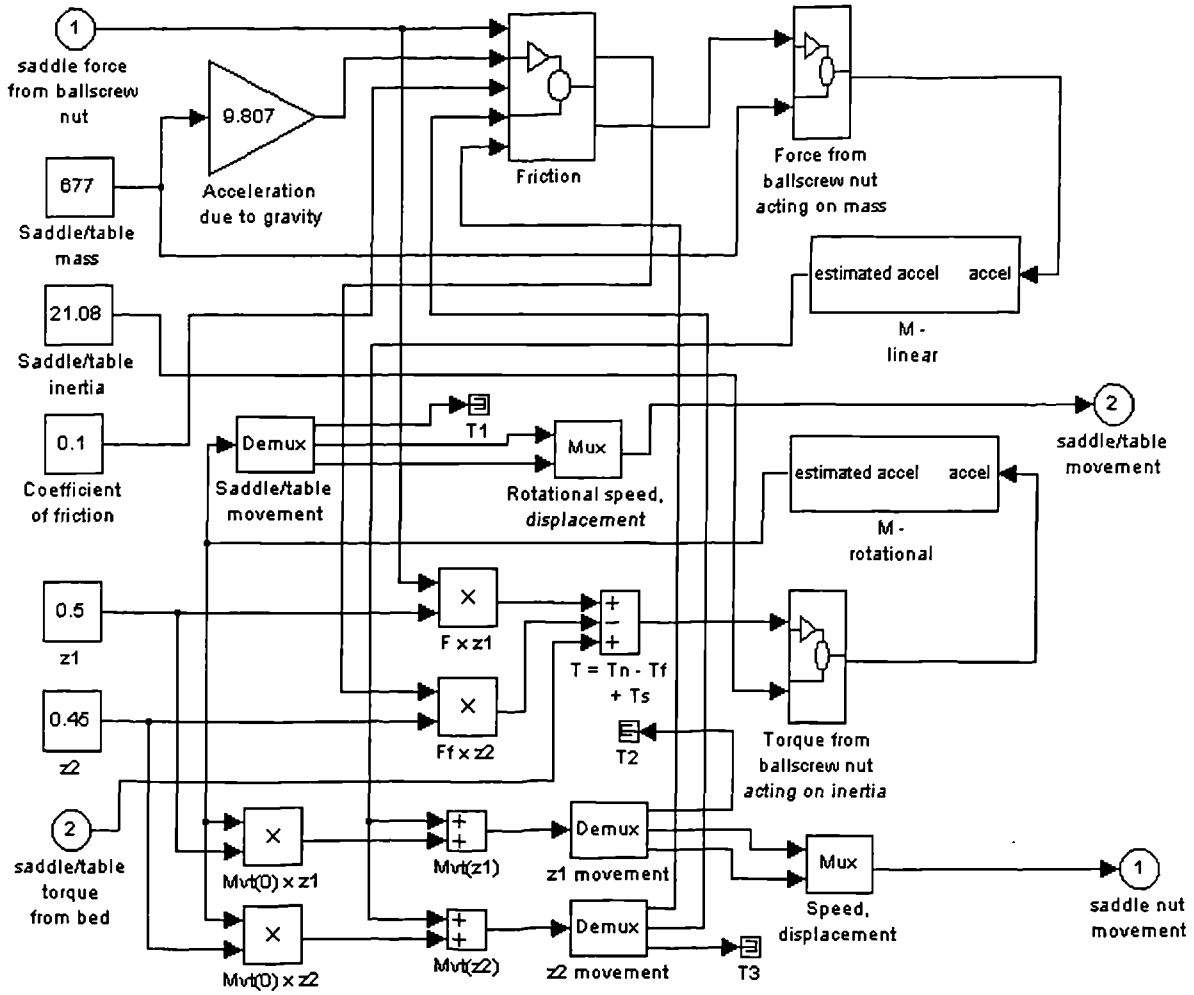

Figure 6. 23. Elements of the block " *Table*" when the rotation of the worktable and saddle is considered

6. 2. Testing the models for deterministic (step and trapezoidal) inputs

6. 2. 1. Lumped parameter model with modular load with backlash and friction

The first stage consists in simulating the action of a single axis drive system using a single set of mathematical models, in response to two categories of deterministic signals, and step and trapezoidal inputs.

The step demand is introduced into the model with distributed parameters corresponding to the experimental set up for the open-loop position control (Figure 6. 24).

The simulated linear velocity of the worktable has the value of 24 mm/ s (Figure 6. 25) when a voltage of 1 V is applied to the pre-amplifier while the measured velocity for the worktable is 26 mm/s. The simulated results are similar to the measured ones, but there are no

ripples on the simulated worktable velocity because the damping coefficients do not have explicit values in the SIMULINK model.

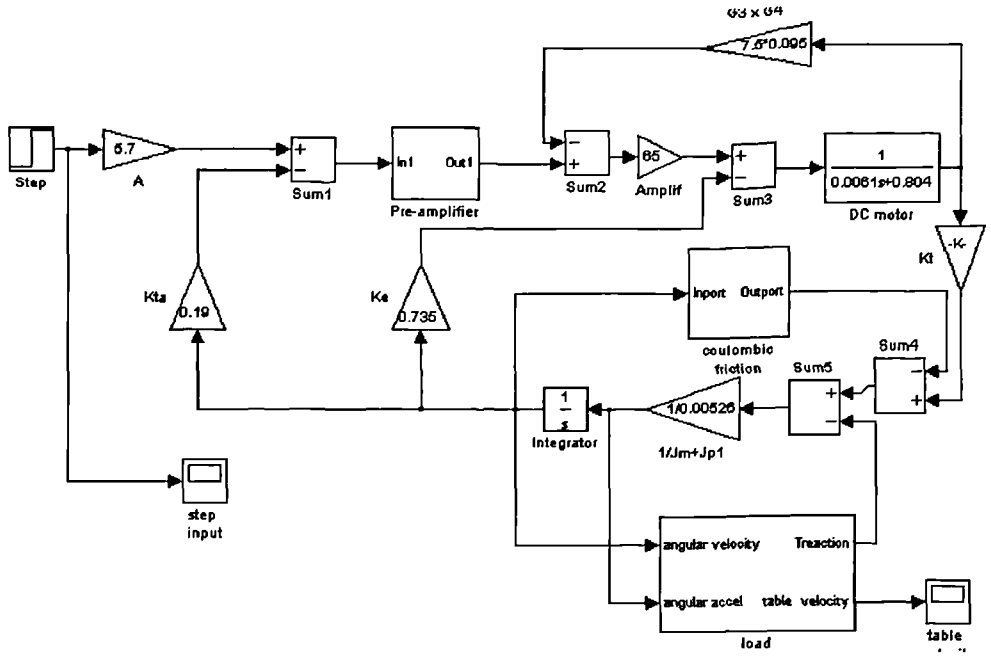

Figure 6. 24. SIMULINK 2. 0. model with distributed parameters corresponding to the experimental set-up for measurements in open-loop position control

The values of the parameters were calculated in the previous chapters on the basis of theoretical and practical considerations.

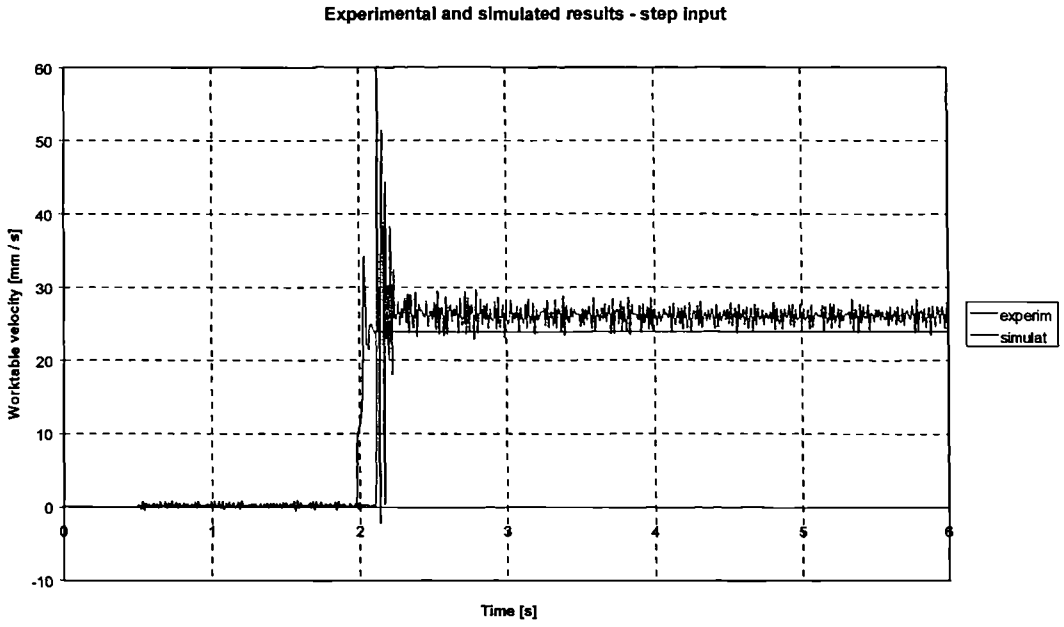

Figure 6. 25. Simulated and measured worktable velocity for a step input considering the model with distributed parameters

The second stage comprises the use of a *trapezoidal signal* as an input stimulus to check out the performance of the CNC machine tool model during acceleration, deceleration and functioning at constant rate. In the case of a Beaver VC 35 CNC machine tool, the half fast traverse rate of 5 m / min = 83. 33 mm /s is selected and the maximum of the simulated value for the controller error is 3. 5 V (as the measured one - Figure 5. 35).

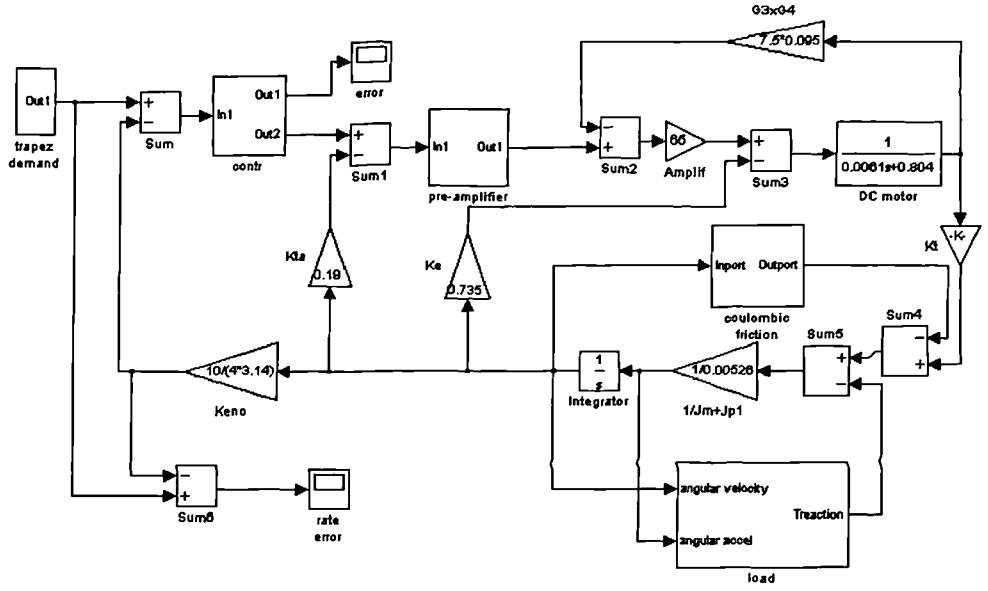

Figure 6. 26. SIMULINK 2. 0. model with distributed parameters corresponding to the experimental setup for measurements in closed -loop position control

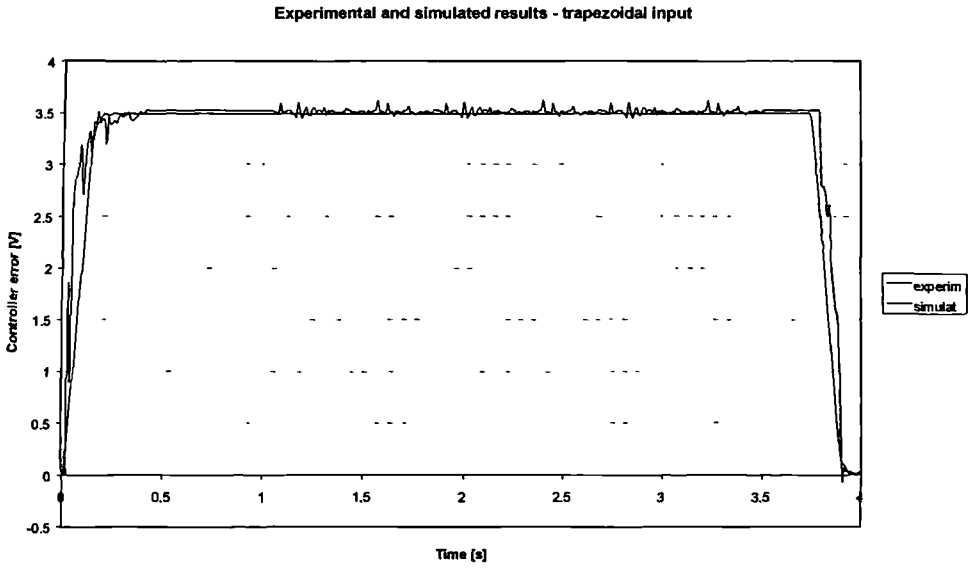

Figure 6. 27. Simulated and measured worktable velocity for trapezoidal input considering the model with distributed parameters

The rate error and the controller error for Y-axis model to the trapezoidal stimulus are shown in Figure 6. 27. It could be observed that the rapid response is circa 0.2 s with no overshoot. Therefore this system is approaching the critically damped situation as required.

It is evident that the drive response lags behind the demand signal especially during acceleration and deceleration phases of simulation. Some lag is inevitable as the system is error driven. The greatest values of the armature current produced by the DC motor appear as the drive attempts to accelerate the load in response to the demand signal ramp up. This is because the motor must generate sufficient torque to accelerate the load and overcome the effects of friction.

After the slide velocity has reached the requested value, the transient state settles and the motor current reduces in magnitude. The drive is now at constant velocity and is overcoming only the effects of friction.

6. 2. 2. Hybrid model with distributed load, explicit damping factors, backlash and friction

The step demand is introduced into the model with explicit damping coefficients corresponding to the experimental set up for the open-loop position control. The simulated linear velocity of the worktable has the value of 24 mm/ s when a voltage of 1 V is applied to the pre-amplifier while the measured velocity for the worktable is 26 mm/s. So the simulated results are similar to those measured.

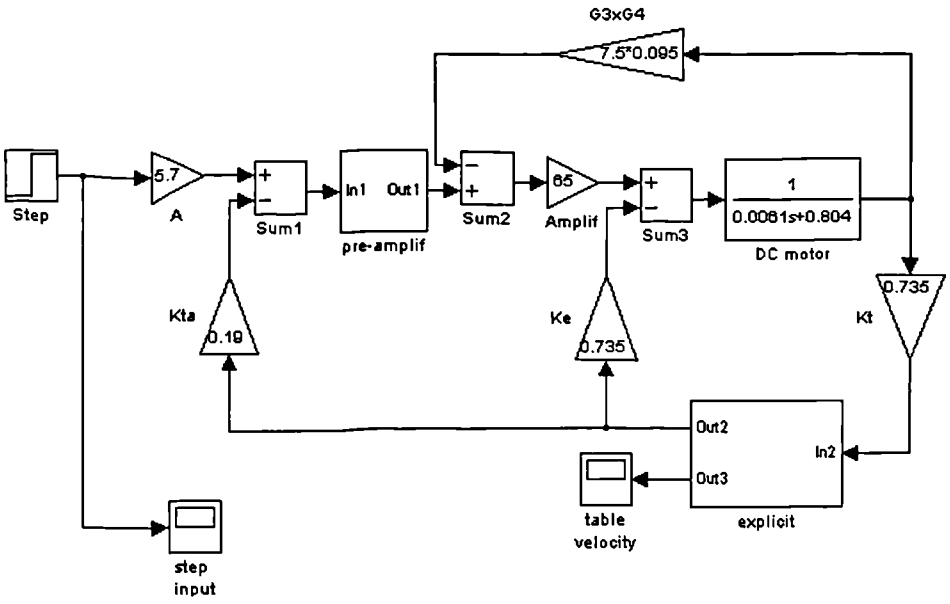

Figure 6. 28. SIMULINK 2. 0. model with explicit damping coefficients corresponding to the experimental setup for measurements in open -loop position control

Simulation of SIMULINK models involves the numerical integration of sets of ordinary differential equations (ODEs). SIMULINK provides a number of solvers for the simulation of such equations and some solvers may be more efficient than others at solving a particular problem.

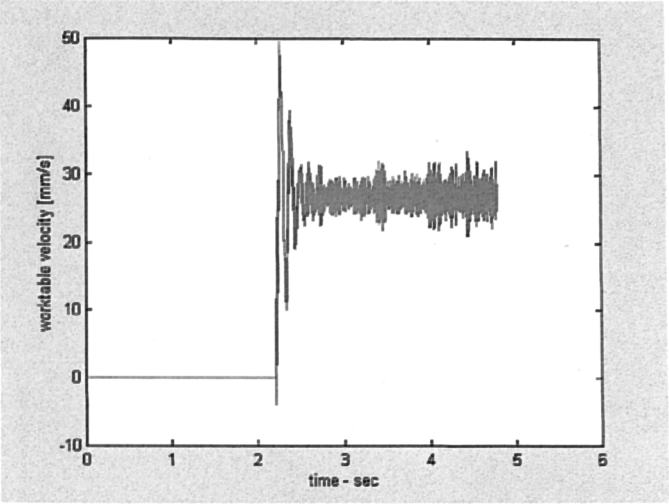

Figure 6. 29. Simulated values for worktable velocity using the solver *ode 45*

First, the same solver (*ode 45* – Dormand / Prince) was applied as for the simulation of the model with distributed parameters. The variable-step solver *ode 45* is based on an explicit Runge-Kutta (4, 5) formula, the Dormand-Prince pair and is considered to be the best solver to apply as a " first try " for most problems. Because the table velocity did not settle down (see Figure 6. 29) for a long period of time after the input had a constant value, it was decided to use another solver.

In accordance with [93] " *For a stiff problem, solutions can change on a time scale that is very short compared to the interval of integration, but the solution of interest changes on a much longer time scale. Methods not designed for stiff problems are ineffective on intervals where the solution changes slowly because they use time steps small enough to resolve the fastest possible change.* "

The characteristics of the model with explicit damping coefficients correspond to this description. So for solving this stiff problem different solvers were tried and the most suitable one is ode23t (mod. stiff / trapezoidal) which is a modified Rosenbrock formula of order 2. The simulation results presented in Figure 6. 30 are identical with the measured ones (see Figure 5. 31) and with simulated results using the model with distributed parameters (Figure 6. 25).

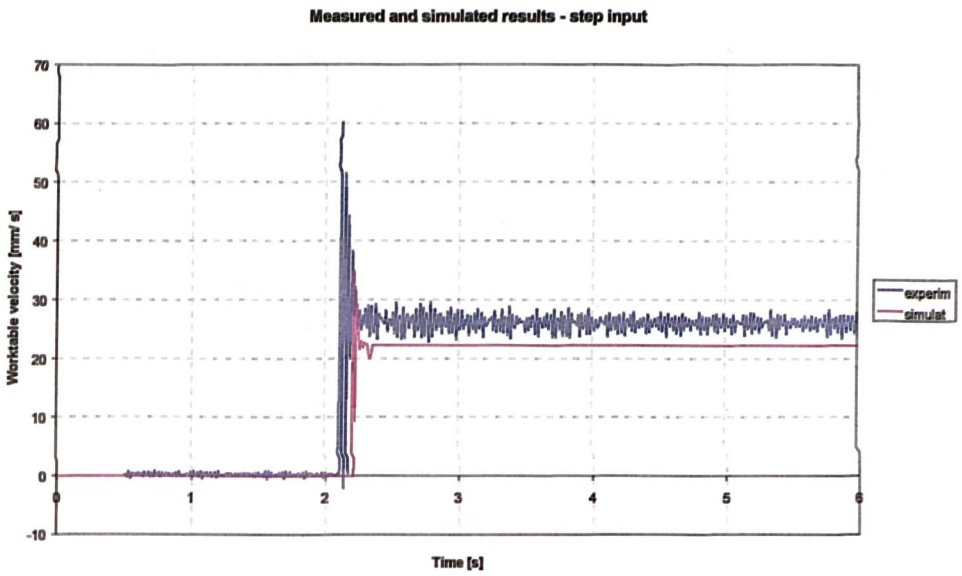

Figure 6. 30. Simulated step input and step response for open-loop position control considering the model with explicit damping coefficients

A *trapezoidal signal* is introduced as an input in the SIMULINK 2. 0. model with distributed parameters corresponding to the experimental setup for measurements in closed - loop position control. The simulated rate demand and response of the Y-axis model when the trapezoidal stimulus has the acceleration time of 140 ms and steady-state value of 83. 33 mm/s are the same like in Figure 6. 27. It could be observed that the controller error is 3. 5 V for a rate demand of 5 m / min = 83. 33 mm / s, entirely equivalent to the experimental value.

The simulated results are similar to the measured ones so the implementation in SIMULINK 2. 0. of the model with distributed parameters and the model with explicit damping coefficients is validated for step and trapezoidal inputs.

6. 3. Simulation of frequency response using swept sine and white noise inputs

As technological processes increase in complexity and the required performance specifications become more severe, it has become essential for engineers to have an understanding of the nature of the dynamic behaviour of systems, and of the methods available for analysing and improving dynamic performance. In the research field regarding the dynamic behaviour of CNC machine tools, frequency response methods are used extensively because they represent a simple way to describe the resonance effect is by observing the system response to *sinusoidal input signals* at various frequencies. The ratio of the response amplitude to the amplitude of the input signal indicates the closed-loop gain (or

sensitivity of the system at various frequencies). The Bode diagrams have two main advantages:

1. For terms that are multiplied together, the logarithm of the magnitude of the whole group is found by *adding* the logarithms of each individual term (by plotting the magnitude on a logarithmic scale). Thus, if the open-loop transfer function consists of a series of factors in the numerator and denominator, each can be plotted separately on the logarithmic scale, and the final result obtained by summing all the graphs, rather than multiplying the factors.
2. Bode diagrams can yield almost at a glance good information on the nature of the transfer function. The slope of the gain curve and phase shift at high frequency indicates the order of the characteristic equation, whilst the slope and phase shift at low frequency indicate whether it is a type 0, 1 or 2 system. In between, a close examination of the phase shift and the intermediate slopes of parts of the plots will yield the "break points" and hence the components of the transfer function. The influence of each lead and lag element can be clearly seen, but the effect of the two components may be added together to give the overall frequency response.

The sinusoidal inputs included in the category of deterministic signals are widely used by control engineers. However, in certain conditions these signals subject the system to strenuous requirements that could damage the system in the case they act for a prolonged period. As it was explained in Chapter 5, in order to increase the amplitude of the input without damaging the CNC machine tool axis drive, random white noise was applied to the open-loop position control system.

6. 3. 1. Lumped parameter model with modular load, backlash and friction

A sinusoidal input with the amplitude equal to half the fast traverse rate of 5 m / min = 83. 33 mm /s is selected with an angular velocity of 1 rad / s is introduced into the model with distributed parameters corresponding to the experimental setup for measurements in closed - loop position control (Figure 6. 26). The difference between rate demand and model response displayed in Figure 6. 31. (a) is not so evident, but it still exists and is illustrated in Figure 6. 31. (b). The oscillations on the rate error (Figure 6. 31 (b)), which occur when the velocity change the direction, are due to backlash and friction effects.

Simulation results are similar to those obtained by applying control and machine tool theoretical analysis. This represents the first step in validating the proposed model. The next step is to compare with the actual data taken from the CNC machine tool.

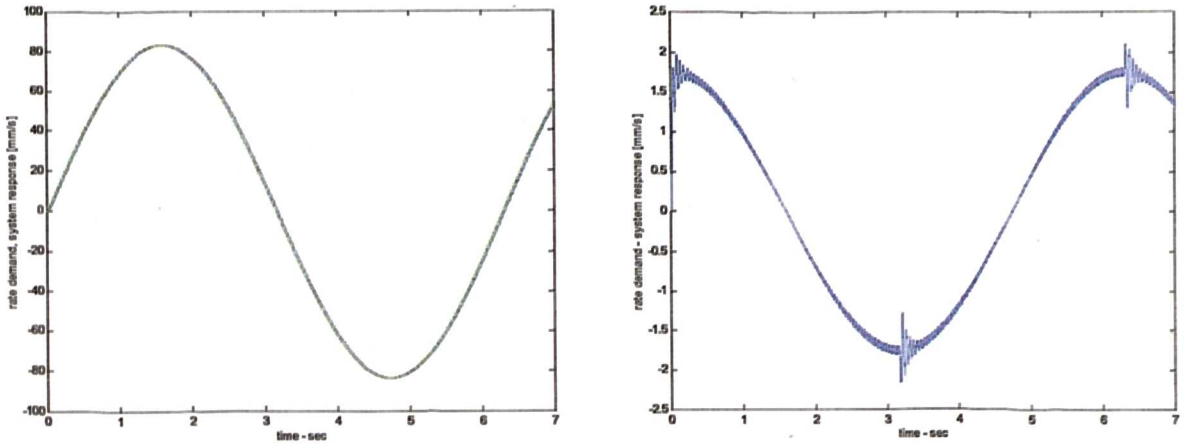

(a) (b)

Figure 6. 31. (a) Sinusoidal rate demand (green) and response of Y-axis model (blue)
(b) Difference between rate demand and model response

A swept sine is applied to the simulation of the model with distributed parameters shown in Figure 6. 24. The "chirp" block from the SIMULINK library generates the swept sine signal whose frequency increases at a linear rate with time. The amplitude of the input is 750 mV and the interval of frequency is 10 – 200 Hz.

The output signal could be detected by:

- rotary encoder attached to the DC motor
- rotary encoder attached to the end of the ball-screw
- linear encoder attached to the bed of the machine tool

Figure 6. 32. illustrates the simulation of the model with distributed parameters when rotary encoder attached to the DC motor generates the output signal. The gain $A_1 = 0.75$ is introduced because the *"chirp"* block produces a signal with amplitude equal with unity and the input signal used for experiments had an amplitude of 0. 750 mV.

At the first stage, the Bode diagrams are plotted using SIMULINK LTI (Linear Time Invariant) Viewer [94] of the Control System Toolbox that performs linear analysis of any portion of a SIMULINK model. The analysis model is specified by using special blocks to locate the inputs and the outputs of the analysis model on the SIMULINK diagram and the model is linearised around the specified operation point. Generally, sharp spikes and dips in the Bode diagrams reveal that the model contains resonant poles and also zeros.

There are no evident resonant poles and zeros in the simulated Bode diagrams presented in Figure 6. 33. and the bandwidth of the open-loop system is approximately 500 rad/s =112 Hz.

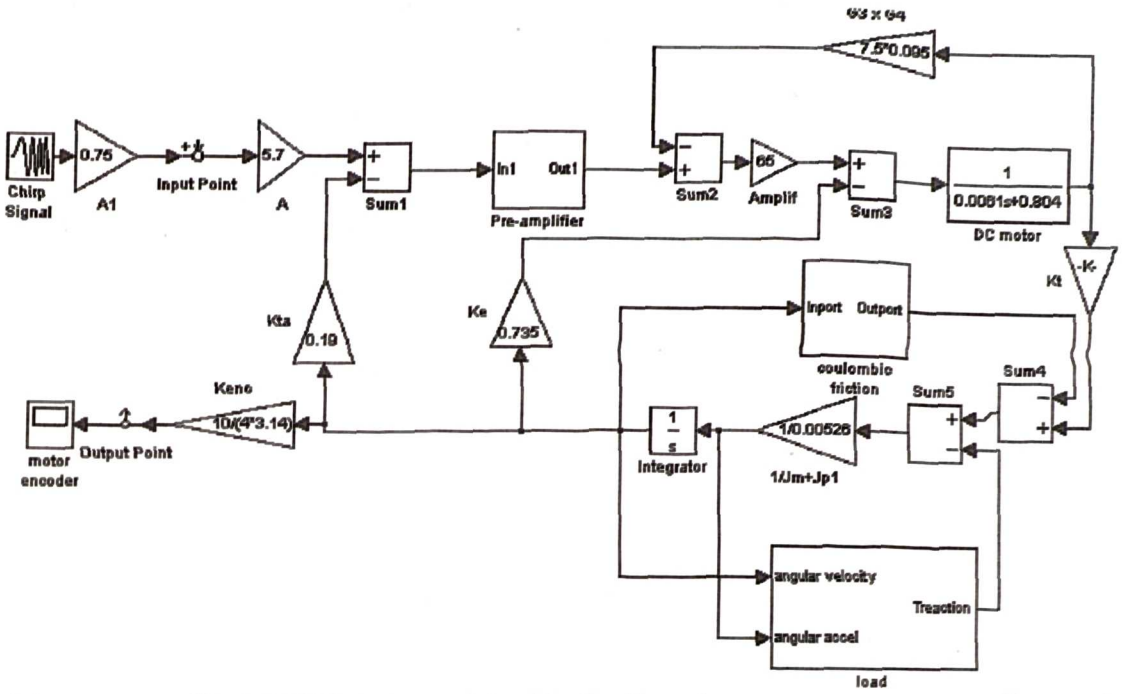

Figure 6. 32. SIMULINK 2. 0. model with distributed parameters corresponding to the experimental setup for measurements in open -loop position control using a swept sine input

However, the experimental Bode plots (see Figure 5. 27.) reveal peaks and troughs for various frequencies so the model with distributed parameters does not represent the system accurately because the explicit damping coefficients are not introduced into the model. To overcome this deficiency, several simulations were performed using the model with explicit damping coefficients.

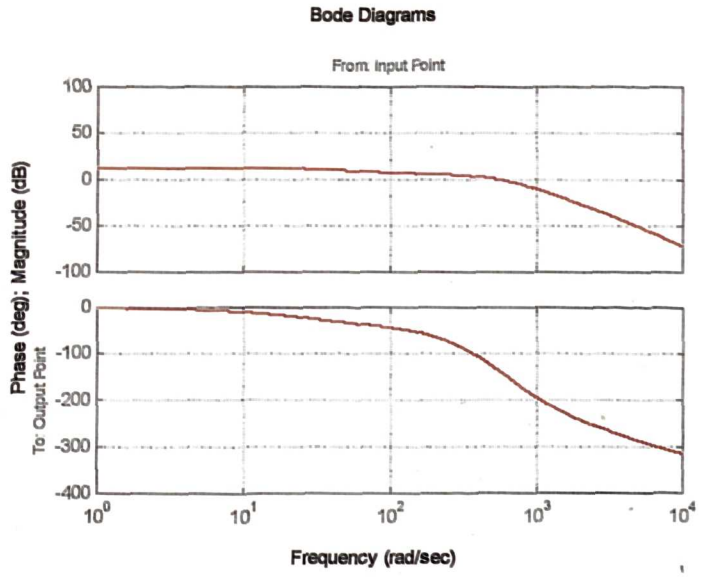

Figure 6. 33. Simulated results for the open-loop position control using LTI viewer

A probabilistic signal (white noise) is introduced into the model with distributed parameters corresponding to the experimental set-up for measurements in open-loop position control (Figure 6. 34). The amplitude of the random white noise is 1V, the standard deviation is 0. 4 and sampling time is 2 ms. This input signal with 2 ms sampling time is produced by the ***Band-Limited White Noise*** block from the SIMULINK library.

During simulation, the input data is saved into the workspace as a variable and the output data as three variables corresponding to the three encoders which measure the feedback signal. An interpolation is performed because the input vector has a different number of elements to the output vector. The *System Identification Toolbox* is used to estimate the spectral model of the system that is exported to MATLAB workspace. The command **getff** is used to retrieve the frequency functions that are plotted as Bode diagrams. Details about this procedure are discussed in Appendix D4.

The simulated results (Figure 6. 35) show a gain change and a phase shift at around 20 Hz and are then very smooth for the rest of the frequency range. This aspect is due to the fact that the factors characterising the dynamics of the system (stiffness, damping coefficients) are not introduced explicitly into the model.

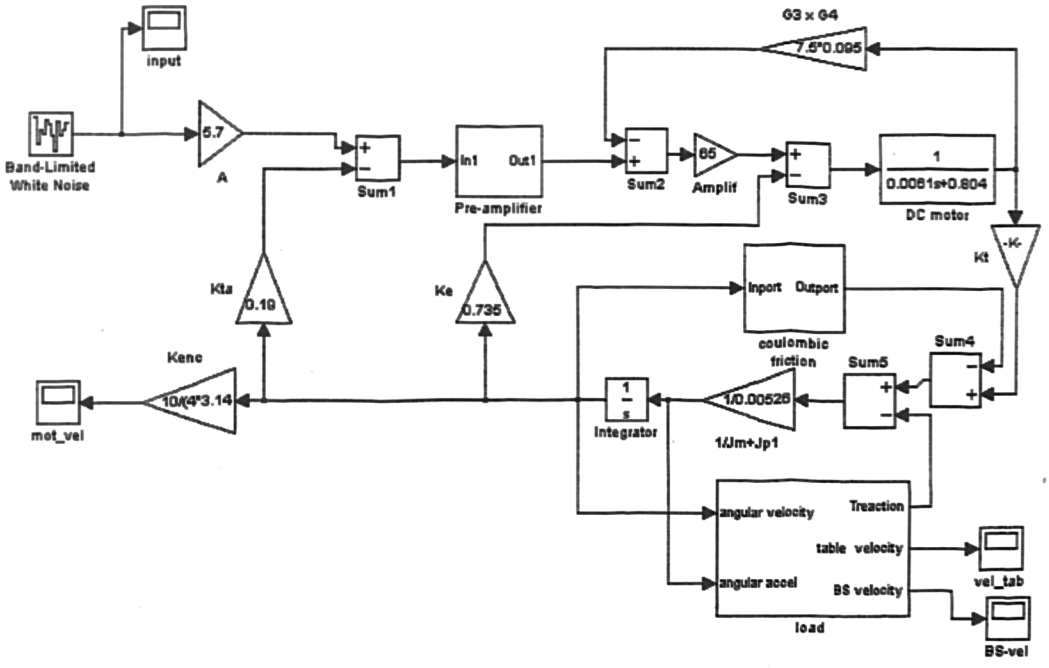

Figure 6. 34. SIMULINK 2. 0. model with distributed parameters corresponding to the experimental setup for measurements in open -loop position control for random white noise input

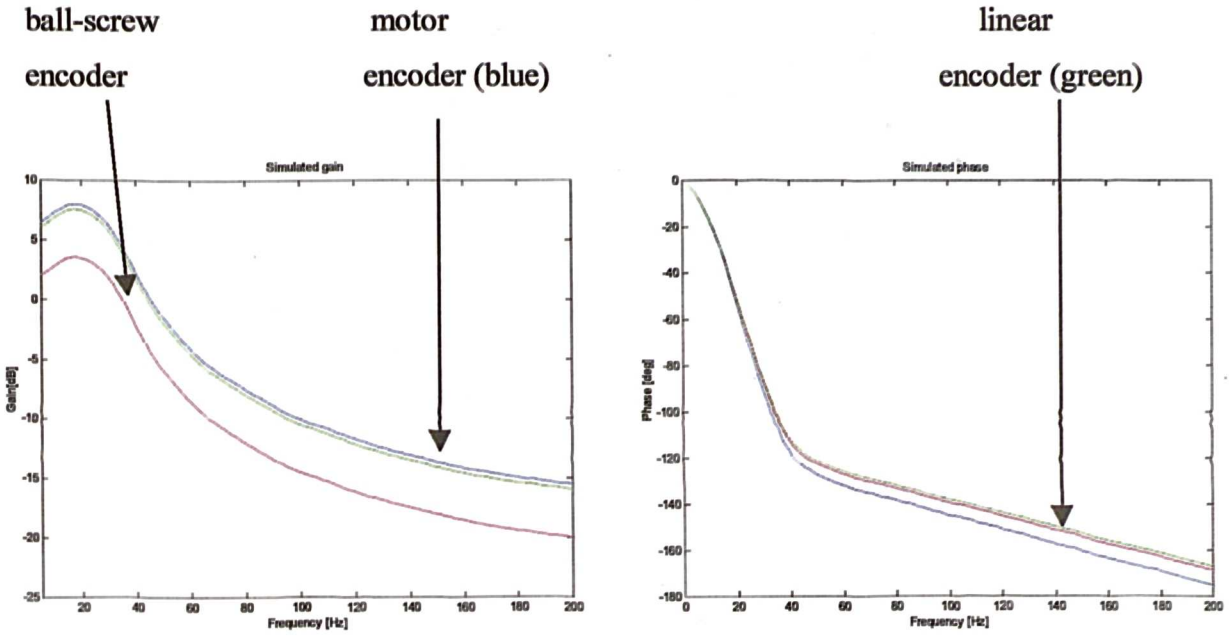

Figure 6. 35. Simulated results for the open-loop position control using the model with distributed parameters for white noise input

6. 3. 2. Model with explicit damping coefficients for one axis drive

The implementation in SIMULINK 2.0. of the model with explicit damping coefficients corresponding to the experimental set-up for measurements in open-loop position control when the input signal is a random white noise with amplitude of 1 V and sampling time of 2 ms is shown in Figure 6. 36. The output signals of the three encoders are estimated simultaneously.

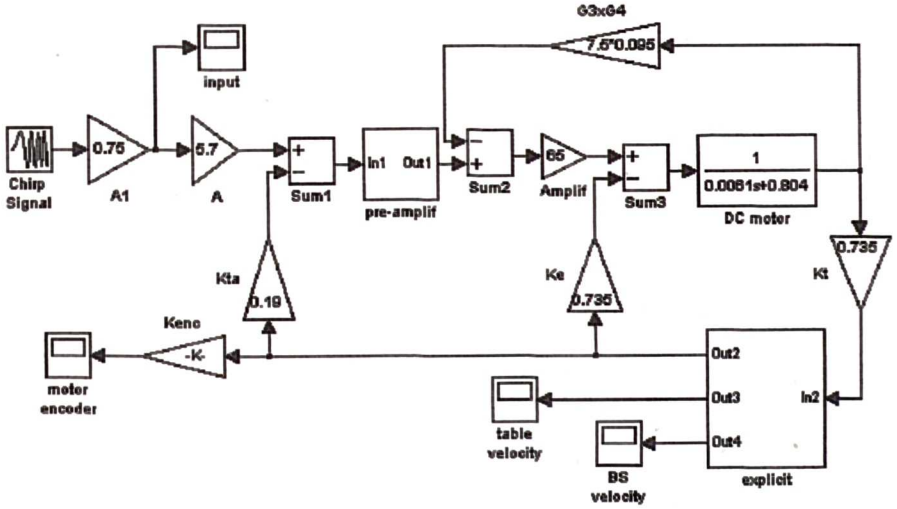

Figure 6. 36. SIMULINK 2. 0. model with explicit damping coefficients corresponding to the experimental setup for measurements in open -loop position control for swept sine input

The same method as used for the model with distributed parameters was implemented:

- The values for the input and output signals are saved into workspace.
- Calculate FFT (Fast Fourier Transform) for the input and output signal for discrete values of the frequency included in the interval 10-200 Hz for which the measurements were performed.
- Plot in MATLAB the Bode diagrams on the basis of the values for FFTs. For every discrete value of frequency, the FFT of the output is divided by the FFT of the input.

The details of this method and the MATLAB program are included in Appendix D3.

The Bode diagrams must have enough points to present a smooth curve. It was considered that 200 points / decade (401 points in total) are sufficient to obtain a reasonable curve and the simulated results are shown in Figure 6. 37.

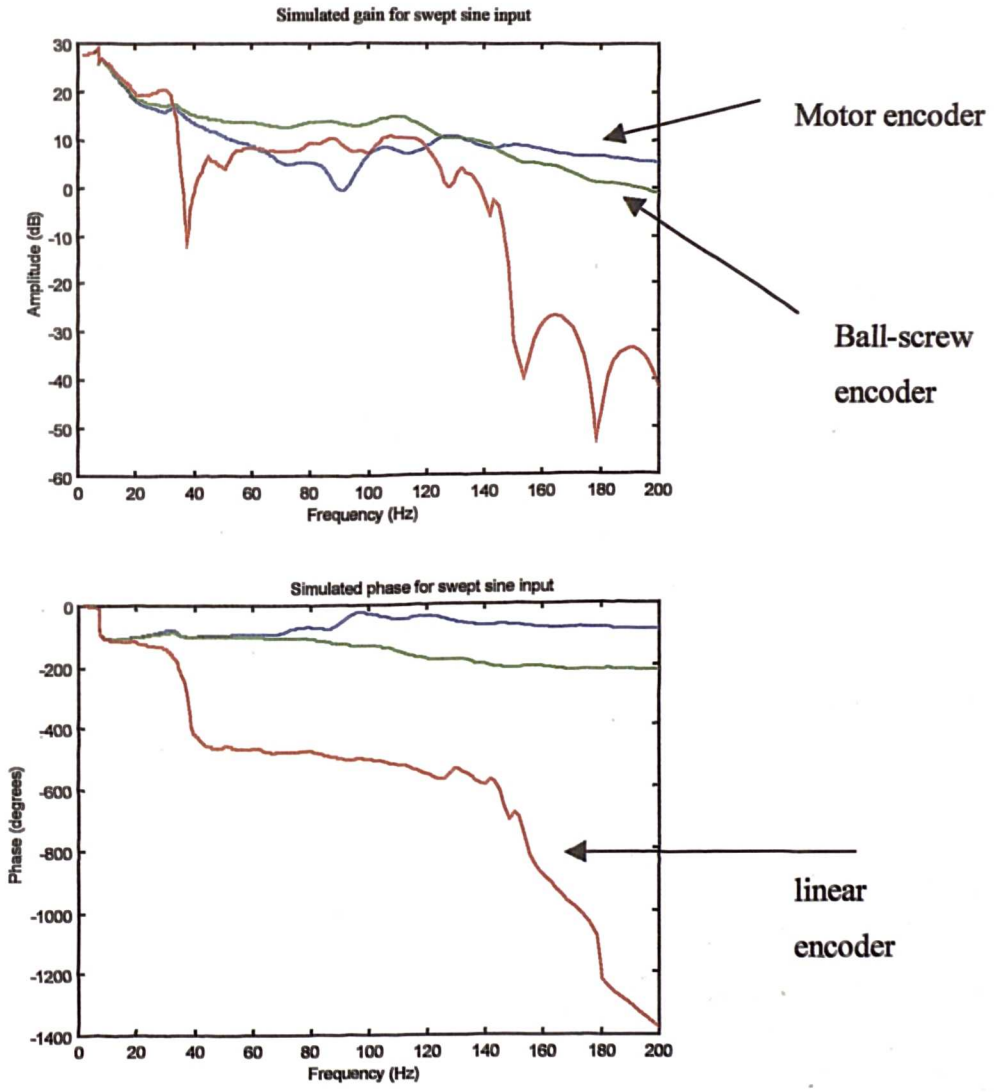

Figure 6. 37. Simulated results using the model with explicit damping coefficients for swept sine input

A white noise input (A=1V, standard deviation 0. 4 and sampling time 2 ms) is introduced into SIMULINK 2. 0. model with explicit damping coefficients corresponding to the experimental setup for measurements in open -loop position control (Figure 6. 36). There are generated 4096 points for the input signal and following the same procedure as for the model with distributed parameters, the gain and phase are plotted considering 128 points.

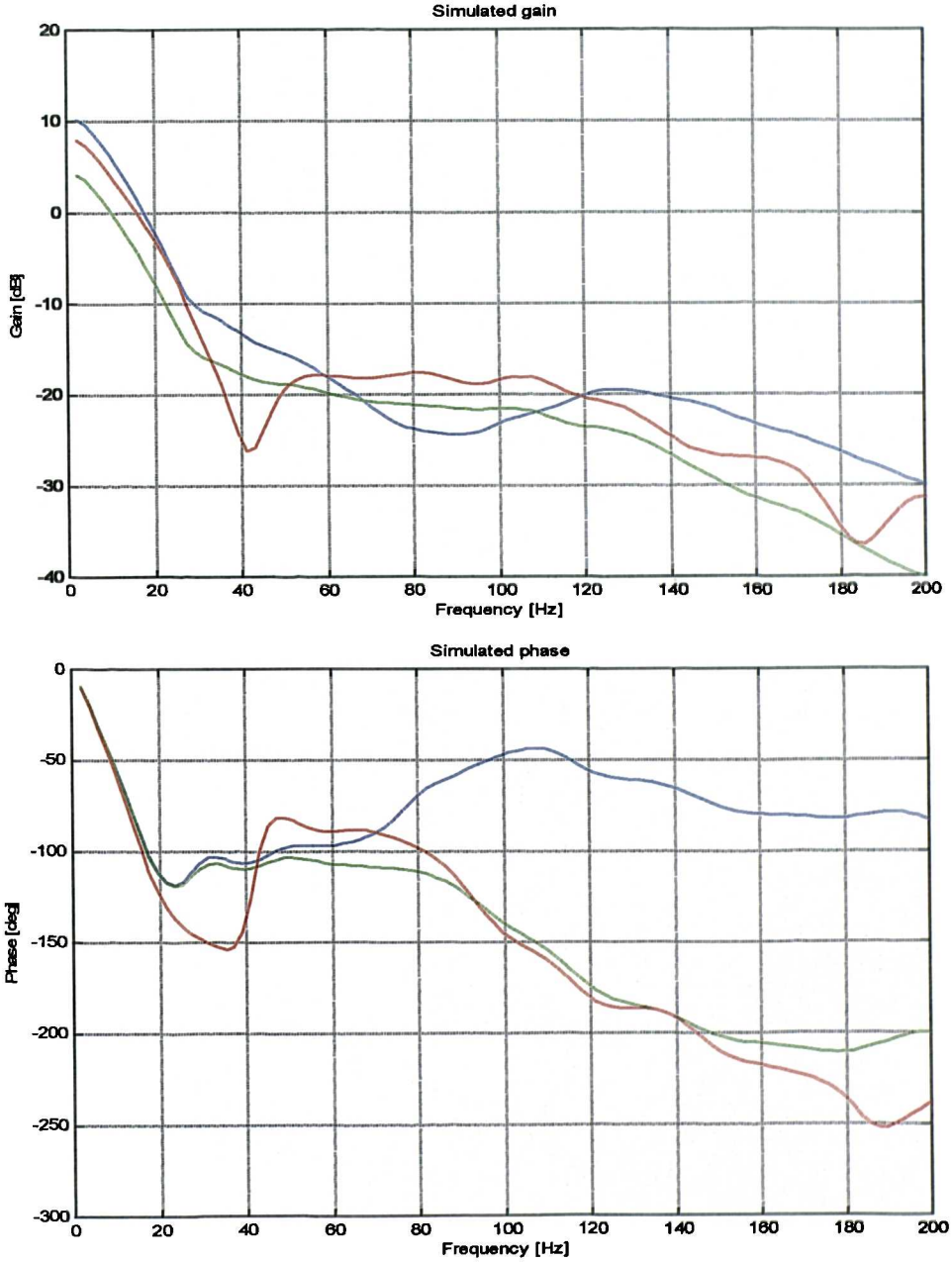

Figure 6. 38. Simulated results for the open-loop position control using a white noise input and optimal values for damping coefficients

The Bode diagrams are plotted considering that the output signal is produced by:

- the rotary encoder attached to the DC motor (blue)

The Bode diagrams are plotted considering that the output signal is produced by:

- the rotary encoder attached to the DC motor (blue)
- the rotary encoder attached to the end of the ball-screw (green)
- the linear encoder attached to the bed of the machine tool (red)

The Bode diagrams for the linear encoder show a trough at 35 Hz (the experimental diagrams present a peak at 35 Hz) and there are no evident peaks or troughs at 119 Hz and 178 – 194 Hz as in the experimental plots. It is possible that the coefficients do not have the best optimum value or it is necessary to consider other stiffness and damping factors for other joints that are influencing the dynamics of the system.

The optimum values of the coefficients of damping are determined using a *generalised eigenvalue method* (details discussed in Appendix E). This method allows one to determine the damped natural frequencies and mode shapes of the CNC machine tool drives and the sensitivity of the various modes to changes in the stiffness and damping characteristics of the machine drives.

6. 4. Two-axis simulation including geometric errors

A two-axis model allows the interaction of dynamic performance and geometric errors in a plane to be generated and subsequently examined. As a first stage, the two-axis model (Figure 6. 39) contains the separate models with distributed parameters for X-axis drive and Y-axis drive, presented previously. A sine wave is introduced as an input to the X-axis and a cosine input to the Y-axis. The amplitude and frequency of both stimuli are the same and the two axes are asked to prescribe a circle. The output signals of the two models (ball-screw positions) are introduced into a XY Graph block which when plotted X against Y produces a trace approaching the form of a circle. The difference between the trace and a circle is drawn under the form of a ball-bar plot and discussed in section 6. 5.

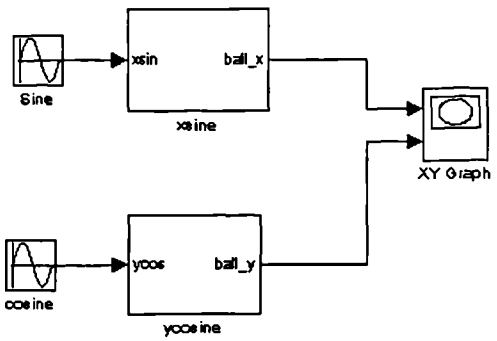

Figure 6. 39. Two-axis model for CNC machine tool axis drives considering velocity demands

Because the ball bar practical test requires that the worktable of the machine has to be commanded to prescribe a circle, the inputs for the two separate models are changed from velocity to position (see Figure 6. 40). The input signals for the subsystem "*calcul* "' are:

- The co-ordinates of the centre of the circle (x_0 , y_0)
- The radius of the circle (R)
- Linear velocity ($v = \omega / R$
- Ramp input representing time vector (t)

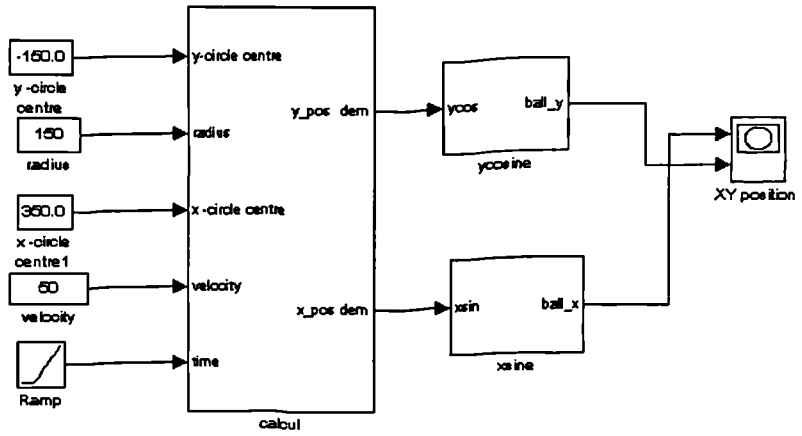

Figure 6. 40. Two-axis model for CNC machine tool axis drives considering position demands

Simon [95] has introduced the equations needed for prescribing a circle in a given co-ordinate system when considering circular interpolation:

$$y = y_0 + R \cos \varphi = y_0 + R \cos (\omega * t) = y_0 + R \cos [(v / R) * t] \quad (6.31)$$

$$x = x_0 + R \sin \varphi = x_0 + R \sin (\omega * t) = x_0 + R \sin [(v / R) * t] \quad (6.32)$$

where φ - angle at centre [deg] ω - angular velocity [rad /s]

The equations are extracted from the analytical geometry and are implemented into the internal interpolator of the CNC machine tool.

To provide a model that conforms more closely to an actual machine, it is necessary to model the geometric error components for each axis and incorporate them into the simulation.

6. 4. 1. Geometric errors integration into two-axis model

Postlethwaite [21] defined a method of predicting the volumetric geometric error of 3-axis machines of all types and configurations. Blake [30] confirmed the geometric error equations for the Beaver type VC 35 configuration and also included non-rigid errors. The following

equations are for a Beaver type configuration where the X- axis worktable travels on top of the Y- axis saddle:

$$Ex = ex(x) + ex(y) + ex(z) + \theta xy(x,y) * Y + \phi z(y) * Y \quad (6.33)$$

$$Ey = ey(y) + ey(x) + ey(z) - \phi z(x) * X \quad (6.34)$$

where X, Y - position co-ordinates of the axes;

ex (x), ey (y) - X- axis, and Y-axis linear positioning error

ey (x), ex (y) - X, Y straightness errors in the XY plane;

ex (z), ey(z) - Y, Z straightness errors in the YZ plane;

ϕz (x), ϕz (y) - X,Y axis pitch errors; θxy - squareness errors in the XY plane;

Ex, Ey - actual error movement of X, Y axes.

The geometric model equations (6. 33 - 6. 34) are derived from equations (5. 1 - 5. 3), but all the components regarding Z-axis have been removed (except Z-axis straightness) because in simulation only the XY (horizontal) plane is considered.

These equations have been implemented in SIMULINK 2. 0. into the subsystems "*X-axis error calculation* " and " *Y-axis error calculation*". The detailed SIMULINK models of the two subsystems are presented in Figure 6. 41. and Figure 6. 42.

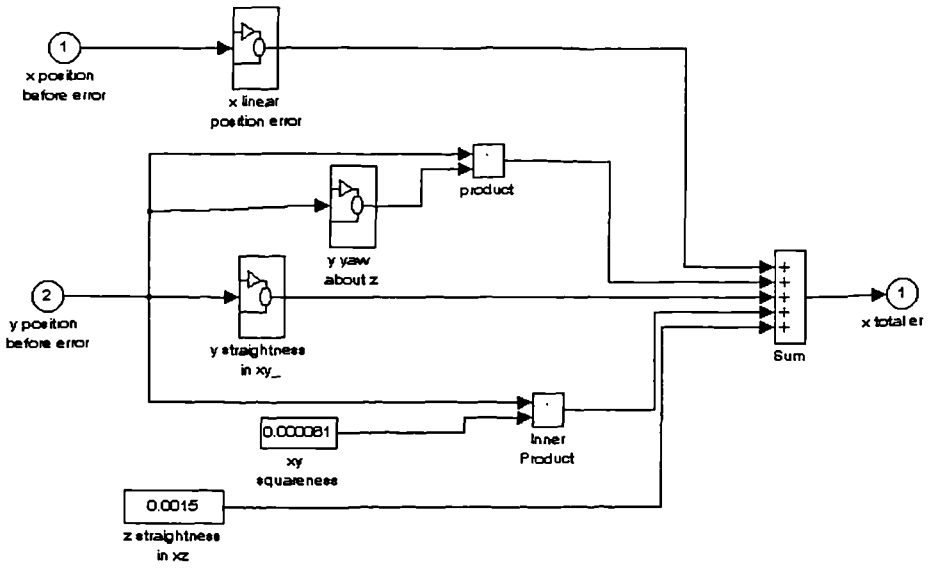

Figure 6. 41. X-axis positional error calculation

A set of geometric error data was collected from the two-axis table of a vertical machining centre Beaver VC 35 using laser interferometer. The data is stored in the form of a number of look-up tables and some constants (such as Z straightness) for use by the geometric model. The positioning errors at each position of the axes are calculated using Equations (6.33

- 6. 34). The X and Y ball-screw positions, produced by the simulation of the two-axis model, are used as inputs to the geometric model. The errors are then added to X and Y ball-screw positions. In this way both the axis drives characteristics and the geometric characteristics of the machine tool are taken into account.

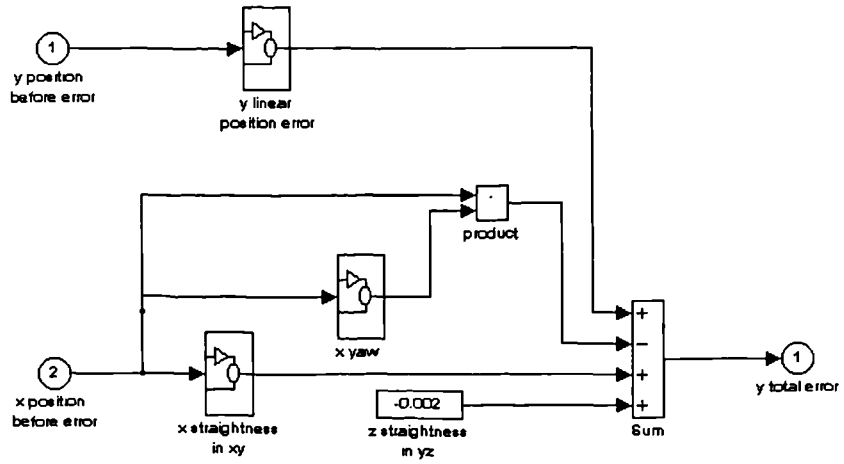

Figure 6. 42. Y-axis positional error calculation

The Renishaw laser interferometer system ML10 was mounted on the spindle of the CNC machine tool when the geometric errors were measured. The reflector was fixed on the worktable that moved under control by the controller program.

The zero positions and directions of travel for worktable were as follows:

- X-axis measurements - length of travel was 700 mm in the positive direction
  - zero position of laser software corresponded to reflector being near the interferometer

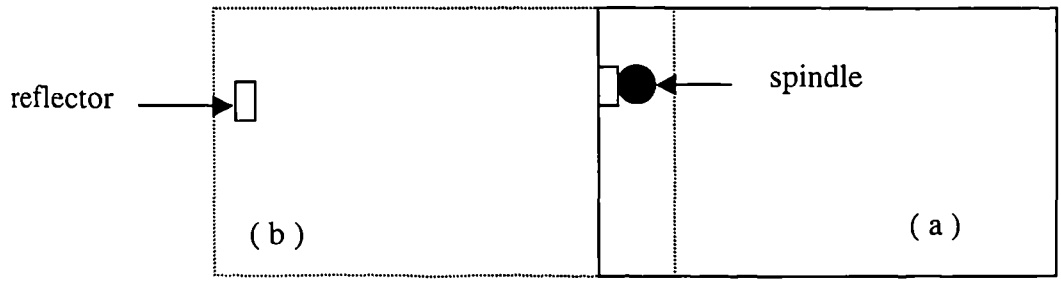

Figure 6. 43. Worktable position relative to spindle for X-axis measurements:
(a) x = 0 ; (b) x = 700 on laser software.

- Y-axis measurements - length of travel was 300 mm in the negative direction
  - zero position of laser software corresponded to reflector being near the interferometer

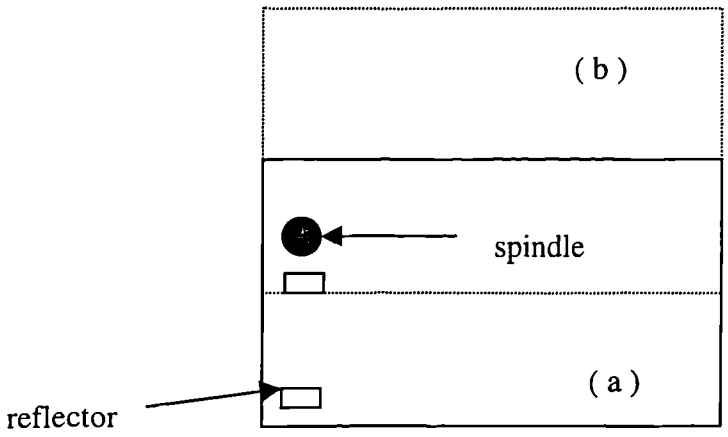

Figure 6. 44. Worktable position relative to spindle for Y-axis measurements:
(a) y = - 300 ; (b) y = 0 on laser software.

Ball bar data is captured as the machine tool moves simultaneously in X and Y axes and their combined movements generate a circular arc. The worktable was moved before the test to position the spindle in the middle of the worktable. The co-ordinates of the circle centre become the co-ordinates for laser system software datum and are $x_0 = 350$ and $y_0 = -150$.

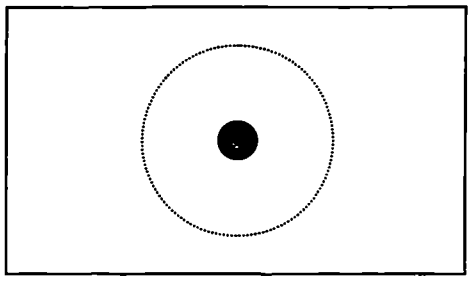

Figure 6. 45. Worktable position relative to spindle for ball bar test

The positions of the circle prescribed by the worktable written in co-ordinates for laser system software are shown in the Figure 6. 46.

The relationship between the circle prescribed in the case of a 150 mm ball bar transducer and the geometric errors measured with laser system could be established. Introducing the co-ordinates of the centre of circle and the radius, the equations (6. 31) - (6. 32) become:

$$x = 350 + 150 \sin \varphi = 350 + 150 \sin (\omega * t) = 350 + 150 \sin [(v / R) * t] \quad (6.35)$$

$$y = (-150) + 150 \cos \varphi = (-150) + 150 \cos (\omega * t) = (-150) + 150 \cos [(v / R) * t] \quad (6.36)$$

The relationships between the different points on the circle and the sign of velocity could be reflected into logic diagrams (see Figure 6. 47).

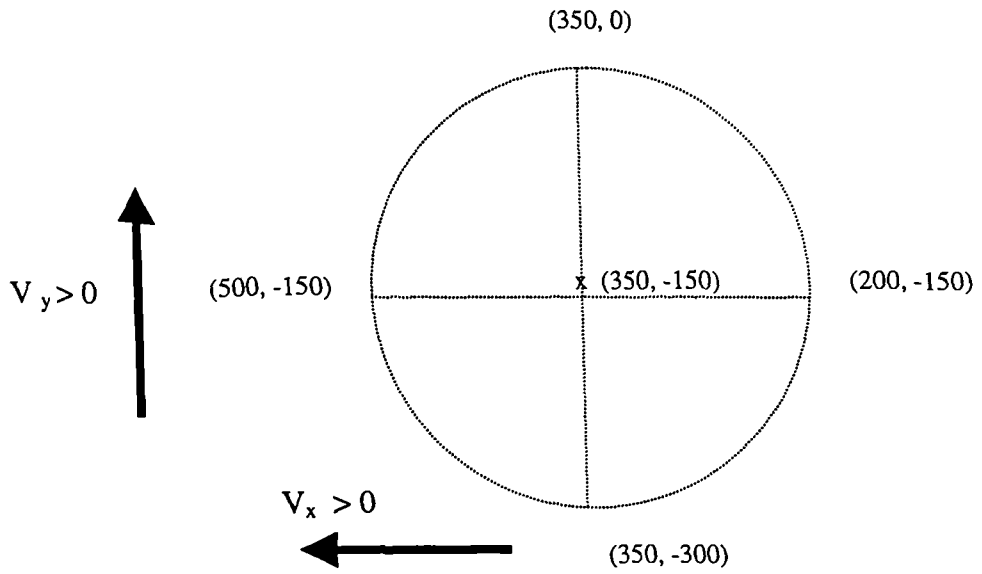

Figure 6. 46. The co-ordinates of points for the circle prescribed during ball bar test

The logic diagrams were implemented in SIMULINK using the switch block which propagates one of two inputs to its output depending on the value of the control input.

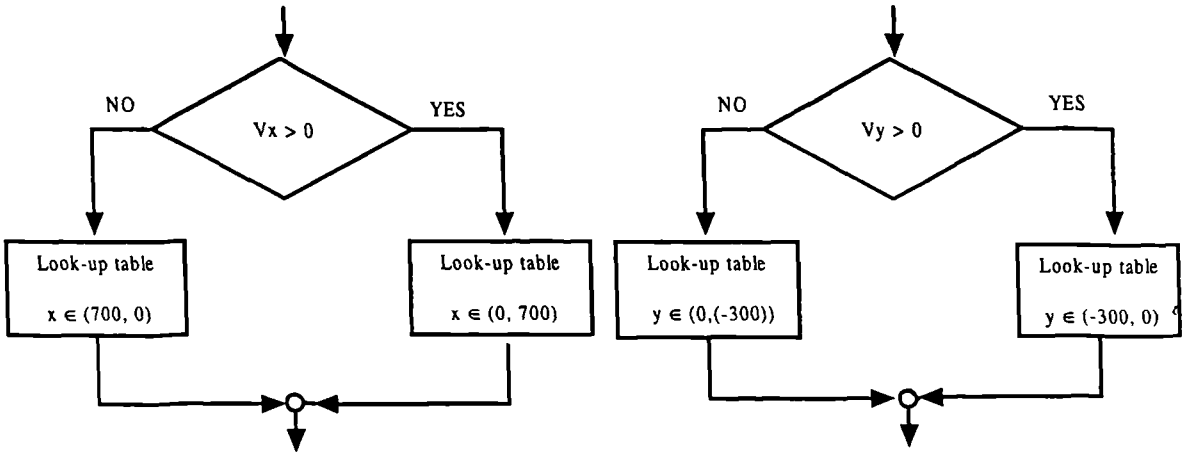

Figure 6. 47. The logic diagrams connecting the laser system measurements with co-ordinates of points from the circle prescribed during ball bar test

The implementation routines were used to build up the elements from subsystems " *X-axis error calculation*" and "*Y-axis error calculation*" presented in Figure 6. 42 and Figure 6. 43. The subsystems " *X-axis error calculation*"' and " *Y-axis error calculation* " have been used for the integration of geometric errors into the simulation (Figure 6. 50). The results of summation between X-axis and Y-axis ball-screw positions and geometric errors can then be

analysed to produce information in the form of a polar plot as described in the following section.

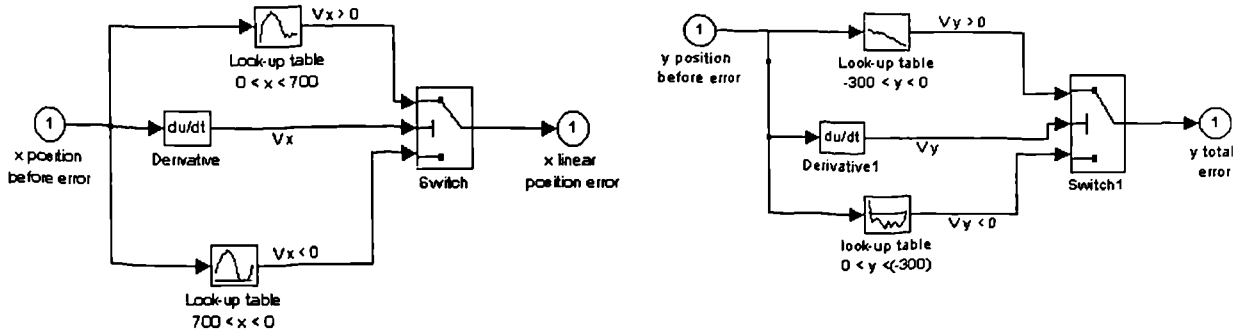

Figure 6. 48. SIMULINK logic diagram connecting laser and ball bar measurements: (a) X-axis ; (b) Y-axis

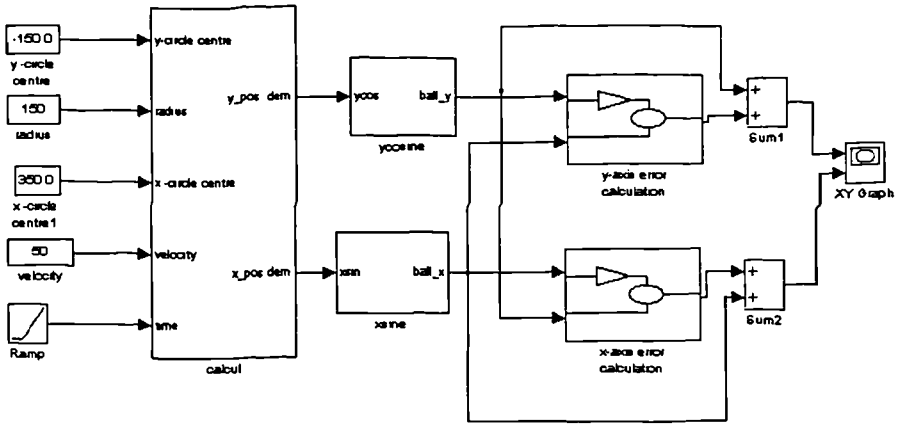

Figure 6. 49. Integration of geometric errors into simulation

6. 5. Ball bar plot simulation and comparison with measurement results

The trace obtained by introducing sine and cosine wave position inputs into the models for X and Y-axis drives and incorporating the geometric errors into the simulation, presented deviations from a circular trace. The deviations from the demand were in microns, therefore some signal processing must be carried out in order to display the actual errors. The errors were calculated by converting the Cartesian co-ordinates to polar co-ordinates and subtracting the circle radius from the radius value of the simulation data. The errors could then be displayed as a conventional X-Y plot by conversion back to Cartesian co-ordinates.

This procedure has been applied first for the case of the two separate models commanded by rate demands (see Figure 6. 42). The radius of the ideal circle was 83. 33 mm because half

c f the fast traverse rate for Beaver VC 35 CNC machine tool was considered to be 5 m / min = 0. 0833 m /s.

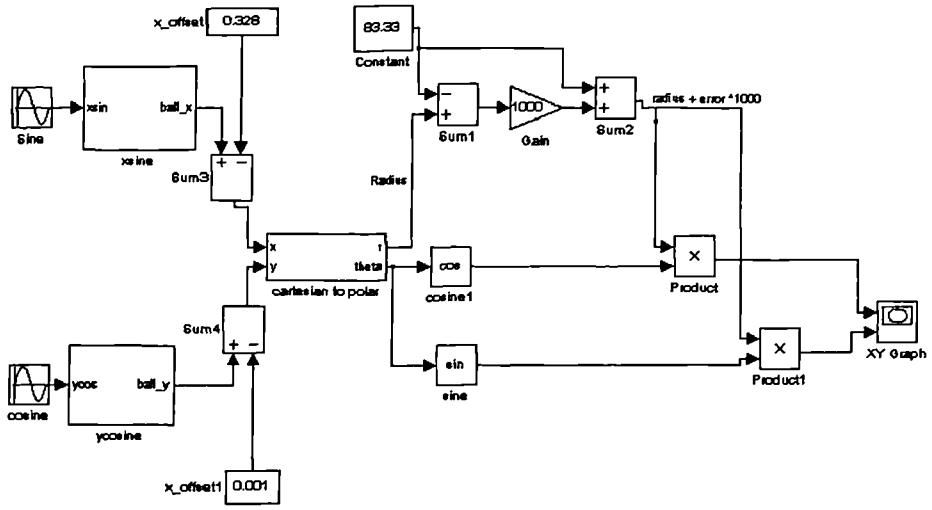

Figure 6. 50. Determination of the errors between the trace obtained from two models and the circle with the radius 83. 33 mm

The models for X-axis respectively Y-axis included backlash only as a non-linearity (10 μm for X-axis and 50 μm for Y-axis) and the error plot (Figure 6. 51) showed that the outputs of the models differ from a pure sine wave for X-axis and the pure cosine wave for Y-axis. This data is representative of the dynamic performance of the axis drive model (with the addition of axis backlash) (see Figure 6. 24). In order to provide a model that conforms more closely to an actual machine tool it is necessary to model the geometric errors and incorporate these into the simulation, rather than to assume a single backlash figure.

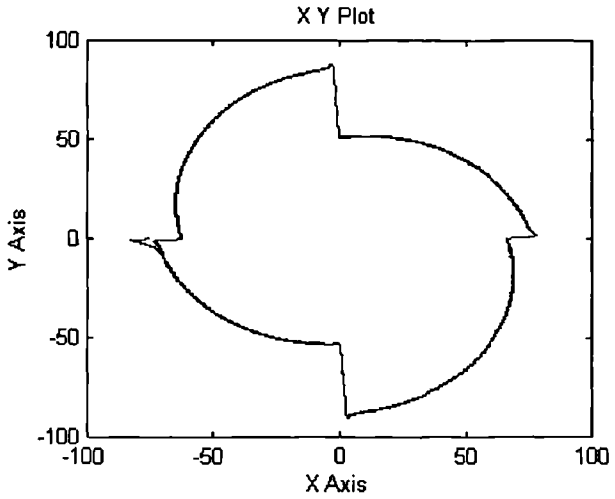

Figure 6. 51. Simulation plot showing purely axis drives positional errors

After the geometric errors were integrated into simulation (see Figure 6. 52), the ball bar plot procedure was applied again. This time the velocity (feedrate) was considered to be 3000 mm / min = 50 mm / sec because this was the value used for the ball bar test.

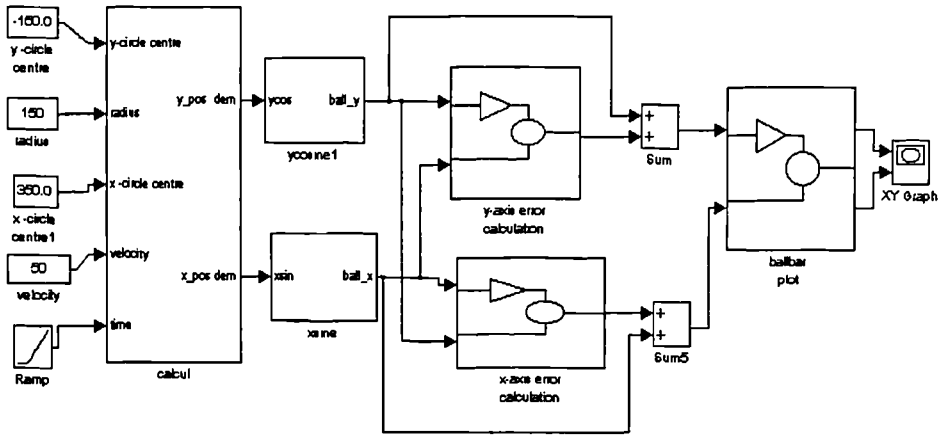

Figure 6. 52. Ball bar plot simulation considering position demand

The co-ordinates of the centre of the circle prescribed by the ball bar are $x_0 = 350$ and $y_0 = -150$ and they are introduced into the subsystem " *Ballbar plot*". Without these offsets, any negative errors would confuse the polar graph, providing misleading data.

The following operations have been performed in order to obtain the ball bar plot:

- introducing offsets for the results of summation between X-axis and Y-axis ball-screw positions and geometric errors;
- conversion from Cartesian co-ordinates to polar co-ordinates;
- subtracting the radius of ideal circle $R_0 = 150$ mm from the simulated radius;
- multiplying the errors by 1000 to make them visible (conversion from μm to mm);
- conversion from polar co-ordinates to Cartesian co-ordinates to display the errors.

The Y axis backlash is particularly evident (the step change at the 90 and 270 degree poles) in the simulated results (Figure 6. 53) and the inertial spikes are present at each pole of the plot, due to axis characteristics (friction, inertia etc.). The spikes are larger in Y direction because the Y-axis saddle is carrying X-axis worktable.

As a result of the axis squareness error (22 arcsec for actual machine), the plot has an oval shape. A similar oval shape would result from a servo mismatch, however the counter-clockwise run (lighter trace) would be shifted 90 degrees. These traces are imposed over each other The two-axis model shows that the combination of different geometric errors (linear, angular, squareness) generates a progressive error deviation when the machine worktable

pr cribes a circle. The simulated results are similar with the experimental ball bar plot so the two-axis model including the geometric errors is validated.

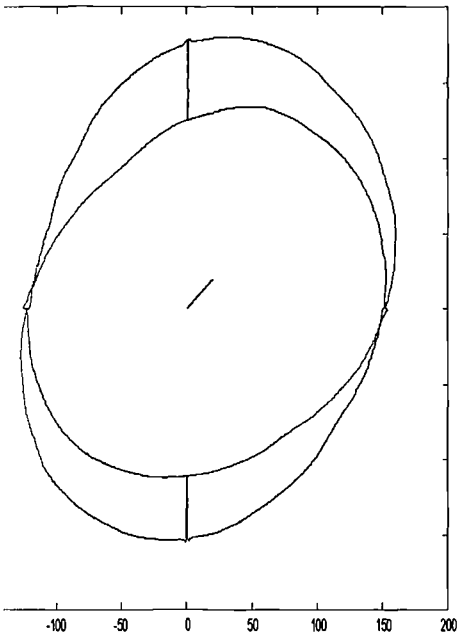

igure 6. 53. Simulation plot

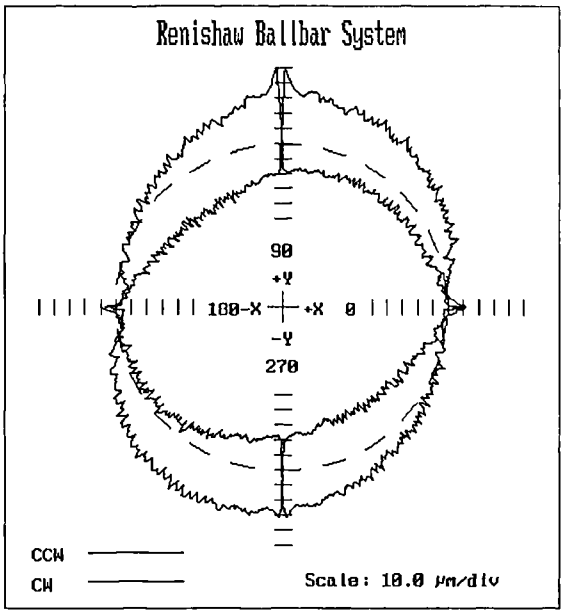

Figure 6. 54. Measured ball bar plot

The next step is to investigate parameter identification techniques which is undertaken in Chapter 7.

7. PARAMETER IDENTIFICATION AND PERFORMANCE OPTIMISATION TECHNIQUES APPLIED TO CNC MACHINE TOOL AXIS DRIVES

7. 1. Introduction

System identification is a field where one tries to intelligently determine a mathematical model for the global behaviour of a system on the basis of observing its response around a local operating point for a limited period of time. While such a model can be obtained by considering the physical laws governing the system, the results are labour intensive and require considerable expertise to produce, and can be quickly made redundant due to a change in operating conditions and / or component wear.

The behaviour of the real systems is generally very complex with various aspects unknown or not studied sufficiently. Consequently, the task of identification of a given dynamical system is equivalent to approximation; the aim is to build a model of the dynamical system of interest such that the predictions of the model are within some tolerance of the actual system output.

As real systems encountered in the engineering environment become increasingly versatile, the task of system identification for building accurate models of complex systems from noisy data is becoming ever more important. Although considerable success has been achieved in non-linear systems identification, much work still remains to be done to devise improved algorithms and better methods of displaying and interpreting the multi-dimensional estimates that are produced.

The work presented in this thesis addresses the time-domain and frequency-domain system identification methods used for modal analysis of non-linear control systems (CNC machine tools). The use of periodic and random excitations in continuous-time non-linear system identification is also reported, with the identification methods illustrating the worth of frequency-domain measurements in this area. In particular, the interpretation of the higher order frequency response functions is comprehensively studied and non-linear effects are related back to the physical models of the systems.

Wavelets are used for practical identification of the modal parameters due to their advantages over traditional Fourier methods in analysing physical situations where the signal contains transient discontinuities and sharp spikes. Wavelets offer simultaneous information

about the behaviour of the system in time domain and frequency domain. The wavelet transform provides better frequency resolution at low frequencies and better time resolution at high frequencies, which are advantageous in generating time-frequency representations that are able to handle signals containing stationary and non-stationary components with high levels of noise.

7. 2. Parameter identification methods suitable for use with machine tools

7. 2. 1. Control performance of CNC machine tools drives

The interval of time between input and output and the quality of the output signal for an axis drive from a CNC machine tool are affected by disturbances such as:

- Resistant forces due to friction;
- Forces dependent upon acceleration (masses) and speed (friction, damping);
- Deformations of the control elements caused by operating forces and loading conditions.

Ford [2] has shown that the effects of disturbances could be classified in three categories:

1. *" Non-linearities - dead zone, saturation, backlash, friction (Coulomb, static and viscous), quantisation;*
2. *Effect of noise on saturable elements - if signal to noise ratio is low, the effect may be a gain reduction and consequently loss of accuracy;*
3. *Effect of element tolerances - these affect the gain and time constants of the system and therefore the dynamic and static accuracy. "*

These effects manifest themselves in different parts of the machine tool axis drives as is shown in Table 7. 1. They affect static and dynamic accuracy of the machine tool, terms that specify the performance of this system.

Different types of stimuli (deterministic or stochastic) could be applied to identify the parameters reflecting the effects of disturbances (see Table 7. 2.). The details of the identification procedures are presented later.

It is unrealistic for the purposes of analysis to consider attempting to investigate the response of the system for all conceivable types of input function; thus usually only certain specific types of function are studied. These are chosen primarily for reasons of analytical simplicity and because design criteria have been developed for them. They include an instantaneous change, which is the most severe input change that a system can undergo, and certain other typically encountered input functions such as an input changing in a sinusoidal manner, or one changing at a constant rate.

Part of motion control system	Effect of disturbances
Controller	Quantisation
	Effect due to sampling time
	Saturation limits
	Effect due to interpolation
Mechanical transmission	Dead band
	Backlash in the driving elements
	Friction between moving parts and slideway
	Stiffness

Table 7. 1. The effects of disturbances in different parts of CNC machine tool axis drive

Parameter	Stimuli
Velocity bandwidth Check overshooting	Step
Backlash Dead band	Triangular signals
Coulomb friction Position gain	Trapezoidal signals
Resonance frequencies for different elements Damping coefficients	Random white noise Swept sine

Table 7. 2. Parameters intended to be identified and stimuli used for this purpose

Another aspect which should be considered is that in practice external disturbances, often of unpredictable form, may act as additional inputs and modify the response in a random manner. Such disturbance inputs, generally referred to as *noise* when they consist of random fluctuations about a mean value, have negligible effect in many situations and hence are usually ignored in the earlier stages of the analysis of a system. However, the disturbance can also be a change in mean value of a variable which causes an alteration in the system datum operating point, and hence in the parameters of the system equations. This is the case when the signal-to-noise ratio has small values.

Generally, when performing parameter estimation of dynamical systems, one must evaluate unknown variables given uncertain measurements. Often the problem is approached using a probabilistic description of the uncertainty and statistical estimation theory is applied.

Much of the statistical signal processing rests on two basic stochastic assumptions (stationarity, Gaussianity) that allow the development of a frame of reference that is mathematically elegant and can be insightful in a practical way. However, the majority of the physical phenomena responsible for generating the practical signals are both non-stationary and non-Gaussian. Consequently, one of the tasks of modern signal processing is to take into account this aspect in order to provide reliable solutions to practical signal processing problems. Haykin [96] enumerated a list of performance tasks for modern signal processing evolution:

- Acquire prior information from the underlying physics of the problem;
- Stabilise the solution by embedding prior information in a computationally efficient manner into algorithm design;
- Adapt to the non-stationary behaviour of the operational environment;
- Use robust algorithms which are insensitive to small deviations of the actual probability distribution from the assumed model;
- Apply properly the feedback principle which will lead to improved convergence, reduced sensitivity to parameter variations etc.

7. 2. 2. Identification of bandwidths, gains and phases of different loops of the system

Frequency response analysis can be used to identify the transfer function of practical systems by following a simple procedure:

- Generate excitation signals over the bandwidth of interest (sine waves, white noise);
- Record input and output data;
- Plot Bode diagram (spectral analysis) ;
- Draw asymptotes and estimate the terms of the transfer function.

The effective bandwidth of the position loop for the Beaver VC35 CNC machine tool is 33 rad / sec. It could be calculated using Equation (4. 34) and was measured using a trapezoidal rate input (Figure 5. 31). The position loop has unity gain and damping factor $\zeta = 1$ (system critically damped).

The effective bandwidth of the velocity loop could be determined from the Bode diagram (Figure 7. 1) plotted using the experimental setup described by Figure 5. 24. The Signal Analyzer HP3566A generated a swept sine input signal for the drive and the output was a differential of the signal produced by the rotary encoder attached to DC motor.

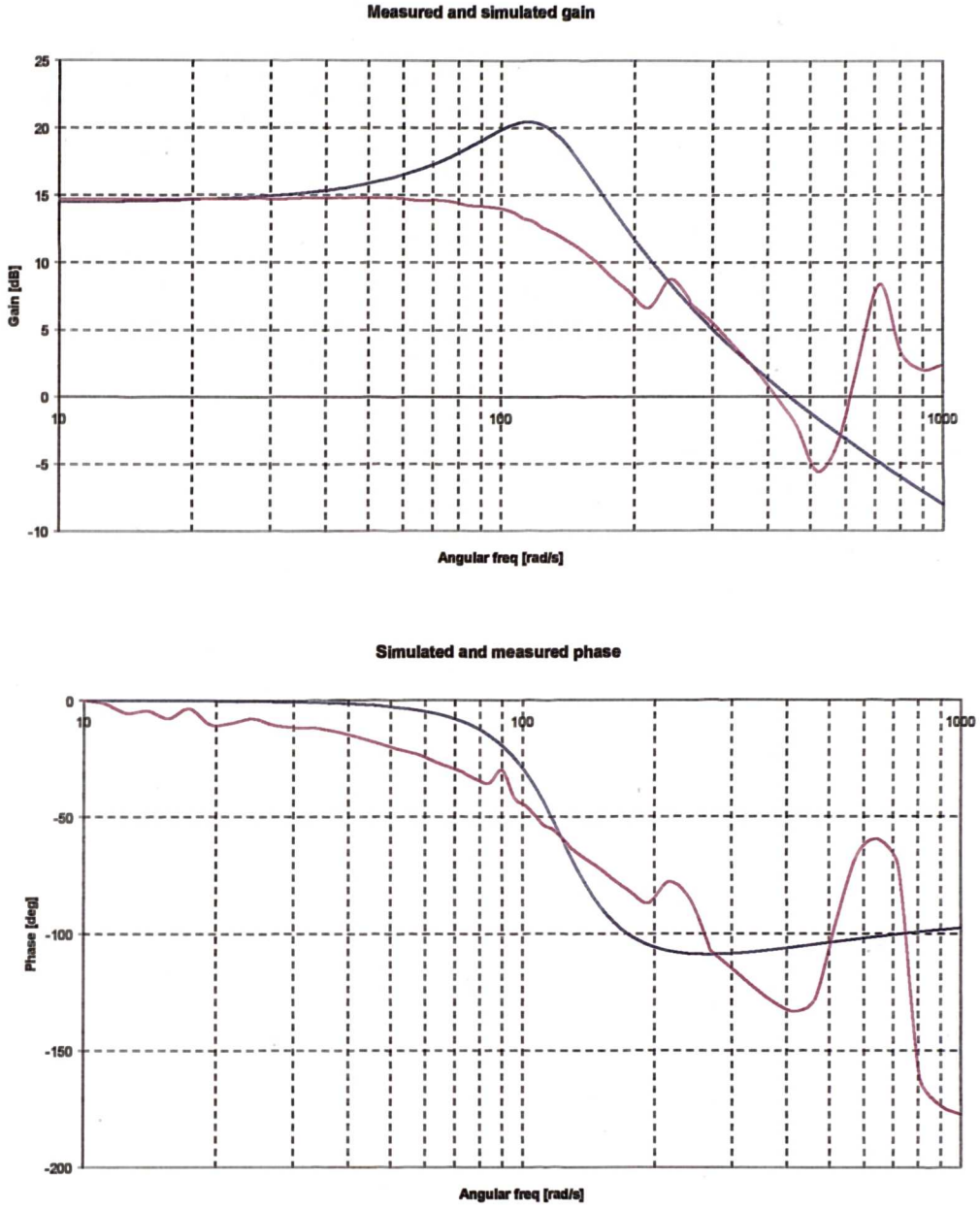

Figure 7. 1. Simulated (blue) and experimental (magenta) Bode diagrams considering the lumped parameter model with a swept sine input

The measured gain is (-3 dB) at a frequency of 72 Hz whilst the simulated gain has the same value at a frequency of 96 Hz. So there is a difference between the bandwidth obtained experimentally for the velocity loop and the calculated value when considered the lumped parameter model with load inertia reflected to the motor.

The bandwidth is reduced in the case of experimental data because some aspects such as distributed load parameter effects and non-linearities were not included into the lumped parameter model. Their effect could be seen in the phase diagram – experimental phase diagram presents phase shifts while the simulated one is smoother.

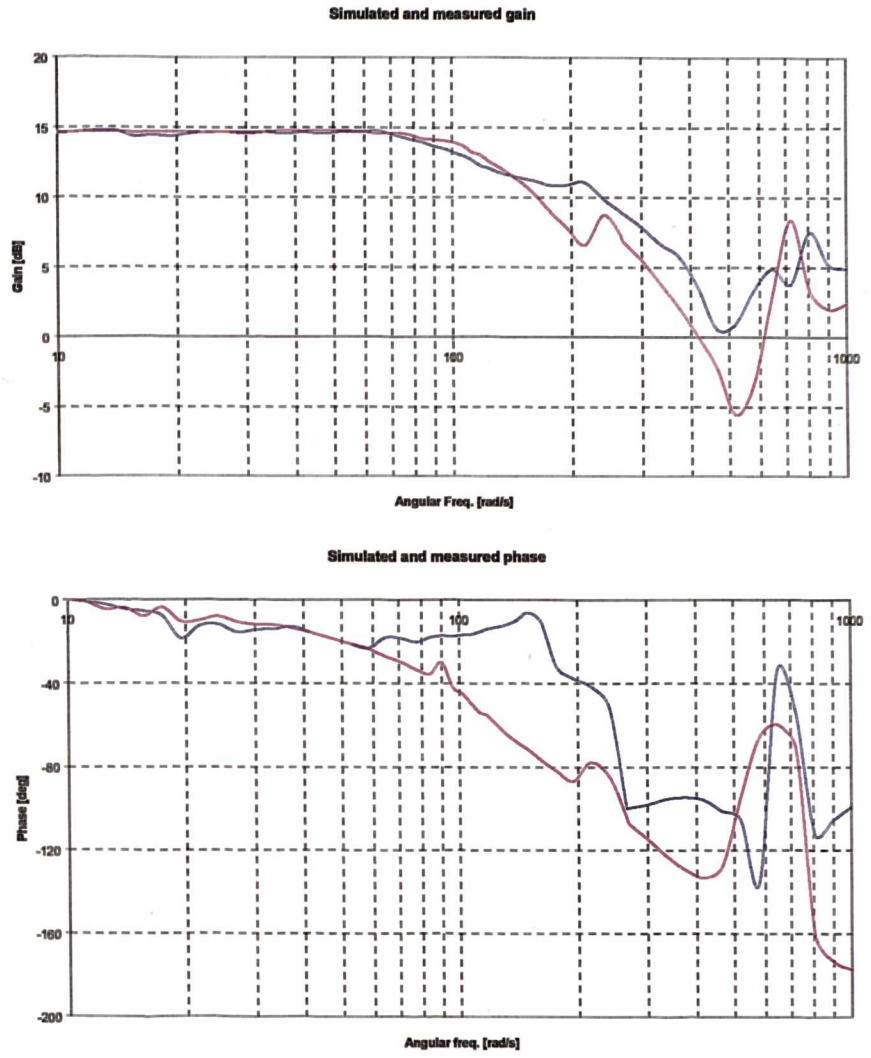

Figure 7. 2. Simulated (blue) and experimental (magenta) Bode diagrams considering the hybrid model with a swept sine input

The simulated gain when using the hybrid model with distributed load and explicit damping factors is similar to the measured one (Figure 7. 2), while the phase presents important differences when compared to the experimental one. The differences are considered to be due to non-linearities and damping terms from the load not being optimised and also due to the effect of magnetic coupling between the tachogenerator and the DC motor over the motion control range.

Awtar and Craig [97] developed an accurate tachogenerator model which takes into account the effect of magnetic coupling between DC motor and tachogenerator. The finite shaft stiffness introduces resonance and shaft ringing and the mutual inductance between the tachogenerator winding and the motor winding leads to sensor dynamics that affect the overall system dynamics. In this way the conventional tachogenerator model [98] which treats the tachogenerator as a simple gain has been proven to be inadequate for predicting the high-frequency system response.

These aspects must be taken into account in an attempt to develop a model for a system that has multiple flexible elements. The model has to be as accurate as possible because it will be used for parameter identification and feedback motion control.

7. 3. Modal parameters identification using experimental modal analysis

Modal analysis represents the process whereby a structure is described in terms of its dynamic properties (frequency, damping and mode shapes). The dynamic response of a structure is the sum of a discrete set of independent predictable motions called *modes.* A resonant frequency, a damping factor and a mode shape define each mode of vibration and dynamic models can be completely represented in terms of these parameters. The modes can be real (all points are either moving in phase or out of phase) or complex (travelling waves).

The goal of modal analysis is to develop a dynamic model which can be used for verification, simulation / prediction, optimisation, diagnostics, prediction, control engineering and monitoring. Gatzwiller [99] mentioned that in modal analysis a number of assumptions are made: linearity (the structural response can be described by linear second order differential equations), time invariance, observability, and modes are defined in a global sense.

Ewins [100] enumerated the essential stages of a modal test:

- Controlled excitation of the structure;
- Measurement of excitation force and response levels;
- Derivation of the frequency response function (FRF) by application of FFT to the time data. The peaks from the FRF occur at frequencies where the time response would have maximum values corresponding to the rate of oscillation of the input excitation. So the time trace could be used to determine the frequency at which maximum amplitude increases occur or the FRF could be used to ascertain where these natural frequencies appear.

- Identification of modal parameters from measured FRF;
- Construction of the modal model of the test structure – this stage is composed from different operations (see Figure 7. 3).

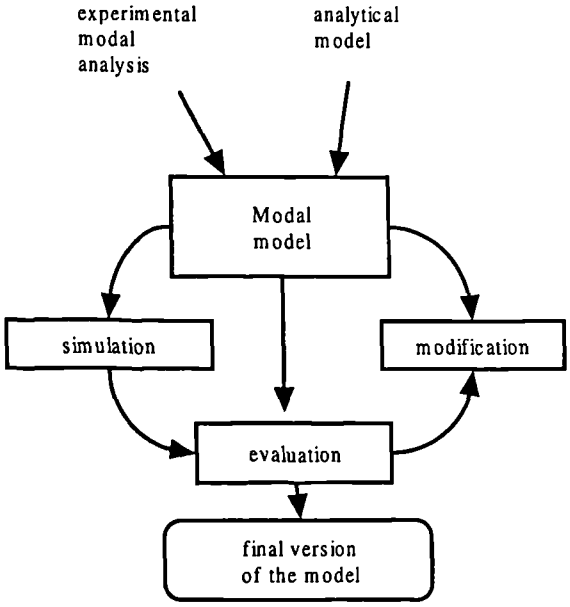

Figure 7. 3. The stages in elaborating a modal model

Also Ewins identified some factors which complicate the presentation of the theory which describes the dynamics of rotating structures into a format that is compatible with conventional modal analysis:

- the use of stationary and / or rotating axes frames;
- the addition of gyroscopic effects;
- damping acting in both stabilising and de-stabilising ways;
- likelihood of non-linear behaviour;
- multi-frequency responses to harmonic excitation.

There is a very strong link between the type of the stimuli and the results of a modal test. In this sense, Verboven et. al [66] presented some interesting conclusions derived from the analysis of these data obtained by using an improved modal parameter identification method based on non-parametric modelling of the measurement noise:

- Lower resonance frequencies correspond to the most important structural modes, so it is important to estimate these values accurately in order to obtain correct modal parameters;
- The type of excitation signal affects the estimates of damping ratios and the mode shapes;

- The bias effect is less apparent in the measurements using a multi-sine excitation due to higher signal-to-noise ratio.

The aims of this chapter are to review some basic modelling and identification concepts from modal analysis, so as to evaluate the state of the art of modal analysis techniques applied to the structures in machine tools and to develop new methods which permit the calculation of reliable modal parameters.

7. 3. 1. Basic modelling and identification concepts from modal analysis

Machine tools are assemblies of individual elements so they may be considered as multi-mass vibrators or oscillators with respect to their dynamic behaviour. For simplicity, considering the machine as a system of unconnected single-mass vibrators may approximate to the behaviour of a machine tool under dynamic loading. The dynamics of multi-degree-of-freedom (MDOF) systems are better understood by analyzing the dynamics of single degree-of-freedom (SDOF) elements.

The time response or frequency response for each of the SDOF systems are easier to determine when the analytical model of a MDOF system is broken up into a set of SDOF systems. In practice it has been demonstrated that a random excitation causes all the modes to be activated therefore the principle of superposition is applied. The total response can be obtained from the contribution of each of the modes of vibration.

The analysis of the dynamics of a SDOF system is generally performed considering an analytical lumped mass model which treats a rigid body system (assembly of a rigid mass connected by spring and damper elements). In cases when the elastic behaviour has to be modelled more accurately, the model based on partial differential equations is used. The two analytical methods mentioned above are not able to adequately describe the dynamic behaviour of a complex structure.

This disadvantage was overcome in recent years by the finite element modelling method. The structure is depicted by combination of small elements. The equations of motion are generated by computer and based on the physical properties of the structure. The equations are 'diagonalised' to find their eigenvalues and eigenvectors. However, the computer programs require a large amount of memory and the model could be proven to be inaccurate for various reasons. The validity of a finite element model has to be confirmed by dynamic (modal) testing.

Workable identification procedures are necessary in connection with the prediction of behaviour for real vibrating systems. These should go beyond a classic determination of

vibration modes and frequencies, for instance to evaluate the coefficients in matrices of stiffness, mass and damping coefficients. Valid identifications are possible for stiffness and mass matrices ([101], [102]) working from measurements of vibration responses to hammer-blow excitations - providing that modelling conforms to an exact model order.

Identification of damping matrices is also feasible, in the ideal case, but is beset with difficulties as soon as one considers observational error, uncertainty of model order and departures from the classic "proportional" distribution of damping throughout a vibrating system.

These are the main theoretical ideas of the majority of specialist software packages used to locate unwanted vibration in machinery. The practical procedure has the following steps:

1. Use vibration sensors to measure the characteristics of vibration in order to track down and eliminate vibration;
2. Carry out the Fast Fourier Transform analysis to produce a complete spectral analysis of the vibration.
3. Measure and analyse the structural response of the machine to excitation by impact or shaker.
4. Use modal analysis to identify the structural deflection mode associated with the resonance involved.

The commercially available software packages enable clients to see for themselves the nature of the flexing responsible for the resonance, using a slow-motion animated sequence displayed on a laptop computer (Figures 5. 9 to 5.13).

Detailed modal analysis determines the fundamental vibration mode shapes and corresponding frequencies. This can be relatively simple for basic components of a simple system, but extremely complex when qualifying a complex mechanical system such as a CNC machine tool.

7. 3. 2. State of the art for modal analysis techniques

A vast majority of FRF measurements are done today by using FFT analyzers and one of the following methods:

1. *Shaker excitation* - may be performed by attaching a shaker at one point and moving the accelerometer to each of several other points;
2. *Transient excitation (impact testing)* - an accelerometer is attached at one fixed point and each other point is excited with a hammer.

The deformation patterns at the natural frequencies take on a variety of different shapes depending on which frequency is used for the excitation force. These deformation patterns are referred to as the mode shapes of the structure. The mode shapes and natural frequencies depend on the weight and stiffness of the structure.

A mode of vibration is really the manifestation of energy trapped within the boundaries of a structure that cannot be readily dissipated. As this energy travels back and forth within the structure, it causes the structure to deform with various well-defined wave-like motions called mode shapes. These mode shapes will "decay" in amplitude if all external sources of energy are removed from the structure.

The data resulting from a modal test is called an operating deflection pattern. The mode shapes are summed together in a linear way to form the deflection pattern because the deformations that are measured represent the actual response of the structure due to input excitation. The contribution of each particular mode is generally greatest in the vicinity of its resonance peak. Unlike modal analysis, an operating deflection pattern does not require measurement of a forcing function for monitoring purposes and it allows visualisation of weak points in a structure.

The contribution from adjacent modal resonances to the overall FRF value at a mode's resonance is called modal coupling. The modal damping and the frequency separation of the modes govern the degree of modal coupling.

For light modal coupling, the FRF value at a modal resonance can be treated as if it is the response to a SDOF system. So it is assumed that the contribution of adjacent modes near each modal resonance peak is negligible. In this case, SDOF curve fitting methods can be used to identify the modal parameters. Because residues are usually of real value in the case of light damping, they can be identified by picking the imaginary value of FRF for every modal peak frequency.

When modal coupling is heavy, the parameters of all modes must be estimated simultaneously using MDOF methods because an SDOF modal parameter estimation method may yield parameter estimates with large errors.

The most difficult part of the whole experimental modal analysis is the modal parameter estimation (the process of extracting modal parameters such as frequency, damping and mode shapes from the measured data). The modal parameters can be determined from a set of FRF measurements, acquired by exciting the structure and measuring its responses at various points across its surface. A frequency domain model of the structure is created from FRF measurements following two steps: identify the mode locations and estimate the modal

parameters of frequency, damping, and residues. Understanding and correctly applying the rigorous mathematical processes involved in developing the modal model is no easy task without in-depth knowledge of structural dynamics.

A computer is able to offer aid at different stages of modal analysis:

- Measurements - controls the Signal Analyser, prompts operator
- Data management - create files, store / recall measurements with labels or modal parameters
- Parameter estimations - methods for SDOF or MDOF systems
- Geometrical model - co-ordinates of points in the structure, connect points by lines, add unmeasured points, co-ordinate transformations
- Animation - shows in slow motion how the structure vibrates at measured modes (see Figures 5. 9 to 5. 13)
- Simulation - analytical modification of structures, analytical excitations.

The modal analysis software calculates the modal parameters from the fitted data and combines this with the geometric model to produce the mode shapes.

Referring to the assistance offered by computers to modal analysis methods for MDOF systems, Beards [103] remarks that:

" Although computational and computer techniques are extensively used in the analysis of multi-degree-of-freedom systems, it is essential for the analytical and numerical bases of any program used to be understood, to ensure its relevance to the problem considered, and that the program does not introduce unacceptable approximations and calculation errors."

A great deal of effort is put into the development of new and sophisticated curve fitting algorithms and excitation techniques and perhaps too little attention has been placed on the FRF measurements themselves. It is essential that great care be taken in measuring the original FRFs because poor original measurements can only lead to poor results.

Curve fitting methods consist in building a mathematical model around the analysed results and calculating the modal parameters by using this model.

Some aspects have to be taken into account when these methods are applied:

- How many data points should be used?
- What should be the order of the model?
- Are there any effects from modes outside the band of the curvefitter?
- Does the same technique need to be applied to all the modes?
- When to use a SDOF versus a MDOF technique?

- Is time domain or frequency domain best for the specific application?

The SDOF techniques are applied when light modal coupling is present in the experimental data. The most used techniques are: quadrature picking, circle fitting, polynomial fitting, complex division and difference formulae.

When heavy modal coupling appears in the experimental data, the MDOF methods (polynomial fitting from FRF or complex exponential algorithm from Impulse Response Function) are applied.

Gatzwiller [99] showed the various aspects of the strong link between modal testing and modal analysis (see Figure 7. 4). Tremendous effort has been expended in developing better measurement and reduction techniques to develop highly accurate models. The practical experiences reinforced the need for a thorough understanding of the fundamentals upon which modal testing is based, and of the detailed workings of the various phases and processes that make up a successful test: planning, executing, interpreting and applying the results from a modal test in straightforward terms.

Excitation techniques to better excite the structure and reduction techniques using multiple reference data, have helped in the process. However, the development of the experimental modal model is always troubled by difficult measurement situations and non-linearities which cause distortion of the extracted model.

Within the last two decades experimental modal analysis has evolved into one of the common tools in the sound and vibration analysis toolbox, readily available to most test engineers. This was due to the advent of the PC and the development of inexpensive, user-friendly modal parameter extraction software packages.

However, despite its recent widespread use, there are some important difficulties which have not yet been overcome, such as:

- Modal testing remains a notoriously difficult application especially in critical applications where high accuracy and high precision are of paramount importance.
- Existent modal analysis software packages are able to perform modal parameter estimation for linear systems of first or second order only because the modal testing explicitly assumes an ideal physical model - time-invariant, linear, causal and observable. However, most systems are non-linear to some degree and the results of modal tests are excitation-specific. Ewins [104] commented on the current advances regarding modal testing in this way:

  " ... *it must be noted that the marked increase in accuracy which has accompanied recent developments in modal testing technology has resulted in a much higher incidence*

of non-linearity observations than in previous years. It is ironic that an improvement in a technique should lead to an increase in difficulties rather than a reduction. Not only is non-linearity visible in the measured data as slight distortions in the usual plots of FRF, but it is also responsible for sometimes significant discrepancies in the modal analysis process. Some of the algorithms used to extract modal parameters can be surprisingly sensitive to the small deviations (from linear characteristics) which accompany the presence of slightly non-linear elements in the structures."

- The existent modal analysis software packages do not offer very accurate results when the modal coupling is heavy.

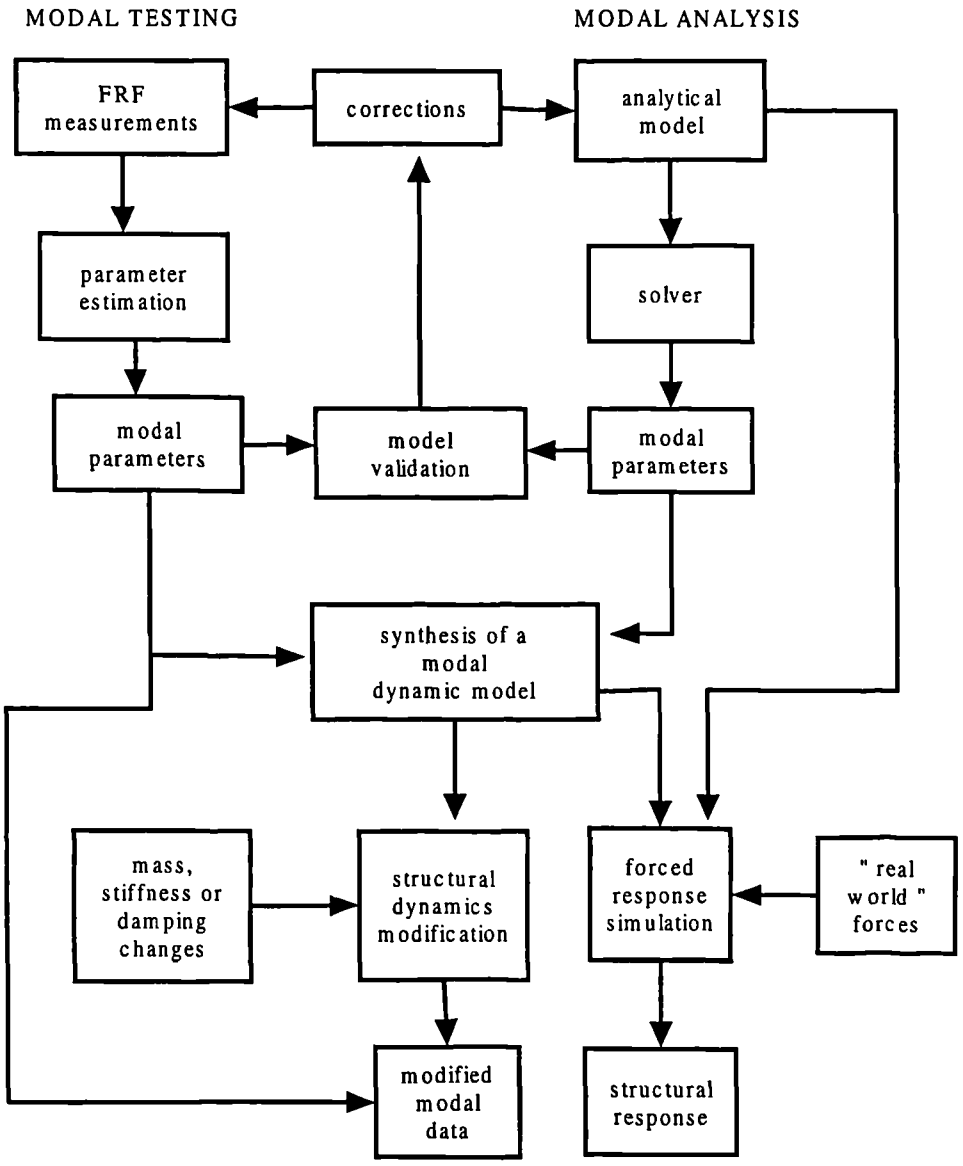

Figure 7. 4. The relationships between modal testing and modal analysis [99]

CNC machine tools are non-linear systems with an order greater than two so one of the purposes of this thesis is to determine a method for parameter estimation suitable for this type of system on the basis of previously developed modal analysis theory.

7. 3. 3. Classical methods for measurement of damping

Damping is an important factor in the behaviour of non-linear dynamic systems because the levels of forced and free vibration are influenced by it. De Silva [105] underlined the importance of the way in which the damping measurements are performed:

"It is extremely difficult to develop a realistic yet tractable model for damping in a complex piece of equipment operating under various conditions of mechanical interaction. Even if a satisfactory damping model is developed, experimental determination of its parameters could be tedious.

A major difficulty arises because it usually it not possible to isolate various types of damping (e. g. material, structural, and fluid) from an overall measurement. Furthermore, damping measurements must be conducted under actual operating conditions for them to be realistic."

De Silva also mentioned the various parameters (damping capacity, loss factor, Q-factor, damping ratio) which represent damping and its models (viscous, hysterectic, structural and fluid) that characterise the nature of mechanical energy dissipation in the system. A review of the most used damping measurement methods was performed and the principal characteristics are shown in Table 7. 3.

In the case of the last two methods, modal damping values for MDOF systems could be estimated from the magnitude of the gain plot when the modal frequencies are not too closely spaced and the system is slightly damped. The width of the peak from the gain diagram gives a value for the damping coefficient and an idea of the central value for the frequency interval.

The phase shift of 180° has to take place at a frequency in the vicinity of the central frequency determined from the gain diagram. This frequency could be in the interval including frequencies up to 10 times the frequency shown by the gain diagram.

The phase shift is 180° in the case of a second order system. When the system has a higher order, the phase shift could be greater or smaller than 180°, depending on the existence of other resonance frequencies.

The author highlighted some limitations to the use of damping values determined from experimental data:

- Damping is assumed to be proportional to the desired resonant frequency at which the system is excited. Therefore, the modal interactions from the resulting transient vibration are neglected.
- Damping parameters are computed from test measurements on the basis of linear system theory. These values will not represent the actual system behaviour when the system has a high degree of non-linearity.
- Damping results are affected by modal interference in closely spaced modes.

Method	Measurements	Formulas
Logarithmic decrement method	A_i – first significant amplitude A_{i+r} – amplitude after r cycles	Logarithmic decrement $\delta = \frac{1}{r} \ln \frac{A_i}{A_{i+r}} = \frac{2\pi\zeta}{\sqrt{1-\zeta^2}}$
Step-response method	M_p – peak value of response PO – percentage overshoot (over steady-state value)	$M_p = 1 + \exp\left[\frac{-\pi\zeta}{\sqrt{1-\zeta^2}}\right]$ $PO = 100 \exp\left[\frac{-\pi\zeta}{\sqrt{1-\zeta^2}}\right]$
Hysteresis loop method	ΔU – area of displacement-force hysteresis loop x_0 – maximum displacement of the hysteresis loop k – average slope of the hysteresis loop	Hysterectic damping constant $h = \frac{\Delta U}{\pi x^2}$ Equivalent damping ratio $\zeta = \frac{h}{2k}$
Magnification-factor method	Q – magnitude of FRF at resonance frequency	$Q = \frac{1}{2\pi\zeta\sqrt{1-\zeta^2}}$
Bandwidth method	$\Delta\omega$ – bandwidth at 0.707 of resonant peak ω_r – resonant frequency	$\zeta = \frac{\Delta\omega}{2\omega_r}$

Table 7. 3. Classical damping measurement methods

Ewins [104] emphasised the difficulties of extracting meaningful damping quantities from measured FRF data:

- Associated with the measurement techniques themselves (damping effects are usually an order of magnitude smaller than the corresponding mass and stiffness effects);

- The underlying equations of motion are much more complex than considered;
- The features which influence damping – joint tightness, surface finish, temperature, wear etc. – are variable and unrepeatable from day to day and system to system.

Under these considerations, *" most attempts to describe the dynamic behaviour of damping elements with any degree of realism will result in very complicated and certainly non-linear expressions."*

The methods enumerated by De Silva [105] consider that the system has only one type of damping. However, the research and development efforts are concentrated on performing modal parameter estimation in MDOF systems which have several forms of damping present. The major drawback of these methods is in determining an equivalent level of damping for the models. Equivalent viscous damping assumes a forced sinusoidal motion, but some damping models depend on amplitude. When the amplitude reduces, so does the damping force in the system. Thus, the use of equivalent damping for transient decay is not recommended.

Wavelet transformation is a powerful tool for the analysis and synthesis of signals. Localization of signal characteristics in spatial (or time) and frequency domains can be accomplished very efficiently with wavelets. This allows the simultaneous determination of sharp transitions in the spectrum of the signal and the positions (or time) of their occurrence. Due to this fact, wavelets can be used to overcome the above mentioned shortcomings and the methodology is described in the following sections.

7. 3. 4. Wavelets used for modal parameters identification

The majority of modal analysis methods use *impulse response data* and employ the Least Squares approach as an integral part of their formulations. When the standard least squares approach is used to analyse noise corrupted data, the system parameters that are obtained are biased and the damping values are most sensitive to corrupted data. To overcome the resulting bias, the solution order is over-specified. Alternatively, the least squares element can be replaced with one of the many methods that attempt to eliminate bias by either modelling the noise, or avoiding the terms that give rise to the bias.

Frequency domain methods for non-linear systems have developed into an established class of procedures with the advent of modern spectral analysis, high precision data acquisition equipment and the development of sophisticated estimation algorithms. The analysis of non-stationary signals whose spectral character changes with time (such as vibration signals) calls for specific time-variant techniques which go beyond those employing

the classical Fourier transform because when a signal is transformed into the frequency domain, time information is lost.

Wavelet analysis is one of these techniques and uses windows with variable size: long time intervals – when more low frequency information is required, shorter regions – when more high frequency information is wanted. This could be observed from the definition of the continuous wavelet transform (CWT) of a signal f (t) at time τ and scale *a* given by Mallat [106]:

$$CWT_f^{\Psi}(\tau,a)=\frac{1}{\sqrt{a}}\int_{-\infty}^{\infty} f(t)\,\psi^*\left(\frac{t-\tau}{a}\right)dt \qquad (7.18)$$

where Ψ (τ, a) – wavelet (mother) function * symbolises complex conjugation

τ - time delay (translate parameter) which gives the position (centre) of the wavelet

a – scale factor (dilation parameter) which determines the frequency content

The factor of $a^{-1/2}$ is a normalisation to keep the total energy of the scaled wavelet constant.

The term wavelet comes from the fact that it is a little wave. There is an infinite number of wavelets that can be used for analysing a series, and nearly this many are in use today. Wavelets have many valuable properties such as:

- The properties of all individual wavelets in a family are the same as those of the mother wavelet because all of the individual wavelets are derived from the same mother wavelet.
- Wavelets can easily be shifted in time therefore a feature that appears at some particular time will reveal itself in a wavelet analysis in a consistent way. Its wavelet characteristic will be the same, no matter when the feature occurs.
- Wavelets are inherently based on a meaningful time scale which helps the users to think in terms of phenomena whose cycle length is a specified number of samples.
- The wavelet analysis takes the signal decomposition to a space-scalar (time-frequency) plane and separates then re-constructs these components in the space domain.

Strang and Nguyen [107], Aldroubi and Unser [108] showed that an advanced signal processing technique such as wavelet transform is capable of performing an evolutive time-frequency analysis of the non-stationary signal.

Luo et. al [109] used the wavelet analysis and global Fourier transforms for analysis and modelling of vibration signals from machine tools and demonstrated the superiority of the wavelet transform. A vibration model was developed considering the combination between continuous wavelet transform (CWT) and the discrete harmonic wavelet transform (DHWT) and the coefficients were identified with the least-square algorithm.

Different applications are better served by different wavelets. Aldroubi and Unser [108] demonstrated that Morlet (modulated Gaussian) wavelets yield the best time-frequency localisation. Morlet wavelets are complex wavelets, which for some applications confer some advantages since the phase may contain useful information.

Also Ruzzene et al. [110] have taken over the idea of estimating the modal parameters from the impulse response of a system, an idea presented before by Agneni and Crema [111] and Spina [112]. Ruzzene et al. have shown that the wavelet transform (WT) represents a good improvement of techniques based on the Hilbert transform ([103, 104]). The technique was applied to the acceleration responses from a real bridge under ambient excitations and the authors emphasised that:

" The decay rate of the envelope for each mode was calculated from the slope of the linear interpolation performed on the wavelet modulus decay, while the damped natural frequency was estimated as the mean value of the instantaneous frequency time history, calculated deriving the phase of the WT. "

Staszewski [113] compared three techniques based on the continuous wavelet transform (CWT) used to estimate damping: the WT cross-section procedure, the impulse response recovery procedure based on wavelet domain filtering and the wavelet ridge detection procedure. The advantage of WT over the classical complex envelope function consists in decoupling the MDOF system into single modal components. The best accuracy (especially in the case of noisy data) is given by the wavelet ridge detection procedure.

The same author published a recent paper [114] where he tried to bring together some recent applications of wavelet analysis to non-linear systems from engineering. After he referred to relevant publications [115-120] containing the fundamentals of wavelet analysis, he discussed about the three methods above mentioned and about cross-wavelet analysis, self-similar signals, coherent structures and chaos. Some of the conclusions are worthy of mention:

- Wavelet analysis used for the identification of non-linear systems is an area of research which offers promising results and could be developed further in the future. Between the directions which present interest are the damping estimation and modal parameters estimation for MDOF systems with close modes.
- Different levels of accuracy and description are reached due to wavelet analysis's capability of representing solutions of partial differential equations at different scales.
- Wavelets could be used for finite element applications as shown by preliminary studies.

From this brief literature survey regarding the use of WT in engineering applications, it is evident that previous modal parameter identification using WT applied to CNC machine tools was not performed (except [109]). The previous publications refer to the use of WT for identifying the modal parameters of civil engineering buildings (bridges, blocks).

This thesis introduces a new procedure to extend the use of the wavelet transform to identify hybrid models of non-linear systems based on a frequency domain description and utilises this to solve practical problems in the CNC machine tools field.

The wavelet transform applied to experimental signals is shown to be capable of detecting variations in the amplitude levels of weak components embedded in strong noise and non-stationary processes and the wavelet analysis is used to de-noise the signals without any appreciable signal degradation.

7. 3. 4. 1. Brief theoretical basis of wavelet analysis

The Fourier transform is the ideal tool when dealing with stationary signals, whose statistical properties are invariant over time because the Fourier transform is an infinite linear combination of dilated cosine and sine waves. This was the standard method for solving and analysing differential equations and for analysing and treating signals.

The weakness of Fourier analysis is shown in dealing with sharp spikes and chopped signals because sines and cosines are, by their very nature, non-local smooth curves which stretch into infinity. The non-stationary signals could be represented by linear combinations of atomic decompositions known as wavelets. These wavelets allow the extraction of the simple constituents, localised in both time and frequency space, that make up a complicated structure or signal. This unique characteristic makes wavelets particularly useful in approximating data with sharp discontinuities.

Wavelet techniques enable the analysis of non-stationary time series by decomposing a time series into time and frequency space simultaneously. A time-frequency representation maps a 1D signal to a 2D time-frequency image that displays how the frequency content of the signal changes over time. Such transformation allows one to localise the occurrence of a particular frequency in the non-stationary signal. Using the wavelet transform one obtains simultaneous information on the amplitude of any "periodic" signals within the series and how this amplitude varies with time.

Wavelet analysis is the new fashionable technology of the age, but its mathematics are not in themselves new because much of the research for the development of wavelets was

carried out in the 1930s. However, a commercial use has been found for them only in recent years.

The wavelet theory was first explicitly introduced by Grossman and Morlet [121] in their works on geophysics, where they showed that any signal of finite energy can be represented as a linear combination of wavelets. Other applications of wavelets are in astronomy, acoustics, earthquake predictions, fingerprint analysis, pure mathematics, multi-resolution signal processing, image and data compression, telecommunications, numerical analysis, speech processing etc.

Farge [122] demonstrated that the wavelet (mother) function from Equation (7. 18) must have a zero mean, be bandpass (have no energy at zero frequency) and be localised in both time and frequency space to be admissible as a wavelet. The Continuous Wavelet Transform (CWT) represented by Equation (7. 18) is a windowing function that shifts frequency by *scaling* (scale a is dimensionless). Rioul and Duhamel [123] have reviewed several algorithms for discrete and continuous transforms and mainly two of them are used in practice:

- The CWT integral could be computed as a discrete convolution and the wavelet transform as a cross correlation between the wavelet and the signal;
- The CWT is calculated in the frequency domain and due to the fact that a convolution in the time domain is a multiplication in frequency domain, this algorithm is significantly faster than the previous one. The algorithm is implemented in the WaveLab library of MATLAB routines for wavelet analysis developed by Department of Statistics, Stanford University, USA. This is a freeware software that can be retrieved by Internet and the basic concepts were treated by Mallat [106]. More details about this algorithm will be discussed later when its use is analysed in depth.

For the identification of the modal parameters of CNC machine tools, the Morlet wavelet was chosen because of its advantages:

- Natural robustness against shifting a feature in time because little or no special precautions are needed to ensure that a feature will make itself known in the same way no matter when it occurs;
- The best filter at simultaneously locating a feature in terms of its period and when it appears. The Heisenberg Uncertainty Principle decrees for this application that no filter can, with arbitrary accuracy, simultaneously locate a feature in terms of both its period

and its time of appearance. In order to gain more precision in one, the other must be sacrificed;

- Very intuitive nature and definition.

The Morlet wavelet transform (Figure 7. 5) has proven to be especially convenient for analysing signals with a wide range of dominant frequencies which are localised in different time intervals or amplitude and frequency modulated spectral components. This wavelet has the advantage of incorporating a wave of a certain period, as well as being finite in extent. In fact, the wavelet is nothing more than a sine wave multiplied by a Gaussian envelope:

$$\Psi(t) = (e^{i\omega_0 t}) \times \left(e^{-\frac{t^2}{2}} \right) = [\cos(\omega_0 t) + i \sin(\omega_0 t)] \times \left(e^{-\frac{t^2}{2}} \right) \quad (7.19)$$

First of all it is necessary to choose the wave number ω_0 which gives the number of oscillations within the wavelet itself. In practice, when $\omega_0 = 6$ then the errors due to non-zero mean are smaller than the typical computer round-off errors ([122]). The Morlet wavelet does not have zero mean because the Fourier transform of the Morlet wavelet presents a DC component. The DC component has a value of 10^{-6} when $\omega_0 = 5.4285$. Flandrin [124] showed that it is common to use a value between $5 < \omega_0 < 6$ which makes the Morlet wavelet practically admissible due to a very small mean value.

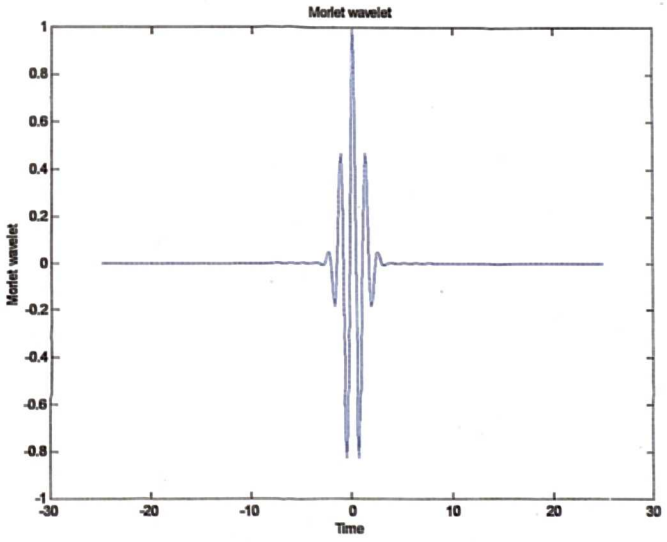

Figure 7. 5. The Morlet wavelet

The next choice is a set of scaling parameters a (see Equation (7. 18)), such that all the frequencies present in the time series are adequately sampled. The first step is choosing the

smallest resolvable scale a_0 as some multiple of time resolution dt (for example $a_0 = 2 \times dt$). The larger scales (longer periods) are chosen as power-of-two multiples of the smallest scale:

$$s = 2^j \times s_0 \qquad , j = 0, 1, 2 \ldots. \tag{7.20}$$

The scales are called octaves and each octave contains 2^j voices. The largest scale should be less than half the length of the entire time series. Usually, the scales could be over-sampled (for example, 10 voices within each octave) to provide information on frequencies in between the dyadic scales.

The Morlet wavelet kernel is formulated to implement the linear wavelet transform, which localises at every frequency channel and can be interpreted by the 2*D* or 3*D* time-frequency wavelet spectrogram.

Staszewski [113] presented the relationship between the scale parameter a, the wavelet, sampling rates and analysing frequency:

$$f_x = \frac{f_0 \times f_s}{a \times f_w} = \frac{\frac{\omega_0}{2\pi} \times f_s}{a \times f_w} \tag{7.21}$$

where f_x – analysing frequency f_0 – centre frequency of the mother wavelet

f_s – sampling rate of the signal f_w – sampling rate of the wavelet

The frequency resolution is proportional to bandwidth, so it will decrease at higher frequencies and increase at lower frequencies. Accordingly, this results in higher time resolution at higher frequencies (lower scales) and lower time resolution at lower frequencies (higher scales). This approach makes sense especially when the signal at hand has high frequency components for short intervals and low frequency components for long intervals.

The Morlet wavelet is complex, being obtained by taking a complex sinusoid and localising it with a Gaussian envelope. This makes the wavelet transform to be complex, too. It is useful to represent the real and imaginary part of the wavelet transform in polar co-ordinates: the norm is the magnitude of the transform while the angle (phase) completes the representation. The alternative display in polar form enables increasing time resolution with increasing frequencies.

7. 3. 4. 2. Identification of damping parameters using wavelets

Damping in machine tools basically is derived from two sources: material damping and interfacial slip damping. Material damping is the damping inherent in the materials of which the machine is constructed. The magnitude of material damping is small comparing with the

total damping in machine tools. A typical damping ratio value for material damping in machine tools is 0. 003 and it accounts for approximately 10% of the total damping.

The interfacial damping results from the contacting surfaces at bolted joints and sliding joints. This type of damping accounts for approximately 90% of the total damping. Among the two types of joints, sliding joints contribute most of the damping. Welded joints usually provide very small damping which may be neglected when considering damping in joints.

Friction is present almost in all mechanical systems as a non-linear parasitic effect that needs to be modelled and understood very well in order to achieve high-accurate positioning of mechanical systems in a very short time period. The friction torque (or force) that corresponds to very low velocities is still a very big challenge for modelling purposes.

Control strategies attempting to compensate for the friction effects require a suitable model that captures the behaviour of friction throughout the entire range of velocity. A realistic friction model must include viscous friction, Coulomb friction, Stribeck effect (negative viscous friction at low velocities), changing break-away torque (torque rate dependence), and stick-slip motion, so that a quasi-real friction can be imposed in simulation procedures to achieve very high-performance positioning.

In the hybrid model elaborated in Chapter 4, only viscous friction and Coulomb friction are considered. Coulomb friction leads to a non-linear mathematical model, while viscous friction produces a linear mathematical model.

The complete information about the dynamic behaviour of a vibrating system can be obtained by knowing its natural frequencies of vibration, modal damping coefficients and the mode shapes. Generally, examining the response frequency spectrum when an impulse is applied as a forcing function can identify the natural frequencies of a system because all frequencies are excited simultaneously.

Landee et al. [125] illustrated that the bandwidth for a SDOF system is directly proportional to the levels of damping. The classical method using the Fourier Transform presents some limitations connected with the type of analysed signal. For example, spectral leakage develops in the case of analysed data which is not periodic in the rectangular analysis window. The side lobes generated by the Fourier Transform of the window will permit leakage of the spectral peak. The common procedure ([126], [127]) to suppress the leakage in time-series theory is to gradually taper the data at the beginning and end of the series with a Hanning or other window. The deficiency of the procedure consists of the modification of the bandwidth of the signal by changing the energy content and distorting spectral estimates.

WT minimises the windowing effects by increasing the duration of the window. The effective damping contribution due to windowing effects can be identified and removed by knowing the central frequency f_0 of the wavelet chosen for the analysis. Thus the parameter f_0 not only dictates the frequency resolution of the WT, but also determines the windowing effects. Its minimum value must allow the capture of the signal components and its maximum value has to be lower than the value that leads to distortion of signal and roughness of the spectral peak.

A MATLAB program for the identification of the modal parameters (resonance frequencies, damping factors) is written on the basis of some **.m** files (CWT, Wavelet etc.) included in the *WaveLab* package. The program is included in Appendix F.

The CWT of the impulse response is calculated considering the following steps:

1. select a mother wavelet – Morlet in this case;
2. for a given scale a, sample the wavelet with N data points within the range of its support (for Morlet wavelet the support is [-5, 5]);
3. compute the FFT of the signal and the wavelet at scale a – the FFT function in MATLAB is a built in primitive function assuming that the signal is periodic and giving a very short execution time. By using the FFT function, one cannot alter the boundary conditions;
4. multiply the FFT of the signal by the modulus of the FFT of the wavelet;
5. compute the IFFT (inverse FFT) to obtain the wavelet coefficients for scale a.

The Morlet wavelet has a maximum scale of 4, the number of octaves is 2 and the scales are over-sampled by choosing 50 voices within each octave.

If the signal has a spectral component that corresponds to the current value of scale a, the product of the wavelet with the signal at the location where this spectral component exists gives a relatively large value. If the spectral component that corresponds to the current value of the scale a is not present in the signal, the product value will be relatively small, or zero.

The CWT applied to experimental data (Figure 5. 42) obtained by measuring the differential of the linear encoder output when random noise is introduced into the system (see Figure 5. 24) produces a 3D graph displayed in Figure 7. 6.

It is important to underline that the axes are translation and scale, not time and frequency. However, translation is strictly related to time, since it indicates where the mother wavelet is located. The translation of the mother wavelet can be thought of as the time elapsed since t=0. The scale is actually the inverse of frequency therefore whatever it is said about the properties

of the wavelet transform regarding the frequency resolution, the inverse of it will appear on the figures showing the WT of the time-domain signal.

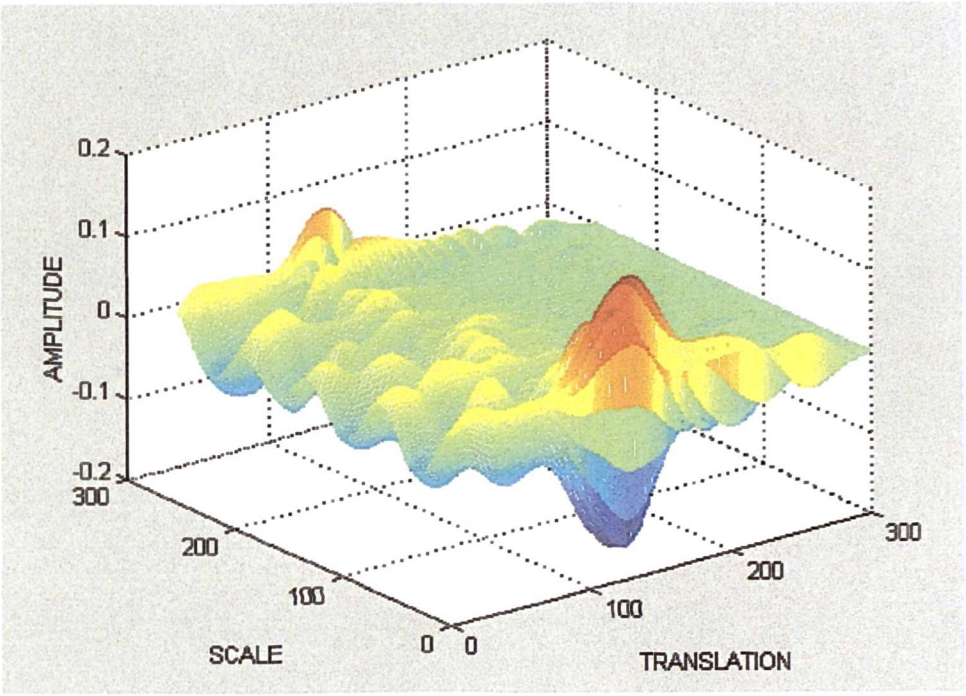

Figure 7. 6. The CWT for the impulse response of the actual control system

The axes of the 3D graph are normalised and should be evaluated accordingly. Roughly speaking, the 300 points from the translation axis correspond to 1070 ms, and the 256 points on the scale axis correspond to a frequency band of 250 Hz. The numbers on the axes are just the numbers of samples in the computation.

The next stage consists of finding the co-ordinates (translation, scale) of the maximum peak from the 3D graph produced by CWT and perform a cross section through 3D graph at this point to obtain an estimate of the damped sine response for this mode. It is obvious that the 3D graph from Figure 7. 6. presents a maximum at a sampling point from translation scale included in the interval 100 and 200. Running MATLAB commands, it was established that the maximum corresponds to sampling point number 127. The damped sine of the cross section is shown in Figure 7. 7.

The decay ratio of the amplitudes for the exponentially damped sinusoid is called *logarithmic decrement* ([128], [129]) and it depends on the damping factor ζ of the sinusoid:

$$\delta = \frac{2\pi\zeta}{\sqrt{1-\zeta^2}} \qquad (7.22)$$

Solving the equation (7. 22), the damping factor is:

$$\zeta = \sqrt{\frac{\delta^2}{4\pi^2 + \delta^2}} = \frac{|\delta|}{\sqrt{4\pi^2 + \delta^2}} \qquad (7.23)$$

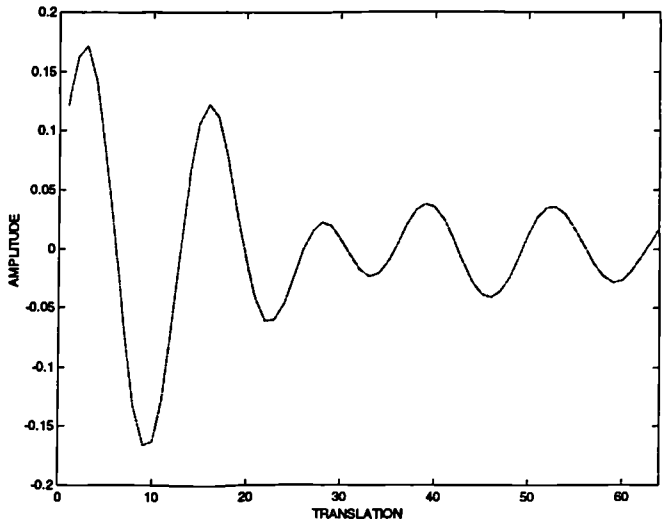

Figure 7. 7. Cross-section through 3D graph corresponding to the maximum value of the CWT

The logarithmic decrement is calculated by applying linear regression to the envelope for the damped sine. In the case of Figure 7. 7., the gradient of the envelope is (– 0. 613) and the damping ratio results:

$$\zeta = \frac{|\delta|}{\sqrt{4\pi^2 + \delta^2}} = \frac{0.613}{\sqrt{4\times(3.14)^2 + (0.613)^2}} = 0.097 \qquad (7.24)$$

The corresponding frequency is determined from the FFT of the damped sine (Figure 7. 8):

$$f = \frac{\text{peak} \times 1000}{n_{FFT} \times \text{sample}} \qquad (7.25)$$

where f – resonant frequency peak – point number of the first maximum of FFT

n_{FFT} – number of points for FFT sample – sampling time in ms

The approximate resonant frequency for FFT from Figure 7. 8. is:

$$f = \frac{\text{peak} \times 1000}{n_{FFT} \times \text{sample}} = \frac{5\times 1000}{64\times 2} = 39 \text{ Hz} \qquad (7.26)$$

These operations are applied for the other peaks and in this way the resonant frequencies and the corresponding damping ratios are extracted from the input and output data. These values

are introduced in Table 7. 4. together with the frequency values that correspond to gain variations from the experimental Bode diagrams shown in Figure 5. 26. Sometimes the gain fluctuations are not very significant, but the corresponding frequencies have been considered with the purpose of comparison with the values obtained by using the wavelet analysis.

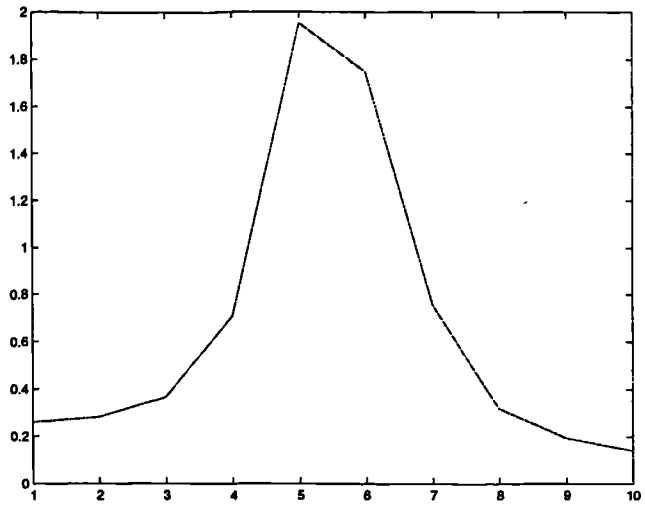

Figure 7. 8. FFT of the cross-section presented in Figure 7. 7.

	f_1	f_2	f_3	f_4	f_5
Bode diagrams	35 Hz	74 Hz	112 Hz	119 Hz	131 Hz
Wavelet Analysis	39 Hz	78 Hz	86 Hz	125 Hz	
Damping ratios	0. 097	0. 126	0. 174	0. 052	

Table 7. 4. Identified values for resonant frequencies and damping ratios using Bode diagrams and wavelet analysis

By applying the bandwidth method in Appendix C3. 2, the damping ratio $\zeta_Y = 0.112$ was calculated for the resonance frequency of 92 Hz from the Bode diagrams showing the torsional movement between the driven and the driving pulleys (see Appendix D2). The damping ratio determined using the wavelet analysis is 0. 174 for a resonance frequency of 86 Hz. Therefore, there is a difference between the values of the damping ratios calculated by using wavelet analysis and bandwidth method. This could be explained by the fact that in the

CWT of the impulse response contains all resonant frequencies of the system while the bandwidth method calculates only one resonance frequency.

The are some obvious advantages of using the wavelet analysis:

- The Bode diagrams were plotted considering the swept sine input that has a great amount of energy for every frequency and is subjecting the CNC machine tool to strenuous effort. The wavelet analysis was performed using the response of the system to random noise which does not generate any problems in the functioning of the machine.
- This application has demonstrated the Wavelet Transform's ability to uncover local and transient features of the signals and to identify the contribution of various modes at different times in the response of the non-linear system.

8. CONCLUSIONS AND SUGGESTIONS FOR FURTHER WORK

8. 1. Conclusions

The main aim of the study was to focus on the parameter identification and the modelling of non-linear control systems associated with the Beaver 3-axis VC35 CNC machine tool. The aims and objectives outlined in section 1.2 have been completed. The intermediate objectives were completed and the following conclusions reached:

(a) The lumped parameter model of each axis with load inertia referred to the motor, without backlash, friction and geometric errors was developed. As expected each single axis model did not reflect the real dynamic behaviour of the system.

(b) The 3-D lumped parameter model with modular load, including backlash and coulomb friction and without geometric errors overcame some of the disadvantages referred to above (a) giving improved dynamic performance. However, the simulated responses did not approach the measured responses (see sections 6.1.1, 6.2.1 and 6.3.1).

(c) The 2-D hybrid model with modular load, including backlash, friction and geometric errors provided a better understanding of the effects of machine tool errors when considering its operating performance. In particular, it was used to simulate the effects of geometric errors on ball-bar plots which were shown to compare very well with the actual data from the machine (see section 6.4).

(d) The dynamic performance for the single axis simulation was still considered not to be good enough when compared to the machine measured data. In particular the response of the system to swept sine and white noise stimuli signals. A single axis hybrid model with distributed load, explicit damping factors, backlash and friction was then developed. The simulation of this model to swept sine and white noise stimuli signals compared favourably with the measured response at the machine (see section 6.3.2). The influence of factors such as damping coefficients, moving mass, velocity and position loop gains, time constants of the servo control system on the machine tool control characteristics has been determined. Different friction models have been investigated and an effective simulation method has been developed. This model represents to a large extent the dynamic behaviour of the axis drive selected. It is considered that the model produced data useful for the prediction of performance, accuracy, stability, and safety issues associated with the drive system.

(e) The control system has been modelled element by element, including for all known non-linear factors as identified by the measurement strategies developed during the research. Specialised equipment such as laser interferometer, ball bar, electronic levels, artefacts, signal spectrum analyser etc. were used to obtain parameter data.

(f) The control system has been modelled element by element, including all known non-linear functions as identified by measurement using the specialised equipment referred to in (e) above. The machine axis drive had encoders fitted to the motor, ball-screw end and to the saddle so that dynamic effects could be evaluated at different load points (see Chapters 5 and 6). The further into the load path the more complex the model needed to become in order to identify the resonant states. Accelerometers with the associated spectrum analysers were used to identify these resonant states and to which element they were related. Essential to satisfy the need for correct data is to build a realistic model.

(g) Modal analysis measurements were carried out on the structure to identify significant structural resonant states in response to impulse, sinusoidal and cutting motion stimuli. Current "state of the art" experimental modal analysis practices were used to determine the salient resonant states (see section 5.3). In this way the theoretical and methodological foundation developed from the control field could be compared with the extensive experimental knowledge from the modal-testing field. Some useful correlation data was produced (see section 5.3.2).

(h) Parameter identification techniques were applied to the CNC machine tool axis drives utilising various stimuli (step input, sinusoidal and trapezoidal signals). A model adjustment technique was used to modify the coefficients of the model. The same signals were applied to both the model and the relevant machine tool axis drive for comparison purposes. The outputs were compared and the coefficients altered by an optimisation algorithm until the model response approaches that of the system. Good correlation was achieved.

(i) The most efficient parameter identification technique was chosen after a detailed survey of existing methods for application with non-linear continuous time systems. The wavelet transform proved useful and versatile in the identification of the damping factors by overcoming the shortcomings of the Fourier transform (only frequency resolution and no time resolution). This multi-resolution analysis technique has the power to retain the information concerning the system and hence enables the user to determine the sensitivity of the parameters to any change in the functioning of the system (see Chapter 7).

The thesis was focused on the development of an efficient identification method of the modal parameters of a non-linear system and has shown promising results to date.

8.2 Contribution to knowledge

Several areas have been identified as giving a significant contribution to knowledge under the scope of this investigation:

(a) The shortcomings of lumped parameter models have been clearly identified in that realistic dynamic responses are not achievable (see sections 4.2, 4.3.3, 7.2.2).

(b) A novel hybrid model with a distributed load, explicit damping factors, backlash and friction was developed (see sections 4.3.3. and 6.1.2) and shown to have a similar dynamic response to the same stimuli as the machine tool axis drive system (see section 7.2.2).

(c) Geometric errors measured by specialised metrology equipment were clearly demonstrated to be essential for inclusion in multi-axis models if realistic contouring accuracy was to be achieved (see sections 5.1, 5.2 and 6.5).

(d) Novel measurement practices (hardware and software) were developed for the decoding of position signals from encoders placed on the motor, ball-screw and saddle (2 rotary and one linear). The techniques were found to be very effective. Machine tool axis drives are known to be difficult systems to gain meaningful data from since they involve heavy mass loads and need stimuli signals of sufficient energy to excite the system. The methodology used in this research has been found to be effective (see Chapter 5).

(e) Measurement strategies for the measurement on non-linear functions and salient resonant states have been defined and validated (see Chapter 5).

(f) Stimuli signals as parameter identifiers applicable to CNC machine tool axis drive applications have been clearly defined (see sections 5.4 – 5.6, 7.2.1).

(g) The Continuous Wavelet Transform (CWT) was used for the first time to estimate the modal parameters of the CNC machine tool axis drives elements and the results obtained agree with those generated by classical methods for measurement of damping factors (see sections 7.3.3. and 7.3.4). The CWT was used before for natural frequencies and damping factors identification in the case of vibrating structures such as bridges, buildings etc., but not for CNC machine tools (see Chapter 7).

8. 3. Suggestions for further work

(a) Improve the realism of the hybrid model with distributed load and explicit damping coefficients by inserting the spectral density of noise measured from the machine, also the effect of mass distribution on the dynamic behaviour of the non-linear system etc.

(b) Develop a 2-D and 3-D hybrid models with distributed load and explicit damping coefficients including geometric errors and those considerations outlined in (a) above which will reflect accurately the dynamic behaviour of vibrating systems.

(c) Convert the SIMULINK model into C++ or equivalent-programming languages as a first step to developing intelligence–based parameter identification and optimising adjustment routine on-line. The intelligence of the system to come from its ability to predict models parameters and checks its system stability.

(d) A major consideration is the development of a series of measurement strategies to optimise the identification process of the machine dynamics. Also to develop a methodology that will analyse the performance of each parameter of the system.

(e) Develop an automatic identifier and algorithm for on-line parameter identification of the non-linear systems based on the wavelet transform by the thorough investigation of the performance and computational considerations associated with the proposed identification technique.

(f) Derive a microprocessor-based identification methodology for application to both analogue and digital drive systems.

(g) The main technical goal of the future work is the derivation of algorithms that track fast variations in the optimal parameters despite noise being present in the measurements of the cost function and the modelling uncertainty that exists in most real systems.

Successful understanding of the dynamic performance of machine tools will lead to improving the machining accuracy through the prediction and compensation control of the machine process errors.

REFERENCES

[1] *Reduction of Errors in the Design and Integrated Manufacture of CNC Machine Tools (REDUCE)*, EPSRC Grant No: GR / R35186 / 01. Precision Engineering Centre, University of Huddersfield.

[2] Ford D. G. - *Machining to Microns - Error Avoidance or Compensation?* Proceedings of International Conference on Laser Metrology and Machine Performance (LAMDAMAP ' 95), Southampton, 1995, pp. 277 - 286.

[3] Ford D. G., Postlethwaite S. R., Blake M. D. - *The Identification of Non-rigid Geometric Errors in a Vertical Machining Centre*, Proc. IMechE, vol. 213, part B, 1999, pp. 555-566.

[4] *ISO 230 - 1: Geometric accuracy of machines operating under no-load or finishing conditions.* ISO Standards 1996.

[5] *ISO 230 - 2: Determination of accuracy and repeatability of positioning of numerically controlled machine tools.* ISO Standards 1996.

[6] *ISO 230-4: Circular test for numerically controlled machine tools.* ISO standards 1996.

[7] *BS 3800 – 3: Method of testing performance of machines under loaded conditions in respect of thermal distortion.* British Standards 1990.

[8] *ISO 230-3: Determination of thermal effects.* ISO Standards 1998.

[9] *Basic Structures for Machine Tools.* AMTRI report, DTI sponsored 1992.

[10] Ford D.G - *Machine Tool Structures – Static, Dynamic and Thermal Errors.* Keynote Speaker for "Sharing Tomorrow's Technology Today". Five UK specialists involved on various topics in a series of Seminars with our Japanese counterparts. Organised by the MTTA/DTI supported by IMechE, I.E.E and leading UK companies. Three Venues: DTI offices, London, Churchill College, Cambridge University, and the Conference Centre, University of Warwick 20, 21 and 22 May 1997.

[11] Bartlett H., Whalley R. - *Power Transmission System Modelling.* Proc.of IMechE, vol.212, part C, pp. 497-508, 1998.

[12] Ford D. G. - *General Purpose CAD / CAE Aid to Design a Machine Tool System*, Ph.D. Thesis, The University of Huddersfield, U. K., December 1987.

[13] Green J. - *Mathematical Modelling and Simulation of CNC Machine Tool Axis Drive Systems.* BSc Project, The University of Huddersfield, U.K., May 1993.

[14] Gross H. - *Electrical Feed Drives for Machine Tools.* John Wiley and Sons Ltd., 1983.

[15] Leonhard W. - *Control of Electrical Drives.* Springer Verlag, Berlin, 1996.

[16] Papiernik W. - *Matching the Components of Modern CNC / Drive Systems.* Proceedings of ' Sharing Tomorrow's Technology ' Conference organised by MTTA and DTI, Warwick-Loughborough, Manchester, 16-18 Nov. 1998.

[17] Papiernik W. - *Structure, Design and Behaviour of Modern CNC Servo Drives.* Proceedings of the Seventh International Seminar on Control Mechanisms, Computer Industry and Electrical Drives, Stuttgart, 26-28 Nov. 1996.

[18] McKeown P. A. - T*he Design of High Precision Machine Systems,* Short Course Notes, Cranfield Unit of Precision Engineering, 15 Oct. 1981.

[19] Forbester I. P. - *Use of Concurrent Engineering in the Optimisation of Machine Tool Design.* Proceedings of International Conference on Laser Metrology and Machine Performance (LAMDAMAP ' 93), Southampton, 1993, pp. 333 - 344.

[20] Donmez A. - *A General Methodology for Machine Tool Accuracy Enhancement - Theory, Application and Implementation.* Ph. D. thesis, Purdue University, USA, 1985.

[21] Postlethwaite S. R. - *Electronic Based Accuracy Enhancement of CNC Machine Tools.* Ph.D. thesis, Huddersfield Polytechnic, U. K., March 1992.

[22] Ford D. G., Postlethwaite S. R., Morton D. - *Error Compensation Applied to High Precision Machinery.* Proceedings of International Conference on Laser Metrology and Machine Performance (LAMDAMAP ' 93), Southampton, 1993, pp. 105 - 112.

[23] Postlethwaite S. R., Ford D. G. - *Geometric Error Analysis Software for CNC Machine Tools.* Proceedings of International Conference on Laser Metrology and Machine Performance (LAMDAMAP ' 97), Huddersfield, 1997, pp. 305 - 316.

[24] Postlethwaite S. R., Ford D. G., Morton D. - *Dynamic Calibration of CNC Machine Tools.* International Journal on Machine Tools and Manufacture. Vol. 37, no. 3, 1997, pp. 287 - 294.

[25] Chen J. S., Yuan J. X., Ni J., Wu S. M. - *Real-Time Compensation of Time-Variant Volumetric Errors on a Machining Centre.* Transactions of the ASME, vol. 155, Nov 1993, pp. 472 - 479.

[26] Hardwick B. R. - *Further Development of Techniques for Software Compensation of Thermally Induced Errors in CNC Machine Tools.* Proceedings of International Conference on Laser Metrology and Machine Performance (LAMDAMAP' 93), Southampton, 1993, pp. 47 - 64.

[27] Allen J. - *A General Approach to CNC Machine Tool Thermal Error Reduction.* Ph.D. thesis, University of Huddersfield, U. K., June 1997.

[28] Postlethwaite S. R., Allen J. P., Ford D. G. - *The Use of Thermal Imaging, Temperature and Distortion Models for Machine Tool Thermal Error Reduction.* Proceedings of Institution of Mechanical Engineers (IMechE), Vol. 212, Part B, 1998, pp. 671 - 679.

[29] Chen J. S., Yuan J. X., Ni J., Wu S. M. - *Compensation of Non-rigid Body Kinematic Effect on a Machining Centre.* Proceedings of the 20th NAMRC, May 1992.

[30] Blake M. D. - *Investigation into Load Effects on Machine Tool Accuracy.* M.Phil thesis, University of Huddersfield, U. K., December 1995.

[31] Ford D. G., Postlethwaite S. R., Allen J. P., Blake M. D. - *Compensation Algorithms for the Real-Time Correction of Time and Spatial Errors in a Vertical Machining Centre.* Proceedings of IMechE, Vol. 214, Part B, Vol. 214, 2000, pp. 221 - 235.

[32] Kirkham E. E. - *Improving Precision in Manufacturing.* IEEE Transactions on Industry Applications, Vol. 25, No. 5, 1989, pp. 800 - 804.

[33] Kakino Y., Ihara Y., Shinohara A. - *Accuracy Inspection of NC Machine Tools by Double Ball Bar Method.* Hanser Publishers, Munich, Germany, 1993.

[34] Smith G. T., Hope A. D., Painter P. R., Blackshaw D. M. S. - *The Assessment of Machining and Turning Centres Using Artifact Based Techniques, Such as the Ball Bar.* Proceedings of LAMDAMAP ' 93, Southampton, 1993, pp. 275 - 286.

[35] Okafor A. C., Ertekin Y. M. - *Machine Tool Accuracy Characterization Using Telescopic Ball Bar.* Proceedings of 11th Annual Meeting of American Society for Precision Engineering (ASPE), Monterey, CA, USA, Nov. 9-14, 1996, pp. 278 - 283

[36] Blackshaw D. M. S., Carr B. - *Positioning Accuracy Optimisation of a Large High Precision Lathe by Linear Error Compensation.* Proceedings of LAMDAMAP ' 93, Southampton, 1993, pp. 141 - 146.

[37] Okafor A. C., Ertekin Y. M. - *Vertical Machining Center Accuracy Characterization Using Laser Interferometer.* Proceedings of 13th Annual Meeting of American Society for Precision Engineering (ASPE), St. Louis, Missouri,USA, Oct. 25-30, 1998, pp. 506 - 511.

[38] Chen J. S., Kou T. W., Chiou S. H. - *Geometric Error Calibration of Multi-Axis Machines Using An Auto-alignment Laser Interferometer.* Journal of the American Society for Precision Engineering, Vol. 23, No. 4, Oct. 1999, pp. 243 - 252.

[39] White A. J. - *Experimental Thermal Error Analysis and Correction Applied to CNC Machine Tools.* Ph.D. thesis, University of Huddersfield, U. K., May 2000.

[40] Ljung L., Soderström T. - *Theory and Practice of Recursive Identification.* MIT Press, 1983.

[41] Bohlin T. - *System Identification: Prospects and Pitfalls.* Springer-Verlag, Berlin, 1991.

[42] Anderson B. D. O. - *Identification of Scalar Errors-in-Variables Models with Dynamics.* Automatica, vol. 21, no. 6, 1985, pp. 709-716.

[43] Brillinger, D. R. - *Time Series Data Analysis and Theory.* New York: Holt, Reinhart and Winston, 1975, pp. 88-115.

[44] Ljung, L. - *System Identification: Theory for User.* Englewood Cliffs, NJ: Prentice- Hall, 1987.

[45] Ljung, L. - *Some Results on Identifying Linear Systems Using Frequency Domain Data.* Proc. of 32nd Conf. On Decisional Control, San Antonio, TX, Dec. 1993, pp. 3534-3538.

[46] Feng, C., Zheng, W. - *On-line Modified Least-Squares Parameter Estimation of Linear Systems with Input-Output Data Polluted by Measurement Noises.* Proc. 1988 IFAC Symp. Identif. and System Param. Estimat., Beijing, China, vol. 3, 1988, pp. 1189-1194.

[47] Guillame, P. G., Pintelon, R. P., Schoukens, J. - *Robust Parametric Transfer Function Estimation Using Complex Logarithmic Frequency Response Data.* IEEE Trans. Autom. Contr., vol. 40, no. 7, July 1995, pp. 1180-1191.

[48] Pintelon R., Guillaume P., Rolain Y., Schoukens J., Van Hamme H. - *Parametric Identification of Transfer Functions in the Frequency Domain - A Survey.* IEEE Trans. Autom. Contr., vol. 39, Nov. 1994, pp. 2245 -2259.

[49] Levi E. C. - *Complex-Curve Fitting.* IEEE Trans. Autom. Contr., vol. AC - 4, Nov. 1959, pp. 37 - 44.

[50] Sanathanan C. K., Koerner J. - *Transfer Function Synthesis as a Ratio of Two Complex Polynomials.* IEEE Trans. Autom. Contr., vol. AC - 9, No. 1, 1963, pp. 56 - 58.

[51] Golub G. H., Van Loan C. F. - *An Analysis of the Total Least Squares Problem.* SIAM Journal Numerical Analysis, Vol. 17, No. 6, 1980, pp. 883 - 893.

[52] Van den Bos A. - *Estimation of Parameters of Linear Systems Using Multiharmonic Test Signals.* Identification of Continuous-Time Systems. Sinha and Rao, Eds. Dordrecht, The Netherland :Kluwer Academic, 1992.

[53] Balmer L. - *On-Line Parametric Identification in the Frequency Domain.* Proc. of the 10th Internat. Conf. On System Engineering, Coventry, Sept. 1994, pp. 80 - 86.

[54] Zhang Y. M. - *Identification of a Multivariable Interval Dynamic Model from Measurements in the Frequency Domain.* Proc. of IMechE, Vol. 212, Part C, 1998, pp. 595 - 603.

[55] Coca D. - *Class of Wavelet Multiresolution Decompositions for Non-linear System Identification and Signal Processing.* Ph.D. thesis, University of Sheffield, U. K., December 1996.

[56] Square D. B. – *Parameter Identification of Non-linear Continuous-Time Systems Using the Hartley Modulating Functions Method.* Ph.D. thesis, Ruhr-University Bochum, Germany, June 1999.

[57] Pavelic V., Cleek A. L. - *Frequency Response and Modal Analysis of a Machine Tool Structure for a Numerically Controlled Machining Center.* Proc. of 6th World Congress On Theory of Machines and Mechanisms, Vol 1, Ch. 333, San Antonio, TX, 1984, pp. 520 - 527.

[58] Gustaveson D. K. - *Direct Parameter Identification for Frequency-Response Measurements.* Proc. of the 5th Internat. Modal Analysis Conf., Imperial Coll. Science& Technology, London, Apr. 1987, vol. 1, Ch. 253, 1987, pp. 1352 - 1356.

[59] Banks H. T., Wang Y. - *Parameter Identification in the Frequency-Domain.* Proc. of the 3rd Bozeman Conf. On Computation and Control, Montana State Univ., Massachussets, 5-11 Aug. 1992, Computation and Control, Vol. 15, Ch. 30, pp. 49 - 62.

[60] Okabe M., Shimizu S., Fukuda R. - *Parameter Identification of Nonlinear Characteristics of Machine-Tool Elements with the Impulsive Response Method.* Proc. of the 7th Internat. Conf. on Production, Chiba, Japan, 15-17 Sept. 1994, Ch. 123, No. 1, pp. 227-232.

[61] Kim S. J., Ha I. J., Kang J. H., Kim C. H., Lim S. G. - *A New Parameter Identification Method for Mechanical Systems with Friction.* Proc. of the 23rd Internat. Conf. On Industrial Electronics, Control and Instrumentation, vol. 1, 1997, Ch. 270, pp. 322 - 327.

[62] Meskell C., Fitzpatrick J. A. - *Parameter Identification In a System with Both Linear and Coulomb Damping.* Proc. of the 3rd Internat. Conf. On Modern Practice in Stress and Vibration Analysis, Ireland, 305 Sept. 1997, Ch. 78, pp. 51 - 56.

[63] Tsuei Y. G., Huang B. K. - *Effect of Modeling for Damping on Parameter Identification.* Proc. of the 16th Internat. Modal Analysis Conf., Santa Barbara, 2-5 Feb. 1998, Vol. 3243, Ch. 262, pp. 1427 - 1432.

[64] Blaszkowski M., SzafarczykM., Al-Taleb M. - *A New Technique for Identification of Servodrives of Machine Tools and Robots.* Journal of Materials Processing Technology, 1998, Vol. 76, no. 1-3, pp. 36-41.

[65] Best M. C., Gordon T. J. - *A Randomized Integral Error Criterion for Parametric Identification of Dynamic Models of Mechanical Systems.* Proc. of IMechE, Vol. 213, Part I, 1999, pp. 119 - 134.

[66] Verboven P., Guillame P., Van Overmeire M. - *Improved Modal Parameter Identification by Non-Parametric Modeling of the Measurement Noise.* Proc. of the 17th

Internat. Modal Analysis Conf., Kissimmee, FL, 8-11 Feb 1999, vol. 3727, Ch. 313, pp. 1984-1990.

[67] *Shape Recognition Techniques Applied to Non-linear Control Systems.* EPSRC Grant: GR/J49679 completed December 1996.

[68] Henderson M., Ingleby M., Ford D.G. - *Robust System Identification Using the Hough Transform.* Proceedings of IMechE, vol. 211, part I, 1997, pp. 135 - 144.

[69] Morton D., Brook D. - *On Load Frequency Response Testing of Electrical Machines.* Proc. of Internat. Conference on Drives, Motors and Controls, Harrogate, 1984, pp. 55 - 60.

[70] Araki K., Liu X., Ohnishi T. - *Frequency-Characteristics Analysis of a Pneumatic Servo System Using M-Sequence and Sinusoidal Input Signals.* Fluid Power Series, 1994, Vol. 6, Ch. 20, pp. 211 - 221.

[71] Smith K. J., Pratt R. W. - *Obtaining Open-Loop Frequency Response Data from a Multi-Input, Mutli-Output Closed-Loop System for Use in Multivariable Controller Design.* Proc. of the 10th Internat. Conf. On System Engineering, Coventry, Sept. 1994, pp. 1159 - 1166.

[72] Jennewein D., Fritzen C. P. - *Optimized and Improved Input Signals for Parameter Identification.* Proc. of the 13th Internat. Modal Analysis Conf., Nashville, Tennessee, 13-16 Feb 1995, Vol. 2460, Ch. 271, pp. 1832 - 1838.

[73] Rivera D. E. - *Introduction to System Identification.* Course notes. Arizona State University, 1998.

[74] Olivetti Corporation - *Introduction to the NC / MT.* Internal report, 28 August 1982.

[75] GEC Ind. Controls - *Gemdrive- Axis Mk 2.* Seminar 15 September 1983

[76] Electro-Craft Corporation - DC Motors, Speed Controls, Servo Systems, Chapter 2, *DC Motors and Generators*, Robbins & Myers / Electro-Craft, pp. 2-16 - 2-21, 1987.

[77] Palmgren H. - *The V-Belt Handbook.* Chartwell - Bratt, 1985

[78] Pislaru C., Ford D. G., Freeman J. M. - *Dynamic Simulation of CNC Machine Tool Axis Drives.* Proc. of Internat. Conf. On Power Conversion and Intelligent Motion PCIM ' 99, Intelligent Motion Section, Nuremberg, Germany, June 22 -24, 1999, pp. 259 - 264 .

[79] Eschmannn, P., Hasbargen, L., Weigand, K. - Ball and Roller Bearings. Theory, Design and Application, Chapter 4, *Friction, Temperature and Lubrication*, John Wiley and Sons, pp. 201 - 247, 1985.

[80] THK LM System - *Ball Screws.* Catalog No 200-2BE, THK Co., Ltd, Tokyo, 1999.

[81] Braasch J., Eberherr A. - *Position Measurement on Machine Tools: by Linear Encoder or Ballscrew and Rotary Encoder?* Proceedings ASPE, Vol. 18, 1998, pp. 437 - 444.

[82] Volland, G. - *Control Systems Modelling and Analysis*, Prentice-Hall, 1986.

[83] Leonhard, W. - *Control of Electric Drives*, Springer-Verlag, 1990.

[84] Fu, K., Gonzalez, R. S., Lee, C. S. G. - *Robotics, Sensing, Vision and Intelligence.* McGraw-Hill International Ltd., 1988.

[85] Pislaru C., Ford D. G., Freeman J. M. - *A New Approach to the Modelling and Simulation of a CNC Machine Tool Axis Drive.* Proc. of Internat. Conf. on Laser Metrology and Machine Tool, CMM and Robot Performance (LAMDAMAP'99), Newcastle upon Tyne, July 13 - 15, 1999, vol. 1, pp. 335 - 343.

[86] D. J. Birchall Ltd - *Vibration & Dynamic Pressure Measuring Instruments - Product Guide*, 2000, pp. 12.

[87] Harris C. M., Crede C. E. - *Shock and Vibration Handbook.* New York , McGraw-Hill, 1976.

[88] Freeman J. M. - *General Data Logging Hardware and Software - User Guide.* Internal Report, University of Huddersfield, February 2001.

[89] Bentley J. P. - *Principles of Measurement Systems.* Longman Scientific & Technical, Harlow, U. K., 1989, pp. 4.

[90] Martin S. J. - *Numerical Control of Machine Tools.* Hodder and Stoughton., 1979.

[91] Smith S. W. - *The Scientist and Engineer's Guide to Digital Signal Processing.* California Technical Publishing, 1997.

[92] *MATLAB - System Identification Toolbox for Use with MATLAB.* The MathWorks, Inc., 1998.

[93] *SIMULINK.- Dynamic System Simulation for MATLAB. Using SIMULINK version 2.* The MathWorks, Inc., MA, 1997.

[94] *Control System Toolbox – For Use with MATLAB. User's Guide version 4.* The MathWorks, Inc., MA, 1998.

[95] Simon W. - *The Numerical Control of Machine Tools.* Edward Arnold Ltd., 1973.

[96] Haykin S. – *Signal Processing: Where Physics and Mathematics Meet.* IEEE Signal Processing Magazine, July 2001, pp. 6-7.

[97] Awtar S., Craig K. C. – *Magnetic Coupling between DC Tachometer and Motor and Its Effects on Motion Control.* The 7th Mechatronics Forum Internat. Conf., Sept. 6-8, 2000, Georgia Institute of Technology, Atlanta, USA, pp. 53 – 59.

[98] McLean D. – *Mathematical Models of Electrical Machines. Measurement and Control*, vol. 11, 1978, pp. 231-236.

[99] Gatzwiller K. B. – *Introduction to Modal Analysis and Operating Deflection Shape*. B & K Course Notes BA 7069-12, Naerum, Denmark, January 1990.

[100] Ewins D. J. - *Modal Testing of Rotating Machinery Structures*. Tutorial at the 5th Internat. Conf. on Rotor Dynamics, Darmstadt, 1998.

[101] Potter R., Richardson M. – *Mass, Stiffness and Damping Matrices from Measured Modal Parameters*. Proc. of the Internat. Instrumentation-Automation Conf. ISA 74, New York, NY, October 1974, pp. 251-255.

[102] Shye K., Richardson M. – *Mass, Stiffness and Damping Matrix Estimates from Structural Measurements*. Proc. of the 5th Internat. Modal Analysis Conf. (IMAC 87), Imperial College, London, April 6-8, 1987, pp. 305-312.

[103] Beards C. F. - *Vibrations and Control Systems*. Ellis Horwood, London. ,1988.

[104] Ewins D. J. - *Basics and State-of-the-art of Modal Testing*. Sadhana, vol. 25, part 3, June 2000, pp. 207-220.

[105] De Silva C. W. – *Vibration- Fundamentals and Practice*. CRC Press, London, 2000.

[106] Mallat S. – *A Wavelet Tour of Signal Processing*. Academic Press, San Diego, 1998.

[107] Strang G., Nguyen T. – *Wavelet and Filter Banks*. Wellesley-Cambridge Press, 1996.

[108] Aldroubi A., Unser M. – *Wavelets in Medicine and Biology*. CRC Press Inc., Florida, 1996.

[109] Luo G. Y., Osypiw D., Irle M. – *Vibration Modelling and Identification Using Fourier Transform, Wavelet Analysis and Least-Square Algorithm*. Proc. of 2nd Internat. Symposium on Multi-Body Dynamics: Monitoring & Simulation Techniques. Bradford Univ., June 27-28, 2000, pp. 153- 167.

[110] Ruzzene M., Fasana A., Garibaldi L., Piombo B. – *Natural Frequencies and Dampings Identification Using Wavelet Transform: Application to Real Data*. Mechanical Systems and Signal Processing, vol. 11, part 2, 1997, pp. 207-218.

[111] Agneni A., Crema L. B. – *Analytic Signals in the Damping Coefficient Estimation*. Proc. of Internat. Conf. on Spacecraft and Mechanical Testing, Noordwijk, The Netherlands, 1988, pp. 133-139.

[112] Spina D. – *Analisi delle Oscillazioni Libere di Sistemi Non Lineari per l'identificazione dei Parametri Meccanici*. Ph.D. thesis, Universita degli Studi La Sapienza, Roma, Italy, 1989.

[113] Staszewski W. J. – *Identification of Damping in MDOF Systems Using Time-Scale Decomposition.* Journal of Sound and Vibration, vol. 203, part 2, 1997, pp. 283 -305.

[114] Staszewski W. J. – *Analysis of Non-linear Systems Using Wavelets.* Proceedings of IMechE, Vol. 214, Part C, 2000, pp. 1339 - 1353.

[115] Daubechies I. – *Ten Lectures on Wavelets.* Society for Industrial and Applied Mathematics (SIAM) Philadelphia, Pennsylvania, 1992.

[116] Meyer Y. – *Wavelets. Algorithms and Applications.* SIAM, Philadelphia, Pennsylvania, 1993.

[117] Chui Ch. K. – *An Introduction to Wavelets. Wavelet Analysis and Its Applications.* Academic Press, Boston, vol. 1, 1992.

[118] Newland D. E. – *Random Vibration, Spectral and Wavelet Analysis.* Longman, Harlow and John Wiley, New York, 1993.

[119] Wojtaszczyk P. – *A Mathematical Introduction to Wavelets.* Cambridge University Press, Cambridge, UK, 1995.

[120] Burke Hubbard B. – *The World According to Wavelets.* A. K. Peters, Wellesley, Massachusetts, *1996.*

[121] Grossman A., Morlet J. - *Decomposition of Hardy Functions into Square Integrable Wavelets of Constant Shape.* SIAM J. Math, Anal., Vol 15, No 4, 1984, pp 723 –736.

[122] Farge M. – *Wavelet Transform and Their Applications to Turbulence.* Annaul Rev. Fluid Mech., vol. 24, 1., 1992, pp. 395 – 457.

[123] Rioul O., Duhamel P. – *Fast Algorithms for Discrete and Continuous Wavelet Transforms.* IEEE Trans. on Information Theory, vol. 38, part 2, pp. 569 – 586.

[124] Flandrin P. – *Time-Frequency / Time-Scale Analysis.* Academic Press, USA, 1999.

[125] Landee R. W., Davis D. C., Albrecht A. P. – *Electronic Designer's Handbook.* McGraw Hill, London, 1957.

[126] Blackman R.B., Tukey J. W. - *The Measurement of Power Spectra.* Dover Publications, New York, NY, 1958.

[127] Ramirez R. W. - *The FFT; Fundamentals and Concepts.* Prentice-Hall, Englewood Cliffs, NJ, 1985.

[128] Raven F. H. – *Automatic Control Engineering.* McGraw-Hill, London, 1987.

[129] Steidel R. F. – *An Introduction to Mechanical Vibrations.* John Wiley & Sons Inc., 1971.

[130] Markhauser A. W. – *Preloading Ball-screws.* Machine Design, March 1967, Penton Publication, pp. 207 –211.

[131] Hildenbrandt H. – *Ball-screw Technology.* Engineering, July 1981.

[132] Contraves – *Leadscrew – Speed Reducer System Application Worksheet.* Contraves Control Systems Research Division, Powertron.

[133] Lorvick R. R. – *Gears and Gear Drives Section 4,* Machine Design, June 1971, Penton Publication, pp. 156-165.

[134] Torrington – *Fafnir Super Precision Ball Screw Bearings and Units.* Catalog No BSB 986, Fafnir Bearings, Wolverhampton, U.K., 1986.

[135] SKF – *SKF Precision Bearings.* Catalog No 4411 E, SKF, Sweden, 1997.

[136] Fenner – *Fenner Power Transmission Products.* Catalog No FEN 5643, Fenner Power Transmission, Blackburn, U.K., 1999.

[137] Coulson C. A. - *Waves- A Mathematical Account of the Common Type of the Wave Motion.* Olive and Boyd Ltd., Edinburgh, 1955

[138] Holroyd G., Pislaru C., Ford D. G. – *Identification of Damping Elements in a CNC Machine Tool Drive.* Proc. of Internat. Conf. LAMDAMAP 2001, Birmingham, July 17 - 20, 2001, pp. 289 - 299.

[139] Holroyd G. – *Identification of Damping Elements in a CNC Machine Tool Drive.* MSc Dissertation, University of Huddersfield, September 2000.

[140] Pislaru C., Ford D. G., Freeman J. M.- *A New 3D Model for Evaluating the Performance of CNC Machine Tool Axis Drives.* Proc. of the First Internat. Conf. of the European Society for Precision Engineering and Nanotechnology (EUSPEN'99), Bremen, Germany, May 31 - June 4, 1999, vol. I, pp. 72 - 75

[141] Quayle J. P. – *Kempe' s Engineers' Year Book.* Morgan Grampian, 1984.

[142] James M. L., Smith G. M., Wolford J. C., Whaley P. W. – *Vibration of Mechanical and Structural Systems with Microcomputer Applications.* Harper & Row, 1989.

[143] Newland D. E. – *Mechanical Vibration Analysis and Computation.* Longman Scientific and Technical, 1989.

[144] Holroyd G. – *Undamped and Damped Natural Frequencies of CNC Machine Tool Drives.* Internal Report, University of Huddersfield, May 2001.

[145] Gourlay A. R., Watson G. A. - *Computational methods for matrix eigenproblems,* John Wiley, 1973.

[146] Wilkinson M. A. - *The algebraic eigenvalue problem,* Clarendon, 1965.

APPENDIX A

A1. Data for CNC Machine Tool BEAVER VC35 sited at the University of Huddersfield

The vertical machining centre BEAVER VC35 is of *bed type construction* with a sliding saddle assembly that fully supports the machine table all times. The sliding member is faced with turcite for low friction high response and long life.

Axis / Characteristic	X	Y	Z
Spatial position	Horizontal	Horizontal	Vertical Pneumatic counterbalance
Maximum travel [mm]	750	400	450
Fast traverse rate [m / min]	10	10	10

Table A1. Characteristics of Beaver VC35 CNC machine tool

Automatic lubrication is provided for all axis slideways and ball-screws; a warning light indicates low tube or oil supply failure.

The *CONTRAVES Spindle Unit,* type ADB/F are basic units equipped with a field controller and used together with the appropriate spindle motor, at constant armature current over specific speed range.

The *SIEMENS electrical drives* contain permanent magnet-excited servomotors 1HU3 074 - OAC01 with toothed belt reduction 2 : 1 to ball-screws with 10 mm pitch.

Beaver VC35 is equipped with a *FANUC 6MB control* which enables simultaneous 3 axis movement at speeds up to 10m/min. Feedback is provided by rotary encoders mounted on the motor end of each DC servo drive. Hardware and software faults are reported back to the user via the diagnostic user interface.

5000 pulses / rev = 10 mm pitch controller sampling time = 10 ms

Other particulars of CNC machine tool Beaver VC35:

Capacity		Spindle	
Table size	930 mm x 490 mm	Spindle motor - cont. rating	10. 97 hp (8.18 kW)
Table area	800 mm x 400 mm	Frequency	1140 r.p.m.
T-slots	3 x 18 mm x 125 mm	Power at 416 r.p.m.	4 hp (2.98 kW)
Max. table weight capacity	300 kg	Spindle speeds	63 - 5600 r.p.m.
Approx. machine weight	5272 kg	Max. total weight (18 tools)	125 kg

A2. The MATLAB source code used to determine the optimised coefficients for the PI compensator which is equivalent with initial transfer function $H_{preampl}$

Objective function

```
function y=obj2(x,a)
n=x(1)*[x(1) x(2)];
d=[x(1) 0];
[m,p]=bode(n,d,a);
y=[m p];
```

The actual routine is **lsqcurvefit** (solve non-linear curve-fitting problems in the least-square sense) which is calling the objective function *obj2*:

```
nump=[0.0052 1];
denp=[0.0015 10.25 1];
w=logspace(-1,3,500);
[magp,phsp]=bode(nump,denp,w);
preamp=tf(nump,denp)
num=[0.0052 1];
den=[10 0];
picomp=tf(num,den)
grid;
bode(preamp,'b',picomp,'r',w);
pause;

options=optimset('Display','iter','MaxFun',1e6,'MaxIter',1e6,'TolX',1e-
6,'TolFun',1e-6);
[x,resnorm]=lsqcurvefit('obj2',[num(1) num(2)],w,[magp phsp],[0
0],[],options);
pause;

num=x(1)*[x(1) x(2)];
den=[x(1) 0];
picomp=tf(num,den);
bode(preamp,'b',picomp,'r',w);
grid
sprintf('The value of Kp=%0.2g and the value of Ki=%0.2g',x(1),x(2))
```

The following values are shown on the MATLAB Command Window after 25 iterations:

Norm of First-order

Iteration	Func-count	f(x)	step	optimality	CG-iterations
1	4	71358.7	1	7.7e+003	0
2	7	69758.8	0.194344	900	1
3	10	68627.6	0.425451	364	1
4	13	68366.1	0.292385	98	1
5	16	68311	0.192287	389	1
6	19	68301.6	0.112595	620	1
7	22	68300.7	0.048379	496	1
8	25	68300.7	0.0094157	142	1

Optimization terminated successfully:

The value of Kp = 0. 00039 and the value of Ki = 0. 082

A3. Data for permanent magnet motor Siemens 1HU3 074 - OAC01

Rated torque	$m_{0M} = 7$ Nm
Weight	$W_m = 40$ kg
Rated current at m_{0M}	$I_{0M} = 9.7$ A
Armature voltage	$U = 167$ V

Speed	$n_M = 2000$ rot / min
Moment of inertia	$J_m = 0.0048$ kg m^2
Mechanical time constant	$T_{mech\,M} = 7.1$ ms
Electrical time constant	$T_e = 7.6$ ms
Thermal time constant	$T_{th} = 90$ min
Torque constant	$K_T = 0.735$ Nm / A
Voltage constant	$K_E = 77$ V / 1000 min^{-1} = 0.735 V / (rad/sec)
Armature resistance with brushes at 20 ° C	$R = 0.804\ \Omega$
Armature inductivity	$L_a = 6.1$ mH

Table A2. Technical data for DC permanent magnet motor [14]

The DC servomotors from series 1HU produced by Siemens have the behaviour of a shunt motor due to permanent magnet-excitation. The magnet material used is highly coercive ferrite material which is suitable for armature voltage control down to the lowest speeds.

A4. Data for mechanical transmission elements

Toothed belt transmission

Element / Axis	X-axis	Y-axis
Driving pulley	Uniroyal 28 - 8M - 30F $D_{exterior} = 71.3$ mm Width = 25 mm	Uniroyal 28 - 8M - 30F $D_{exterior} = 71.3$ mm Width = 25 mm
Belt	Uniroyal 880 - 8M - 30 Length = 880 mm Width = 30 mm	Uniroyal 720 - 8M - 30 Length = 720 mm Width = 30 mm
Driven pulley	Uniroyal 56 - 8M - 50F $D_{exterior} = 142.6$ mm Width = 56 mm	Uniroyal 56 - 8M - 30F $D_{exterior} = 142.6$ mm Width = 30 mm

Table A3. Components of the belt drive

Calculations for X-axis

Specific steel density V steel = 7.68×10^{-5} N / mm 3

$\rho = V\ steel / 9.81 = (7.68 \times 10^{-5}) / 9.81 = 0.7869 \times 10^{-5}$ kg /mm^3 = 7860 kg /m^3 (A1)

Motor shaft

Diameter = 17 mm Material = steel Length = 120 mm

$$J_{shaft} = \frac{m \times r^2}{2} = \frac{\pi}{32} \times D^4 \times L \times \rho = \frac{3.14}{32} \times (0.017)^4 \times 0.120 \times 7860 = 7.5 \times 10^{-6}\ \text{kg m}^2 \quad \text{(A2)}$$

Driving pulley Uniroyal 28 - 8M - 30 F

Diameter (exterior) = 71.3 mm Diameter (interior) = 0 mm Thickness = 25 mm

$$J_{pl} = \frac{\pi}{32} \times D^4 \times L \times \rho = \frac{3.14}{32} \times (0.0713)^4 \times 0.025 \times 7860 = 4.9 \times 10^{-4} \text{ kg m}^2 \quad \text{(A3)}$$

Ball-screw (driven) pulley (considered as a hollow cylinder) Uniroyal 56 - 8M - 30 F

Diameter (exterior) = 142. 6 mm Material = steel Thickness = 56 mm

Diameter (interior) = ball-screw diameter = 38. 1 mm

$$J_{p2} = \frac{\pi}{32} \times (D^4 - d^4) \times L \times \rho = \frac{3.14}{32} \times [(142.6)^4 - (38.1)^4] \times 59 \times 0.7860 \times 10^{-5} = 17.78 \times 10^{-3} \text{ kg m}^2 \quad \text{(A4)}$$

Ball-screw inertia

Diameter = 38. 1 mm Material = steel Length = 1675 mm

$$J_{BS} = \frac{\pi}{32} \times D^4 \times l \times \rho = \frac{3.14}{32} \times (0.0381)^4 \times 1.675 \times 7860 = 2.725 \times 10^{-3} \text{ kg m}^2 \quad \text{(A5)}$$

Working table (the dimensions are shown in Figure A3. 1.)

material = Cast iron

$\rho_{\text{cast iron}} = V_{\text{cast iron}} / 9.81 = (7.769 \times 10^{-5}) / 9.81 = 7920 \text{ kg / m}^3$

L = 883 mm l = 495 mm h = 29. 5 mm

$M_1 = 7920 * 0.883 * 0.495 * 0.0295 = 10.31 \text{ kg} = 102.12 \text{ kg}$

Strips (up) L = 883 mm l = 495 mm h = 32 mm

$V_{tot} = 0.883 * 0.495 * 0.032 = 0.013986 \text{ m}^3$ (A6)

$V_{air} = 3 [(0.032 * 0.015 + 0.018 * 0.017) * 0.803] + 2 (0.04 * 0.3855 * 0.032) = 0.0024 \text{ m}^3$ (A7)

$V = V_{tot} - V_{air} = 0.013986 - 0.004712 = 0.011586 \text{ m}^3$ (A8)

$M = \rho_{\text{cast iron}} * V = 7920 * 0.011586 = 91.76 \text{ kg} \approx 92 \text{ kg}$ (A9)

Strips (down) L = 546 mm l = 406 mm h = 76. 2 mm

$V_{tot} = 0.546 * 0.406 * 0.0762 = 0.01689 \text{ m}^3$ (A10)

$V_{air} = 2 [0.075 * 0.03 * 0.546] = 0.002457 \text{ m}^3$ (A11)

$V = V_{tot} - V_{air} = 0.01689 - 0.002457 = 0.014433 \text{ m}^3$ (A12)

$m = \rho_{\text{steel}} * V = 7920 * 0.014433 = 114 \text{ kg}$ $m_{\text{guards}} = 44 \text{ kg}$

Total working table mass $m_{\text{work table}} = 102 + 92 + 114 + 44 = 352 \text{ kg}$ (A13)

Total moving mass (moving nut)

$m_{tot\,x} = 352 + 7 = 359 \text{ kg}$ (A14)

Inertia of the load referred to the ball-screw

$$J_L = m_{tot} \frac{p^2}{(2\times\pi)^2} = 359 \frac{100}{4\times(3.14)^2} = 9.1 * 10^{-4} \text{ kg m}^2 \quad \text{(A15)}$$

Total inertia at the motor

$$J = J_m + J_{shaft} + J_{pl} + \frac{J_{p2} + J_{bs} + J_L}{R^2} = \quad \text{(A16)}$$

$$= 0.0048 + 0.0000075 + 0.000498 + \frac{0.0178 + 0.0027 + 0.00091}{4} = 0.0072 \text{ kg m}^2$$

Scaling term for armature current loop feedback

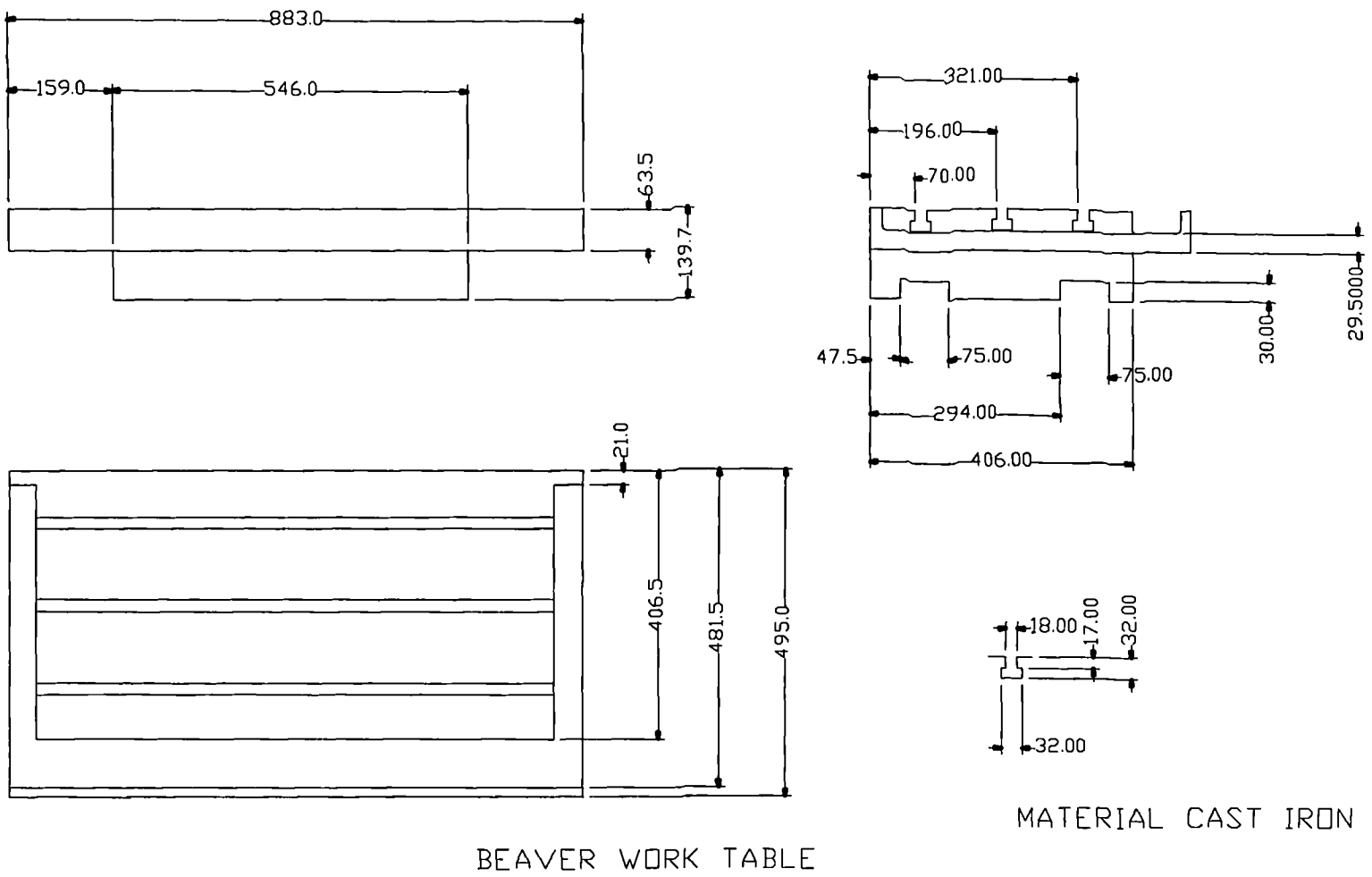

Figure A3. 1. Worktable dimensions for CNC machine tool Beaver VC35

$$G_3 \times G_4 = 4.4 \times 0.095 = 0.418 \quad \text{(A17)}$$

Friction force (moving nut) $F_f = \mu * W = 0.1 * 9.8 * 359 = 352$ N (A18)

W_{tot} - total moving weight [N] μ - coefficient of friction for slideway material

Maximum acceleration force

$F_{acc} = (W * G_a * V_1) / 60 * 10^3 = (359 * 9.8 * 33 * 10000) / 60000 = 19350$ N (A19)

$G_a = 33$ mm / s / mm (control system gain) (A20)

$V_1 = 10000$ mm / min (fast traverse rate) Data source: Ford [12]

Total slide force (acceleration + friction) $F1 = F_{acc} + F_f = 19350 + 352 = 19702$ N (A21)

Contingency factor for screw force (preload force for screw)

$F5 = 0.35 * F1 = 0.35 * 19702 = 6896$ N (friction + acceleration) (A22)

Data source: Markhauser [130] Hildenbrandt [131]

Running torque at the screw

$$\tau_{bp} = T_{screw} = \frac{(F1 + F5) * p}{2\pi * E1} = \frac{(19702 + 6896) * 0.01}{6.28 * 0.9} = 47.06 \text{ Nm} \quad \text{(A23)}$$

where p - ball-screw pitch $p = 0.01$ m

E1 - efficiency factor for ball-screw E1 = 0.9 (precision ball-screw)

Data source: Contraves [132]

Running torque at the motor $$\tau_L = T_{motor} = \frac{T_{screw}}{R * E2} = \frac{47.06}{2 * 0.95} = 24.76 \text{ Nm} \quad \text{(A24)}$$

where R - overall reduction ration R = 2

E2 - drive efficiency E2 = 0.95 (toothed belt and pulley)

Data source: Contraves [132] Lorvick [133]

The difference between tight and loose belt tensions:

$$T_x = \frac{\tau_L J_{p2} r_{p1} + J_{p1} r_{p2} \tau_{bp}}{2(r_{p1}^2 J_{p2} + r_{p2}^2 J_{p1})} = \frac{24.76 * 0.00049 * 0.035 + 0.00049 * 0.07 * 47}{2 * (0.035^2 * 0.0043 + 0.07^2 * 0.00049)} = 351.27 \text{ N} \quad \text{(A25)}$$

Calculated data for Y – axis		***Calculated data for Y - axis***
DC motor moment of inertia	$J_m = 0.0048$ kg m²	$J_m = 0.0048$ kg m²
Armature current feedback scaling	$G_3 \times G_4 = 0.7125$ V / A	$G_3 \times G_4 = 0.95$ V / A
Motor shaft inertia	$J_{shaft} = 0.0000075$ kg m²	$J_{shaft} = 0.0000075$ kg m²
Driving pulley inertia	$J_{p1} = 0.0004986$ kg m²	$J_{p1} = 0.0004986$ kg m²
Driven pulley inertia	$J_{p2} = 0.009524$ kg m²	$J_{p2} = 0.009524$ kg m²
Ball-screw inertia	$J_{bs} = 0.002724$ kg m²	$J_{bs} = 0.002017$ kg m²
Load moving mass	$m_L = 677$ kg	$m_L = 281$ kg
Load inertia referred to the ball-screw	$J_L = 0.0017$ kg m²	$J_L = 0.00712$ kg m²
Total load inertia referred to the motor	$J = 0.0069$ kg m²	$J = 0.0084$ kg m²
Friction force	$F_f = 663.5$ N	$F_f = 275$ N
Acceleration force	$F_{acc} = 36490$ N	$F_{acc} = 14822$ N
Total slide force	$F1 = 37154$ N	$F1 = 15097$ N
Preload force for screw	$F5 = 13004$ N	$F5 = 5284$ N

Running torque at screw	τ_{bp} = 88. 74 Nm	τ_{bp} = 36 Nm
Running torque at motor	τ_L = 46. 7 Nm	τ_L = 19 Nm
Difference between tight and loose belt tensions	T_x = 673 Nm	T_x = 538 Nm

Ball-screw (identical data for X-axis and Y-axis)		***Z-axis***
Diameter	38. 1 mm	38. 1 mm
Root diameter	35. 28 mm	35. 28 mm
Length	1675 mm	1270 .mm
Distance between bearings	1520 mm	1115 .mm
Screw	10 mm pitch, single start	10 mm pitch
Mass of ball-screw	15 kg	11 kg
Mass of nut	7 kg	7 kg
Efficiency coefficient	0. 95	0. 95
Critical speed	2306 rpm	3465 rpm
Buckling strength	67 kN	100. 7 kN
Maximum speed	1837 rpm	1837 rpm

Bearings

Bearing Nadella ARNBT 30 - 105 (equivalent with MM 30 BS 62 Q M) - set of 4 taper roller bearings - 'fixed' end (attached to the structure of the machine)

Bearing SKF 6206 - 2RS - single row deep groove ball bearing - ' free' end (attached to driven pulley)

Bearing type	Axial stiffness N / μm	Length mm	Bore diameter mm	Outside diameter mm
Nadella ARNBT 30 - 105	800	52	30	62
SKF 6206 - 2RS	1560	16	30	62

Table A4. Technical data for bearings [134], [135]

Taper roller bearings have higher stiffness than ball bearings because of the contact conditions between rolling elements and raceways. The greater the contact angle, the greater the stiffness of the bearing in axial direction. Applying a preload force axially or radially depending on the type of bearing can further enhance bearing stiffness. Deep groove ball bearings, thrust ball bearings and taper roller bearings are generally preloaded axially.

Calculations for X - axis

- *Fixed end*

$T_{0\,fixed} = f_0 * 10^{-7} * (\nu * n)^{2/3} * T^3$ friction torque – load free (A26)

f_0 - coefficient increasing with the rolling element size (bearing cross-section)

$f_0 = 2$ oil mist / grease lubrication (A27)

ν - operational viscosity of oil / grease base oil $[mm^2 / s]$ $\nu = 0.2$

n – speed of bearing $=(60 / 2*pi) * \omega$ $[min^{-1}]$ $n = 9.55 * \omega$

$$T = \frac{d+D}{2} = \frac{30+62}{2} = 46\,mm$$ pitch circle diameter (A28)

$d = 30$ mm – bearing bore diameter $D = 62$ mm – bearing outside diameter

$T_{1\,fixed} = (\mu_1 * f_1 * F_{fixed} * T) / 2$ friction torque – load dependent

μ_1 - friction coefficient dependent on load and bearing design

$\mu_1 = 0.001$ tapered roller bearings, single-row

f_1 - coefficient taking into account direction of load application

$f_1 = 1$ for $F_a / F_r = 0.5 / Y$ (purely radial)

- the force due to ball screw weight $$F_w = \frac{m_{bs}\, g}{2} = \frac{15 \times 9.8}{2} = 73.5\,N$$ (A29)

- axial force acting upon 'fixed' end of the ball-screw $$F_a = \frac{F_{free}}{3} = \frac{706.4}{3} = 235.5\,N$$ (A30)

F_{fixed} – resulting bearing load acting upon the "free" end of the ball-screw model:

$$F_{fixed} = \sqrt{F_a^2 + F_w^2} = \sqrt{(73.5)^2 + (235.5)^2} = 246.7\ N$$ (A31)

$T_{0\,fixed} = f_0 * 10^{-7} * (\nu * n)^{2/3} * T^3 = 2 * 10^{-7} * 0.2 * (9.55 * \omega)^{2/3} * (46)^3$ [Nmm] =

$= 0.01724 * (\omega^{2/3})$ Nmm $= 0.01724 * 10^{-3} * (\omega^{2/3})$ Nm (A32)

$T_{1\,fixed} = (\mu_1 * f_1 * F_{fixed} * T) / 2 = (0.001 * 1 * 246.7 * 0.046) / 2 = 5.7 * 10^{-3}$ Nm (A33)

- *Free end*

$T_{0\,support} = f_0 * 10^{-7} * (\nu * n)^{2/3} * T^3 = 2 * 10^{-7} * 0.2 * (9.55 * \omega)^{2/3} * (46)^3$ [Nmm] =

$= 1.724 * 10^{-5} * (\omega^{2/3})$ Nm (A34)

F_{free} – resulting bearing load acting upon bearing from the "free" end of the ball-screw model:

$$F_{free} = \sqrt{F_w^2 + 4T_x^2} = \sqrt{(73)^2 + 4*(351.27)^2} = 706.4\ N$$ (A35)

$T_{1\,support} = (\mu_1 * f_1 * F * T) / 2 = (0.001 * 1 * 706.5 * 0.046) / 2 = 16.25 * 10^{-3}$ Nm (A36)

Calculations for Y - axis

- *Fixed end*

$T_{0\,fixed} = f_0 * 10^{-7} * (\nu * n)^{2/3} * T^3 = 1.724 * 10^{-5} * (\omega^{2/3})$ Nm (A37)

- axial force acting upon 'fixed' end of the ball-screw $$F_a = \frac{F_{free}}{3} = \frac{1348}{3} = 449\,N$$ (A38)

F_{fixed} – resulting bearing load acting upon the "free" end of the ball-screw model:

$$F_{fixed} = \sqrt{F_a^2 + F_w^2} = \sqrt{(73.5)^2 + (449)^2} = 455\ N$$ (A39)

$T_{1\,fixed} = (\mu_1 * f_1 * F_{fixed} * T) / 2 = (0.001 * 1 * 455 * 0.046) / 2 = 10.5 * 10^{-3}$ Nm (A40)

- *Free end*

$$T_{0\,support} = f_0 * 10^{-7} * (\nu * n)^{2/3} * T^3 = 1.724 * 10^{-5} * (\omega^{2/3}) \text{ Nm} \quad \text{(A41)}$$

F_{free} – resulting bearing load acting upon bearing from the "free" end of the ball-screw model:

$$F_{free} = \sqrt{F_w^2 + 4T_x^2} = \sqrt{(73.5)^2 + 4*(673)^2} = 1348 \text{ N} \quad \text{(A42)}$$

$$T_{1\,support} = (\mu_1 * f_1 * F * T)/2 = (0.001 * 1 * 1348 * 0.046)/2 = 31 * 10^{-3} \text{ Nm} \quad \text{(A43)}$$

A5. Transducers fitted on Beaver VC35 CNC machine tool sited at the University of Huddersfield

X-axis motor encoder - Leine & Linde Rotary Incremental Encoder 7102350

Model: 63603 Volt : 5W46 Pulse rate: 2500

Y-axis motor encoder & Y-axis ball-screw encoder

Litton G60 S S LD BI 2500 5 2 3 05

Y-axis sealed linear encoder- HEIDENHAIN LS 106

1 pulse = 0.4 μ m, defined thermal behaviour, withstands high vibration

- generates sinusoidal signals, protected against chips, swarf, dirt and splashwater by an aluminium housing with flexible sealing lips, providing protection to IP 53 according to IEC 529.

EXE 650 B – with 50-fold interpolation of the encoder signal

- internal clock frequency 8 MHz - delivers output signals in cadence with an internal cycle time of t = 2.5 μ s
- maximum frequency of the input signal 40 kHz

APPENDIX B

B1. Analysis of zero-order hold element

The D / A converter reconstructs a continuous-time signal *from* the discrete-time signal. *A simple and* practical method is to hold the sample value at the beginning of the sample interval over the sample interval. The reconstructed signal, however, can take on only certain real values *(quantised signal).*

The switching in the D / A converter causes transients that corrupt the output of the summing amplifiers. Many D / A converters contain a zero-order hold (ZOH) to isolate the output signal from the transients.

Raven [128] presented the equation the equation of a zero-order hold generator considering that its output y (t) is a series of steps because the zero-order hold retains the discrete values of the input f (0), f (T), f (2T), f (3T)... for every value of sampling time :

$$y(t) = f(0)[u(t) - u(t-T)] + f(T)[u(t-T) - u(t-2T)] + f(2T)[u(t-2T) - u(t-3T)] \quad \text{(B1)}$$

The Laplace transform for the output y (t) is:

$$Y(s) = f(0)\left(\frac{1-e^{-sT}}{s}\right) + f(T)\left(\frac{e^{-sT}-e^{-2sT}}{s}\right) + f(2T)\left(\frac{e^{-sT}-e^{-3sT}}{s}\right) + \ldots\ldots \quad \text{(B2)}$$

$$Y(s) = \left(\frac{1-e^{-sT}}{s}\right)\left[f(0) + f(T)e^{-sT} + f(2T)e^{-2sT} + \ldots\ldots\right] = \left(\frac{1-e^{-sT}}{s}\right) \times F^*(s) \quad \text{(B3)}$$

So the Laplace transform of the output Y(s) is equal with the product between the Laplace transform of the zero-order hold and the Laplace transform of the sampled input F*(s).

When sampling period T=10 ms (the case of FANUC controller), the output could be considered an analogue signal (the steps are not very evident).

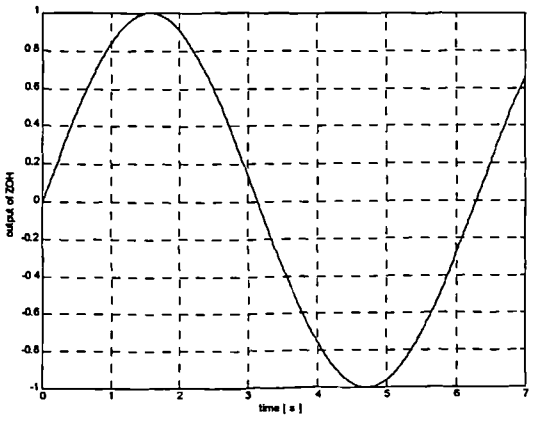

Figure B1.1. Output of ZOH with sampling period T = 10 ms

B 2. Data for lumped parameter models

Calculated data for X - axis

Transfer function of armature current - motor rate control loop

$$H_{motor+\ load} = 88.47 \times \frac{122727}{s^2 + 456819s + 122727} \rightarrow \omega_n = 110.78 \text{ rad/s},\ \zeta = 20.61 \quad \text{(B4)}$$

Equivalent transfer function for armature current - motor rate control loop

$$H_{\text{motor+ load equiv}} = 88.47 \times \frac{1}{0.4s+1} \tag{B5}$$

Transfer function of the velocity control loop

$$H_{\text{velocity}} = \frac{948.85\,s + 199499.85}{s^2 + 182.78\,s + 37904.98} \qquad \rightarrow \omega_n = 195 \text{ rad/s},\ \zeta = 0.469 \tag{B6}$$

Transfer function of the position control loop

$$H_{\text{position}} = \frac{7528.966\,s + 1588018.8}{s^3 + 182.78\,s^2 + 45434\,s + 1588018.8} \tag{B7}$$

Equivalent transfer function for the position control loop

$$H_{\text{position equiv}} = \frac{1600}{s^2 + 80s + 1600} \qquad \rightarrow \omega_n = 40 \text{ rad/s},\ \zeta = 1 \tag{B8}$$

Calculated data for Z - axis

Transfer function of armature current - motor rate control loop

$$H_{\text{motor+ load}} = 88.47 \times \frac{12387.7}{s^2 + 2059.05s + 12387.7} \qquad \rightarrow \omega_n = 111.3 \text{ rad/s},\ \zeta = 18.5 \tag{B9}$$

Equivalent transfer function for armature current - motor rate control loop

$$H_{\text{motor+ load equiv}} = 88.47 \times \frac{1}{0.2s+1} \tag{B10}$$

Transfer function of the velocity control loop

$$H_{\text{velocity}} = \frac{821.7\,s + 17899.6}{s^2 + 180.96\,s + 30276} \qquad \rightarrow \omega_n = 174 \text{ rad/s},\ \zeta = 0.52 \tag{B11}$$

Transfer function of the position control loop

$$H_{\text{position}} = \frac{5412.85\,s + 1668127.6}{s^3 + 180.96\,s^2 + 41343\,s + 1668127.6} \tag{B12}$$

Equivalent transfer function for the position control loop

$$H_{\text{position equiv}} = \frac{1482}{s^2 + 77s + 1482.5} \qquad \rightarrow \omega_n = 38.5 \text{ rad/s},\ \zeta = 1 \tag{B13}$$

% MATLAB program for calculation of the transfer function for motor + load loop

```
» num1=47.775; den1=[0.000042  0.454  0.54];
» w = logspace(-1,5);
» bode(num1,den1,w)
» sys1 = tf(num1,den1);
» dcgain(sys1)                    % calculation of DC gain
» damp(sys1)                      % calculation of damping ratio
```

% MATLAB program for calculation of the transfer function for velocity loop

```
» num2=[379.54  79799.94];      den2=[1  73.12  15162];
» w = logspace(-1,3);
```

```
» bode(num2,den2,w)
» sys2 = tf(num2,den2);
» dcgain(sys2)
» damp(sys2)
```

% MATLAB program for calculation of the transfer function for position loop

```
» num3=7.96;                den3= [1 0];    sys3= tf(num3, den3);
» num4=[36. 09 7581];den4=[1  73. 12 15162];
» sys4=tf(num4, den4);
» w = logspace(-2,6);
» sys5 = series(sys3, sys4)          % TF of the open loop for position control
```

$$\frac{287.24\ s + 60344.76}{s^3 + 73.12\ s^2 + 15162\ s}$$

```
» sys6 = tf (1,1)
» sys7 = feedback(sys5, sys6)       % TF of closed loop for position control
```

$$\frac{287.24\ s + 60344.76}{s^3 + 73.12\ s^2 + 15449.24\ s + 60344.76}$$

```
» damp(sys7)
```

Eigenvalue	Damping	Freq. (rad/s)
-3.98e+001	1.00e+000	3.98e+001
-3.46e+001 + 1.18e+002i	2.81e-001	1.23e+002
-3.46e+001 - 1.18e+002i	2.81e-001	1.23e+002

By applying the curve fitting method, the best estimate for the natural frequency is 35 rad / s and the comparison with the initial Bode diagrams is made running the following program:

```
» num8=1225;    den8=[1  70  1225];        sys8=tf(num5,den5);
» bode(sys7,'b',sys8,'r',w)  % red – initial TF; blue - equivalent TF
```

B 3. Data for distributed parameters models

Calculated data for X-axis and Z-axis

T_{p2} - torque due to driven pulley inertia $T_{p2}(s) = J_{p2}\ s\omega_2 = 0.0095\, s\omega_2$ $T_{p2\_z}(s) = 0.009\, s\omega_2$

T_{BSd} - torque due to ball-screw friction $T_{bsf} = 11 \times \text{sign}(\omega_2)$ $T_{bsf\_z} = 10 \times \text{sign.}(\omega_2)$

T_{BSi} - torque due to ball-screw inertia $T_{bsi}(s) = J_{bs}\ s\omega_2 = 0.0027\, s\omega_2$ $T_{bsi\_z}(s) = 0.002027\, s\omega_2$

T_{sr} - torque due to slideway reaction $T_{sr}(s) = 0.000019\,\omega_2 + 0.019\, s\omega_2$ $T_{sr\_z}(s) = 0.000023\,\omega_2 + 0.012\, s\omega_2$

$T_{friction}$ - torque due to friction in bearings

$$T_{0fixed} = T_{0support} = f_0\, 10^{-7} (\upsilon n_b)^{2/3} D^3 = 1.724 \times 10^{-5} \times (\omega_2)^{2/3} \quad \text{(B14)}$$

$$T_{0fixed\_z} = T_{0support\_z} = f_0\, 10^{-7} (\upsilon n_b)^{2/3} D^3 = 1.475 \times 10^{-5} \times (\omega_2)^{2/3} \quad \text{(B15)}$$

$T_{1fixed} = \mu_1 f_1 F_{fixed} (D/2) = 0.0057$ Nm $T_{1fixed\_z} = \mu_1 f_1 F_{fixed\_z} (D/2) = 0.0072$ Nm

$T_{1support} = \mu_1 f_1 F_{support} (D/2) = 0.01625$ Nm $T_{1support\_z} = \mu_1 f_1 F_{support\_z} (D/2) = 0.01872$ Nm

B4. Belt drive stiffness preliminary estimation

The synchronous belt from the Y- axis drive was considered as an example.

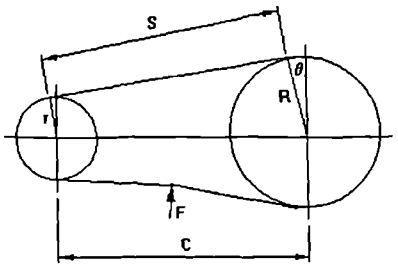

Figure B4.1. Diagram of timing belt drive

The length L of the belt is given by:-

$$L = \pi\ (R + r)\ +\ 2(R - r)\theta\ +\ 2S \tag{B16}$$

and the tangent of the angle of the belt from the plane containing the shafts of the drive:

$$\tan\theta\ = \frac{R - r}{S} \tag{B17}$$

where S - the belt span C - the drive centre distance

r - the radius of the driving pulley R - the radius of the driven pulley

θ - the angle of the belt from the plane containing the shafts of the drive

The belt span and the angle are obtained by solving these equations. The drive centre is calculated from the angle of the belt considering $C = \frac{R - r}{\sin\theta}$,.

The following MATLAB program solves the equations:

```
function[output]=b_centre(r,R,L,prec)
theta=0.;done=0.;k=0.
if (r==R)
  S=(L-pi*(R + r))/2.; C=S; theta=0.;
else
  pi=4.*atan(1.);dtheta=0.1; S=(L-pi*(R+r))/2.; S1=(R-r)/1e-6;  S1S_old=S1-S;
  while (done==0. & k<1000)
    k=k+1; theta=theta + dtheta; S=(L-pi*(R+r)-2.*(R-r)*theta)/2.; S1=(R-r)/tan(theta); S1S = S1-S;
    if (abs(S1S) < prec * S)
      C=(R-r)/sin(theta); Done = 1.
    else
    if (S1S * S1S_old < 0.)
      dtheta = dtheta / (-2.); S1S_old = S1S; end
    end
  end
end
output(1) = S; output(2) = C; output(3) = theta;
output(4) = done; output(5) = k;
```

The results are presented in the following table:

Drive	X	Y
Belt length [mm]	880	720
Driving pulley radius [mm]	35.65	35.65
Driven pulley radius [mm]	71.30	71.30
Span [mm]	267.28	185.22
Centre distance [mm]	269.64	188.62
Belt angle [rad]	0.1326	0.1901

Table B1. Calculated geometrical data regarding the toothed belt drives

The belt for the Y drive should have a tension T of 365 N when considering the factor Y from the Fenner catalogue [136].

The force F needed to push the belt sideways a distance of 10 mm per metre of span in the middle is given by

$$F = \frac{T_{belt} + \frac{S}{L} \times Y}{25} \tag{B18}$$

where Y = 200 N for a 30 mm wide belt. In the case of the Y drive this gives:

$$F = \frac{365 + (\frac{185.22}{720}) \times 200}{25} = 16.66 N \tag{B19}$$

The tension in the belt when pushed sideways is:

$$T_{tens} = \sqrt{T^2 + F^2} = \sqrt{365^2 + 16.66^2} = 365.4 \text{ N} \tag{B20}$$

The additional tension caused by the sideways push is:

$$T_{+} = \sqrt{T^2 + F^2} - T = \sqrt{365^2 + 16.66^2} - 365 = 0.380 \text{ N} \tag{B21}$$

This stretches the belt by

$$\delta = 2 \times \sqrt{\left(\frac{185.22}{2}\right)^2 + \left(\frac{10 \times 185.22}{1000}\right)^2} - \frac{185.22}{2} = 0.0370 \text{ mm} \tag{B22}$$

The stiffness of the full belt is therefore 0. 380 / 0. 0370 = 10. 257 N / mm.

The torsional stiffness of the belt referred to the motor shaft and corrected to the span between the pulleys is:

$$K_{\tau} = 2 \times 10257 \times \frac{720}{185.22} \times \left(\frac{35.65}{1000}\right)^2 = 101.3 \text{ Nm / rad} \tag{B23}$$

The inertias referred to the motor shaft at either side of the torsional spring are :

- from the motor side

$$J_1 = J_m + J_{shaft} + J_{p1} = 0.0048 + 0.0000075 + 0.0004986 = 0.005306 \text{ kg.m}^2 \tag{B24}$$

- from the ball-screw side

$$J_{2\_Y} = \frac{J_{p2} + J_{BS} + J_{LY}}{4} = \frac{0.009524 + 0.002724 + 0.0017}{4} = 0.003487 \text{ kg m}^2 \tag{B25}$$

The equivalent "mass on a spring" value is

$$J_{eq\_Y} = \frac{J_1 \times J_{2\_Y}}{J_1 + J_{2\_Y}} = \frac{0.005306 \times 0.003487}{0.005306 + 0.003487} = 0.00210 \text{ kg m}^2 \quad \text{(B26)}$$

The natural frequency of this simple equivalent system is 219. 44 rad / s or 34. 9 Hz.

The same calculations have been performed for X-axis considering the data from Appendix A4 and the results of the analysis for X-axis and Y-axis are summarised in Table B2.

Drive	X	Y	Units
Extra tension caused by side push	0. 397	0. 380	N
Stretch caused by side push	0. 0535	0. 0370	mm
Linear stiffness for full belt length	7429	10257	N/m
Torsional stiffness	62. 1	101. 3	N.m/rad
Motor side inertia	0. 005306	0. 005306	kg.m²
Ball-screw side referred inertia	0. 005353	0. 003487	kg.m²
"One mass" equivalent	0. 00266	0. 00210	kg.m²
Natural frequency	152. 68	219. 44	rad/sec
Natural frequency (Hz)	24. 3	34. 9	Hz

Table B2. Calculated mechanical data regarding the toothed belt drives

B5. Coefficients for the model using explicit damping coefficients determined considering the experimental data for the closed-loop position control

- *motor mechanical*

rated torque $m_{0M} = 7$ Nm speed $n_M = 2000$ rot / min

Assumption: 2 % of rated torque is dissipated in the bearings : $m_{bearings} = 0.02 \times 7 = 0.14$ Nm

The damping coefficient is resulting from the Equation (4. 47):

$$c_{\theta\_m} = \frac{m_{oM}}{2 \times \pi \times n} = \frac{0.14}{2 \times \pi \times \frac{2000}{60}} = 0.668 \times 10^{-3} \frac{\text{N m s}}{\text{rad}} \quad \text{(B27)}$$

- *motor shaft*

Diameter = 17 mm Material = steel Length = 120 mm

The rotational stiffness is calculated considering Equation (4. 55): $K_1 = \frac{\pi}{32} D^4 \times \frac{G}{L} = 5466 \frac{\text{N m}}{\text{rad}}$ (B28)

where G - modulus of rigidity $8.104 \times 10^{10} \text{ N / m}^2$

For the damping coefficient, it was chosen a conventional value: $c_1 = 1 \times 10^{-3} \frac{\text{N m s}}{\text{rad}}$

- *driving (first) pulley*

$$J_1 = \frac{J_{shaft}}{2} + J_{pl} = \frac{0.0000075}{2} + 0.0004986 = 5.024 \times 10^{-4} \text{ kg m}^2 \quad \text{(B29)}$$

- reduction ratio $u = 2$
- *belt drive - X-axis* (considering the experimental results for closed-loop position control)

The inertia referred to the motor shaft from the ball-screw side is:

$$J_{2\_X} = \frac{J_{p2} + J_{bs} + J_L}{4} = \frac{0.0178 + 0.0027 + 0.00091}{4} = 0.005353\ \text{kg m}^2 \qquad \text{(B30)}$$

A peak of 10 dB at 75 Hz could be observed from the Bode diagrams showing the torsional movement between the driven and the driving pulleys (see Appendix C2).

10 dB = 20 x log (x) $\rightarrow x = 3.164$ The damping ratio is: $\zeta_X = \frac{1}{2*x} = \frac{1}{2*3.164} = 0.158$

The torsional stiffness of the belt is: $K_{2x} = J_{2\_X} \times \omega_n^2 = 0.005353 \times (2 \times \pi \times 75)^2 = 1188 \frac{\text{N m}}{\text{rad}}$ (B31)

The coefficient of critical viscous damping is:

$$c_{cx} = 2 \times \sqrt{J_{2\_calc} \times K_{belt\_X}} = 2 \times \sqrt{0.005353 \times 1188} = 5.044 \frac{\text{N m s}}{\text{rad}} \qquad \text{(B32)}$$

The coefficient of viscous damping is: $c_{2x} = c_{cx} \times \zeta_x = 0.797 \frac{\text{N m s}}{\text{rad}}$

- *belt drive - Y-axis* (considering the experimental results for closed-loop position control)

The inertia referred to the motor shaft from the ball-screw side is:

$$J_{2\_Y} = \frac{J_{p2} + J_{bs} + J_L}{4} = \frac{0.0095 + 0.0027 + 0.0017}{4} = 0.003481\ \text{kg m}^2 \qquad \text{(B33)}$$

A peak of 13 dB at 92 Hz could be observed from the Bode diagrams showing the torsional movement between the driven and the driving pulleys (see Appendix C2).

13 dB = 20 x log (y) $\rightarrow y = 4.47$

The damping ratio is: $\zeta_Y = \frac{1}{2*y} = \frac{1}{2*4.47} = 0.112$ (B34)

The torsional stiffness of the belt is:

$$K_{2y} = J_{2\_Y} \times \omega_n^2 = 0.003481 \times (2 \times \pi \times 92)^2 = 1167 \frac{\text{N m}}{\text{rad}} \qquad \text{(B35)}$$

The coefficient of critical viscous damping is:

$$c_{cy} = 2 \times \sqrt{J_{2\_Y} \times K_{belt\,y}} = 2 \times \sqrt{0.003481 \times 1167} = 4.037 \frac{\text{N m s}}{\text{rad}} \qquad \text{(B36)}$$

The coefficient of viscous damping is: $c_{2y} = c_{cy} \times \zeta_y = 0.452 \frac{\text{N m s}}{\text{rad}}$

- *driven (second) pulley - X-axis* $J_{2x} = \frac{J_{bs}}{4} + J_{p2} = \frac{0.0027}{4} + 0.0178 = 18.46 \times 10^{-3}\ \text{kg m}^2$ (B37)
- *driven (second) pulley - Y-axis* $J_{2y} = \frac{J_{bs}}{4} + J_{p2} = \frac{0.0027}{4} + 0.009524 = 10.2 \times 10^{-3}\ \text{kg m}^2$ (B38)

The coefficient of viscous damping is chosen to be $c_2 = 0.668 * 10^{-3}$ N m s / rad due to the fact that there is a low friction force which occurs between driven pulley and ball-screw

- *ball-screw 1 = ball-screw 2 (X-axis and Y-axis)*_ (the two halves of the screw)

The inertia referred to the driven pulley from the ball-screw side is calculated considering the inertia of the half of the ball-screw and of the quarter of the ball-screw connected in series:

$$J_{BS\ ref} = \frac{\frac{J_{BS}}{2} \times \frac{J_{BS}}{4}}{\frac{J_{BS}}{2} + \frac{J_{BS}}{4}} = \frac{0.001362 \times 0.000681}{0.001362 + 0.000681} = 0.000454 \text{ kg m}^2 \quad \text{(B39)}$$

The torsional inertia for the full length of the ball-screw is: $K_{BS} = \frac{\pi}{32} D^4 \times \frac{G}{L} = 9880 \frac{\text{N m}}{\text{rad}}$

The torsional inertia for the half length of the ball-screw is:

$$K_3 = K_4 = K_{\frac{BS}{2}} = 2 \times K_{BS} = 2 \times 9880 = 19760 \quad \frac{\text{N m}}{\text{rad}} \quad \text{(B40)}$$

The coefficient of critical viscous damping is:

$$c_c = 2 \times \sqrt{J_{BS\,ref} \times K_{\frac{bs}{2}}} = 2 \times \sqrt{0.000454 \times 19760} = 5.98 \frac{\text{N m s}}{\text{rad}} \quad \text{(B41)}$$

Because there is necessary to consider a ' light ' damping for the two halves of the screw, the 1 % of the critical viscous damping is introduced into the model:

$$c_3 = c_4 = c_{0.01} = c_c \times 0.01 = 0.059 \frac{\text{N m s}}{\text{rad}} \quad \text{(B42)}$$

The inertia of the half of the ball-screw is: $J_3 = \frac{J_{BS}}{2} = 0.001362 \frac{\text{N m}}{\text{rad}}$ (B43)

- *ball-screw end (X-axis and Y-axis)* $J_4 = \frac{J_{BS}}{4} = \frac{0.0027}{4} = 0.000681 \text{ kg m}^2$ (B44)

- *coefficient used to transform rotational movement into translational movement*

$$\text{conv} = \frac{p}{2\pi} = \frac{10}{2 \times 3.14} \quad \text{(B45)}$$

The effect of the ball-screw mass on the springs corresponding to each half of the total length is represented by a third of the ball-screw mass due to Coulson 's [137] remark:

" *It thus appears that the effect of the mass of the spring is equivalent, in a close approximation, to adding a mass* ***one-third*** *as great as bottom of the spring.* ". So $m_1 = m_{BS} / 3 = 5$ kg

- m_2 - *the mass attached to the spring of the ball-screw nut* is the load moving mass plus a third of the ball-screw mass

  $m_2 = 359 + 5 = 364$ kg for X-axis $\quad m_2 = 677 + 5 = 682$ kg for Y-axis

- *ball-screw nut* $K_5 = K_{axial\_nut} = 10^9 \frac{\text{N}}{\text{m}}$

It was estimated a great value due to the big friction forces which appear between the screw and nut. The coefficient of viscous damping was chosen in the sense that the simulation of the model to run in good conditions. The estimated value is: $c_5 = 82110 \frac{\text{N m s}}{\text{rad}}$

The theoretical calculations of the equivalent stiffness (K_6) for the system ball-screw - bearings are performed in Appendix C4.

APPENDIX C

C1.Geometric errors from Beaver VC35 measured using laser interferometer system

X-axis linear positioning error – ex (x)

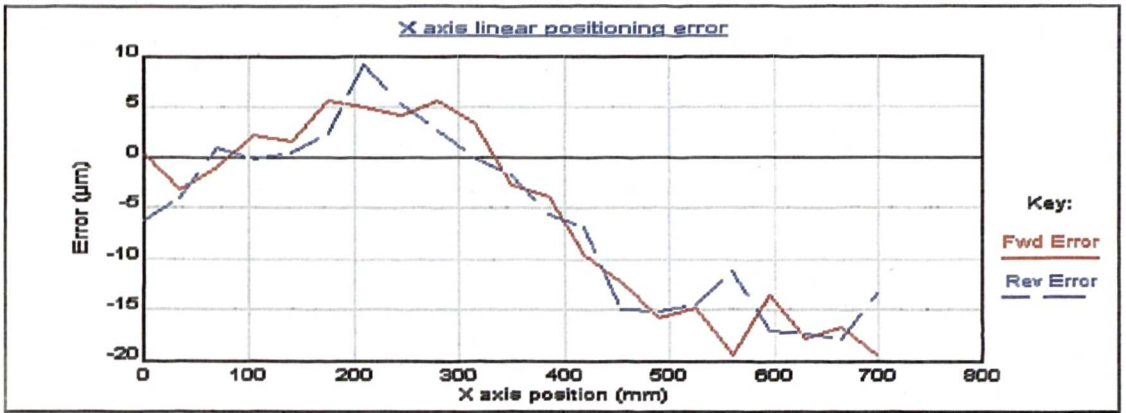

M/c:Beaver VC35	Ser.No:	Loc:UoH	Date:August 2001
Source:x1.rtl - X axis linear positioning error			By:CP
Comment:Figure C1.1. X-axis linear positioning error			

Y-axis linear positioning error –ey (y)

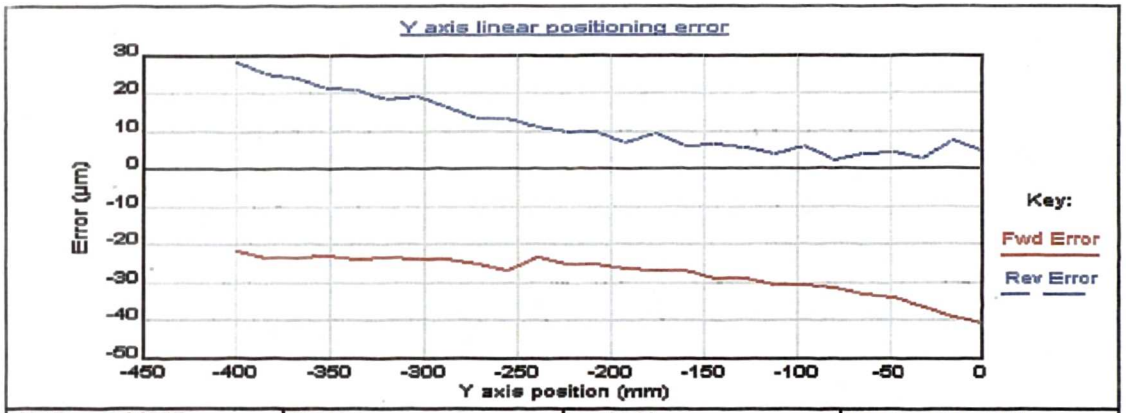

M/c:Beaver VC35	Ser.No:	Loc:UoH	Date:August 2001
Source:Y1.rtl - Y axis linear positioning error			By:CP
Comment:Figure C1.2. Y-axis linear positioning error			

Z-axis linear positioning error – ez (z)

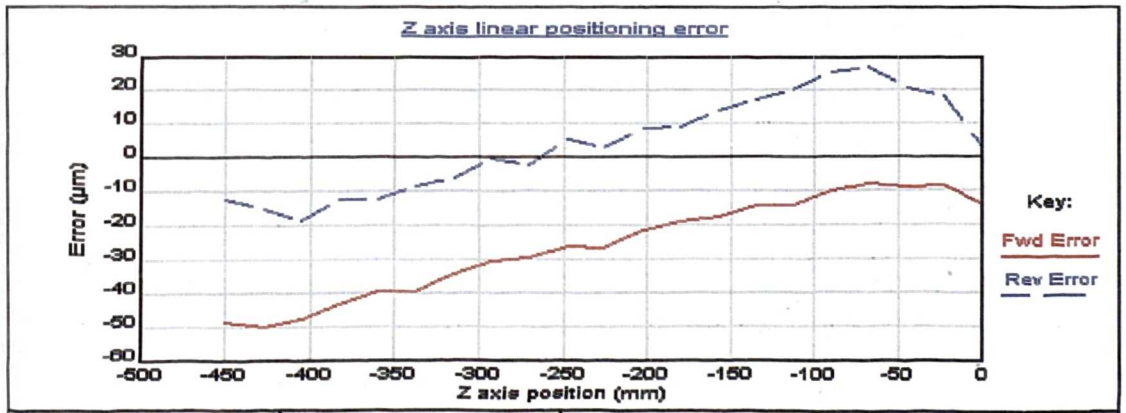

M/c:Beaver VC35	Ser.No:	Loc:UoH	Date:August 2001
Source:z1.rtl - Z axis linear positioning error			By:CP
Comment:Figure C1.3. Z-axis linear positioning error			

X-axis angular error about X-axis - $\phi x(x)$

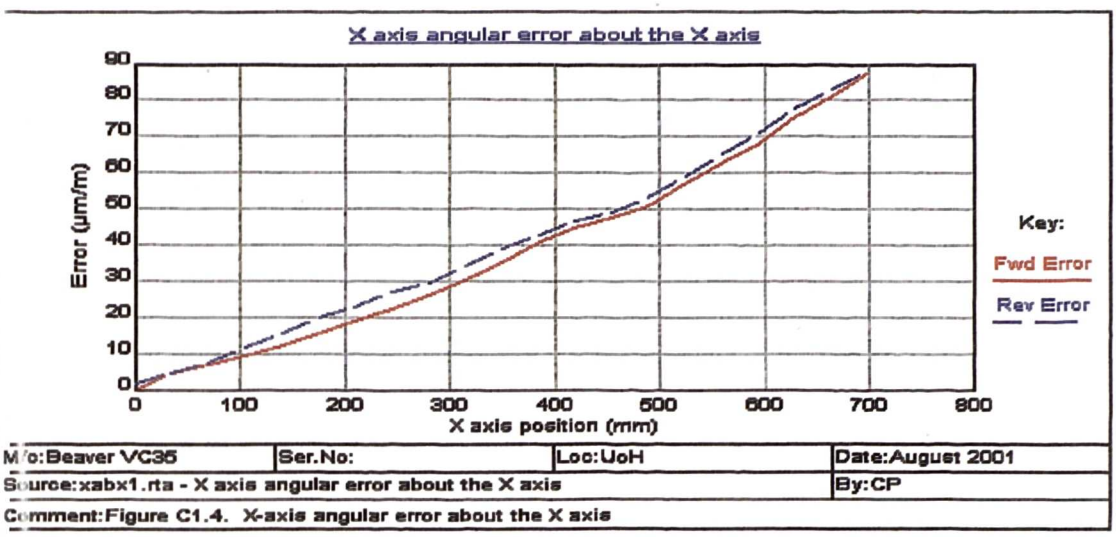

M/c:Beaver VC35	Ser.No:	Loc:UoH	Date:August 2001
Source:xabx1.rta - X axis angular error about the X axis			By:CP
Comment:Figure C1.4. X-axis angular error about the X axis			

X-axis angular error about Y-axis - $\phi y(x)$

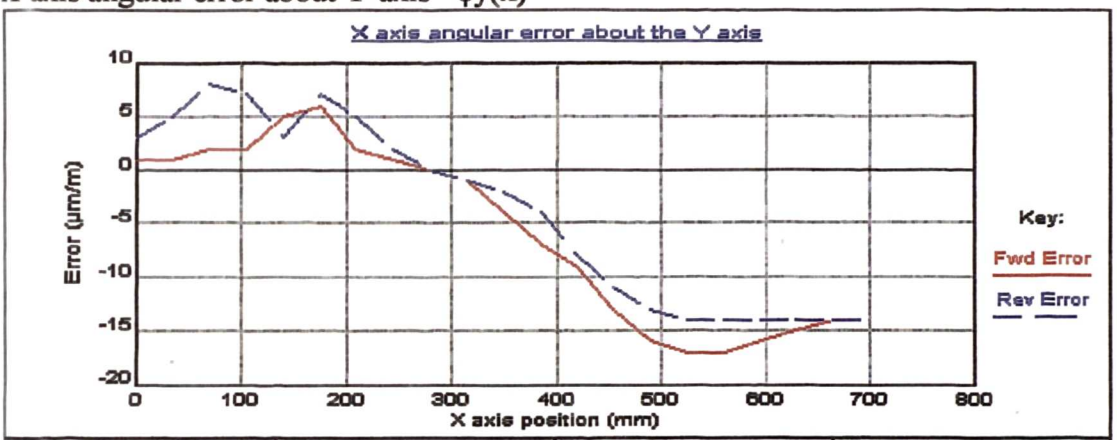

M/c:Beaver VC35	Ser.No:	Loc:UoH	Date:August 2001
Source:xaby1.rta - X axis angular error about the Y axis			By:CP
Comment:Figure C1.5. X-axis angular error about the Y axis			

X-axis angular error about Z-axis - $\phi z(x)$

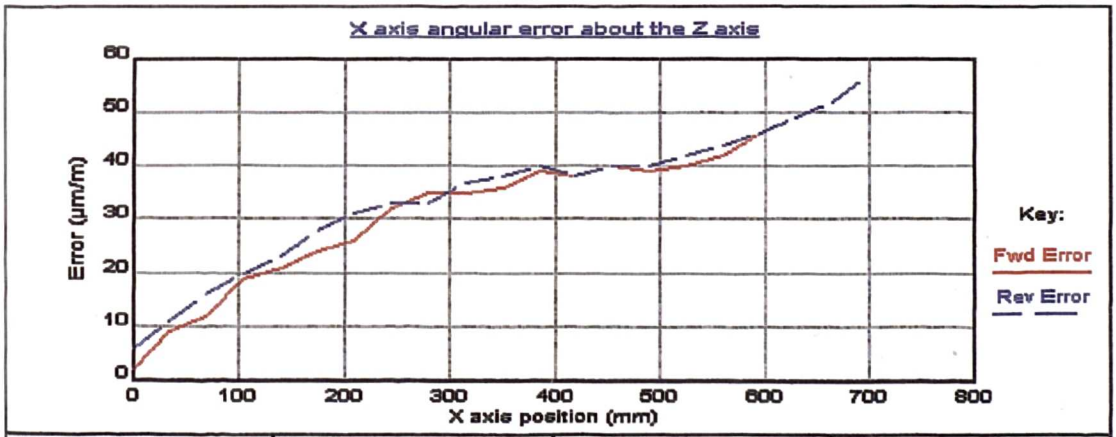

M/c:Beaver VC35	Ser.No:	Loc:UoH	Date:August 2001
Source:xabz1.rta - X axis angular error about the Z axis			By:CP
Comment:Figure C1.6. X-axis angular error about the Z axis			

Y-axis angular error about Y-axis - $\phi y(y)$

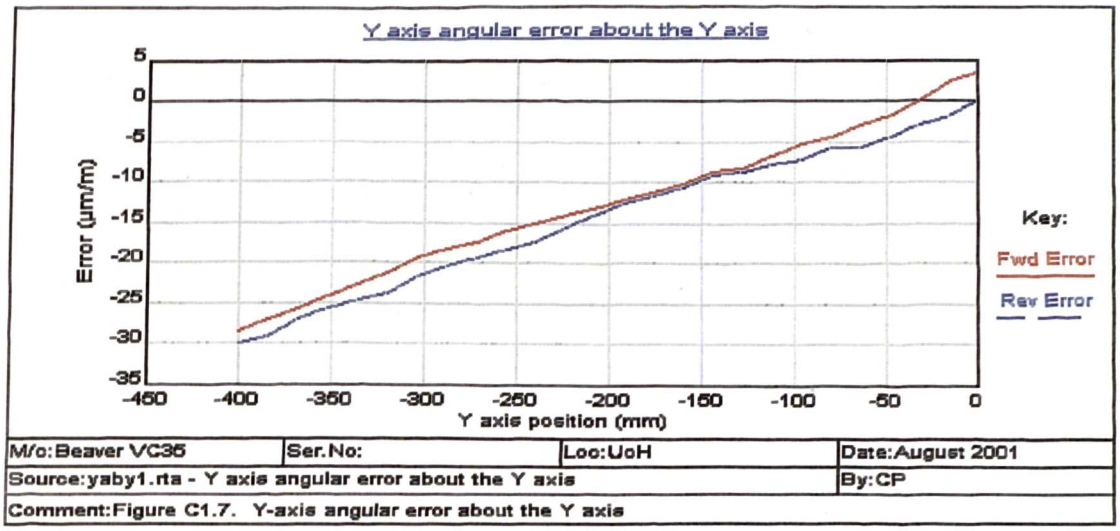

M/c:Beaver VC35	Ser.No:	Loc:UoH	Date:August 2001
Source:yaby1.rta - Y axis angular error about the Y axis			By:CP
Comment:Figure C1.7. Y-axis angular error about the Y axis			

Y-axis angular error about X-axis - $\phi x(y)$

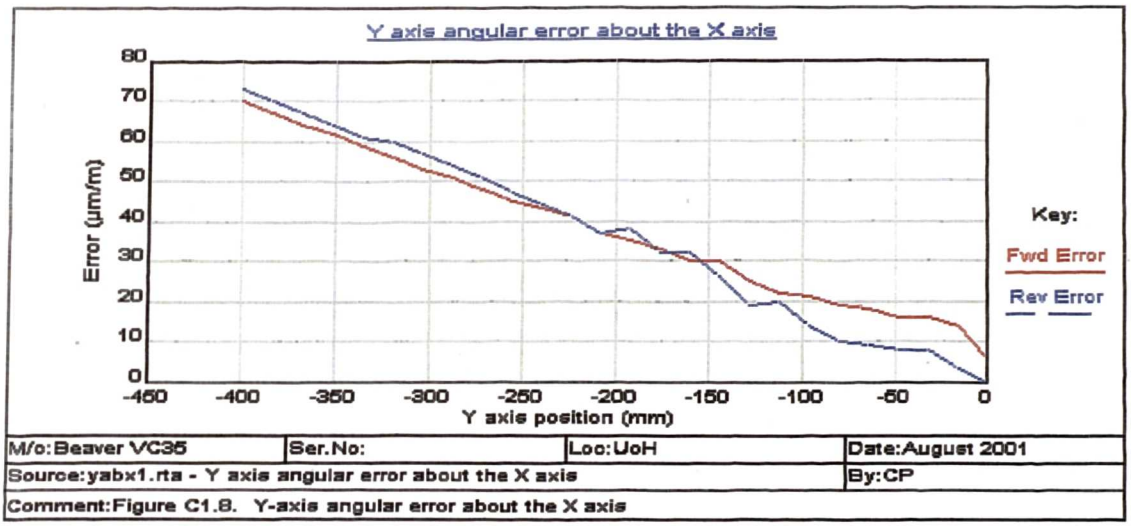

M/c:Beaver VC35	Ser.No:	Loc:UoH	Date:August 2001
Source:yabx1.rta - Y axis angular error about the X axis			By:CP
Comment:Figure C1.8. Y-axis angular error about the X axis			

X-axis straightness in the Y-axis direction – ey (x)

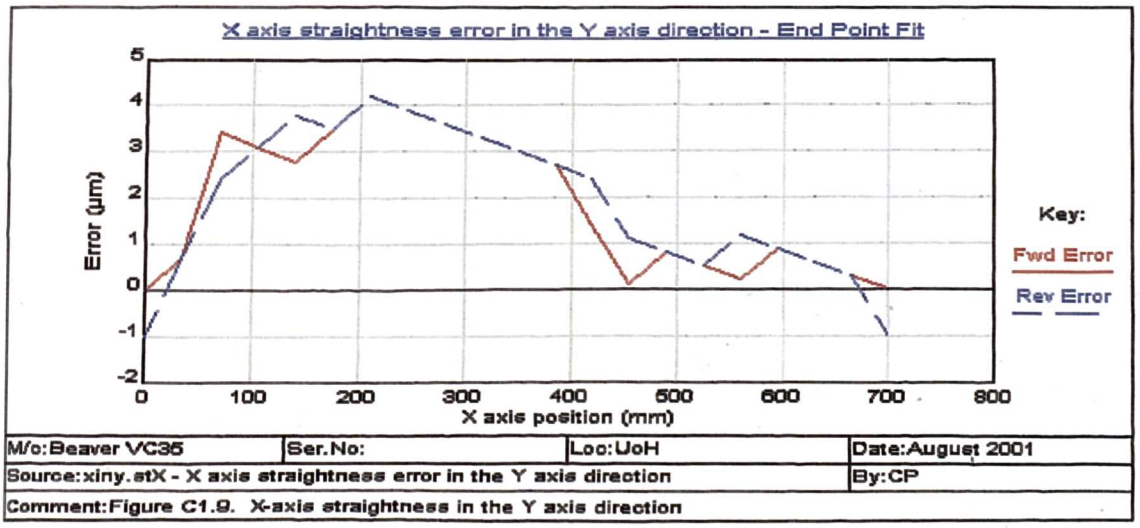

M/c:Beaver VC35	Ser.No:	Loc:UoH	Date:August 2001
Source:xiny.stX - X axis straightness error in the Y axis direction			By:CP
Comment:Figure C1.9. X-axis straightness in the Y axis direction			

X-axis straightness in the Z-axis direction – ez (x)

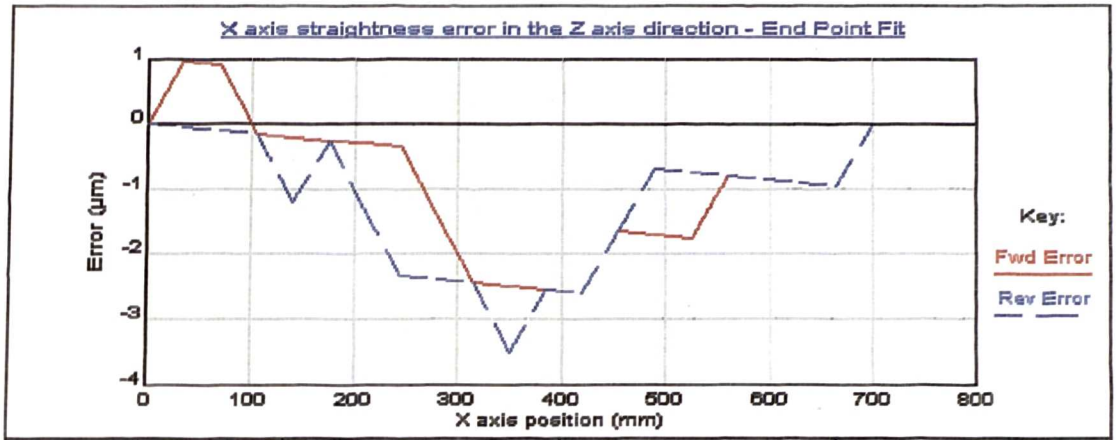

M/o:Beaver VC35	Ser.No:	Loc:UoH	Date:August 2001
Source:xinz1.stX - X axis straightness error in the Z axis direction			By:CP
Comment:Figure C1.10. X-axis straightness in the Z axis direction			

Y-axis straightness in the X-axis direction – ex (y)

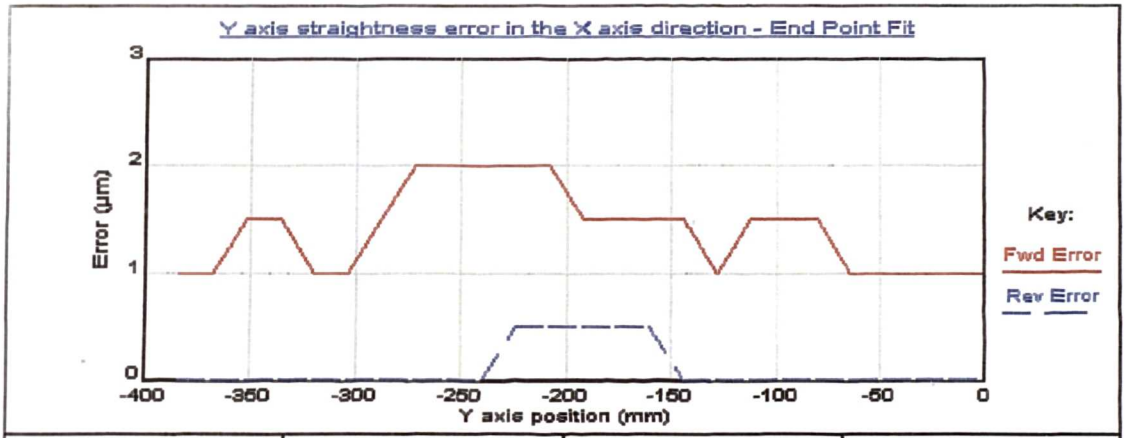

M/o:Beaver VC35	Ser.No:	Loc:UoH	Date:August 2001
Source:yinx1.stY - Y axis straightness error in the X axis direction			By:CP
Comment:Figure C1.11. Y-axis straightness in the X axis direction			

Y-axis straightness in the Z-axis direction – ez (y)

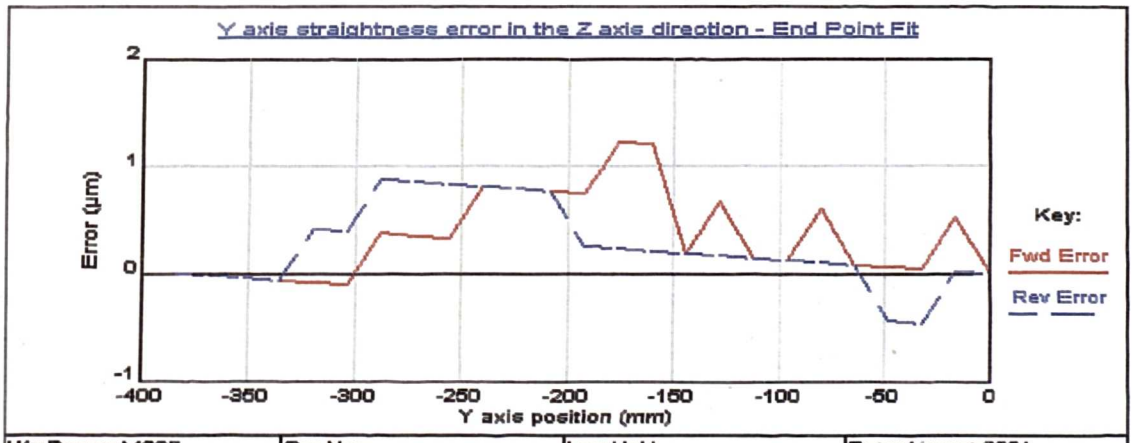

M/o:Beaver VC35	Ser.No:	Loc:UoH	Date:August 2001
Source:yinz1.stY - Y axis straightness error in the Z axis direction			By:CP
Comment:Figure C1.12. Y-axis straightness in the Z axis direction			

Z-axis straightness in the Y-axis direction – ey (z)

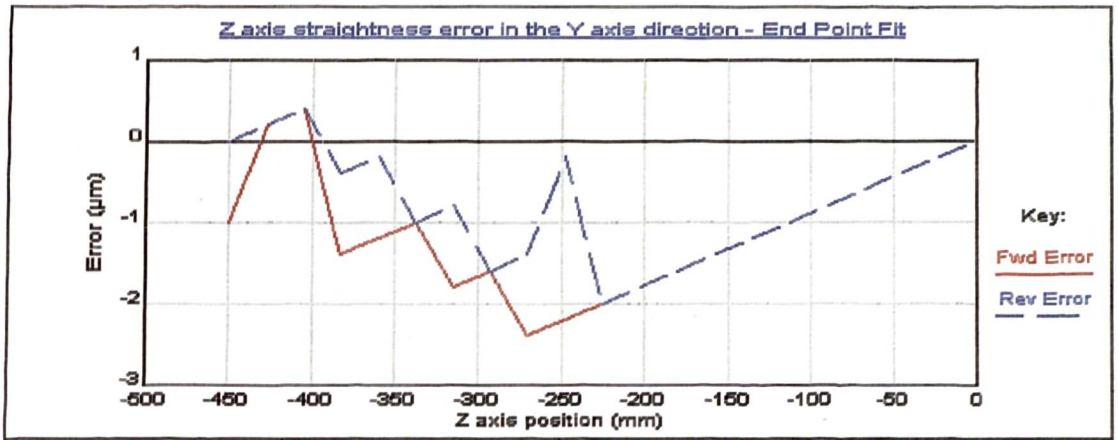

M/c:Beaver VC35	Ser.No:	Loc:UoH	Date:August 2001
Source:Ziny3.stz - Z axis straightness error in the Y axis direction			By:CP
Comment:Figure C1.13. Z-axis straightness in the Y axis direction			

Z-axis straightness in the X-axis direction – ex (z)

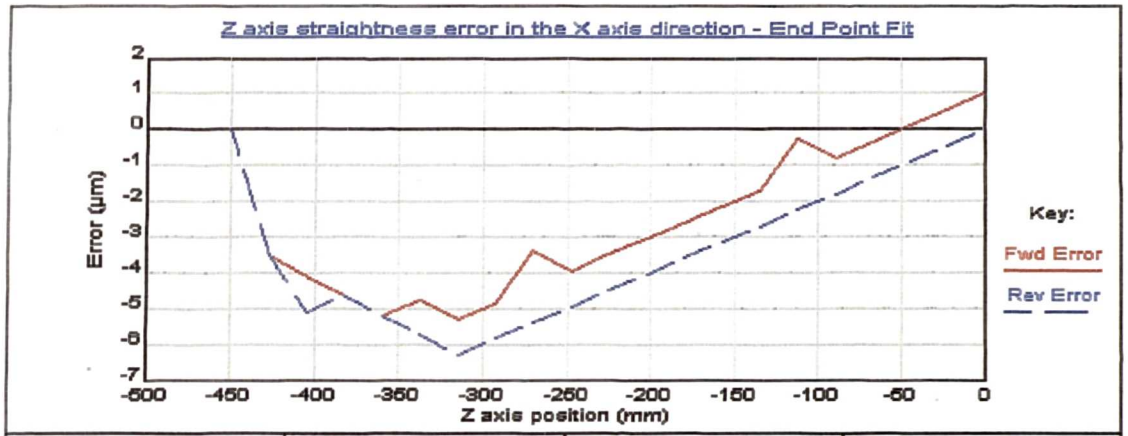

M/c:Beaver VC35	Ser.No:	Loc:UoH	Date:August 2001
Source:zinx1.stZ - Z axis straightness error in the X axis direction			By:CP
Comment:Figure C1.14. Z-axis straightness in the X axis direction			

Y-axis angular error about Z-axis - ϕz (y)

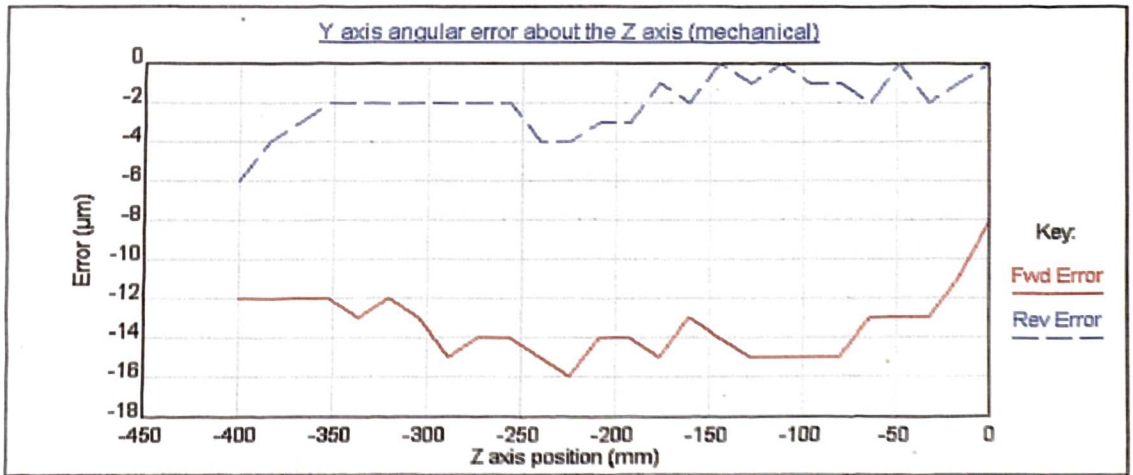

M/c:Beaver	Ser.No:	Loc:Workshop	Date:August 2001
Source:yabz1.rta - Y axis angular error about the Z axis (mechanical)			By:CP
Comment:Figure C1.15 Y axis angular error about the Z axis			

Z-axis angular error about X-axis - $\phi x(z)$

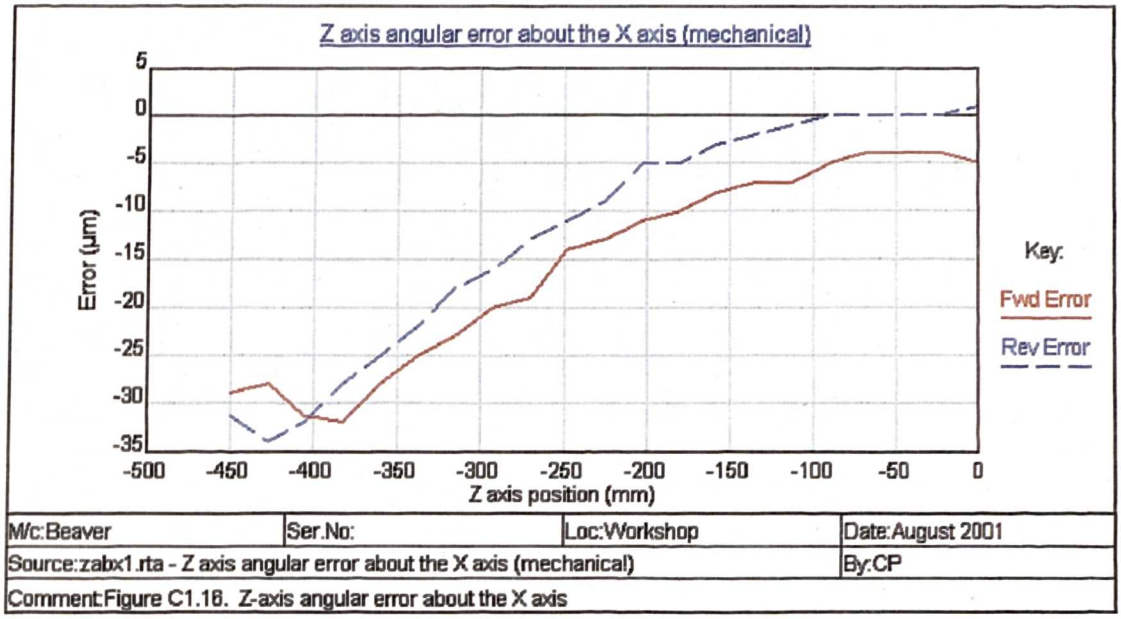

Z-axis angular error about Y-axis - $\phi y(z)$

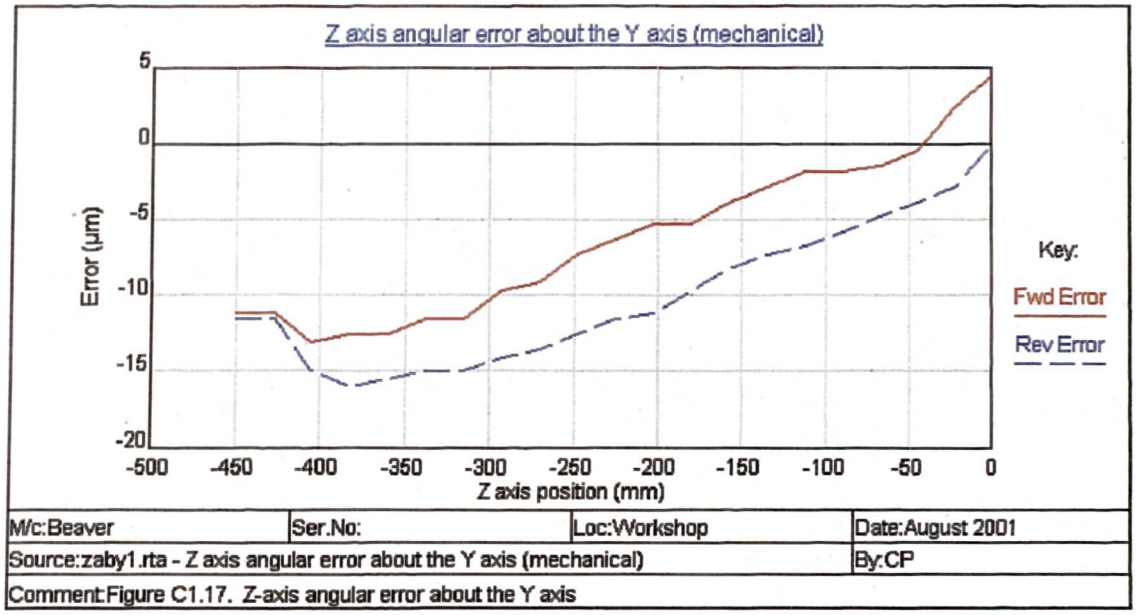

The squareness errors were measured using electronic precision levels (talyvels):

XY squareness = 10. 42 arc sec = 10. 42 * 4. 7 µ m / m = 49 µ m / m = 0. 049 µ m / mm

YZ squareness = 5 arc sec = 5 * 4. 7 µ m / m = 22. 5 µ m / m = 0. 0225 µ m / mm

XZ squareness = -5. 5 arc sec = -5. 5 * 4. 7 µ m / m = - 26 µ m / m = - 0. 026 µ m / mm

The XY squareness error had to be converted in mm / mm because it was multiplied by Y-axis position before error.

C2. Measurement results using accelerometers attached to the drive systems for X-axis and Y-axis

Bode diagrams reflecting the characteristics of the belt drive in the case of both axes

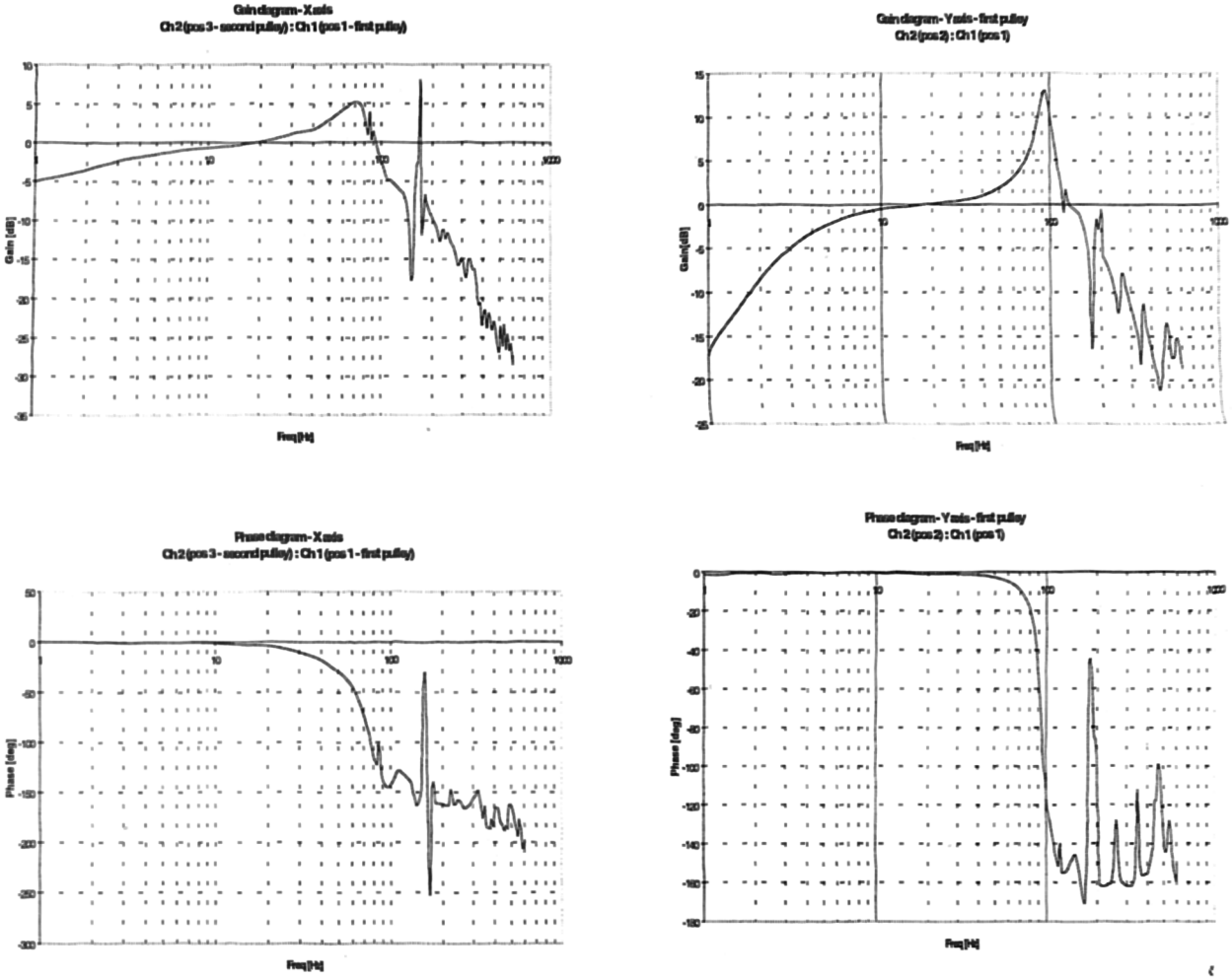

The vibration characteristics of the belt drive for X-axis result by comparing the acceleration picked up by one of the accelerometer fitted on the driving (first) pulley with that of one fitted on the driven (second) pulley.

By comparing the acceleration picked up by the two accelerometers on the driving pulley, it is obvious that the vibration is torsional. These measurements were not performed for the Y-axis because the driving pulley is not easily accessible.

Bode diagrams presenting the axial linear movement of the thrust bearing housing versus torsional movement of the driven pulley in the case of both axes

The measurements of the axial linear movement of the thrust bearing housing versus torsional movement of the driven pulley in the case of both axes showed relatively small activity so these vibrations were neglected.

X -axis

Y -axis

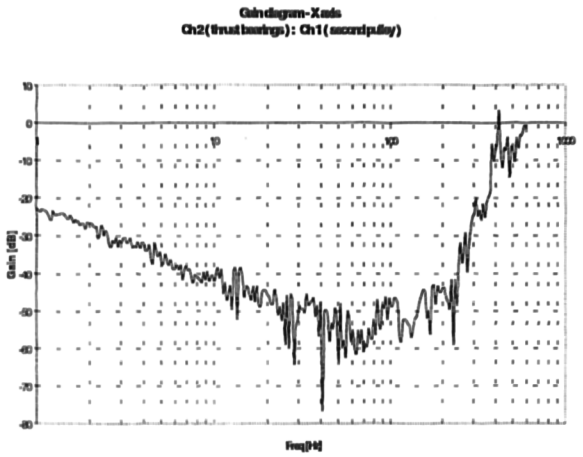

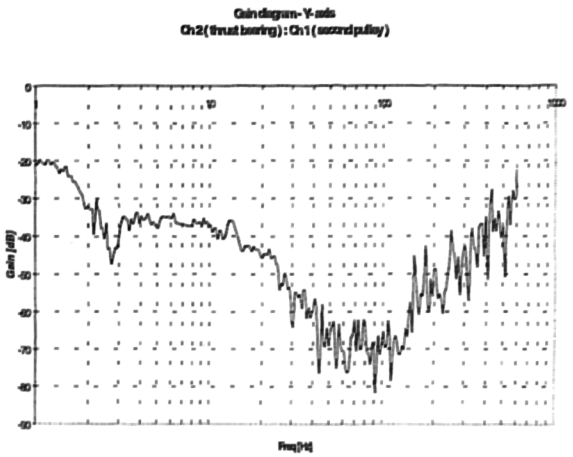

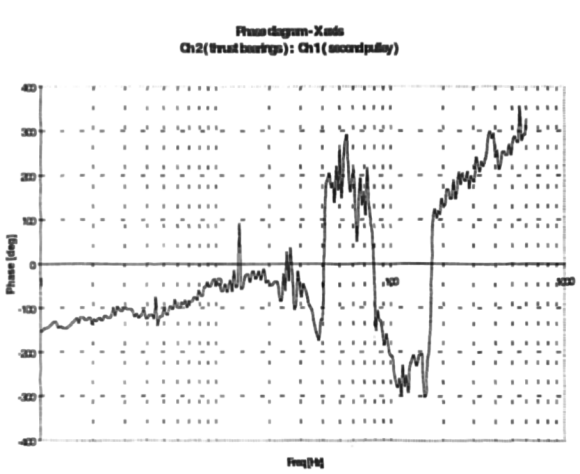

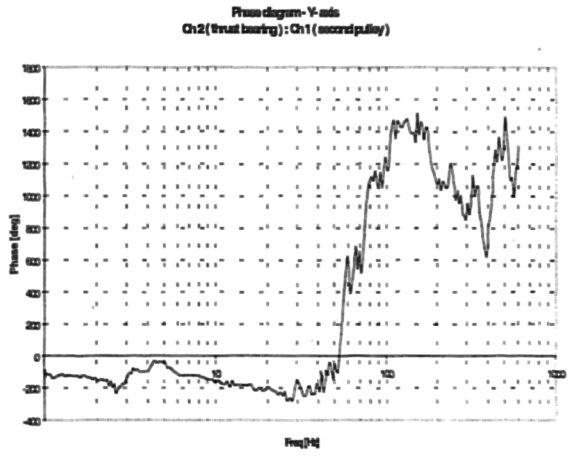

Bode diagrams presenting the radial linear movement of the thrust bearing housing versus torsional movement of the driven pulley in the case of both axes

X - axis

Y -axis

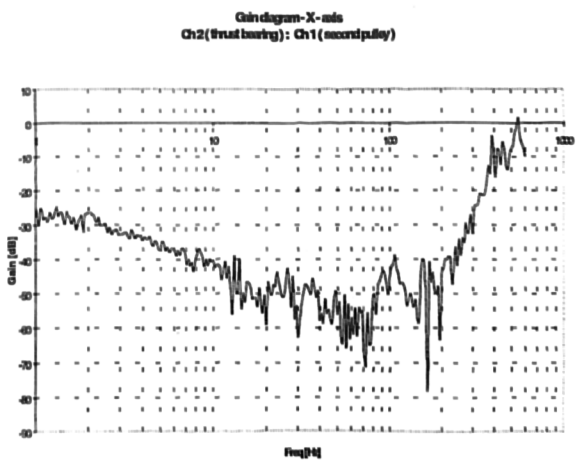

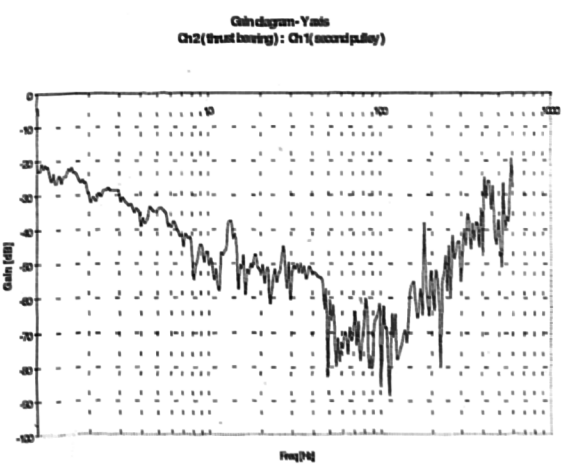

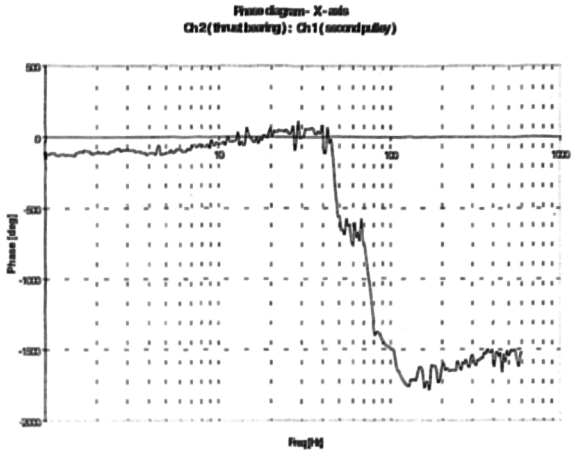

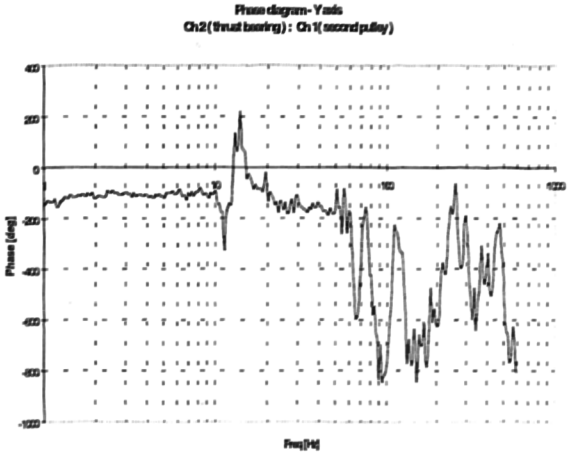

Also the measurements of the radial movement of the thrust bearing housing versus torsional movement of the driven pulley in the case of both axes showed relatively small activity so these vibrations were neglected.

Bode diagrams displaying the axial linear movement of the ball-screw nut housing versus torsional movement of the driven pulley in the case of both axes

X - axis

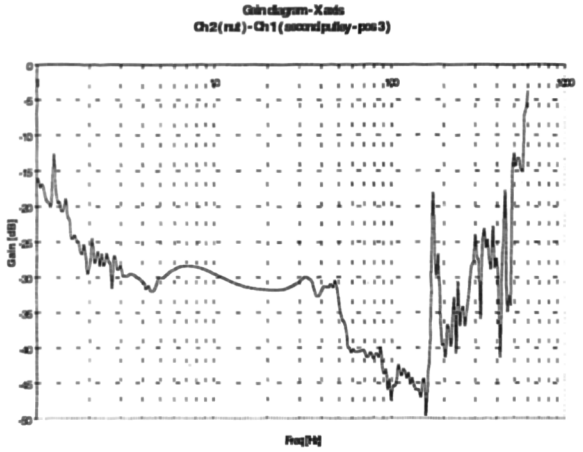

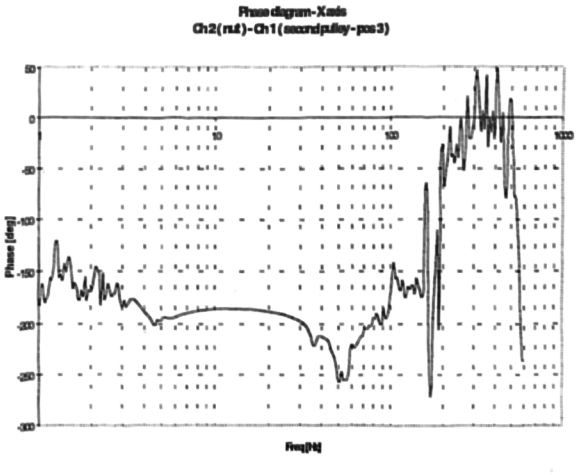

Y - axis

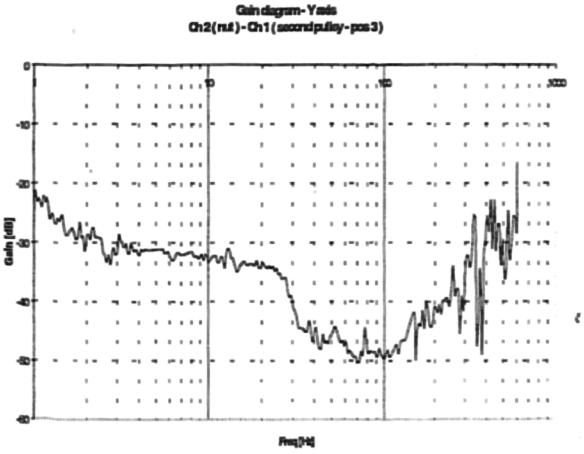

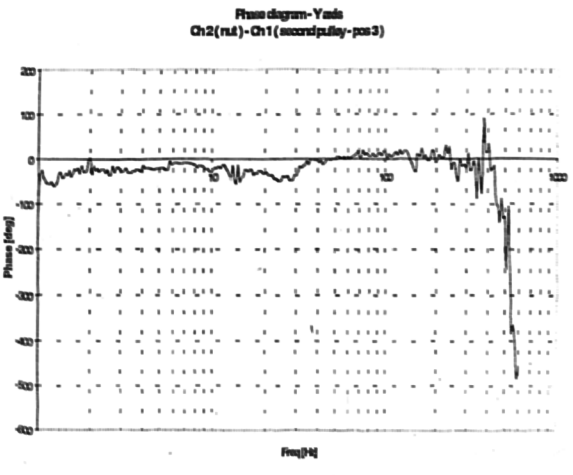

The measurements of the axial vibration of the ball-screw nut showed low levels so these values were ignored in the modelling process.

C3. Measurement results using accelerometers to determine the source of resonant frequency at 35 Hz

INPUT - swept sine with A = 750 mV generated by HP 3566A, applied to the pre-amplifier of the Y-axis - OPEN LOOP position control

OUTPUT - signal generated by charge amplifier (~ acceleration measured by accelerometer)

Accelerometer DJB A / 20 - sensitivity 25 - 38 pC /g → charge amplifier set at 31. 5 pC / g

Charge amplifier FYLDE 128 CA

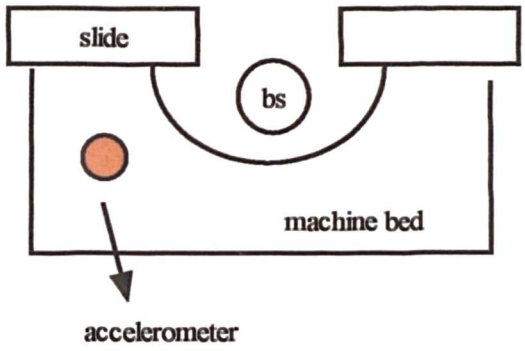

Frequency 30 - 45 Hz

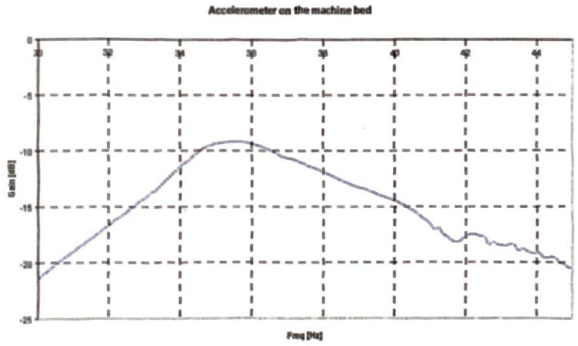

Frequency 5 - 100 Hz

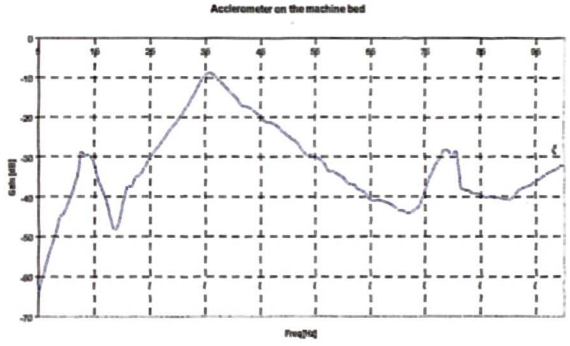

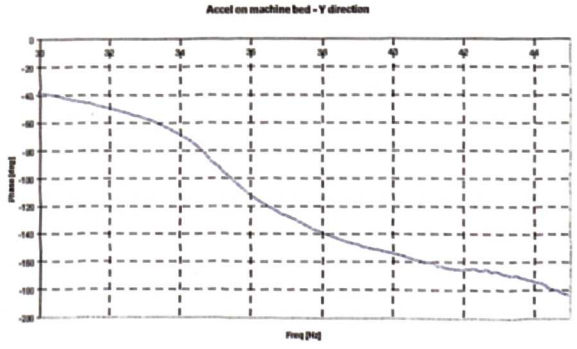

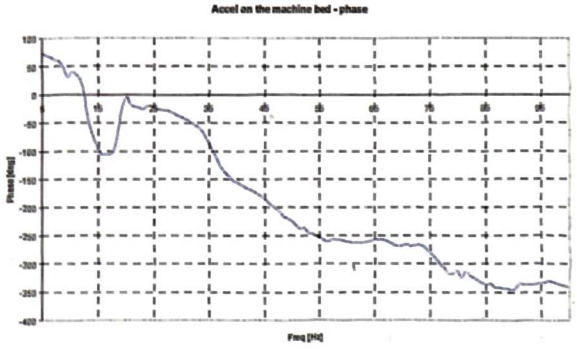

X axis direction

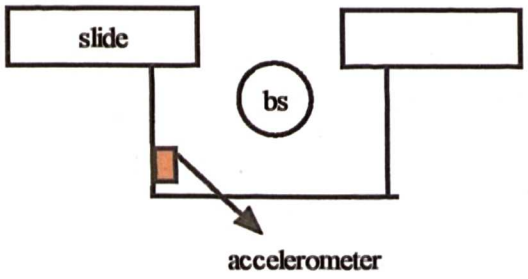

Z-axis direction

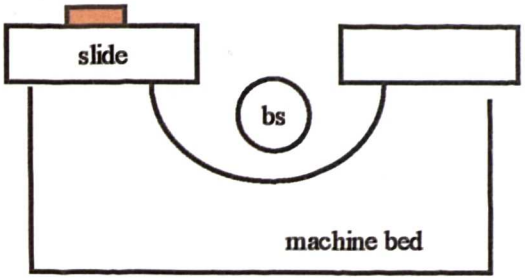

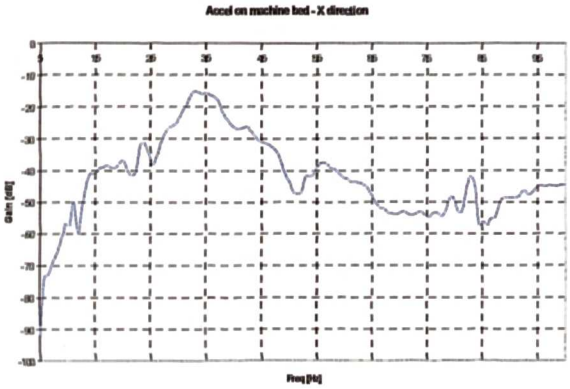

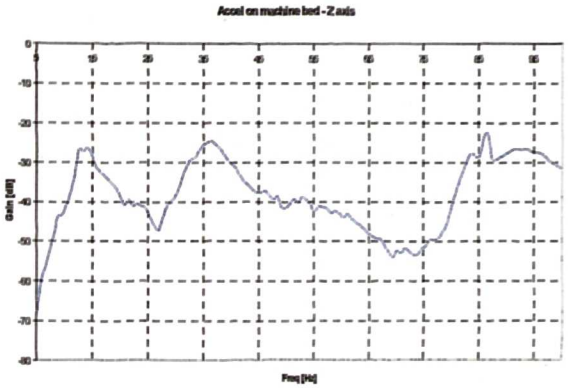

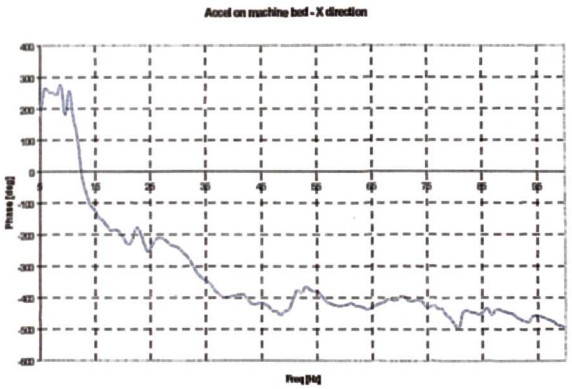

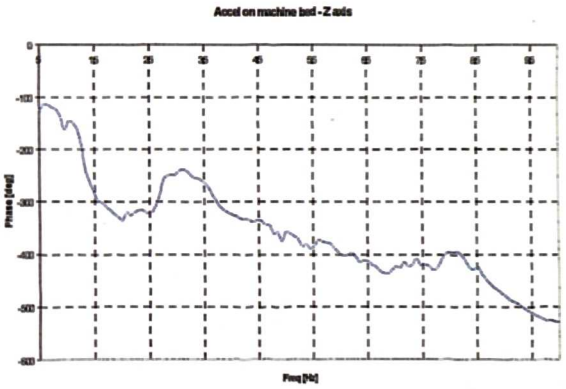

SADDLE

Y -axis direction

X direction

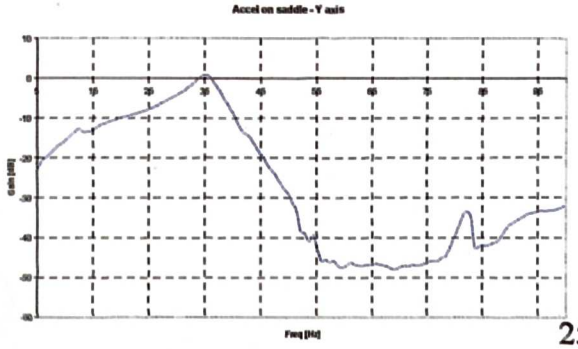

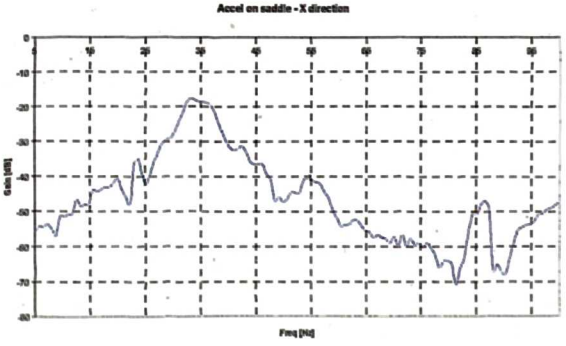

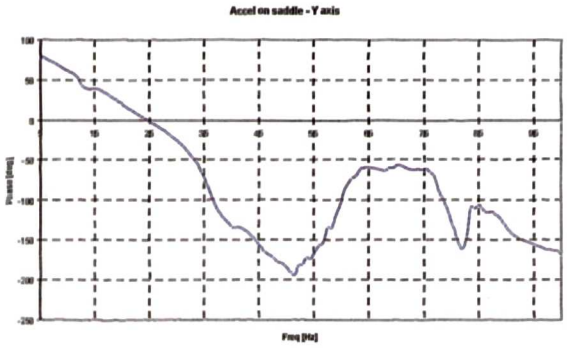

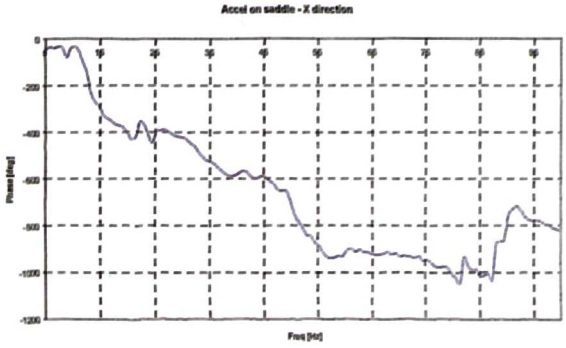

Z direction

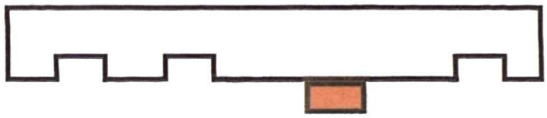

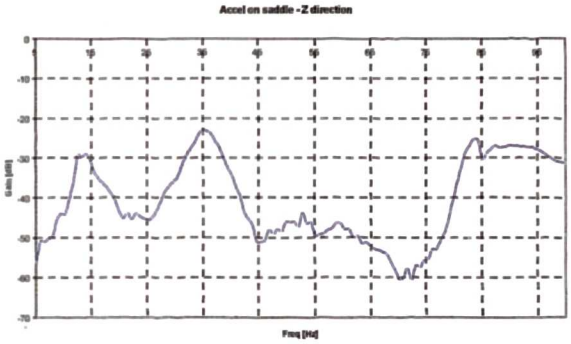

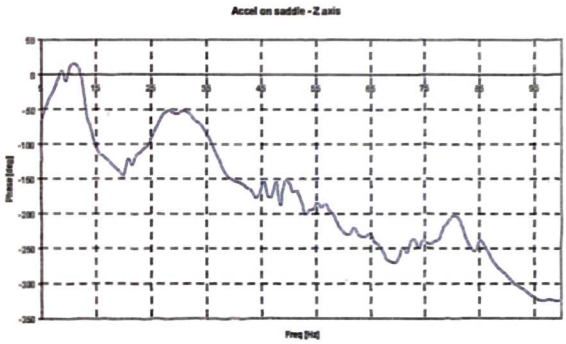

WORKTABLE Z direction

1	4	7
2	5	8
3	6	9

Position 1

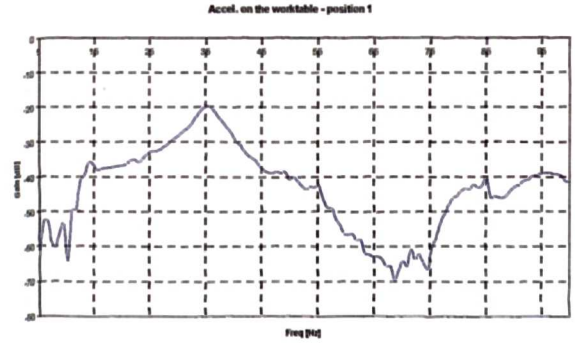

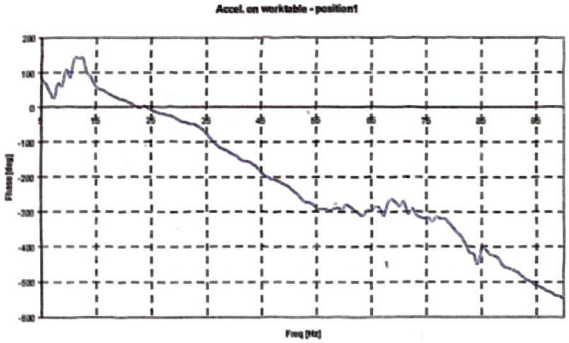

Position 2

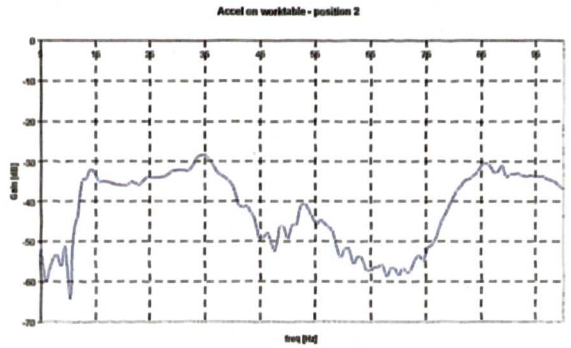

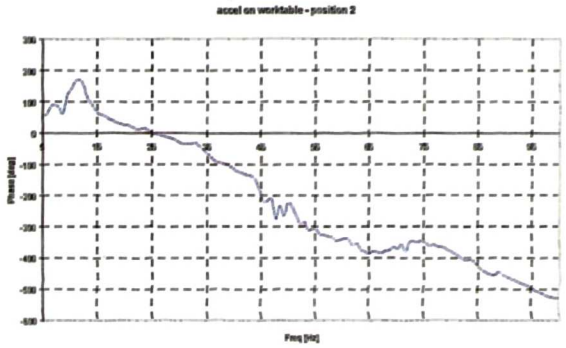

Position 3

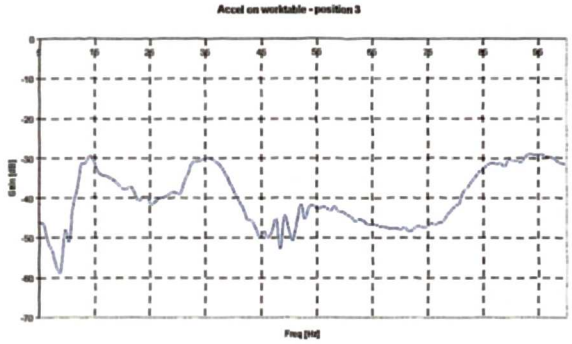

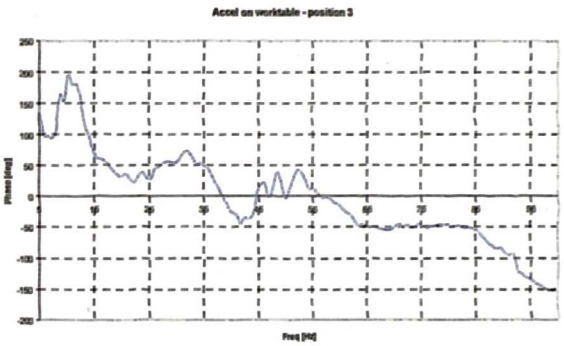

Position 4

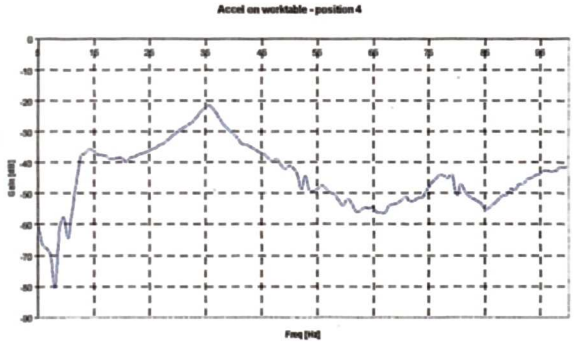

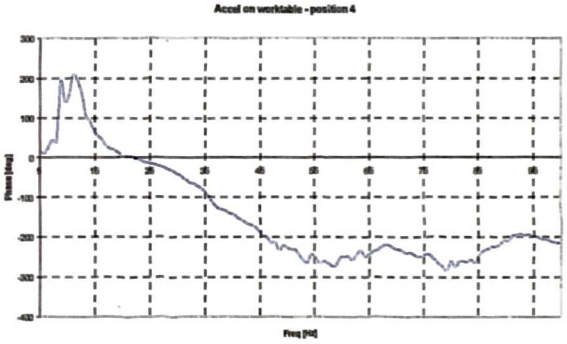

Position 5

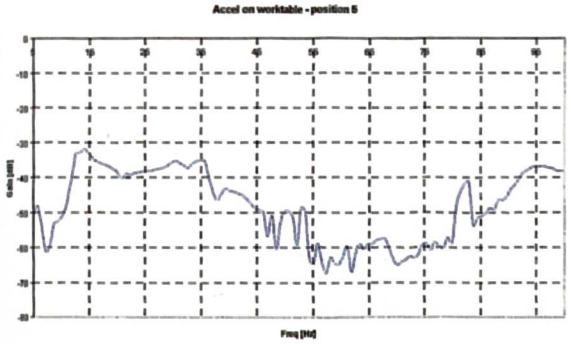

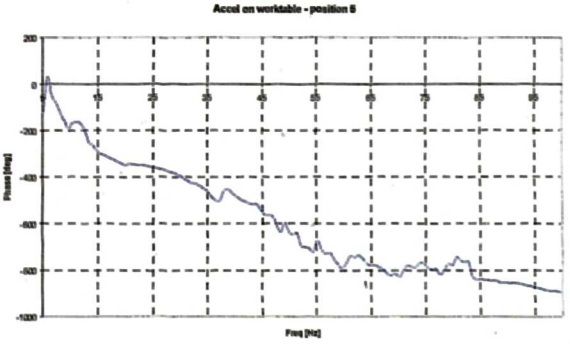

Position 6

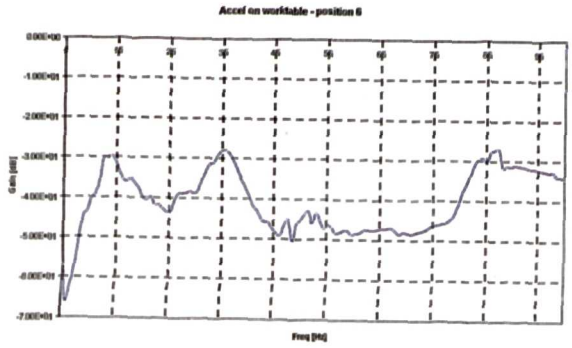

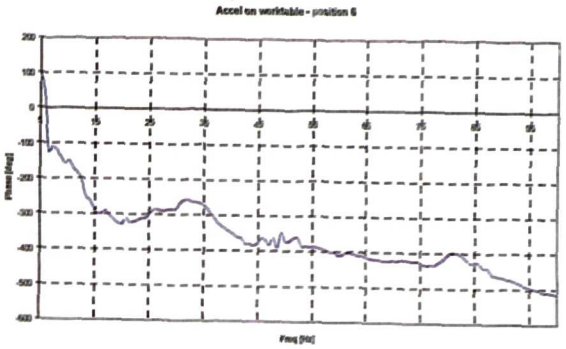

Position 7

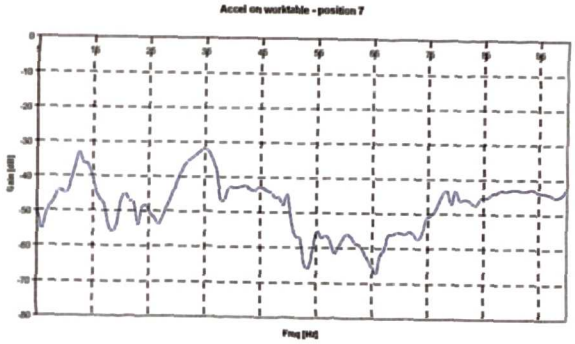

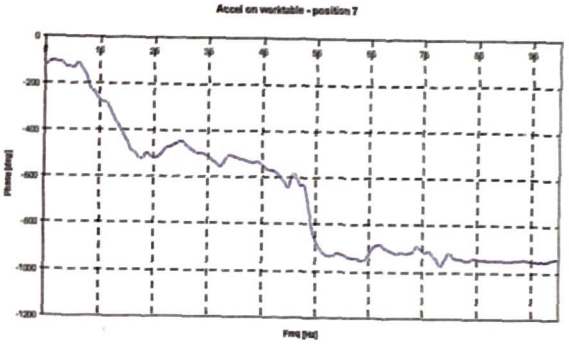

Position 8

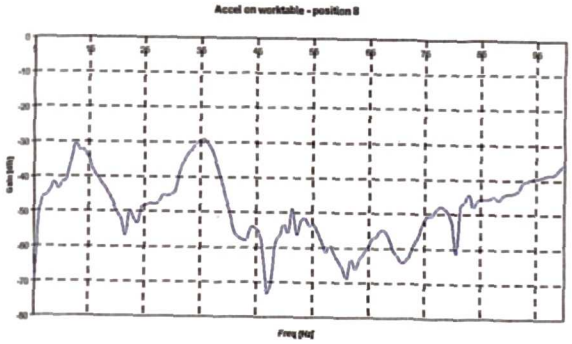

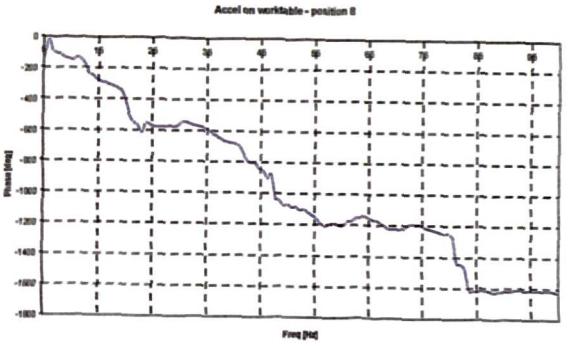

Position 9

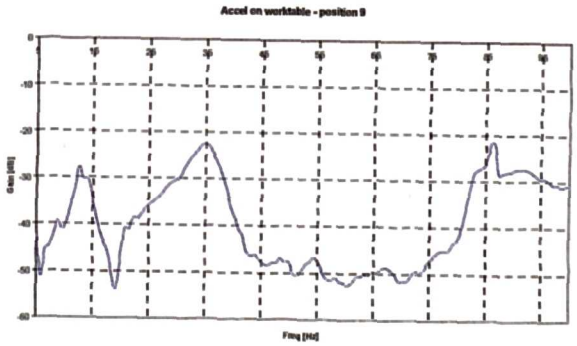

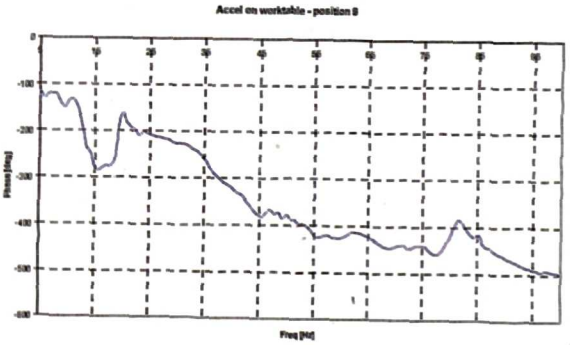

By reading the values of gain and phase (θ) for 35 Hz in the various mountings of the accelerometer (on machine bed, saddle or worktable), it is obvious that the greatest values for the gain are in the case that accelerometer is mounted on the worktable in Z-direction of the machine tool.

The amplitude of the gain is calculated considering the definition of the gain in dBs:

$G\ [dB] = 20 * \log_{10}(gain) \rightarrow gain = 10^{G/20}$

The distribution of the product gain * sin θ for the nine point considered on the worktable is:

- 0. 1	- 0. 08	0
- 0. 03	- 0. 01	0. 03
0. 02	0. 04	0. 08

Considering the values on the columns corresponding to three values of the X-axis [1 0. 5 0], the following graphs could be plotted:

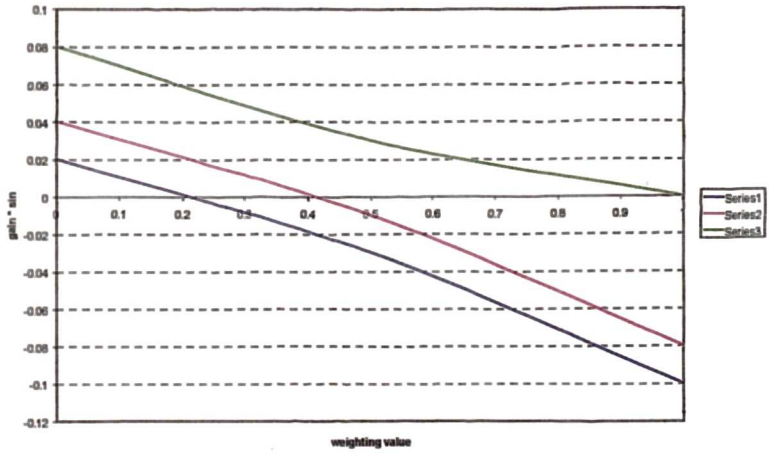

The three lines are crossing the X-axis at the values x = 0. 2, 0. 4 and respectively 0.

This is representing that fact that the saddle and the worktable are rocking around X-axis when the input into the open-loop position control system has a frequency of 35 Hz.

C4. Theoretical calculations of the stiffness considering the system: ball-screw - bearings - nut

The axial stiffness of the whole ball-screw for X-axis respectively Y-axis could be calculated considering the ball-screw as a cylinder with dimensions given in Appendix A4:

$$K_{axial\_bs} = \frac{\pi}{4} D^2 \times \frac{E}{L} = \frac{3.14}{4} \times (0.0381)^2 \times \frac{207 \times 10^9}{1.520} = 155.3 \times 10^6 \frac{N}{m} \quad (C1)$$

The axial resonance of the whole ball-screw is:

$$\omega_{axial\_bs} = \sqrt{\frac{K_{axial\_bs}}{m_{bs}}} = \sqrt{\frac{155.3 \times 10^6}{15}} = 3218 \frac{rad}{s} \quad (C2)$$

However, the resonant frequency of the ball-screw depends upon the way that the ball-screw is mounted in the CNC machine tool. The next figure illustrates a ball-screw supported by the bearings on each end (the case of Beaver VC35 CNC machine tool). The worst case is with the nut at the centre of the ball-screw, when the springs corresponding to each half of the total length are connected in parallel.

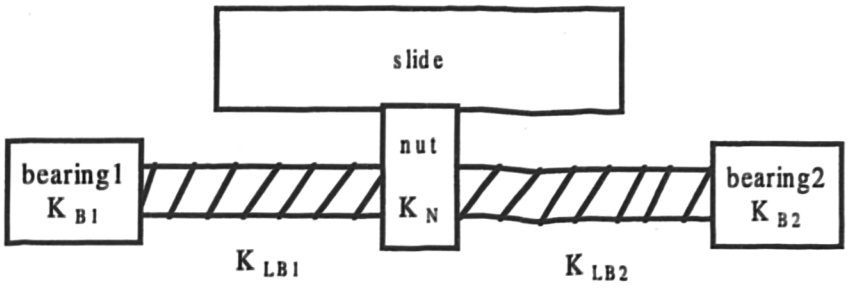

Each half of the ball-screw will have the following stiffness:

$$K_{axial\_bs\_1} = 2 \times K_{axial\_bs} = 310.6 \times 10^6 \frac{N}{m} \quad \text{(C3)}$$

The stiffness of one bearing in series with one half of the screw is:

$$K_{LB1} = \frac{K_{axial\_bs\_1} \times K_{B1}}{K_{axial\_bs\_1} + K_{B1}} = \frac{(310.6 \times 10^6) \times (1560 \times 10^6)}{(310.6 + 1560) \times 10^6} = 259 \times 10^6 \frac{N}{m} \quad \text{(C4)}$$

The stiffness of the other type of bearing in series with one half of the screw is:

$$K_{LB2} = \frac{K_{axial\_bs\_1} \times K_{B2}}{K_{axial\_bs\_1} + K_{B2}} = \frac{(310.6 \times 10^6) \times (800 \times 10^6)}{(310.6 + 800) \times 10^6} = 223.7 \times 10^6 \frac{N}{m} \quad \text{(C5)}$$

The two halves working in parallel have a combined stiffness:

$$K_{LB12} = K_{LB1} + K_{LB2} = (259 + 223) \times 10^6 = 482.7 \times 10^6 \ N/m \quad \text{(C6)}$$

The axial resonance of the X- axis drive yields:

$$\omega_{LB12\_x} = \sqrt{\frac{K_{LB12}}{m_L}} = \sqrt{\frac{482.61 \times 10^6}{364}} = 1152 \frac{rad}{s} = 183.3 \, Hz \quad \text{(C7)}$$

In the same way, the axial resonance of the Y- axis drive could be calculated:

$$\omega_{LB12\_y} = \sqrt{\frac{K_{LB12}}{m_{Ly}}} = \sqrt{\frac{482.61 \times 10^6}{682}} = 841.3 \frac{rad}{s} = 133.9 \, Hz \quad \text{(C8)}$$

C5. Measurement results for closed-loop position control

Input signal - swept-sine generated by PC Spectrum/Network Analyser HP 3566A

Output signal - the error generated by the controller

Feedback - rotary encoder attached to the DC motor (Y-axis)

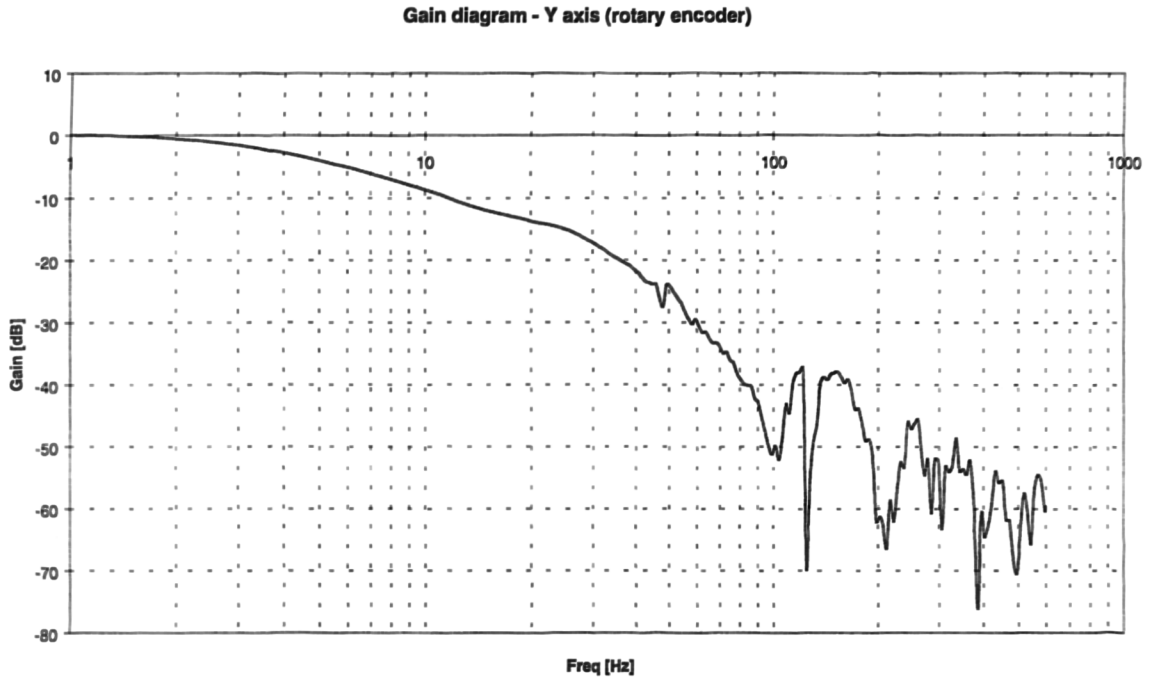

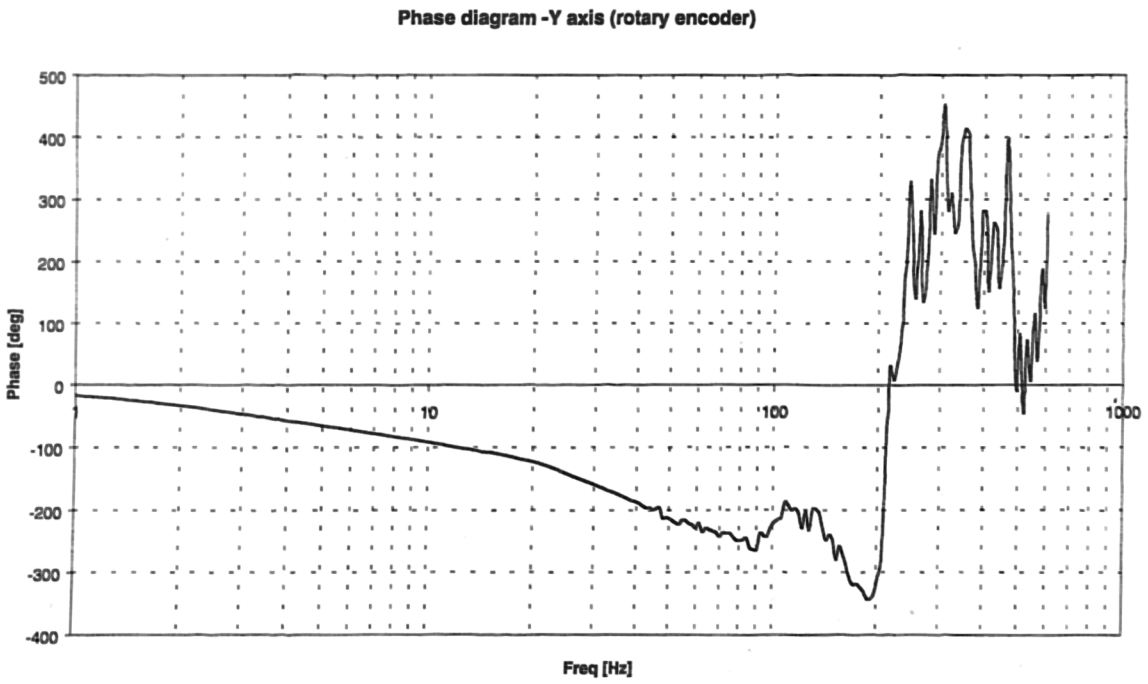

Input signal - swept-sine generated by PC Spectrum / Network Analyser HP 3566A

Output signal - the error generated by the controller

Feedback - rotary encoder attached to the end of the ball-screw (Y-axis)

Gain diagram - Y- axis (encoder at the end of ball-screw)

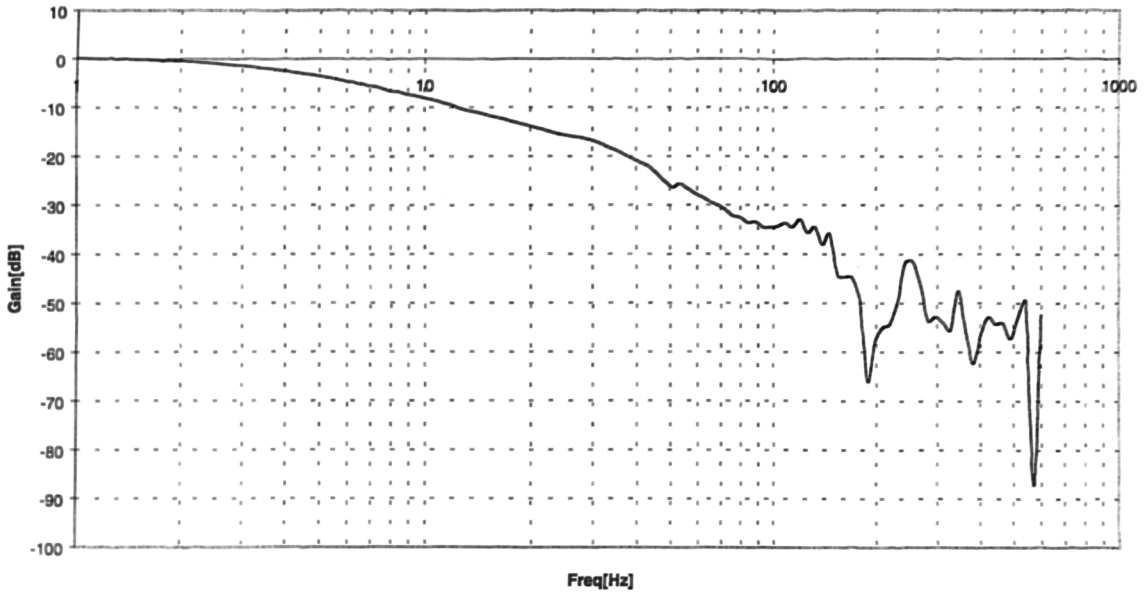

Phase diagram - Y- axis (encoder at end of ball-screw)

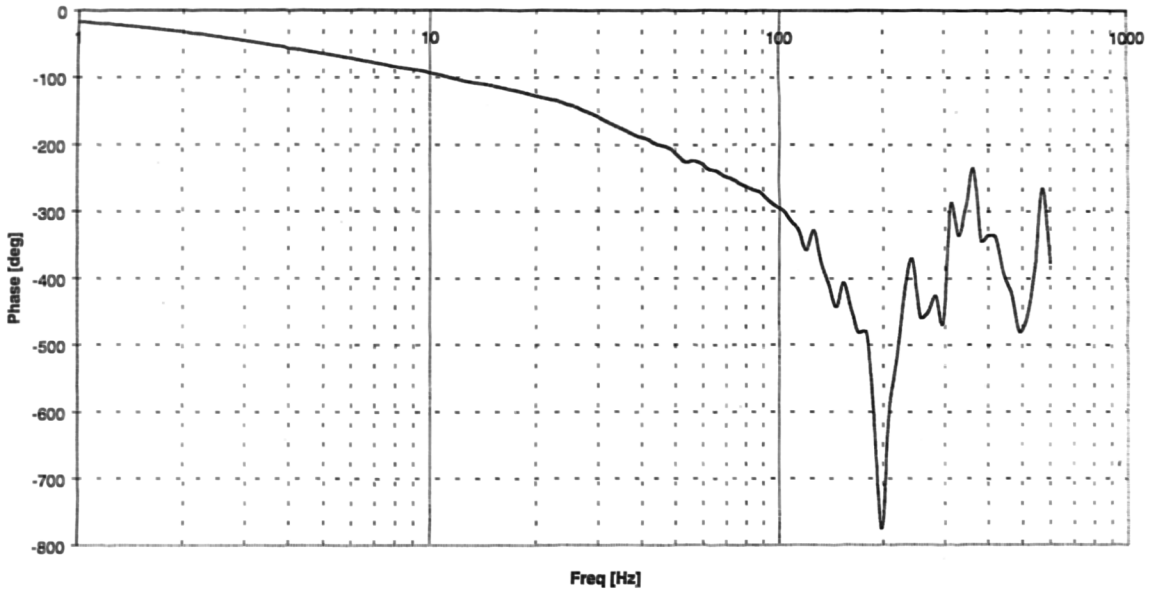

Input signal - swept-sine generated by PC Spectrum / Network Analyser HP 3566A

Output signal - the error generated by the controller

Feedback - linear encoder attached to the bed of the CNC machine tool (Y-axis)

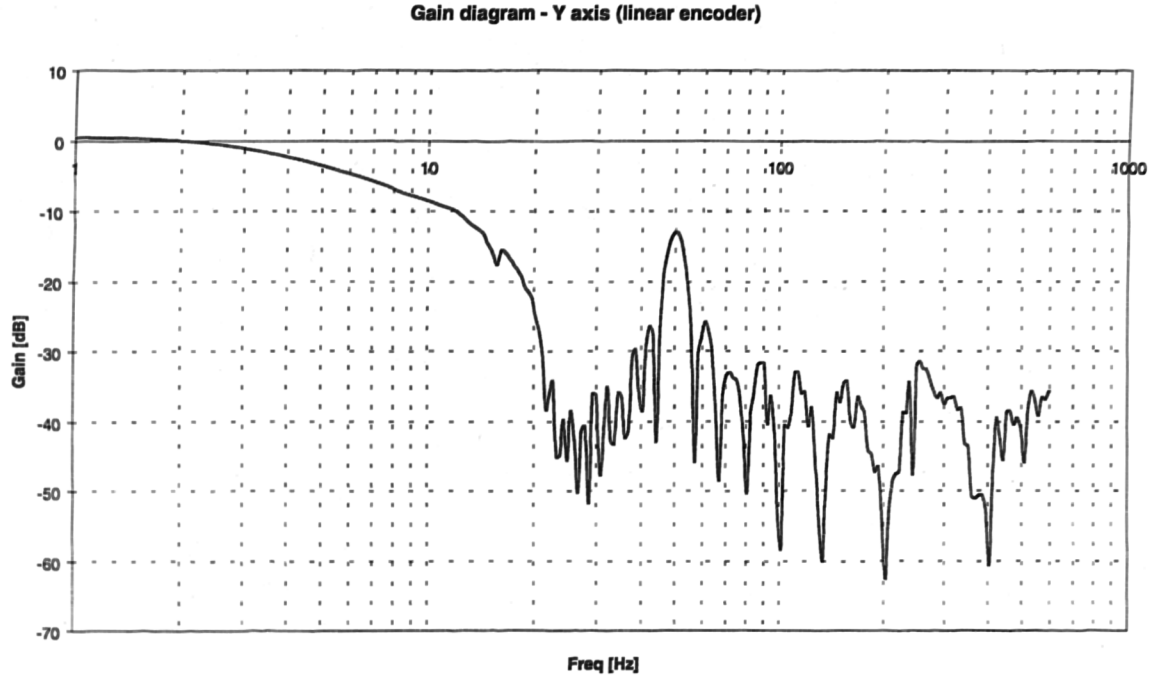

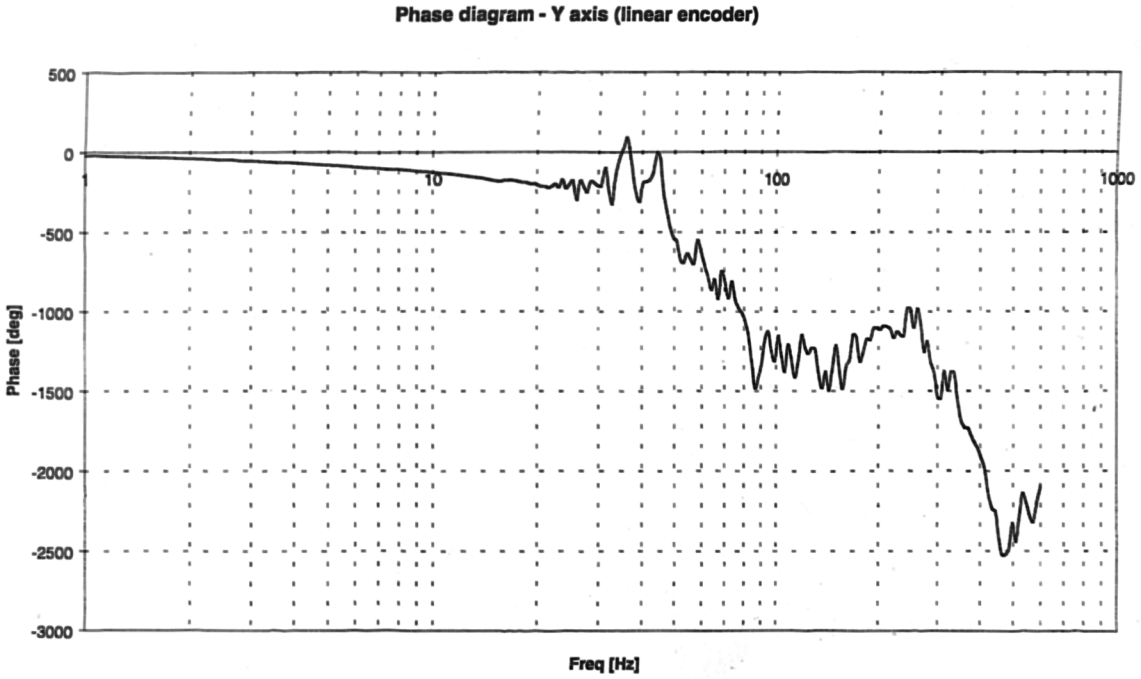

Input signal - swept-sine generated by PC Spectrum/Network Analyser HP 3566A

Output signal - the error generated by the controller

Feedback - rotary encoder attached to the DC motor (X-axis)

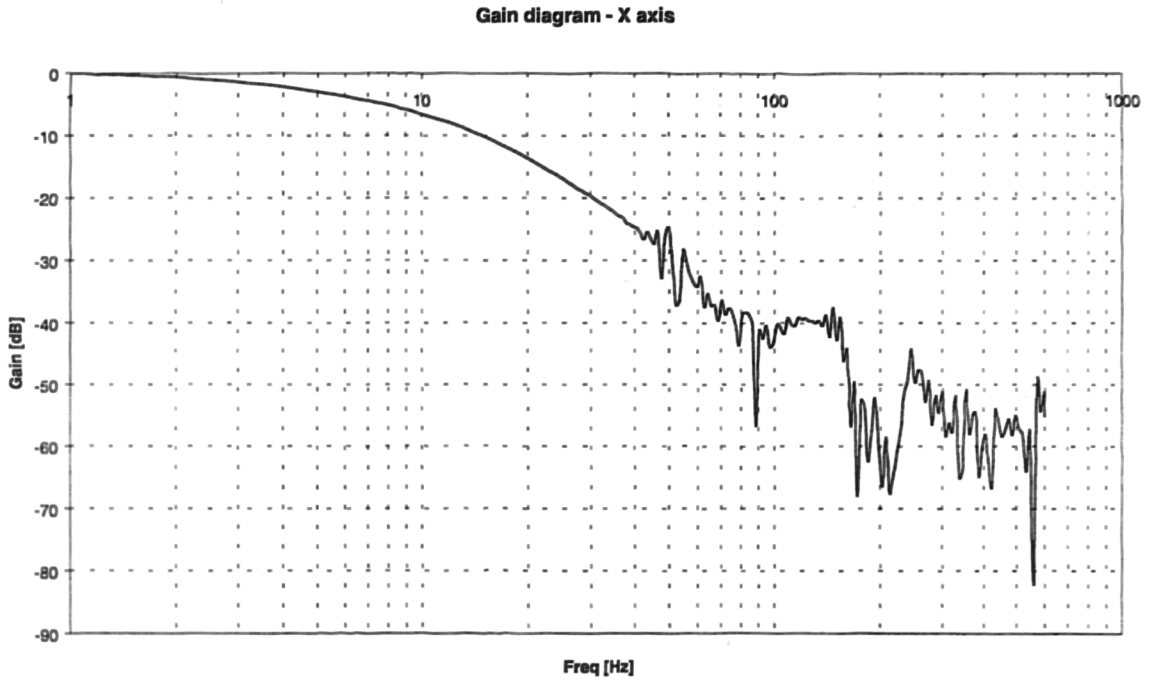

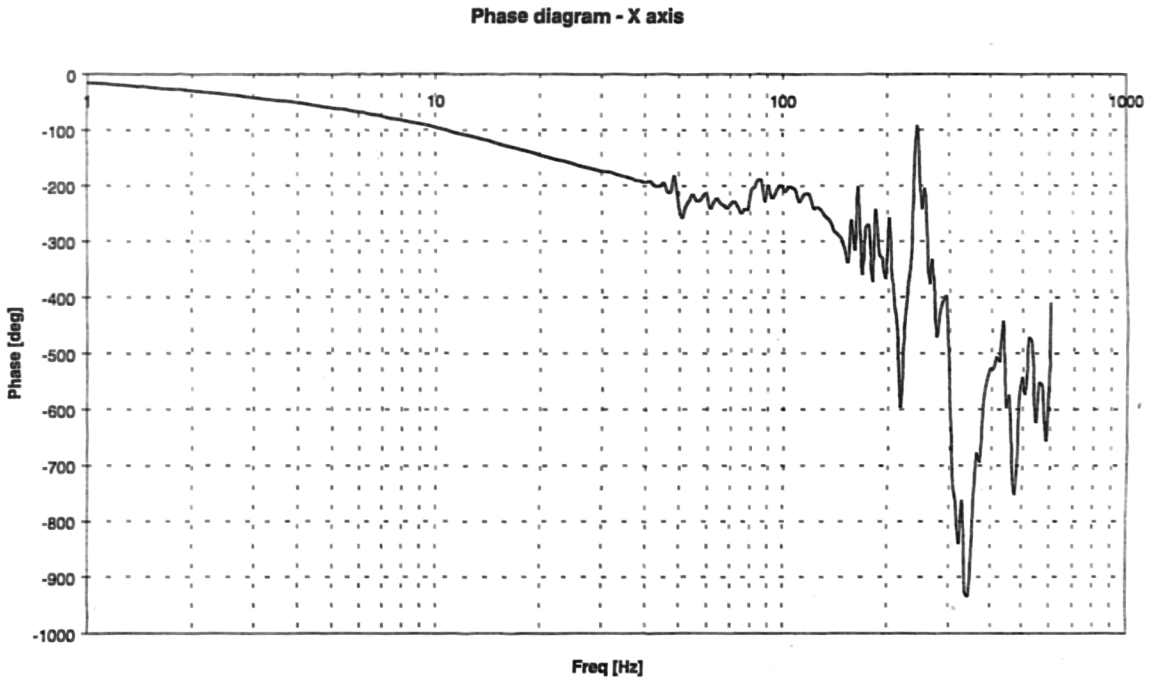

C6. Brief description of the General Data Logging Software (GDLS) developed at the University of Huddersfield

The system aims to provide a versatile software environment to allow data collection in real-time. Data generation and collection are enabled by simulation and by on-line data processing through all available hardware interfaces (for input and output) present on the user's system. It uses a configuration file which specifies the detailed set-up for a particular application or experiment. It also provides on-line data analysis and reporting of results for further processing.

The necessary hardware comprises a standard or industrial PC with one or more interface cards installed to enable data collection of one or more signals from transducers installed on the studied system (such as a machine tool). The data is collected in real-time (at regular intervals of time, or whenever a movement stops). Each signal collected is said to constitute a channel. One channel is usually used to store a record of the time as read from the real-time clock in the PC. The maximum number of channels is 50 and the maximum number of samples is 10000 per channel.

The channels are sampled under control of the software until the user intervenes. Then the results are processed and plotted on screen. The information is also recorded to disk for future analysis. Various channels are provided to generate signals such as step, ramp, white noise, PRBS etc to produce test signals for use as input to the rig. Other channels allow one or more of the input channels to be processed in some way, for example FFT, SUM of two channels, moving average, digital filters, simulated analogue transfer functions etc. Some of the processing channels work in real-time, while others work in batch mode at the end of data collection. Thus FFT is batch only, while SUM and digital filters can be used in real-time or batch mode. The A/D and D/A channels operate in real-time only.

More details about this software written in TURBO PASCAL, are discussed by Freeman [101] in the manual dedicated to the users of this software package.

As an example, here is the configuration file used during the measurements when the white noise is generated by GDLS and the Bode diagrams are plotted using the differential of the signal produced by linear encoder:

```
Channel Specification   {Up to 20 channels (19) }
1 Time Interpolate
2 Signal RandomWhite Delay 2 0 0.6  {delay 1 - mean 0V - approx. 1500 mV max}
3 DAC16 0 2 -1    {DAC channel A, from channel 2, factor -1}
4 Digital DST 3 384 0.24 {To convert to equivalent volts - includes correction for 1/lambda squared and
                          new linear encoder factor of 0.1}
5 DFil 4 1 1 2 0.1 -0.1 0.102 -0.1 0   {High Pass digital filter T=0.1}
6 CUT 2 1 500
7 CUT 5 1 500
8 Correlation 6 7 1024 {Correlation of signals 6 and 7 to give impulse. response-1024pts}
9 FFTREAL 8 1
10 FFTIMAG 8 1
11 LOGGAIN 9 10
12 PHASEANGLE 9 10 UNWRAP
```

13 MovingAverage 11 4 {signal 6 = 4 point average}

14 MovingAverage 12 4 {signal 6 = 4 point average}

19 GAIN 9 10

C7. Calculation of the coefficients of the high pass digital filter

The transfer function of the digital filter is:

$$G_{filter}(s) = 1 - \frac{1}{1+sT} = \frac{sT}{1+sT} \tag{C9}$$

where T - threshold time

The equivalent of the operator s in the z-domain is calculated as follows:

$$s\,y = \frac{dy}{dt} = \frac{y_n - y_{n-1}}{\Delta T} = \frac{1-z^{-1}}{\Delta T} \times y_z = \frac{z-1}{z \times \Delta T} \times y_z \tag{C10}$$

where ΔT - sampling interval

Therefore, the equivalent of the operator s is: $s = \frac{z-1}{z \times \Delta T}$ (C11)

The transfer function in z-domain yields:

$$G_{filter}(z) = \frac{\frac{z-1}{z \times \Delta T} \times T}{1 + \frac{z-1}{z \times \Delta T} \times T} = \frac{(z-1) \times T}{z \times \Delta T + (z-1) \times T} = \frac{(z-1) \times T}{z \times (\Delta T + T) - T} = \frac{(1-z^{-1}) \times T}{\Delta T + T - z^{-1} T} \tag{C12}$$

The formula for the digital filter introduced into GDLS is:

$$G_{filter}(z) = \frac{a + b \times z^{=1}}{a_1 + b_1 \times z^{-1} + c_1 \times z^{-2}} \tag{C13}$$

The coefficients of the digital filter could be identified from the last two relations:

$a = T$ $\qquad$ $b = -T$ (C14)

$a_1 = \Delta T + T$ $\qquad$ $b_1 = -T$ $\qquad$ $c_1 = 0$ (C15)

C8. CNC machine tool part program for a trapezoidal rate contour

O001;	- program number
G91 G01;	- incremental programming; linear interpolation for feedrate
F5000;	- feedrate goes from 0 to 5000 mm/min
Y-300.000;	- worktable will travel with this speed for 300 mm
G04 X4.0;	- dwell for 4 sec
Y300.000;	- worktable travel back for 300 mm
M30;	- end of program

The interval of time necessary for the worktable to move 300 mm is:

5000 mm .....60 s

300 mm x

x = (300 x 60) / 5000 = 3. 6 s

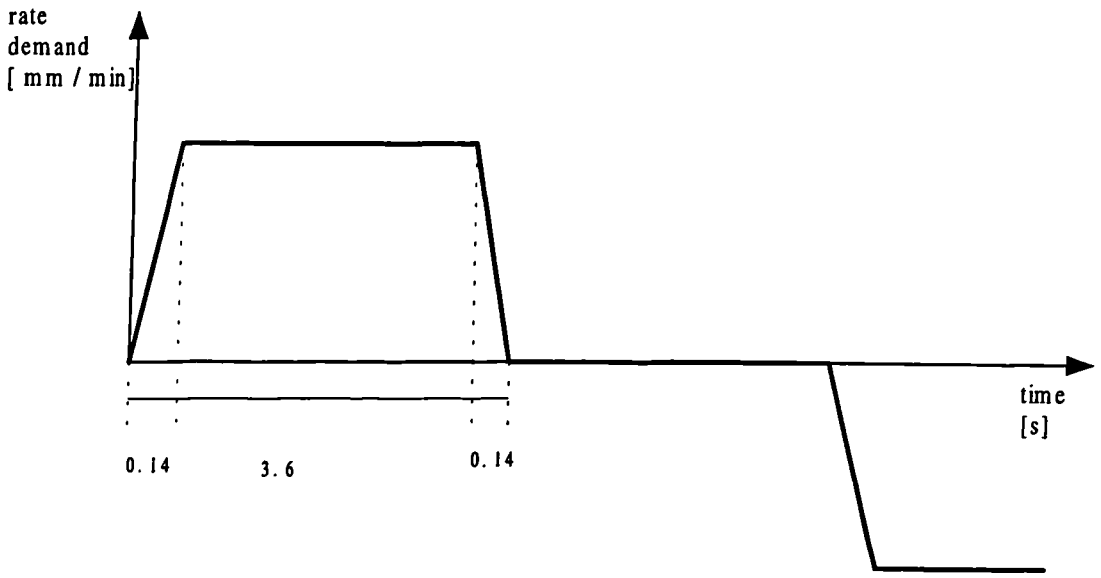

The time for one trapezoidal demand when the acceleration / deceleration time is 0. 14 s yields:

T = 0. 14 + 3. 6 + 0. 14 = 3. 88 s

APPENDIX D

D1. Configuration of the subsystem " *Ballscrew* " for the linear encoder

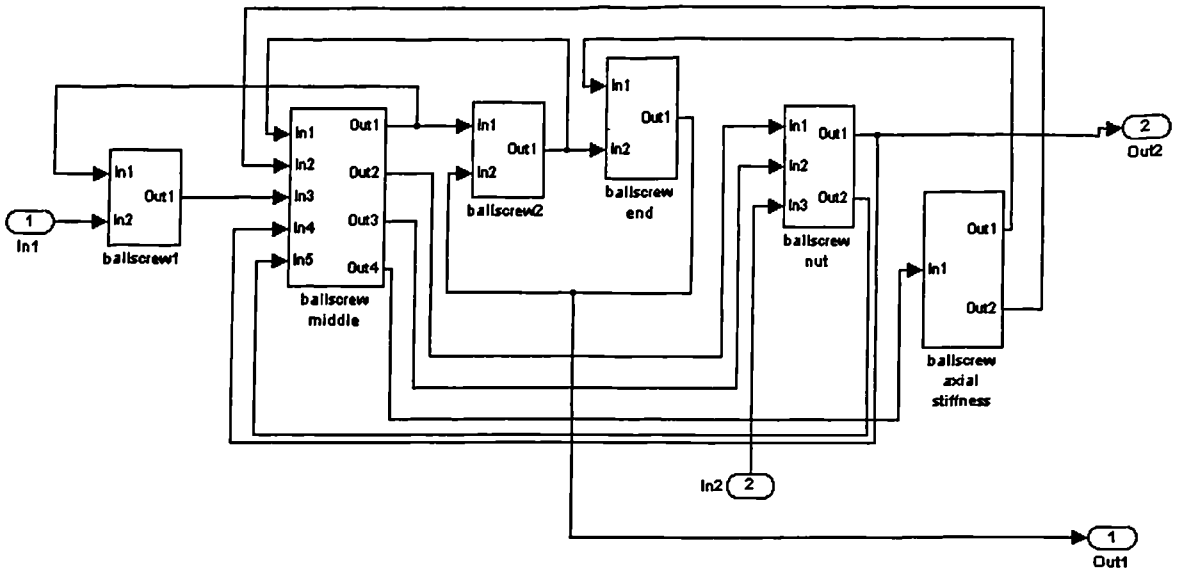

Figure D1.1. Configuration of "Ballscrew" subsystem for linear encoder

D2. Simulation results using SIMULINK 1 and a simplified model with explicit damping coefficients

The simplified model does not contain:

- Transverse inertia and spring elements;
- A non-linear model for drive belt which takes into account the belt tensions, friction between the belt and pulley and transverse vibration of the belt;
- Viscous damping for various elements.

The torsional behaviour of the motor, belt drive and ball-screw coupled with the axial movement of the table or saddle and the ball-screw nut were considered. The effect of the distributed mass in the ball-screw was also investigated.

Holroyd et al .[138], [139] showed the movement of the table predicted by the simplified model when a perturbation signal of about 250 mV was injected at the pre-amplifier and the controller was included into the position loop. In the simulated results it is obvious the controller step time of 10 ms and a further 80 ms delay occurs before the table starts with a jerk because of the friction forces which have to be overcome. The velocity response is damped down quickly after the initial step, but continues to exhibit vibratory behaviour on top of a typical time delayed response.

The same model also predicted a phenomenon observed during the measurement process: the table or saddle would cease to vibrate above a certain frequency under swept sine excitation due to the backlash in the ball-screw nut.

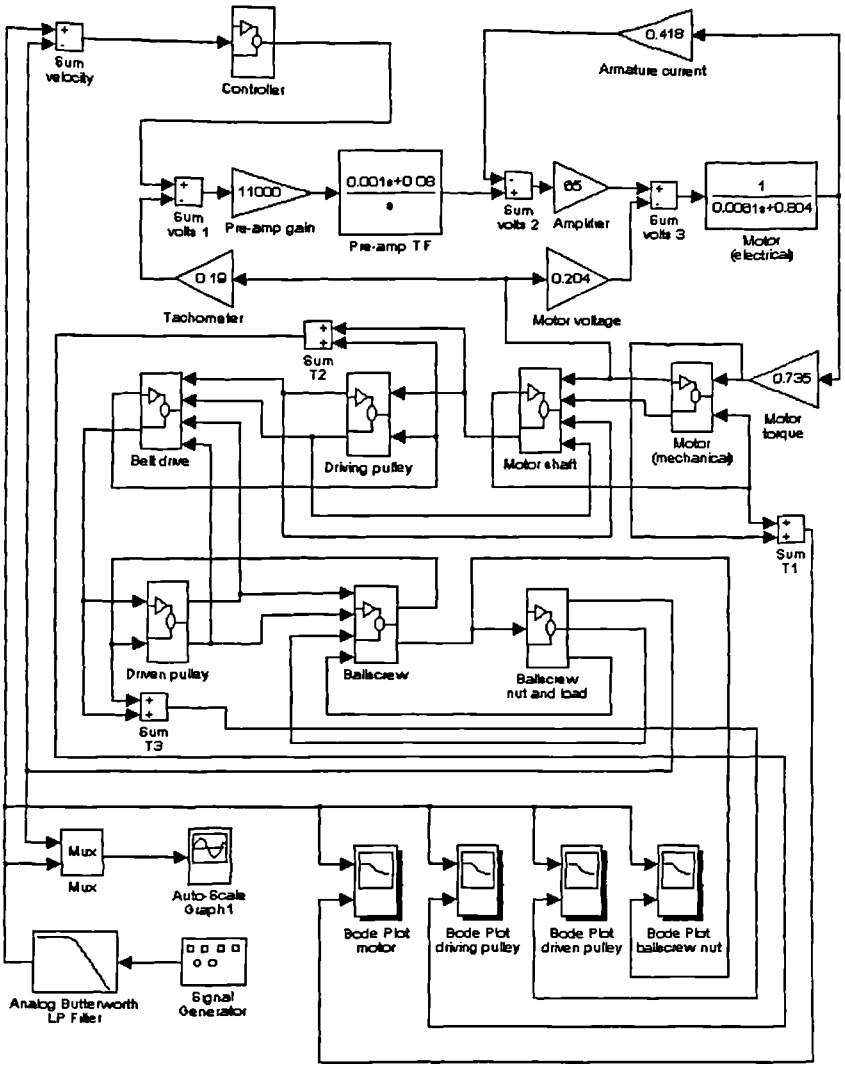

Figure D1.2. SIMULINK 1 implementation of the simplified model

The authors mentioned that: " *The results of this investigation are being fed into a larger project in hand at Huddersfield University which to improve our understanding of the mechanisms involved in dynamic errors in machine tools.*"

A more sophisticated model was developed meanwhile and the details of its components and the simulated results are examined in Chapter 6.

D3. MATLAB programs for plotting Bode diagrams in the case of swept sine input

Function [f, a_m, a_b, a_l, p_m, p_b, p_l] = bode_3 (inp_gain, fs, ff, N, Nc, Nf)
% calculates and plot Bode diagrams for three output variables
*% input variables - **inp_gain** - amplitude of input*
*% **fs** - start frequency*
*% **ff** - final frequency*

```
%                N          - number of samples for Fourier Transform (typical 4096 or 2048)
%                Nc         - number of periods for swept sine (typical 5)
%                Nf         - number of points for frequency interval (example: 401 when
%                           there are 200 points / decade and frequency is between 10 Hz and 100 Hz)
% output variables -   f -   frequency vector
%                a_m, p_m   - gain and phase vectors for the motor encoder output
%                a_b, p_b   - gain and phase vectors for the ball-screw encoder output
%                a_l, p_l   - gain and phase vectors for the linear encoder output

pi = 4.* atan (1.);                          % define the constant pi
ud = 2.;
R = 0. 010 /(2.*pi);                         % constant equal with (screw pitch / 2 *pi)
for i=1 : Nf
  f (i) = fs * ( ff / fs) ^ (( i -1) / (Nf - 1));
  x = f (i);
  [Ns, dt, T, t, u, tu] = def_imp ( f(i), N, Nc);      % generate input signal as swept sine
  save input tu;                             % save the content of the vector tu into input. mat file
  [T, X, Y] = sim ( ' name ', T+0. 001);     % run the simulation of the model ' name ' from the command line
     % calculate values of the Bode diagrams for the motor encoder output
  load motor mv_r;
  [mv] = interpol (t, mv_r);
  [inp,out] = bode_out (f(i), dt, N, Nc, Ns, t, u, mv);  % call function bode_out which calculates the FFT
                                             % for input and output
  bode_m(i) = out (Nc+1) / (inp (Nc+1) * inp_gain * 0. 001);
  a_m (i) = 20.* log10 (abs (bode_m (i)) / ud * R);   % gain in dBs
  p_m (i) = 180. / pi * angle ( bode_m (i));          % phase in degrees

     % calculate values of the Bode diagrams for the ball-screw encoder output
  load bscrew bv_r;
  [bv] = interpol (t, bv_r);
  [inp, out] = bode_out (f(i), dt, N, Nc, Ns, t, u, bv);
  bode_b ( i ) = out (Nc + 1) / (inp (Nc + 1) * inp_gain * 0. 001);
  a_b ( i ) =20.*log10 (abs ( bode_b (i) ) * R);
  p_b (i) = 180. / pi * angle (bode_b (i) );

     % calculate values of the Bode diagrams for the linear encoder output
  load linear lv_r;
  [lv]=interpol(t,lv_r);
  [inp, out] = bode_out (f (i), dt, N, Nc, Ns, t, u, lv);
  bode_l (i) = out ( Nc + 1 ) / ( inp ( Nc + 1) * inp_gain * 0. 001);
  a_l (i) =20. * log10 (abs ( bode_l (i)));
  p_l(i) = 180. / pi * angle (bode_l (i));
  end
 save o_loop inp_gain  fs  ff  N  Nc  Nf  f a_m  a_b  a_l  p_m  p_b  p_l     % save the mentioned variables
                                                                  % in o_loop inp_gain. mat file
 [p1_m] = unwrap_2 (p_m, 270.);              % call function unwrap_2 which unwrap the phase
 [p1_b] = unwrap_2 (p_b, 270.);
 [p1_l] =unwrap_2 (p_l, 270.);
     % plot the gain diagram
plot (f,a_m,f,a_b,f,a_l)
title ( ' Y drive - Amplitude plot ' )
xlabel ( 'Frequency (Hz)' )
ylabel ( 'Amplitude (dB)' )
figure
     % plot the phase diagram
plot( f, p1_m, f, p1_b, f, p1_l)
```

```
title ( 'Y drive - Phase plot' )
xlabel ( 'Frequency (Hz)')
ylabel ( 'Phase (degrees)' )
********** ********** **********
function [ f, amp, phase] = bode_2  ( inp_gain, fs, ff, N, Nc, Nf )
    % ONLY ONE OUTPUT VARIABLE
    % input variables - inp_gain - amplitude of input
    %                   fs       - start frequency
    %                   ff       - final frequency
    %                   N - number of samples for Fourier Transform (typical 4096 or 2048)
    %                   Nc - number of periods for swept sine (typical 5)
    %                   Nf - number of points for frequency interval (example:  401 when
    %                   there are 200 points / decade and frequency is between 10 Hz and 100 Hz)

pi=4.*atan(1.);                          % define the constant pi

for i=1:Nf
  f (i) = fs *  ( ff / fs) ^ ( (i-1) / (Nf-1));
  x = f (i);
  [Ns, dt, T, t, u, tu] = def_imp ( f (i), N, Nc);   % call function def_imp
  save input tu;                         % save the content of the vector tu into input. mat file
  [T, X, Y] = sim ( ' name ', T+0.001);  % run the simulation of the model ' name ' from the command line
  load vel_res  ans;                     % load .mat output data file with associated variable ans
  [v] = interpol (t, ans);               % call function interpol to make the same number of points for
                                         %  input and output data
  [inp, out] = bode_out (f (i), dt, N, Nc, Ns, t, u, v);  % call function bode_out which calculates the FFT
                                                          % for input and output
  bode (i) = out (Nc+1) / ( inp (Nc+1) * inp_gain * 0. 001);
  amp (i) = 20. * log10 (abs ( bode (i) ) );              % gain in dBs
  phase (i) = 180. / pi * angle (bode (i));               % phase in degrees
end
******** ******** **********
function [Ns, dt, T, t, u, tu]=def_imp (f, N, Nc)
% Ns - no of points in the input data set for SIMULINK model
% dt - time interval determined by sample rate                T - time of simulation
% t - time sequence                                           u - input sequence
% tu- single array of time and input - for simulation

pi = 4. * atan ( 1.);
dt = Nc / f * 1. / N;
Ns = N + round (0. 04 / dt);
T= ( Ns - 1) * dt;
t = 0. : dt : ( Ns - 1) * dt;          %Time array
u = sin (2. * pi * f * t) ;            %Sine array for Nc cycles
for i =1 : Ns,    tu (2, i) = u ( i );        tu (1, i) = t ( i );
end
******** ******** **********
function [v] = interpol (t, ans)
% reduce the number of points for ans to value t
N=length ( t );
N1=length ( ans );
V =interp1(ans(1,:),ans(2,:),t);
v(N)=ans (2, N1);
******** ******** **********
function [inp, out] = bode_out (f, dt, N, Nc, Ns, t, u, v)
pi=4.*atan(1.);
```

```
 i1=N;   i2=Ns;
 for i=1:N,
   t1(i1)=t(i2);     u1(i1)=u(i2);     v1(i1)=v(i2);     i1=i1-1;     i2=i2-1;
 end
 inp = fft (u1, N);                                % FFT for input data
 out = fft (v1, N);                                % FFT for output data
 freq=0. : 1. / ( dt * N ) : ( N - 1 ) / ( dt * N);   %Frequency array
******* ******* *********************************************
 function [p1] = unwrap_2 (p, jump)
 % unwrap the phase p when it becomes bigger than jump
 N = length (p);
 for i=1:N
   p1(i) = p(i);
 end
 for i=1:N-1
   dp = p1 (i+1) - p1 (i);
   if abs ( dp ) > jump
     for j=i+1:N
       p1 (j) = p1 (j) – sign ( dp ) * 360. ;
     end
   end
 end
```

D4. Simulation procedure for plotting Bode diagrams using white noise

- Run SIMULINK model and save input data as matrix **inbs** and output data as matrix **outbs**
- [v] = **interpol** (inbs, outbs); *% reduce the number of points for **outbs** to that of **inbs***
- Use the *Identification Toolbox* to estimate the spectral model **spad** for I / O data
- [w, amp, phas] = getff(spad); *% calculate Bode diagrams values from **spad***
- ampdB = 20 * log 10 (amp); *% amplitude in decibels*
- wHz = log 10 (w / 6.28); *% frequency in Hz*
- subplot (211), plot (wHz, ampdB); subplot (212), plot (wHz, phas);

D5. See pages 275 and 276

D6. CNC machine tool part program for circular contouring test of XY plane using ball bar (length 150 mm)

```
0001 N010 G 90 G54;               - program number & initialisation
N020 M19;                         - stop spindle rotation
N030 F3000;                       - feedrate 3000 mm / min
N040 G1 X151. 5 Y0. 0 Z0. 0;      - move direct to start point
N050 M1;                          - optional stop
N060 G1 X150. 0 Y0. 0;            - perform feed in
N070 G2 I-150. 0 J0. 0;           - prescribe first circle, CW direction
N080 G2 I-150.0 J0. 0;            - prescribe second circle, CW direction
N090 G1 X151.5 Y0. 0;             -  perform feed out
N100 M1;                          - optional stop
N105 G1 X151. 5 Y0. 0 :           - consider the start point for CCW direction
```

```
N110 G1 X150.0 Y0.0;        - perform feed in
N120 G3 I-150.0 J0.0;       - prescribe first circle, CCW direction
N130 G3 I-150.0 J0.0;       - prescribe second circle, CCW direction
N140 G1 X151.5 Y0.0;        - perform feed out
N200 M30;                   - end of program
```

D7. MATLAB programs used in the simulation of ball bar plots

```
function [r, th] = car2pol (x, y)
% Converts the cartesian coordinates (x,y) to the polar co-ordinates (r, th)
[n,p] = size(x);
r = zeros(n, p);
th = zeros(n, p);
r = (x.^2 + y.^2).^0.5;
th = atan2(y, x);
```

D8. Simulation results using 3D lumped parameter model with modular load, friction and backlash

Pislaru et al [140] showed that the simulation response of the 3D model when sine wave is applied to X-axis, cosine wave is applied to Y-axis and ramp input is introduced in Z-axis is a three dimensional helix.

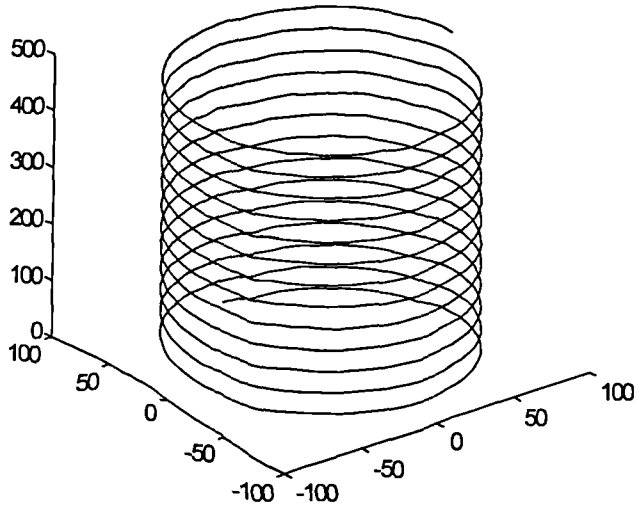

The rate demand was considered to be 5000 mm / min. The simulated response is in accordance with the theoretical approach and it excludes at this stage the geometric errors. The non-linearities considered are the backlash and Coulomb friction.

Figure D1.3. Response of 3D lumped parameter model with modular load, friction and backlash

D5. Values for look-up tables extracted from the laser measurements data

X -axis

FILE	0	35	70	105	140	175	210	245	280	305	340	375	410	445	480	515	550	585	620	655	700
XPOS [μm]	0.3	-3.1	-0.9	2.2	1.7	5.6	4.9	4.2	5.6	3.3	-2.7	-3.8	-9.5	-12.3	-15.8	-14.8	-19.4	-13.5	-17.8	-16.8	-19.6
XSTRY [μm]	0	0.8	3.4	3.1	2.9	3.4	4.3	3.7	3.3	3.2	3	2.8	1.9	0.1	0.9	0.5	0.2	0.9	0.8	0.5	0
XABZ [μm / m]	2	9	12	19	21	24	26	32	35	35	36	39	38	40	39	40	42	46	49	52	57

FILE	700	655	620	585	550	515	480	445	410	375	340	305	280	245	210	175	140	105	70	35	0
XPOS	-13.2	-17.9	-17.3	-17.1	-11.2	-14.5	-15.1	-15	-6.8	-5.6	-1.8	0.1	2.8	5.3	9.2	2.4	0.5	-0.1	1	-4	-6.2
XSTRY	-1	0.5	0.8	1.2	1.1	0.5	0.9	2	2.5	2.8	3	3.2	3.3	3.7	4.3	3.4	2.9	3.9	2.7	0.8	0
XABZ	57	52	49	46	44	42	40	40	38	40	38	37	33	33	31	28	23	20	16	11	6

Values for look-up tables extracted from the laser measurements data

Y -axis

FILE	0	-16	-32	-48	-64	-80	-96	-112	-128	-144	-160	-176	-192	-208	-224	-240	-256	-272	-288	-304	-320
YPOS [μm]	-41.2	-38.6	-36.6	-33.9	-32.8	-30.8	-30	-30.4	-28.3	-28.4	-26	-26.4	-26	-24.6	-24.5	-23	-25.9	-24.7	-23.4	-23.2	-22.9
YSTRX [μm]	1	1	1	1	1.2	1.5	1.5	1.5	1	1.5	1.5	1.5	1.7	2	2	2	1.8	1.4	1	1.3	1.5
YABZ [μm /m]	0	-1	-2	0	-2	-1	0	-1	0	-2	-1	-3	-3	-4	-4	-2	-2	-2	-2	-2	-2

FILE	-320	-304	-288	-272	-256	-240	-224	-208	-192	-176	-160	-144	-128	-112	-96	-80	-64	-48	-32	-16	0
YPOS	18.4	18.9	15.8	13.3	12.6	10.2	9.5	8.9	6.1	8.2	5.4	5.6	4.7	2.8	4.6	1.2	2.9	3.8	1.9	6.6	9.3
YSTRX	0	0	0	0	0	0	0.2	0.5	0.5	0.5	0.5	0	0	0	0	0	0	0	0	0	0
YABZ $*10^{-4}$	-12	-13	-15	-14	-14	-15	-16	-14	-14	-15	-13	-14	-15	-15	-15	-15	-13	-13	-13	-11	-8

APPENDIX E

Generalised eigenvalue method used to determine undamped and damped natural frequencies

One of the common analysis techniques employed to evaluate the dynamic responses of systems is the *eigenvalue method.* The eigenvalue method [141, 142, 143] was used extensively to determine the undamped natural frequencies and mode shapes by approximating the kinetic and potential energies by quadratic forms. The limitation of the method is the assumption that there is no damping in the system.

To overcome this disadvantage, Holroyd [144] used the *generalised eigenvalue method* [145, 146] to determine the undamped and damped natural frequencies and mode shapes for the hybrid model with distributed load, explicit damping factors, backlash, friction described in Chapter 6.

In the first stage, the natural frequencies and modes of vibration of the system were calculated considering that there is no damping in the system. This generated a general idea of the vibratory behaviour of the system. The next stage consisted in the study of the influence of the damping over system's behaviour using the generalised eigenvalue method.

Although in the model were represented different types of friction (Coulomb, hydrodynamic and viscous), only linear effects (viscous damping) were taken into account in this simplified approach.

The MATLAB programs developed by Holroyd were used for the following purposes:

- to determine the natural frequencies and damping factors for the elements of the drive using the generalised eigenvalue method;
- to plot the mode shapes in order of ascending natural frequency;
- to perform the sensitivity of natural frequency *(δnf)* to stiffness changes *(δk)*, respectively the sensitivity of damping ratio *(δζ)* to stiffness changes *(δk)* (see Table A7. 1)
- to perform the sensitivity of natural frequency (δnf) to changes in damping (δc), respectively the sensitivity of damping ratio (δζ) to changes in damping (δc) (see Table A7. 1)

These values could be used to identify what element of the drive has to change its damping ratio and event an approximate of the amount of change to make the simulation results to fit the experimental one. This method is just approximative and further work is necessary to be done to accomplish the task.

The variables from Table E1 have the following significance:

k_ms - motor shaft torsional stiffness
k_bl - belt drive torsional stiffness
k_bs - ball-screw torsional stiffness
k_nut - ball-screw nut axial stiffness
k_ax - ball-screw axial stiffness
c_ms - motor shaft torsional damping
c_bs - ball-screw torsional damping
c_bl- belt drive torsional damping
c_nut - ball-screw nut axial damping
c_ax - ball-screw axial damping
c_brg_ms - motor bearings torsional damping
c_brg_bs - ball-screw bearings torsional damping

Mode	1	2	3	4	5
Nat. freq.					
Undamped, Hz	0.0	75.1	111.8	524.7	581.6
Damped, Hz	0.0	75.3	111.6	524.8	574.2
Damping, 1/sec	-0.0	-25.7	-36.7	-21.2	-491.8
δnf/δk					
- k_ms	NaN	0.0605	0.0274	0.0171	0.4002
- k_bl	NaN	0.2653	0.1396	0.0000	0.0978
- k_bs	NaN	0.0107	0.0036	0.4730	0.0145
- k_nut	NaN	0.0773	0.1601	0.0032	0.0000
- k_ax	NaN	0.0781	0.1698	0.0049	0.0001
$\delta\zeta/\delta$**k**					
- k_ms	0.0	0.1115	0.3564	0.1323	-0.4346
- k_bl	0.0	-1.3340	0.0868	0.0007	-0.0578
- k_bs	0.0	0.0424	-0.0226	-0.5528	-0.0125
- k_nut	0.0	0.2698	-0.6709	-0.1723	-0.0004
- k_ax	0.0	0.4185	-0.2532	0.2160	-0.0003
δnf/δc					
- c_ms	NaN	-0.0000	-0.0000	-0.0000	-0.0000
- c_bl	NaN	0.0082	-0.0053	-0.0000	-0.0262
- c_bs	NaN	-0.0000	0.0000	-0.0000	-0.0000
- c_nut	NaN	-0.0013	0.0015	0.0004	0.0000
- c_ax	NaN	-0.0003	-0.0001	-0.0001	0.0000
- c_brg_ms	NaN	-0.0000	-0.0000	-0.0000	0.0000
- c_brg_bs	NaN	0.0000	-0.0000	-0.0000	0.0000
$\delta\zeta/\delta$**c**					
- c_ms	0.0	0.0001	0.0001	0.0016	0.0019
- c_bl	0.0	0.9020	0.7236	0.0001	1.0033
- c_bs	0.0	0.0003	0.0001	0.7386	0.0011
- c_nut	0.0	0.0791	0.2504	0.1925	0.0001
- c_ax	0.0	0.0119	0.0394	0.0435	0.0000
- c_brg_ms	0.0	0.0000	0.0000	-0.0000	0.0000
- c_brg_bs	0.0	0.0011	0.0007	0.0106	0.0000

Table E1 – Sensitivity of natural frequencies, respectively damping ratios to stiffness changes, respectively changes of damping coefficients of the different elements of the drive

APPENDIX F

MATLAB programs for identification of modal parameters from I / O data using continuous wavelet transform

```
%       -- Calculate impulse response from I / O data
%       -- Plot Continuous Wavelet Transform (CWT) for the impulse response
%       -- Determine resonant frequency and damping ratio corresponding to the biggest peak of CWT
%       -- Repeat the procedure for remaining peaks

% Program built Tuesday, June 19, 2001 9:32:10 AM
% This is Copyrighted Material
% For Copying permissions contact Crinela Pislaru (Precision Engineering Centre-University of Huddersfield)
% or send email to c.pislaru@hud.ac.uk

disp ( ' Create the data file containing [output input] ' );
disp ( ' Save it in EXCEL as Tab delimited .txt file ' );
 [z, q] =guiload ( '*. txt ');                          % load data file z containing vectors[y u]
number = input ( ' Number of points for data file ' );
scale = input ( ' Product of scaling factors ' );       % scaling factors introduced during the measurement
for i =1 : number,
  z (i, 1) = z (i, 1) / scale;
end;                                                    % consider the influence of scaling factors over output
disp ( ' Impulse response ' );
lags = input ('Number of lags for which the correlation analysis is computed');
[ir, r, c1] = cra (z, lags, 0, 2);  pause               % calculate the impulse response
                        % z - data entered in two columns
                        % lags - number of lags for which the functions are computed
                        % 0 - no prewhitening is performed
                        % 2 - gives a plot of all covariance/correlation information
 disp ( 'Continuous Wavelet Transform applied to impulse response ' ) ;
disp ( 'PRESS A KEY PLEASE' );  pause
can = cwt (ir, 50, 'Morlet', 2, 4);   % Continuous Wavelet Transform for impulse response
        % ir - signal, dyadic length n=2^J, real-valued,  50 - number of voices/octave,  octave =2,   scale = 4
 figure (1) ;mesh (can);   pause      figure(2) ;contour (can);  pause
 maxima = max(can);                                     % find the first peak
 [ c, d ] = max (maxima);                               % find the column with highest maximum   d= index, c=value
 sprintf ('First peak at point number %d', d);
 damped_sine = can (:,d);                               % cross section of CWT at point of first peak
 figure (3); plot (damped_sine);
 title ('Damped sine for the first peak');   pause
 for j=1 : 7,                                           % save the first 7 maximum values of damped_sine
   [ma, r ] = max (damped_sine);
   u (j) =ma;
  damped_sine (r) = 0;
  end
   [m, c] = lin_reg (u);            % gradient and free term of straight line obtained by applying linear regression
 m2 = m * m;    v2 = 4 * 3. 14 * 3.14;     den = sqrt (m2+v2);     zeta = m / den;        % damping factor
 ff1 = abs (fft (damped_sine(1:64));    [a1, v1] = max (ff1);     sample = 2;             % sampling time
  tot_samp = 64 * sample;        f1 = v1 * 1000 / tot_samp;                              % resonant frequency
  sprintf ('Damping coefficient of d% at frequency %d', zeta, f1);  pause
  % determine the next maximum value
  key = input ('Do you wish to continue ? (Y / N)');
  while key = 'Y'
  contour (can); pause
  disp ('Introduce the interval of points for what you want more details');
```

```
   min_lim = input ('Minimum limit'); pause
   max_lim = input ('Maximum limit'); pause
    figure (1); contour (can (: , min_lim : max_lim));          % display the contour to find the next maximum
    no = input ('Rank of maximum');
    peak = input (' Point number for the next maximum');
    damp = can (: , peak); figure (2); plot (damp); title (' Damped sine for peak %d', no);
    disp ('Determine the maximum values from the vector which will be plotted starting with second positive max');
   damp (1:40)
    for i =1:7,
   u2(i) = input ('Next maximum');
   end;
   [m1, c1] = lin_reg (u2); m2 = m1 * m1;    v2 = 4 * 3. 14 * 3.14;    den = sqrt (m2+v2);       zeta = m / den;
    nfft = input ('Number of points for FFT');
    ff2 = abs (fft (damp(1: nfft));    [a2, v2] = max (ff2);
    tot_samp = nfft * sample;       f2 = v2 * 1000 / tot_samp;
    sprintf (' Peak % d  - Damping coefficient of d% at frequency %d', no, zeta, f2); pause       end
% The program uses part of WaveLab version 802
```

```
function [m,c]=lin_reg(u);  % gradient and free term for a straight line fitted for the initial data using
                            %  linear regression -  Program built Thursday, June 21, 2001 12:02:27 AM
for i=1:length(u),
  y (i) = log (u (i));
  x (i)=i;
  end
sum_x=0;    sum_y=0;    sum_xy=0;   sum_x2=0;
for i=1:length(u),
   sum_x=sum_x+x(i);
   sum_y=sum_y+y(i);
   sum_xy=sum_xy+x(i)*y(i);
   sum_x2=sum_x2+x(i)*x(i);
   end
s1=sum_xy; s2=sum_x*sum_y;    s3=sum_x2; s4=sum_x*sum_x;    n=length(u);       m=(n*s1-s2)/(n*s3-s4);
c=(sum_y-m*sum_x)/n;              sprintf('Gradient m= %d', m);  sprintf('Free term c = %d',c);
```

```
function [data,fname]=guiload(ftypes,writing,stayhere)        % Load a file using the gui
if nargin<3     stayhere=1;
  if nargin<2        if nargin<1            ftypes='*.*';     end
    writing='Select file to view';    end
end
if stayhere==0       olddir=cd; end
[abba,srcpath] = uigetfiles(ftypes,writing);        % Multiple file open dialog box.
     if isempty(abba)    data=[ ]; fname=[ ];   return;  end
cd (srcpath); fname = char (abba (1));
if exist (fname,'file' ) ~ = 2
  if stayhere = = 0
  cd olddir;
  end
  error( 'File not found.' ); end
data=load (fname);
if stayhere==0
cd olddir;
end
% Dynamic Link Library for Windows 95/NTwritten by David J. Warren, Dept. of Bioeng., University of Utah
```